DAMEN

Hydrogen Powered Ship Propulsion for High-Speed Craft

The Implementation of Fuel Cell Battery Propulsion Systems

M. Boekhout

TU Delft

Hydrogen Powered Ship Propulsion for High-Speed Craft

The Implementation of Fuel Cell Battery Propulsion Systems

by

M. Boekhout

to obtain the degree of Master of Science
at the Delft University of Technology,
to be defended publicly on Monday September 28, 2020 at 09:30 AM.

Report number:	SDPO.20.031.m	
Student number:	4290445	
Project duration:	December 16, 2019 – September 28, 2020	
Thesis committee:	Ir. K. Visser,	TU Delft, chairman
	Dr. Ir. P. de Vos,	TU Delft, supervisor
	Dr. Ir. A.A.K. Rijkens,	DAMEN Shipyards Group, supervisor
	Prof. Dr. Ir. P. Colonna di Paliano	TU Delft
	Dr. Ir. H.J. de Koning Gans	TU Delft

An electronic version of this thesis is available at `http://repository.tudelft.nl/`.

Abstract

The shipping industry has a notable share in global greenhouse gas emissions and other pollutants such as sulphur and nitrogen oxides. The International Maritime Organisation (IMO) has adopted its climate change strategy in 2018, which states that greenhouse gas emissions should peak as soon as possible and these should be reduced by at least 50% by 2050. Fuel cells and batteries are identified as relatively new technologies for shipping with high potential and hydrogen is also considered as one of the most promising sustainable fuels, especially for smaller vessels. At this moment however, hydrogen is not yet at a competitive level with fossil fuels and there is insufficient infrastructure to implement it on a large scale. Still, in order to reach the goals set by the IMO it is important that green technologies are developed now and that successful ones are scaled up. This research is executed in cooperation with the Damen Shipyards Group and contributes to three identified knowledge gaps: (1), the potential of hydrogen propulsion for high-speed craft, (2) the hybridisation of fuel cells and batteries for marine applications and (3) the characteristics of the response of a hybrid fuel cell/battery propulsion system under transient loads. The objective of this research is to analyse these aspects based on a series of time domain simulations of various operational conditions. This study uses a reference vessel, which is a fast crew supplier with a length of 12 metres. This vessel has a versatile design which provides the ideal platform for the implementation of a fuel cell propulsion system with a minimum of design amendments. In addition to this, the reference vessel is the smallest vessel from Damen's high-speed craft portfolio. It has a relatively low autonomy (up to 1 day) and installed power, compared to the other vessels. Therefore, it is a good vessel as a starting point for the implementation hydrogen propulsion.

Hydrogen can be stored in various forms: compressed, liquefied, cryo-compressed or solidified. Hydrogen in compressed form (350 bar) is considered in this study, because pure hydrogen has a very high heating value compared to other fuels, but it is also has a very low volumetric energy density. Therefore, it requires much more storage volume compared to more conventional fuel types. Hydrogen is converted to electrical energy with a fuel cell. There are various types of fuel cells, but a LT-PEM fuel cell is considered here due to a high maturity and high feasibility in the short-term. Fuel cells have high efficiencies compared to other driving machines such as combustion engines and gas turbines. However, LT-PEM fuel cells are less responsive and therefore, it is advised to use a lithium-ion battery for support during transient loading. Fuel cells and batteries have excellent characteristics to be combined in a hybrid propulsion system with electric motors as prime mover. This study focuses on the implementation of fuel cell/battery systems for high-speed maritime craft. These vessels usually have a high power demand at top speed, but they only sail at top speed for a limited amount of time. Therefore, the concept of hybridisation ensures efficient operation for both average and peak power demand.

It is proposed that fuel cells and batteries are combined in a hybrid power supply, where the fuel cell (and hydrogen) deliver the majority of the energy. The battery assists the fuel cell stack as power booster and during transient conditions. It is suggested to implement a system with a "floating" DC bus voltage, which is dictated by the battery. The battery voltage is relatively constant for its operational domain, contrary to the fuel cell voltage, which makes it convenient that the voltage is dictated by the battery. The fuel cell voltage is converted to the DC bus voltage, i.e. battery voltage, with a DC/DC converter. This propulsion system is modelled in Simscape Power Systems^{TM}, which is a modelling environment in Simulink. Generic models are used for the fuel cell stack and battery module and these require only a few variables from product specification sheets. These models construct the complete polarisation curve of a fuel cell or battery based on these input values. The first model only includes the hybrid power supply and does not include the electric drive.

With the developed model, it is possible to analyse the energy consumption for various operational conditions of the FCS1204. Two operational profiles are tested: the profiles of a survey vessel and of a harbour patrol vessel. The vessel is equipped with either one or two fuel cell stacks. In addition, five different batteries are designed with increasing size and capacity. This gives a total set of ten potential combinations of fuel cell power and battery energy. These ten configurations are all tested for two different operational profiles and based on this analysis, two configurations are selected (one for the survey vessel and one for the harbour

patrol vessel). It is is recommended to either implement one stack with a medium-sized battery or two stacks with a smaller battery. If the vessel sails at top speed, the fuel cell power packs operate at maximum power and the battery operates as power booster. A strong correlation was found between the endurance (time/range) at top speed and the battery size which is selected. A larger battery has a positive effect on endurance, but it also increases the displacement of the vessel significantly and, hence, required power.

The electric drive is now added to the model in order to complete the propulsion model into a second, more detailed model. Permanent magnet synchronous machines are proposed as driving machines for this propulsion system. Electric motors can deliver a high torque and have a wide speed range, which is an advantage for mobility applications. PMSM's operate on AC power, so DC power is first inverted through and DC/AC inverter. This inverter plays an important role in the control of the motor. The frequency of the three-phase circuit is the same as the rotational speed of the electric circuit in the stator, so the motor's circumferential speed is controlled through the AC current that flows to the motor. The motors are mechanically coupled to the propellers of the FCS1204. The operational conditions of the propellers are determined with a 4-quadrant open water diagram. The coupling of the propeller and motor via a rigid shaft, tells how the propulsion system responds to these transient loads.

The system's performance in transient conditions is analysed by investigating three extreme cases: sailing in waves, slam start manoeuvres and crash stop manoeuvres. The worst intended conditions are modelled in these cases, because it can be expected that the system performs well in moderate conditions if it is also able to operate in extreme conditions. In order to analyse this, it is necessary to identify the limits of the fuel cell, battery and PMSM's. Fuel cells are least responsive and, hence, these should be protected against high fluctuations in a short time. If the power of the fuel cell stack is properly managed, it is found that a fuel cell can only follow low-frequency transient loads. The battery is required to support in high-frequency load changes. Contrary to the fuel cell, both the battery and PMSM were found to have very favourable characteristics in transient conditions. Both have a very high responsiveness and both can deliver a high peak power for a limited amount of time. Due to the characteristics of these components, it was found that the performance of the vessel can be significantly improved during emergency manoeuvres compared to the reference vessel.

Finally, it is concluded that it is feasible to implement fuel cell/battery propulsion on high-speed craft. It is proposed that the fuel cell and hydrogen deliver the majority of the energy and use the battery as power booster and for transient support. Novel energy management strategies are capable of delivering high system efficiencies in both full and part load and this is one of the main advantages of hybridisation. In addition to this, the proposed propulsion system has an excellent performance under transient conditions. The fuel cell is only capable to follow low-frequency loads and is supported by the battery for high-frequency loads.

The implementation of a fuel cell/battery system does, however, come at significant costs in terms of endurance and top speed due to the low volumetric energy density of hydrogen. In practice this would mean that it is possible to sail for a limited prolonged period at top speed (20 knots, over 1 hour) and refuelling is required more often (daily) compared to diesel propulsion. The reference vessel has a high range of 200 nm at a speed of 26 knots, so this shows the main limitation of hydrogen propulsion. Therefore, it should be acknowledged that the functionality of the vessel is also reduced. The FCS1204H2 is not capable to operate as a supply vessel for the offshore energy market, due to the long sailing distance to these locations. In addition to this, the storage of hydrogen requires some deck space, so the cargo capacity in terms of crew and material is also reduced. Therefore, it is recommended to redefine the user profile of the vessel and define a set of operations that can be executed with this vessel, such as survey and harbour patrol operations.

Preface

April 2018 marked a milestone for the global shipping industry, as the International Maritime Organization adopted its climate change strategy to reduce the greenhouse gas emissions from international shipping. The ships we are building today, will remain in service for the coming decades, which means that we must act today. The energy transition is in full swing and now is the time for all stakeholders to redefine their operations in order to reduce their carbon footprint. When I was finishing my bachelor degree I got acquainted with the impact of progressive policies on ship design and operations. My bachelor thesis focused on the design of container vessels under the uncertainty of upcoming ECA regulations. During this semester, however, it struck me that my interests do not lie within the field of ship design and I was inspired by the large number of disruptive technologies that may lead the way through the energy transition. Suddenly, I became aware of my potential contribution to sustainable shipping in the role of a marine engineer. During my master program I pursued this ambition and I can proudly look back at a period where I have developed myself in both professionally and personally.

This master thesis focuses on the implementation of hydrogen propulsion for high-speed vessels. The main challenge with respect to the realisation of hydrogen projects can best be described as a "chicken and egg" problem: shipping companies are not willing to invest in hydrogen technology if there is no infrastructure and energy supplier are not investing in an infrastructure if there are no users. This research project is executed at the Damen Shipyards Group and runs parallel to a subsidised project for the technical and commercial validation of hydrogen technology in the port of Den Helder (the Netherlands). A consortium aims to establish a decarbonised fuel chain and realise a demonstrator project and, hence, the chicken and egg problem is solved due to this inter-organisational collaboration. The close relation between my graduation research and this project gave me a strong motivation to focus on both the practical and academic aspects of this problem.

I would like to thank the Damen Shipyards Group for the opportunity and the thrust that they have put into me. First of all, I would like to thank the campus recruiter, Lisa Weggemans, for finding me an assignment perfectly matching my interests. Furthermore, I would like to thank my supervisors at Damen, Albert Rijkens and Johan de Haas, for their support during the graduation process. Albert has always helped me to set up this research and to discuss the relevance and correctness of my findings. Johan, on the other hand, provided me with valuable insights in terms of the practical side of the assignment. Together, they could help me with any challenge that came in my way. Besides this, I would also like to thank my colleagues at the design & proposal department and the research & development department for their help and for the nice informal moments that we have shared.

I would also like to thank the support that I have received from the Delft University of Technology. In particular, I would like to thank Peter de Vos for his supervision and the interesting discussions that we have had. Also on a personal level, I have received a lot of advise from Peter during my master program, for which I am grateful. I would also like to thank Klaas Visser for his relevant feedback and inspiring words during the formal progress meetings. Finally I would like to thank the other committee members, Henk de Koning Gans and Piero Colonna di Paliano, for their time and effort to review my work.

This research is executed in a period where we have seen how the world changed due to the COVID-19 pandemic. For me this meant that I had to work from home for a large part of this period. This would not have been possible without the support from all the people around me. I would like to thank my colleagues and fellow students for the nice chats and motivating words. However, most of all, I would like to thank my friends and loved ones for their endless support and good company during my studies and the graduation process.

M.Boekhout
Delft, September 2020

Contents

List of Figures

List of Tables

List of Symbols

Abbreviations

AC	Alternating current
AFC	Alkaline fuel cell
BEMF	Back electromagnetic force
BoP	Balance of Plant
COPV	Composite pressure vessel
CPSR	Constant power speed range
CTSR	Constant torque speed range
DC	Direct current
DMFC	Direct methanol fuel cell
DOD	Depth of discharge
EMS	Energy management system
ESS	Energy storage system
FAT	Factory acceptance test
FC	Fuel cell
FCS	Fast crew supplier
FRP	Fibre reinforced plastic
GHG	Greenhouse gas
HFO	Heavy fuel oil
HHV	Higher heating value
HSC	High-speed craft
HT	High-temperature
ICE	Internal combustion engine
IMO	International Maritime Organization
LA	Lead-acid
LHV	Lower heating value
Li-ion	Lithium-ion
LNG	Liquefied natural gas
LT	Low-temperature
MCFC	Molten carbonate fuel cell

MEPC Marine Environment Protection Committee

NiMH Nickel metal hydride

PAFC Phosphoric acid fuel cell

PEMFC Proton exchange membrane fuel cell

PMS Power management system

PMSM Permanent magnet synchronous machine

PSD Power speed diagram

SOC State of charge

SOFC Solid oxide fuel cell

SPS Simscape power systems

SR Steam reforming

SSS Short-sea shipping

TTP Tank to propeller

WGS Water gas shift

WTP Well to propeller

WTT Well to tank

Chemical compounds

H_2SO_4 Sulphuric acid

Pb Lead

PbO_2 Lead dioxide

CH_3OH Methanol

CH_4 Methane (natural gas)

CO Carbon monoxide

CO_2 Carbon dioxide

e^- Electron

H_2 Pure hydrogen

H_2O Water

H^+ Hydrogen ion

LH_2 Liquid hydrogen

NO_x Nitrogen oxide

SO_x Sulphur oxide

Greek symbols

α Charge transfer coefficient

ΔG Gibbs free energy

ΔH Change in enthalpy

ΔS Change in entropy

η Efficiency

μ Wave direction

μ_f Fuel utilisation coefficient

ω Wave frequency

ω_e Electrical rotational speed of motor [rad/s]

ω_m Mechanical rotational speed of motor [rad/s]

Φ Magnetic flux

Φ_w Wave potential

ρ Density

θ_e Electrical angle

θ_m Mechanical rotor angle

ζ_a Wave amplitude

Roman Symbols

$\dot{m}$ Mass flow rate

$\dot{V}$ Volume flow rate

A Tafel curve slope

A Voltage drop exponential area

B Exponential zone time constant inverse

B Strength of magnetic field

C Capacitance

c Wave speed

C_q Torque coefficient

C_t Thrust coefficient

D Duty cycle

D Propeller diameter

E Energy

F Faraday constant

F Viscous friction coefficient

F_L Lorentz force

f_s Switching frequency

I Current

I_0 Exchange current

I_B	Battery current
I_{Bus}	DC bus current
I_{FC}	Fuel cell current
J	Moment of inertia
K	Polarisation voltage constant
k	Wave number
K_M	Motor constant
k_p	Number of propellers
K_T	Torque constant electric motor
L	Inductance
l	length
M	Molar mass
m	Mass
n	Number of moles
n	Number of moving electrons
N_c	Number of cells
N_m	Mechanical rotational speed of motor [rpm]
n_m	Mechanical rotational speed of motor [rev/s]
N_p	Number of battery modules parallel connected
N_p	Rotational speed of propeller [rpm]
n_p	Rotational speed of propeller [rev/s]
N_s	Number of battery modules in series connected
P	Number of pole pairs
P	Pressure
P_B	Battery power
P_b	Brake power of motor
P_{EM}	Mechanical power electric motor
P_{FC}	Fuel cell power
Q	Propeller torque
Q_B	Battery capacity
R	Gas constant
R_0	Load resistance
R_s	Ship resistance
R_{ohm}	Ohmic resistance

T	Propeller thrust
T	Temperature
t	Thrust deduction factor
T_e	Electromagnetic torque of electric motor
T_m	Mechanical torque of electric motor
T_s	Switch period
u	Water particle velocity in x-direction
V	Volume
V_0	Open circuit voltage
V_a	Advance speed
V_B	Battery voltage
V_r	Relative water velocity
V_s	Ship speed
$V_{0,nom}$	Battery voltage constant
V_{act}	Activation voltage
$V_{B,cut}$	Cut-off voltage battery
V_{Bus}	DC bus voltage
V_{FC}	Fuel cell voltage
V_{LL}	Line-to-line voltage
V_{Nernst}	Nernst voltage
V_{ohm}	Ohmic voltage
w	Wake fraction
x_i	Mass fraction of i
y_i	Volume fraction of i
z	height

1

Introduction

The transportation sector is one of the largest emitters of carbon dioxide (CO_2) and shipping has a notable share in this. Besides greenhouse gas emissions (GHG), shipping also emits a range of pollutants, such as sulphur oxide (SO_x) and nitrogen oxide (NO_x), with local health and environmental risks. The *Paris Agreement*, adopted in 2015, prescribes how the parties to this agreement should strengthen the global response to the threat of climate change, in order to keep the increase in the global average temperature below 2°C [90]. However, guidelines for the shipping industry are not directly included in this agreement. The shipping industry could represent about 10% of the global greenhouse gas emissions if other sectors take measures to keep the global temperature increase below 2°C [32].

Some political context is relevant when discussing the mitigation of emissions from shipping. Ship emissions are estimated and reported based on national fuel sales. This measure often gives a false impression: large ships can sail for weeks without bunkering, so often ships call at ports without refuelling. In other words, vessels release emissions in one area, but they are reported somewhere else. Individual countries have been reluctant to impose fuel taxes as ships can easily bunker elsewhere [2]. Laying down regulations at a global level is therefore more effective.

Global standards for the shipping industry are addressed by the International Maritime Organization (IMO). The IMO, however, has long tried to deny the impact of shipping and gave its prevailing view at the time that the Paris Agreement was signed: *"Shipping was already the most efficient form of transport and its emissions could not be capped because shipping was the servant of world trade and would need to continue to grow with it"* [2]. Pressure from high ambition nations and industry has eventually resulted in the acknowledgement of the need to act. The IMO's Marine Environment Protection Committee (MEPC) has adopted its climate change strategy in 2018. Greenhouse gas emissions from international shipping should peak as soon as possible and the total annual amount of GHG emissions should be reduced by at least 50% by 2050 compared to 2008 [44]. Meanwhile, incentives to phase out GHG emissions entirely should be supported.

From 2020, the shipping industry is facing the 0.5% sulphur cap which affects up to 70,000 vessels [22]. Current regulations focus on the reduction of harmful emissions, such as SO_x and NO_x. In the recent past, technical solutions to meet these regulations have been developed to ensure compliance for recently implemented regulations. However, ongoing discussions will lead to new targets for cleaner (and emission-free) shipping. Technical solutions that are retrofitted in a vessel, to meet current regulations, might slow down the transition to the utilisation of decarbonised fuels: a ship that is equipped with scrubbers is unlikely to switch to sulphur-free fuel in the near future. This is referred to as the 'emissions paradox' [22]. That being said, there is a wide range of options under investigation for new-build vessels. At the time of starting this research, December 2019, the maritime industry found itself at the dawn of a decade where the most disruptive set of regulations will be implemented. This moment marked the start of a transition towards sustainable shipping.

1.1. Roadmap to clean shipping

Research into alternative fuels is driven by international initiatives to reduce carbon dioxide emissions. Classification society DNV-GL has identified fuel cells (FC) and battery systems as relatively new technologies for shipping with high potential [27]. Furthermore, methanol, biofuels and hydrogen are considered as most promising fuels without CO_2 emissions from tank to propeller (TTP). From well to tank (WTT), however, a significant amount of CO_2 is emitted in the production process of these "green" fuels. In some cases, when methanol or hydrogen is produced from methane, well to propeller (WTP) emissions are even higher compared to conventional fuel oils [27]. Hydrogen can also be produced from electrolysis by using electricity. The carbon footprint of this method is expected to drop in the near future, since onshore electricity generation is included in many pledges to the Paris Agreement [2]. Alternatively, the utilisation of green electricity opens a pathway to the production of (synthetic) carbon-neutral logistic fuels. This requires that carbon is captured from the atmosphere, which is still challenging due to the low concentration of CO_2 in the atmosphere [95]. Ultimately, the production of hydrogen from green electricity results in full decarbonisation [34].

It is safe to say that the complete decarbonisation of shipping would increase the demand for renewable electricity considerably: EU-related shipping alone is expected to require 11% to 53% additional green electricity [2]. Full-electric battery and hydrogen fuel cell technologies (or hybrid combinations) put the lowest strain on the renewable energy sector. It makes sense to link renewable energy sectors, specifically offshore wind, with the production of green hydrogen: offshore wind turbines run often when the electrical grid is saturated. The excess energy can be stored in hydrogen for later use [16]. Stakeholders should pursue a gradual increase in energy demand by developing green technologies and scaling up successful ones [2, 34]. In this view, short-sea shipping (SSS) is a good starting point for fuel cell electric vessels for two reasons. Firstly, large ocean-going vessels need a developed fuel infrastructure for global fuel availability, which is not yet established [27]. Also, vessels for SSS require relatively small power generation systems; technologies with sufficient power are already commercially available [100]. Ocean-going vessels can use green alternatives for auxiliaries, but remain dependent on conventional combustion engines for propulsion until technology matures.

At this moment, green hydrogen is only economically feasible under the assumption of massive subsidies or high taxes on conventional fuels [27]. Today, almost all hydrogen is produced from natural gas (grey hydrogen). Natural gas is currently at a competitive level with HFO, both ranging between 60% and 80% of the Brent crude oil price [27]. Operational expenditures are often the driving factor for policy makers, so these economic aspects (and governmental support to overcome these barriers) are very relevant in the roadmap towards clean shipping [2]. The expected development of the hydrogen market is analogous to the development of the offshore wind industry [16]: energy from offshore wind used to be significantly more expensive than conventional sources and has achieved competitive levels today. It is expected that hydrogen will come down to a competitive level with fossil fuels by 2030.

1.2. Damen Shipyards Group

This research project is executed within the premises of Damen Shipyards Group. At Damen, ships are designed, engineered, built and serviced. The company is active in a wide range of market segments: dredging vessels, tugs, workboats, ferries, naval vessels, yachts, offshore vessels, high-speed craft and patrol vessels. This study is executed at the design & proposal department for high-speed craft.

1.2.1. DKTI-Transport 2019

The Damen Shipyards Group and a small number of partners have received subsidies from the 'Rijksdienst voor Ondernemend Nederland' (DKTI-Transport 2019) to technically and commercially validate innovative hydrogen technology applied on waterborne craft. An inter-organisational collaboration aims to realise a decarbonised fuel chain and validate the hydrogen chain and technology in a demonstrator project including the delivery of green electricity (Engie), the development of an hydrogen station (Total), the design and realisation of a hybrid hydrogen-electric vessel (Delft University of Technology and Damen Shipyards Group) and the day-to-day operations of this vessel (Port of Den Helder). This consortium will make important steps towards future applications of hydrogen in the domains of short sea shipping and high-speed applications.

1.2.2. Preliminary studies

In the recent past, two bachelor graduation studies, towards the application of hydrogen technology for High-Speed Craft (HSC), are executed within Damen Shipyards. These studies focused on the feasibility of (pure) hydrogen propulsion for HSC [98] and the development of a concept design of a fuel cell/battery propulsion system [28]. For both studies, a small crew supplier with a length of 12 meters was used as benchmark case. This vessel is formally known as the *Fast Crew Supplier 1204 FRP* or 'FCS1204'. From its product sheet it is noticed that this vessel is very versatile when it comes to propulsion configuration and modular accommodation options. This versatility provides the ideal platform for the implementation of a fuel cell propulsion system with a minimum of design amendments [28, 98]. The FCS1204 is one of the smallest vessels in Damen's portfolio and therefore suitable to bear the risks of such a project.

Hydrogen has a low volumetric energy density and due to this very sizeable fuel tanks are required [100]. One previous study [98] has estimated the total amount of available energy from diesel, taking the engine's efficiency into consideration. The original diesel configuration was capable of delivering a total of 12,481 MJ to the outgoing shaft. 200 kg of hydrogen is able to deliver an equivalent amount of energy, assuming an energy density of 120 MJ/kg and fuel cell efficiency of 52.5%. To store this amount of energy, one would need 24 tanks capable of storing 8.4 kg at 350 bar per tank [98]. From figure 1.1 it becomes clear that it is not feasible to bunker an equivalent amount of energy carried in hydrogen compared to diesel, without losing operability. Therefore, it can be expected that the utilisation of pure hydrogen comes at the cost of the vessel's endurance.

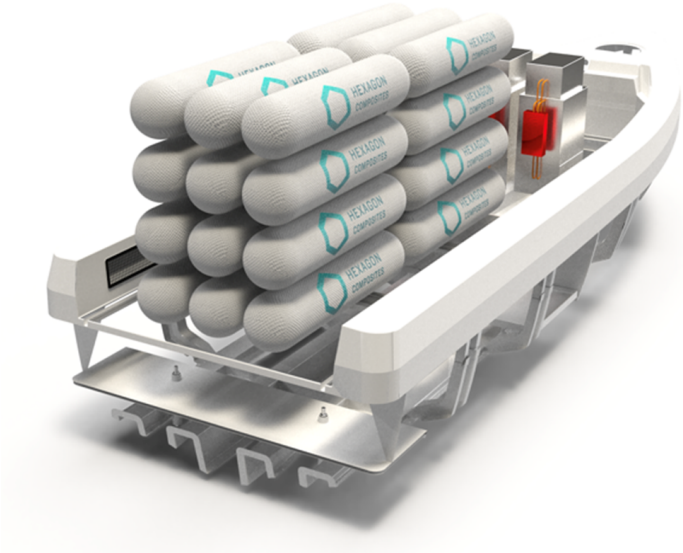

Figure 1.1: Required space for an equivalent amount of energy carried in hydrogen [98]

The second study [28] worked towards the concept design of a fuel cell system for the FCS1204. Three different operational functions were studied: a water taxi, fast crew supplier and harbour patrol vessel [28]. For each function he defined a sailing profile. Based on the sailing speed and some power calculations, the propulsion system was sized. However, little is known about the dynamic behaviour of a hydrogen fuel cell system for high-speed craft. This leads to the incentive to support this master thesis research project.

1.3. Problem definition

In literature a strong focus is found on land-based applications of FC technology. Marine applications of fuel cells are not developed as well as other transport applications of fuel cells for a number of reasons: there is a lack of infrastructure to support this technology, the marine environment presents challenges for a fuel cell system (continuous movements and corrosion), and the price per kWh is much higher for fuel cell modules compared to conventional systems [51]. Also, the former absence of strict regulations on environmental impact at sea has contributed to the fact that the shipping industry is lagging behind [96].

On the other hand, fuel cell systems can be very beneficial for marine applications as well, rather than just for land-based transport. As mentioned before, hydrogen can achieve full decarbonisation if produced from

renewables. Recently, the European Union's Fuel Cells and Hydrogen 2 Joint Undertaking [34] has included the shipping industry in a roadmap towards decarbonisation in the transport sector: it is expected that commercialisation in freight shipping starts from 2023, being business-as-usual from 2047 (2037 in the most optimistic scenario). Regulators, industry and investors should act now to launch the hydrogen roadmap [34, 88].

In order to start commercialisation in the short term in the maritime domain, it is crucial that knowledge is gained regarding hydrogen fuel cell propulsion systems. Currently, little literature is available covering the dynamic behaviour of FC's in waterborne craft [98]. Three knowledge gaps can be identified here:

1. **Operability**: Damen Shipyards sees potential in hydrogen propulsion for high-speed craft. Some researchers, however, note that a hybrid FC/battery system is limited to low-speed watercraft [21]. Power increases rapidly as speed increases and with power so does the complete size of the fuel cell system [21]. This statement is based on qualitative analyses, rather than quantitative. Therefore, it is recommended to study the impact of a FCS's operational profile on the fuel cell, battery and subsystems. Effects on performance indicators, such as range and top speed, should be compared to the vessel's conventional propulsion system.

2. **Hybridisation**: There seems to be consensus that fuel cells are to be implemented alongside other energy storage systems like batteries [21, 23, 59, 85, 96, 100]. However, hybridisation with fuel cells and batteries, capable of following the demanded loads, requires further research [96].

3. **Energy and power management**: Fast peaks in power demand will cause a high voltage drop in the FC in a short time, known as starvation, which might reduce performance and lifetime [85]. Peak loads are not uncommon in marine environments. Waves cause surge motions and changes in propeller submergence (due to heave and pitch), resulting in time varying loads [84]. More importantly, manoeuvring operations also cause high fluctuations in loading. The system's response to these peak loads require further research. In this view, controls and energy management strategies are very important.

The development of a hybrid hydrogen-electric vessel will require research in these domains. This study will aim to develop a propulsion model. An iterative approach with increasing scope and complexity is used to gradually build up the model. With this model different configurations and operations will be tested.

The ultimate goal of the hydrogen project is the construction and testing of the 'FCS1204H2'. This validation will provide valuable information regarding the system's performance (although it is a small vessel). This is a an important first step towards the utilisation of hydrogen on a larger scale. The design of such a vessel and testing, however, is not in the scope of this research, but it emphasises how this project supports an important part of the presented roadmap: the development of hydrogen and fuel cell applications and up-scaling of successfully proven ones [34].

1.4. Research questions

Based on the literature review and identified knowledge gaps, the following main research question is formulated:

What is the impact of implementing a hydrogen fuel cell-battery propulsion system on the operability of high-speed craft, based on time-domain simulations of various operational conditions?

The main objective focuses on operability, which is defined as the ability to keep the vessel in a reliable functioning condition, in accordance with predefined operational requirements. Such requirements may include acceleration/deceleration time, speed and endurance. Operability is also sensitive to physical constraints such as power limits, hydrogen storage capacity or weight limitations. An energy management system is expected to be very important to optimise the energy consumption within these constraints. A propulsion model will be constructed, which is used for time-domain simulations of various operational conditions. These simulations will provide insight in energy consumption for operational profiles, i.e. various day trips, and the transient behaviour of the system. The dynamic behaviour, or transient behaviour, is defined as system's reaction to deviations from a steady-state condition. The system's performance is dependent on the characteristics of individual component's, such as response time and acceleration/deceleration limits. The

operability will be studied by analysing the dynamic behaviour of a hybrid propulsion system, while executing a certain operational profile and being exposed to environmental loads. The different aspects of this problem are addressed in the sub-questions of this research:

- *To what extent is the operability reduced by respecting physical system constraints?*
  Figure 1.1 shows the physical constraint of hydrogen storage resulting from the low volumetric energy density of hydrogen. It is expected that more constraints come into play during this research. One can think of restrictions on weight and volume in a small high-speed vessel. These constraints, imply that some operational profiles or functionalities are technically not feasible. Therefore, the impact of these constraints on operability is included in this study.

- *What are the trade-offs in the selection of a suitable energy management strategy to balance energy demand from the fuel cell stack and battery?*
  The energy management system ensures that sufficient energy is provided by the hybrid system to execute a given task. It decides how much energy is provided by the fuel cell and batteries, i.e. it balances the energy consumption. The relatively low volumetric energy density of fuel cell systems emphasises the importance of a suitable energy management strategy to ensure that all energy is used in the most efficient way. Power, being the rate at which energy is delivered, may not exceed certain limits. A battery should not be discharged below a certain state of charge (SOC), which means that the SOC must be sustained above a certain level at all times, i.e inducing a limit on available power when the SOC is low. This shows that energy management and power management are closely related.

- *What is the most suitable degree of hybridisation for fuel cell/battery vessels?*
  The initial sizing of the electric motors is based on the intended operations and sailing speeds. However, various combinations of fuel cell power and battery size can be used to deliver energy to these motors. A set of configurations will be developed and these configurations are then for these operational profile. The results are used to indicate the most suitable degree of hybridisation for the FCS1204H2. From this set of configurations, the most suitable configurations are selected for the rest of this research.

- *What is the impact of fuel cell/battery propulsion on top speed, endurance and efficiency of high-speed craft?*
  The above steps gradually build up a complete propulsion system with operational profiles (i.e. day trips) as input. It is expected that 'going green' comes at the cost of reduced operational performance indicators. These limitations are important from an operator's perspective. By executing a series of voyage simulations with this developed model, these limitations could be quantified.

- *What are the characteristics of the transient response of the propulsion system to time varying loads?*
  The voyage simulations will be used to analyse the energy consumption during a complete operation and it focuses on time frames up to several hours. However, it is necessary to zoom in on a smaller timescale to analyse how the system responds to sudden load changes. The transient response, i.e. how disturbances are absorbed, is well studied for stand-alone fuel cell applications. However, at the start of this project little information is available about the response when fuel cells are integrated in a propulsion system for marine applications with batteries, current converters and electric motors. During this phase, extreme conditions are studied, such as sailing in waves and emergency manoeuvres. This part provides insight in the dynamic behaviour of integrated systems.

1.5. Report structure

This thesis presents the process of the research and the results that have been found. Chapter 2 presents background information about the main subjects of this research. The production and chemical properties of hydrogen are discussed. Secondly, the working principles of fuel cells and different fuel cell types are introduced. The working principle of batteries is similar compared to fuel cells. The concept of hybridisation and battery functionalities in hybrid systems are also tackled here. The chapter is finished with an introduction to all-electric ship propulsion.

Chapter 3 discusses some initial design choices that have been made. The FCS1204 and intended operational profiles are first introduced in more detail. A power speed diagram is then used to select an electric

motor for the ship's propulsion. This power speed diagram is an important diagram that is used in the whole research project. It contains valuable information about the operational conditions of the propeller and original diesel engines. The diesel engines are replaced by a hybrid power supply with electric driving machines. Hence, the design of the propulsion system will change drastically and the new design is also discussed. The fuel cell module and batteries under considerations are discussed at the end of the chapter.

The next chapter (ch. 4) dives into the modelling of the hybrid power supply. This only includes the fuel cell stack, battery and DC/DC converter. The electric motors are not yet implemented in the model at this point. This model is then put to work in chapter 5, where the energy consumption is analysed for the intended operational profiles. This energy analysis is used to select the most suitable configurations for the FCS1204.

The propulsion model is completed in chapter 6 by adding the electric motors and propellers to the model. Up to this point, the power consumption was estimated with the power speed diagrams and a number of efficiencies for the motors and power conversion components. However, in order to analyse the propulsion system's behaviour under transient conditions, these components must be included in the propulsion system. The dynamic behaviour of the system is then studied in chapter 7.

The final chapter (ch. 8) concludes the research. The research question and sub-questions that are defined in the foregoing section are reviewed and it is tried to answer these question with the knowledge that is gained during the research. Other recommendations or points of discussion are also included in this chapter. At the end of this report, a number of appendices can be found. The confidential appendix is not included in this version, as it is only accessible for supervisors and employees of the Damen Shipyards Group.

2
Background

A positive trend is observed regarding the use of electricity for propulsion, rather than just for auxiliaries: all-electric vessels are becoming more popular due to the low emissions and high energy efficiency [20]. Fuel cells are suggested for these systems as main source of power as they convert chemical energy into electrical energy. Some of the potential benefits of fuel cells are the absence of polluting emissions, a high thermodynamic efficiency and good performance in part load [91]. A fuel cell is the most efficient method to extract energy from hydrogen [67]. Fuel cells effectively run on hydrogen, although other fuels, such as methanol and ammonia, can also be used as logistic fuel [67, 95]. Battery systems are often used as energy storage system and to improve the dynamics and efficiency of such a propulsion system [13]. Both fuel cells and batteries provide electrical energy which is converted to mechanical energy by an electric motor.

In order to be able to analyse characteristics of the dynamic behaviour of hybrid FC/battery systems for high-speed craft, it is important to first understand the basics of such systems. To name a few examples: the chemical properties of hydrogen, the working principles of fuel cells, charge and discharge behaviour of batteries. Hydrogen as fuel is discussed in section 2.1. The working principles and different types of fuel cells and batteries are considered in sections 2.2 and 2.3, respectively. Section 2.4 discusses various configurations for fuel cell and battery hybrid systems. Finally, section 2.5 introduces the electric motors suitable for ship propulsion.

2.1. Hydrogen as fuel

Today's energy demand puts a considerable strain on our environment as fossil fuels are the main source of energy. The energy demand is rapidly rising, while our global fossil fuel reserves are declining [58]. Alternative fuels reduce the fossil fuel dependence and support a sustainable growth of economies. A promising alternative is hydrogen as energy carrier. Many countries may become more independent from fossil fuel-producing nations as it is widely available in the form of water. It provides security of energy since it is globally distributed and can be locally produced. Hydrogen also opens up a way to full decarbonisation of the transport sector. In order to realise this, the demand in renewable electricity will increase inevitably [2]. The price of energy from solar technologies and offshore wind has dropped considerably in the recent past and it is expected that the renewable energy market will grow steadily towards 2030 [45]. In the meantime, hydrogen can also be created from grey electricity or light hydrocarbons by means of transition methods.

2.1.1. Hydrogen production

Under normal conditions, hydrogen is a gas, which is colourless, odourless, non-poisonous and flammable. Hydrogen is rarely found in its pure form (H_2), although it is abundant in its most common form (H_2O) [6, 58]. It can also be found in other compounds like hydrocarbons (diesel and LNG) and methanol, so hydrogen can be produced in various ways. There are two common processes to create pure hydrogen: steam reforming (SR) and electrolysis [58].

The first process is an endothermic process where hydrocarbons (or methanol) are reformed to hydrogen and carbon dioxide [88, 96]. Steam reforming occurs under high temperatures in two steps: after SR the so-

called (exothermic) water gas shift (WGS) occurs more or less automatic and a mixture of CO_2 and hydrogen (referred to as Syngas) is created [96]. The chemical reactions for steam reforming of natural gas (eq. 2.1), the water gas shift (eq. 2.2) and total reaction (eq. 2.3) are given below [88, 96]:

$$CH_4 + H_2O \longrightarrow CO + 3H_2 \tag{2.1}$$

$$CO + H_2O \longrightarrow CO_2 + H_2 \tag{2.2}$$

$$CH_4 + 2H_2O \longrightarrow CO_2 + 4H_2 \tag{2.3}$$

For methanol this occurs in one step due to the presence of one oxygen ion in the compound of methanol (eq. 2.4):

$$CH_3OH + H_2O \longrightarrow CO_2 + 3H_2 \tag{2.4}$$

The hydrogen from either reforming process can be used after purification in a FC, eliminating the harmful emissions in the conversion from chemical to electrical energy. However, as equations 2.3 to 2.4 show, considerable amounts of carbon dioxide are still emitted in the reforming process. Despite the produced GHG emissions, the reforming process of hydrocarbons still has a lower carbon footprint compared to the energy conversion of hydrocarbons inside internal combustion engines (ICE) [100].

The second option, electrolysis, creates hydrogen and oxygen from water by consuming electricity [92]. An electrolyser consists of two electrodes (anode and cathode) and an electrolyte in the middle. Water is split at the anode in oxygen and hydrogen ions, hydrogen ions are transported over the membrane and the electrons flow towards the cathode where hydrogen is formed. The chemical reactions at the anode (eq. 2.5), cathode (eq. 2.6) and final balance (eq. 2.7) are given below [92]. When conventional sources of electricity are used, the carbon footprint remains considerable. However, when renewable energy sources are used, it is feasible to produce green hydrogen [58, 67, 92]. This method reduces the specific pollutant well to tank (WTT) emission to 2 g/MJ with respect to 90 g/MJ for steam reforming (emitted CO_2 per MJ energy carried in hydrogen) [27].

$$2H_2O \longrightarrow 4H^+ + O_2 + 4e^- \tag{2.5}$$

$$4H^+ + 4e^- \longrightarrow 2H_2 \tag{2.6}$$

$$2H_2O \longrightarrow 2H_2 + O_2 \tag{2.7}$$

A lot of development is seen in the field of electrolysers in the recent past and they should be considered economically viable at this moment [67]. In addition to this, the costs for renewable energy have also come down. If these trends continue, it can be expected that hydrogen reaches a competitive level with fossil fuels between 2025 and 2030 [16, 67].

2.1.2. Storage

Hydrogen has a density of 0.09 kg/m^3 at ambient conditions (20°C and 1 bar) [58, 91]. Compared to other compounds, this is rather low. In gaseous form it is 8 and 14 times less dense than methane and air, respectively. In liquid state, hydrogen is 6 and 55 times less dense than liquid methane and gasoline, respectively [89]. The storage capacity of hydrogen will induce challenges for hydrogen powered vessels as ships commonly have limited volume [29]. As a consequence of the low density, hydrogen must be processed before it can be transported efficiently. There are four different methods of storing hydrogen efficiently:

1. Liquefaction: Hydrogen has the second lowest freezing point of all elements: -253°C. After liquefaction at ambient pressure, the ratio between volume and energy is 848 times higher compared to hydrogen at ambient temperature [89]. Temperatures below 200 K (-73°C) are known as cryogenic temperatures and, hence, liquid hydrogen (LH_2) is classified as a cryogenic liquid [91]. The process of liquefaction is very energy-intensive as it requires 40% of the energy content [11]. It is also difficult to store hydrogen in this state for a prolonged period due to the low boiling point [91]. Cryogenic tanks are not capable of withstanding high pressures when LH_2 evaporates, which might result in boil-off losses [11]. However, similar to LNG tankers, hydrogen powered vessels may use boil-off gases for power generation [67].

2. Compression: Compression of hydrogen is another convenient technology. Seamless steel pressure vessels are most commonly used in industry [58]. These tanks are generally limited to pressures up to 200 bar due to the risk of hydrogen embrittlement (premature cracks in the cylinder) [11]. For energy and transport applications, however, higher pressures are desired. The compression of gaseous

hydrogen to 700 bar increases the volume ratio with a factor 440 compared to hydrogen at atmospheric pressure [89]. Composite pressure vessels (COPV) with capacities between 350 bar and 700 bar are developed more recently and commercially available [11].

3. Cryo-compression: The above shows that hydrogen is much denser in liquid state. However, it is challenging to get to this state and difficult to contain hydrogen in a liquid form. A liquid's boiling point can be increased by applying pressure. The boiling point of LH_2 can be increased to -240 °C at a pressure of 13 bar, where additional pressure above this point does not have any result on the boiling point [91]. Additional pressure, however, does have a positive effect on the storage autonomy: a tank capable of withstanding higher pressures allows further pressure increases before evaporated hydrogen has to be boiled off. The technique of combining cooling and pressure is called 'cryo-compression'. High energy densities are expected when the technology matures [11, 96].

4. Solidification: Molecules of hydrogen can diffuse through many "impermeable" materials as they are smaller than all other gaseous molecules. This makes it difficult to contain hydrogen in a tank [91]. This characteristic can also be used in its advantage: under specific temperature and pressure conditions, hydrogen can be stored in solid compounds. This reversible process occurs in two steps: firstly, hydrogen molecules are dissociated on the solid's surface and, secondly, its atoms diffuse in the solid, which is often a metal [11]. Magnesium is a promising host, but technology is still under development. A possible downside for mobile applications is the extra weight of the solid material.

Cryo-compression and solidification might become very interesting in the future to achieve high energy efficiencies. However, these technologies are not yet commercially available. Liquid hydrogen is most attractive when it comes to the density: approximately 1.9 times as much energy can be transported in one volume unit of liquefied hydrogen compared to compressed hydrogen. However, the production is energy-intensive and it is difficult to contain hydrogen in a liquid state. Therefore, it is not advised as solution for on-board storage [11]. In addition to this, some expect that economically viable liquid hydrogen infrastructures will not be completed before within 5 years [19, 82]. Previous studies at Damen Shipyards have analysed hydrogen storage in more detail and for the rest of this study compressed hydrogen (350 bar) is considered [28, 98] .

Compression of hydrogen

Hydrogen is compressed to the desired pressure in multiple stages to make compression less adiabatic and more isothermal [58]. After each stage, the gas is cooled and this process requires approximately 13% of the hydrogen's energy content. The density of most gases can be determined with the ideal gas law, relating volume to pressure and temperature (eq. 2.8), but hydrogen deviates significantly from the ideal gas law. In reality, hydrogen requires more volume than the gas law estimates. The ideal gas law can be corrected for this phenomenon by adding a compressibility factor, but this factor is far from constant for different pressures and temperatures [58]: hydrogen has a density of 20 kg/m^3 at 300 bar and 40 kg/m^3 at 700 bar. The ideal gas law gives a density which is 20% to 50% higher than the real density, for pressures between 300 bar and 700 bar (see fig. 2.1).

$$P \cdot V = n \cdot R \cdot T \qquad \longrightarrow \qquad \rho = \frac{P \cdot M}{R \cdot T} \tag{2.8}$$

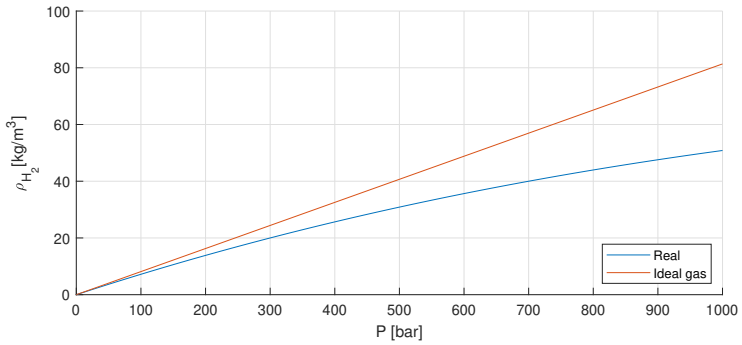

Figure 2.1: Density of hydrogen (at 298K) with respect to pressure

2.1.3. Chemical properties

When the gravimetric energy density of hydrogen is compared to other conventional fuels, hydrogen shows the highest heating value with a lower heating value (LHV) of 120 MJ/kg and higher heating value (HHV) of 142 MJ/kg [94]. The difference between the two values represents, by definition, the extra amount of energy required to vaporise a liquid fuel. Taking the low density of hydrogen into account (0.09 kg/m^3), the LHV is converted to a volumetric LHV of 0.01 MJ/L. Compression or liquefaction increases this number significantly. This can be seen and compared to other fuels in table 2.1.

This table shows that the gravimetric LHV of hydrogen is roughly 2.7 times higher compared to diesel or gasoline. Thus, for a given energy demand, the required mass of hydrogen is about one third of the required mass of diesel/gasoline. On the other hand, the volumetric LHV of liquid hydrogen is 4 times lower, i.e. the required volume is 4 times larger for an equal energy demand. Table 2.1 emphasises the convenience of using diesel or gasoline for mobility. These fuels give the highest energy content based on volume (i.e. tank capacity). This energy content is present at ambient storage conditions, i.e. fuels can be transported in simple containers and do not require any processing to reach a high energy content.

Fuel	**LHV [MJ/kg]**	**HHV [MJ/kg]**	**Storage condition**	**LHV [MJ/L]**
Hydrogen	120	142	Ambient conditions	0.01
			Pressurised at 200bar	1.8
			Pressurised at 700bar	4.8
			Liquefied	8.5
LPG	46	50	Liquefied	26
Methane	50	56	Pressurised at 200bar	8.4
			Pressurised at 700bar	15.8
			Liquefied	20.9
diesel/gasoline	44	46-47	Ambient conditions	31-36

Table 2.1: Gravimetric heating values for different fuels and volumetric lower heating value for different storage methods [91, 94]

Flammability and explosion

Chemical properties with respect to flammability are also important to discuss, in perspective of safety on-board. Fire or an explosion might occur when fuel, oxygen and a source of ignition are present. Hydrogen mixes with oxygen whenever it is released from a container. Sources of ignition are sparks, flames or heat.

Fuels burn in a gaseous state, so liquid fuels must first convert to a vapour. Hydrogen is fully vaporised when it leaks from a container due to its low boiling point, but it has a relatively high auto-ignition temperature of 585°C [89]. This makes it difficult to ignite hydrogen with only heat (without a spark or flame). The ignition energy of hydrogen is rather low and, if ignited, hydrogen flames are pale blue, which makes it difficult to see flames in daylight [55, 91]. In other aspects, they are safer compared to gasoline flames. Hydrogen gas has a high buoyancy and diffusivity and, therefore, gas rises quickly and flames are localised. Gasoline, however, spreads laterally and creates a broad flame zone.

The flammability range of a gas is defined as the range of gas concentrations that support a self-propagating flame when the gas is mixed with air. Within the flammability range, sufficient amounts of air and oxygen are both present. The flammability range for hydrogen is wide: 4% to 75% [91]. Explosions are different from fire, as combustion must be contained in an enclosed space to build up pressure and temperature. At a certain point, there is enough energy to destroy the containment. The explosion range for hydrogen lies between 15% and 59% at atmospheric temperature.

2.1.4. Risk of hydrogen

A business case for hydrogen powered HSC is dependent on the risks which are related to hydrogen. Tank failure and, consequently, fire/explosion risk are the main concerns with respect to on-board safety [1].This literature review briefly discusses this risk to provide a complete figure. Risks and risk mitigation will not be taken into account during the rest of the study.

Pure hydrogen is not flammable nor explosive as long as it is contained in a pressure vessel: the gas con-

centration is 100%, i.e. the content is too rich to allow ignition. A tank rupture (without ignition) may still impose safety risks for passengers and crew since it creates a strong blast wave over a short duration [1]. Severe damage, like hull ruptures and loss of of critical systems, can be expected from such an incident. The mixture with oxygen after a leak also imposes a risk of flammability or explosion, since both the flammability and explosion range are wide. A spark or flame will directly ignite the mixture due to hydrogen's low ignition energy. In this view, it is preferred to place hydrogen tanks on deck rather than in an enclosed space. Leakage and ignition is preferred on deck where localised flames can diffuse in the open air compared to an explosion when hydrogen is released in an enclosed space.

Two phenomena might increase the risk of tank leakage: emptying speed and damage from mechanical impacts [11]. Quick emptying of COPV's may lead to internal deformations of the cylinder liner. This can be attributed to the cooling of hydrogen during quick expansion. As a consequence of heat exchange, the cylinder liner also experiences cooling. Prescribed temperature limits are exceeded during quick emptying and this contributes to ageing and damage effects [26]. Secondly, mechanical impacts, during a car accident for instance, may cause significant degradation of structural integrity in COPV's [11]. When sailing in heavy seas, impacts from slamming are not uncommon: such operations might increase the risk of leakage.

2.2. Fuel cells

A fuel cell is an electrochemical cell that converts chemical energy directly into electrical energy. A conventional diesel generator creates first thermal energy, then mechanical energy and finally electrical energy. When mechanical energy is desired, fuel cells have an equal number of energy conversions. Recent studies have shown that fuel cell systems are significantly more expensive compared to conventional generators: current prices are reported to be over 1000 $/kW, which is expected to drop to 280 $/kW when annual production increases with at least a factor 20 [27, 96]. A price of 50 $/kW would put them in direct competition with generators, but production numbers would have to increase even further. In most cases, however, the expected fuel price over a vessel's lifetime is the most dominant factor, rather than capital expenditure for equipment.

2.2.1. Working principle of fuel cells

A fuel cell consists of three main components: two electrodes (anode and cathode) and an electrolyte in the middle. A fuel (hydrogen) is continuously fed to the the anode and oxygen is fed to the cathode. Redox (reduction-oxidation) reactions occur at the electrodes: ions are formed that will pass through the electrolyte. At the same time, electrons are formed at the anode due to the ionisation of hydrogen. The electrons will flow towards the cathode, creating current [49]. These electrochemical reactions occur in one cell, multiple cells are connected in series to create a fuel cell stack with a higher voltage (and power) [97].

A widely used fuel cell type, a Proton Exchange Membrane Fuel Cell (PEMFC), is now used to demonstrate the working principle. This fuel cell, of which an illustration is given in figure 2.2, uses pure hydrogen and oxygen as reduction and oxidation reactants, respectively. Hydrogen ions are transported across the electrolyte and only water is emitted. The electrochemical reactions for the anode (eq. 2.9), cathode (eq. 2.10) and final balance (eq. 2.11) are given below [83, 88]:

$$2H_2 \longrightarrow 4H^+ + 4e^- \tag{2.9}$$

$$O_2 + 4H^+ + 4e^- \longrightarrow 2H_2O \tag{2.10}$$

$$2H_2 + O_2 \longrightarrow 2H_2O \tag{2.11}$$

Most fuel cells effectively run on hydrogen, but FC's can operate on any hydrogen-containing logistic fuel (diesel, LNG, methanol). Pure hydrogen can be used without extensive pretreatment due to the high reaction rate of hydrogen, even at low temperatures [96]. Other fuel types, however, require reforming as shown in section 2.1.1 and purification to create gaseous hydrogen.

2.2.2. Fuel cell types

A wide range of FC types is available in the market. The classification and naming of fuel cells is based on the material of the electrolyte, which determines the temperature in the cell and cell power [59]. Table 2.2 gives the most important characteristics of fuel cells that are found in industrial applications. Figure 2.3 presents, for the same fuel cells, a schematic overview of reactants in the cell and transfer of ions across the electrolyte.

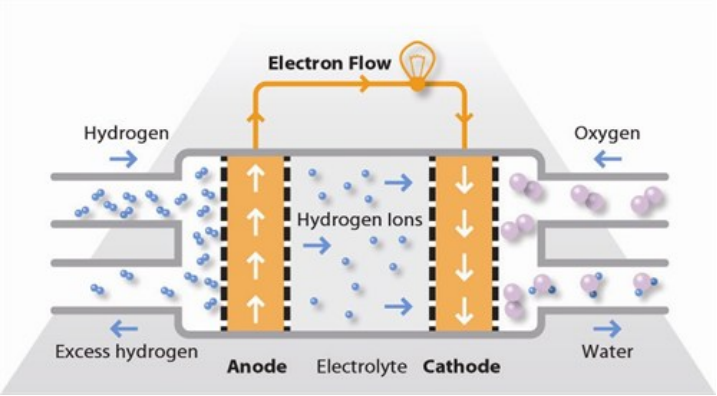

Figure 2.2: Working principle of a PEM fuel cell [88]

Operating temperature plays a dominant role in many fuel cell characteristics. Fuel cells are divided in low- and high-temperature (LT/HT) fuel cells, where high-temperature fuel cells operate above 600°C.

In the foregoing section it was noted that fuel cells effectively run on hydrogen. Other fuel types should be reformed to hydrogen before it enters the cell. A separate reforming unit is required for LT-FC's, if hydrogen is not available as logistic fuel. These fuel cells are sensitive to fuel impurities, so purification is also necessary [96]. A separate reforming unit decreases the overall system efficiency by approximately 15% [92]. HT-FC's, however, operate at sufficiently high temperatures that this unit is unnecessary. The SR and WGS reactions occur automatically and internally as a result of the high temperature. An exception to this rule is the direct methanol fuel cell (DMFC), which operates on a weak methanol/water solution at low temperature without any need for reforming [88].

The fuel cell stack efficiency (η_{stack}) ranges between 50% and 60% for most fuel cell types (tab. 2.2). The emission from a HT-FC or phosphoric acid fuel cell (PAFC) contains a lot of waste heat, which can be recovered [88, 91]. In this case, the energy from the exhaust gases is used to drive a steam turbine to create electricity. Waste heat recovery increases the overall system efficiency to 80%-85%. However, it is expected that such systems add complexity and costs to the total system.

It is reported that high-temperature fuel cells suffer from material degradation during extended operations. Low-temperature fuel cells have fewer problems with this [91]. Degradation results in a reduced efficiency over time and hence increased fuel consumption. Also, LT-FC's have faster start-up times, which makes them interesting for mobility applications.

Fuel cell type	**Power levels [kW]**	**Fuel**	**Maturity**	**Operating temperatures [°C]**	**Efficiency η_{stack} [%]**
Alkaline (AFC)	<500	Hydrogen	High	60-90	50-60
Proton Exchange Membrane (PEMFC)	<120	Hydrogen	High (LT) Low (HT)	60-100 (LT) 140-200 (HT)	50-60
Direct methanol (DMFC)	<5	Methanol	Low	60-90	20
Phosphoric Acid (PAFC)	100-400	Hydrogen	High	180-220	40 (80**)
Molten carbonate (MCFC)	<500	Hydrogen*	High	600-700	50 (85**)
Solid oxide (SOFC)	20-60	Hydrogen*	Moderate	600-1000	60 (85**)

* Internal reforming of other fuels (diesel, methanol, LNG) is possible
** Maximum efficiency with waste heat recovery

Table 2.2: Fuel cell types and characteristics [56, 73, 88, 96]

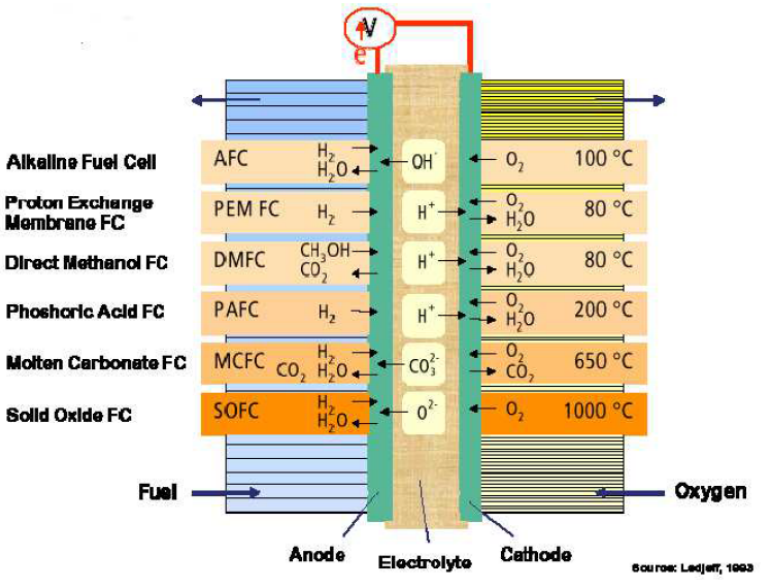

Figure 2.3: Fuel cell types and internal reactions [8]

DNV-GL [88] has analysed these cells in more detail and selected the three most promising fuel cell types. This assessment was based on 11 criteria, on which the fuel cells were ranked. All criteria are also weighted with respect to importance. This study concludes that LT-PEMFC's, HT-PEMFC's and SOFC's are the most promising fuel cell techniques for marine applications. In other literature, there also seems to be consensus that these types have the highest potential, though LT-PEM fuel cells have a higher feasibility in the short-term [23, 51, 80, 83, 88, 97, 100]. LT-PEMFC's have a high degree of maturity and the technology is also continuously under development to improve flexibility, durability and reduce costs, which are already relatively low [88]. Finally, the fast start-up time and favourable power-to-weight ratio are very beneficial for transport applications from an operational perspective [4]. These findings coincide with conclusions from previous studies at Damen Shipyards [28, 98]. Based on these readings, it is decided to focus on LT-PEM fuel cells in this study. All other fuel cell types will not be considered in the rest of this study.

Water management in LT-PEM fuel cells

A LT-PEMFC consists of a ionic hydrogen-conductive polymer electrolyte (the proton exchange membrane) between two porous electrodes. Gas diffusion layers and gas distributor plates on top of the electrodes provide gas distribution and reactant (gas and liquid) removal from the electrodes [97]. Fuel cells are connected in series to create a stack with higher voltage. The stack's reactant in- and outlets, however, are connected in parallel, feeding each cell from a common stream.

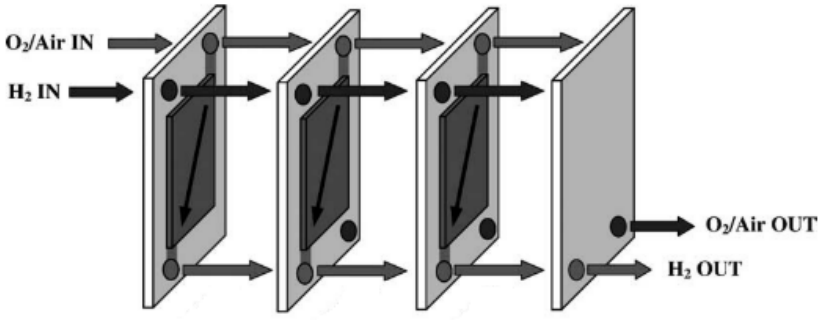

Figure 2.4: Fuel cell stack with parallel fluid distribution [97]

The polymer electrolyte needs to be humidified by liquid water to support ion conduction across the electrolyte [97]. Hence, the operational temperature of a LT-PEMFC is limited at 100°C due to the boiling point of water [83]. This parallel arrangement, however, poses a major challenge for water management. It is difficult

to guarantee a uniform reactant distribution across the cells. If water builds up in one cell (known as flooding), less gas will flow to that cell and, consequently, less water is removed from the cell [97]. This results in a reactant-starved condition and could lead to cell reversal where a fuel cell basically becomes an electrolyser. It is known that operational conditions, such as current draw and gas flow rate, have influence on this, but optimum water management has not been achieved yet [78].

2.2.3. Fuel cell stacks compared to combustion engines

A fuel cell propulsion system converts chemical energy in mechanical energy via an electric motor. An internal combustion engine converts chemical energy into thermal energy and thereafter in mechanical energy. Each transformation is associated with a loss of energy. The most dominant losses are the following:

- Fuel cell: stack efficiency, parasitic power losses for 'balance of plant' (BoP) components, electrical losses and motor efficiency [95]. These losses are discussed in more detail in section 4.1.3.
- Combustion engine: thermodynamic efficiency, incomplete combustion, heat loss to the cylinder and mechanical efficiency [49],

The stack or thermodynamic efficiency is the theoretical maximum efficiency of the system. The maximum stack efficiency is 83% which is derived in more detail in section 4.1.3. The thermodynamic efficiency is the most dominant loss for an ICE. The theoretical thermodynamic efficiency is defined by the shape of pressure-volume and temperature-entropy diagrams of the combustion cycle: it relates the heat input to the work output. The maximum possible thermodynamic efficiency is obtained from a reversible cycle, i.e. a Carnot cycle. However, a Seiliger cycle is more appropriate in case of diesel engines as it approximates the diesel process very well [81]. A thermodynamic efficiency of 53% can be achieved for an ideal Seiliger process, resulting in an overall efficiency around 45%. Fuel cell systems are reported to have higher overall efficiencies compared to ICE's, partly resulting from the direct energy conversion [80, 91, 96, 100]. This is also reflected in figure 2.5.

Energy converter	η_{max}	η_{system}
Fuel cell	83%	50%-60%
Combustion engine	53%	45%

Table 2.3: Maximum efficiency for fuel cells and combustion engines [9, 37, 49]

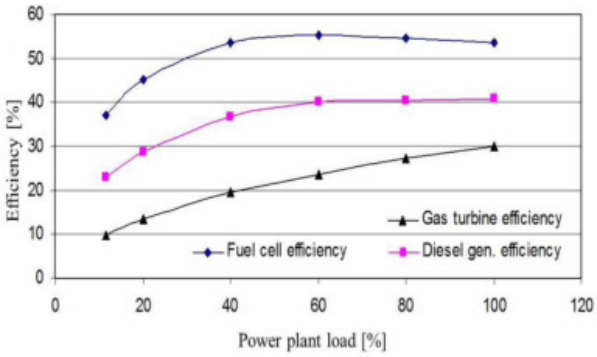

Figure 2.5: Efficiency in relation to power plant load for various energy converters [100]

2.3. Energy storage in batteries

A general challenge for all electric systems is the difficulty to store electrical energy. The storage of electrical energy requires the conversion towards another form of energy [15]. In batteries, chemical compounds act as storage medium for energy. During discharging, electrochemical reactions occur causing the conversion of energy (chemical to electrical) at a certain current and voltage. In this view, batteries are very similar to fuel cells. However, there is a a critical difference: fuel cells require an external supply of reactants, where all reactants in batteries are stored internally. Fuel cells are thus solely energy converters, where batteries also act as energy storage systems (ESS).

2.3.1. Working principle of batteries

The working principle of a battery is very similar compared to a fuel cell. It has a similar construction with two electrodes and an electrolyte. The reactants can be stored in the electrodes, electrolyte or separate tanks (or a combination) [15]. The energy conversion is reversible for some batteries, but not for all. Primary batteries can be discharged only once (disposable batteries), where secondary batteries can be recharged. The first category is not very suitable for transport applications, since it has a very limited lifespan. The (dis)charging characteristics of secondary batteries play an important in the vehicle's performance [38]. Batteries also differ from fuel cells in the sense that they have charge and discharge cycles, while FC's provide electricity as long as fuel is fed to the cell [50].

During discharging, electrons are released from the reactants at the negative electrode. They are absorbed by reactants at the positively charged electrode. Current can be drawn from the battery due to the electron flow between the two electrodes [15]. This is demonstrated for a lead-acid (LA) battery. This battery consists of a negative electrode made of lead (Pb), a positive electrode made of lead dioxide (PbO_2) and a sulphuric acid (H_2SO_4) solution as electrolyte. This gives the following electrochemical reactions, during discharging, at the negative electrode (eq. 2.12), positive electrode (eq. 2.13) and final balance (eq. 2.14) [38]:

$$Pb + H_2SO_4 \longrightarrow PbSO_4 + 2H^+ + 2e^- \tag{2.12}$$

$$PbO_2 + H_2SO_4 + 2H^+ + 2e^- \longrightarrow PbSO_4 + 2H_2O \tag{2.13}$$

$$Pb + PbO_2 + 2H_2SO_4 \longrightarrow 2PbSO_4 + 2H_2O \tag{2.14}$$

These reactions are also visualised in figure 2.6. Different types of batteries have different reactants, but the working principle is the same (and also very similar to the redox reactions in a fuel cell as presented in equations 2.9 to 2.11). If current is then delivered to the battery, this process is reversed and the battery is charged. The final electrochemical equation thus becomes:

$$Pb + PbO_2 + 2H_2SO_4 \Longleftrightarrow 2PbSO_4 + 2H_2O \tag{2.15}$$

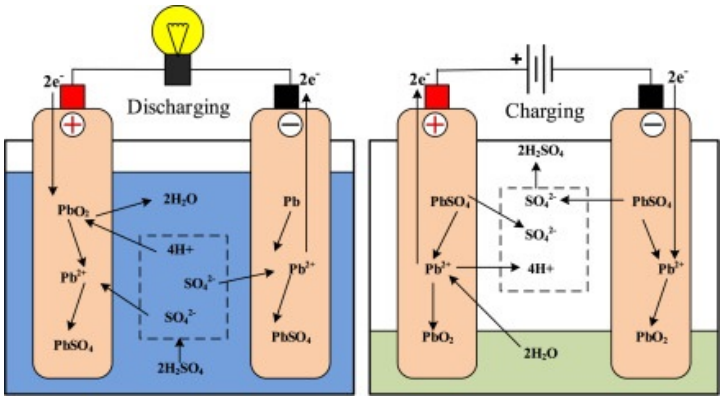

Figure 2.6: Electrochemical reactions for discharging (left) and charging (right) in a lead-acid battery [38]

The available energy from a battery is defined by the state of charge (SOC). The SOC gives the remaining capacity in the battery. However, a battery can not be fully discharged as this will cause irreversible crystallisation and damage to the electrodes. Manufacturers often give a recommended depth of discharge (DOD) limit. The DOD expresses the consumed energy, discharges beyond the recommended limit reduces the battery's lifetime significantly [15, 43].

2.3.2. Batteries for marine vehicles

The obvious motivation for electric propulsion is the zero-emission potential. However, ICE propulsion has been the absolute norm for the shipping industry due to the former absence of stringent emission-related regulations. Meanwhile, the use of batteries is not uncommon for automotive applications and, hence, most literature regarding battery technologies for transportation is focused on automotive applications. There are two fundamental differences between electric vessels and cars: typical mission profiles are much longer for

vessels and cars have more potential for energy recovery via regeneration [75]. This leads to higher battery capacity requirements for marine vehicles. High-speed craft, however, have limited space and weight available for propulsion machinery. The selection of a battery type is expected to have a large impact on the performance. This section compares three types of batteries that fit the needs for high performance electric power systems: lead-acid batteries, nickel metal hydride (NiMH) batteries and lithium-ion (Li-Ion) batteries [47].

Lead-acid batteries
LA batteries have already been introduced in the preceding section. They are commonly used as starters for ICE's, emergency power supply systems and grid storage and have been used for over 150 years [38]. A maximum of 1500 charge/discharge cycles, electrical efficiencies up to 90% and a DOD limit of 80% are reported at relatively low costs [43]. LA batteries are commonly used in submarines, but they do not seem the most appropriate battery type for (high-speed) surface vessels. The dominant reason for this is the low energy and power density of LA batteries (both volumetric and gravimetric) [15, 43]. Another disadvantage is the reduced capacity at high discharge rates: only 50% to 70% of the rated capacity is available if a LA battery is discharged in one hour [43]. High discharge rates can be expected for high-speed craft at top speed, so this would reduce the vessel's operability significantly.

Nickel metal hydride batteries
NiMH batteries are built with nickel as positive electrode and different alloys as negative electrode [38]. The negative electrode absorbs hydrogen from the electrolyte following the battery reaction [15]:

$$H_2 + 2NiOOH \Longleftrightarrow 2Ni(OH)_2 \tag{2.16}$$

Nickel-based batteries have a slightly higher energy and power density compared to LA batteries [43]. In addition to this, NiMH batteries are more favourable for a number of reasons: they are available over a wide range of stored energy and provide safe operations at high voltage [3, 43]. The maximum number of cycles is comparable to LA batteries. Batteries in hybrid configurations are usually fully charged initially and then discharged to a certain SOC at which the charge level is sustained by an energy source. This deviates from a full charge/discharge cycle with negative influences on the lifetime of the battery [3]. The lifetime of NiMH batteries can be improved by periodic full discharge cycles.

Lithium-ion batteries
Li-Ion batteries are made with many different materials, but in general they are made of a lithium metal oxide as positive electrode, dissolved lithium salts as electrolyte and lithiated graphite carbon as negative electrode [15, 38]:

$$Li_xC_6 + Li_{(1-x)}Mn_2O_4 \Longleftrightarrow C_6 + Li_xMn_2O_4 \tag{2.17}$$

Lithium-ion batteries have the highest power density of the discussed battery types: 90-100 Wh/kg, compared to 20-50 Wh/kg for LA batteries and 50-80 Wh/kg for NiMH batteries [3, 15]. Li-Ion batteries require less space and provide the most lightweight solution. It can be expected that Li-Ion batteries deliver a 40%-50% weight reduction and 20%-30% volume reduction compared to NiMH batteries [47]. Batteries with a lifetime of 5000 cycles are available, but they are subject to ageing [3, 15]. Lithium-ion batteries have a maximum voltage up to 3.6 V, compared to 1.9 V and 1.3 V for LA and NiMH batteries, respectively. So, less cells are required to achieve the desired voltage [43]. Li-Ion batteries operate at ambient temperature at efficiencies between 85% and 98%. Disadvantages of Li-Ion batteries are the high prices and the need for circuit control to limit voltage and current [3, 38]. The main characteristics of different battery types are summarised and compared in table 2.4.

	Unit	**LA**	**NiMH**	**Li-Ion**
Power density	Wh/kg	20-50	50-80	90-100
Efficiency	%	70-90	75-90	85-98
Maximum voltage	V	1.9	1.3	3.6
Cycles (lifetime)	-	250-1,500	600-1,200	500-10,000

Table 2.4: Characteristics of LA, NiMH and Li-Ion batteries [3, 15, 38, 43, 47]

The table shows that Li-Ion batteries are preferred to achieve the highest system performance for high-speed craft. The high gravimetric power density and efficiency are the main advantages of Li-Ion batteries. Both

characteristics contribute to reduced weight and volume for the propulsion system. This is crucial for high-speed craft since the required power to sail at a given speed increases with the vessel's weight. Internal research at Damen Shipyards has also concluded that a Lithium-based battery is currently the best technology for HSC. Three different technologies are considered and compared in table 2.5: lithium ferrophosphate (LFP), Lithium Nickel Manganese Cobalt Oxide (NMC) and lithium-titanate (LTO) batteries. The naming is based on the materials used for the cathode (positive eletrode).

	LFP	**NMC**	**LTO**
Lifetime	+	++	+++
Costs	$	$	$$
Safety	+++	++	+++
Volume	++	+++	+
Weight	++	+++	+

Table 2.5: Comparison between lithium-based batteries [Source: Damen Shipyards Group]

2.4. Fuel cell and battery hybrids

For high-speed craft average power usually deviates from peak power requirements as vessels do not constantly sail at top speed. If the energy is delivered by one energy source, the system must be sized based on peak power requirements. Consequently, some components are oversized during average load conditions. The philosophy of hybridisation is to utilise multiple energy sources to ensure efficient operation for both average and peak power demand [74]. A fuel cell is strictly an energy converter, but a fuel cell system, including hydrogen supply, can be seen as source of electrical energy. Combined drives involving diesel engines and/or gas turbines have been used on-board fast ships and diesel-electric drives can be found on all kind of vessels [49]. These concepts are far from novel, but marine hybrids involving ESS are relatively new [75].

A diesel-electric system is an example of hybrid propulsion, where a combustion engine and electric motor (power take-in) are mechanically coupled to drive the propeller and separate generator sets supply the electrical power [18]. Hybrid propulsion should be distinguished from hybrid power supply, where only an electric motor drives the propeller (all-electric ship propulsion) and different energy sources provide electrical power. For operational purposes it is beneficial to combine high specific power sources (with fast response characteristics) with high specific energy sources (slow response) [57]. In this view, fuel cells and batteries are a good combination for hybrid power supply, since batteries have a relatively high power density but low energy density (and vice versa for fuel cell systems) [42]. In such a hybrid system batteries can compensate the FC's slow response [85]. The combination of both improves the overall operating point of the power supply and the overall fuel efficiency [75].

There are three common strategies for a hybrid power supply: series hybrid, parallel hybrid and combined hybrid (also known as series-parallel hybrid). When discussing power supply, it is important to understand the differences between these configurations and the implications for the overall performance. These strategies have the following characteristics [42]:

1. Series hybrid: the motor is directly driven by the battery and a fuel cell stack is used as generator to recharge the battery or sustain a certain SOC. The system's layout is the simplest of the three. However, during charging or charge-sustaining modes, the maximum current draw from the battery is limited to its peak charge current. Hence, the maximum load is limited.

2. Parallel hybrid: the FC and battery can be connected either individually or together to the motor. This system will still provide power if one supply fails and peak power can be as high as the sum of both power supplies. The coupling is either mechanical (gearbox) or electrical (regulator and diodes) and energy is lost here. Also, the battery can not be charged in a parallel hybrid.

3. Combined or series-parallel hybrid: as the name says, this configuration combines both series and parallel hybrids. The fuel cell power pack is used here to recharge the battery or sustain a certain SOC and deliver power to the consumers.The main advantages are flexibility and high peak power.

Large variability in loading profiles increases the attractiveness of the concept of hybridisation, as energy sources can operate closer to their optimal operating points [75]. However, the above shows that different

load cases ask for different strategies. A series hybrid is more appropriate for low-load conditions where the FC stack can be used to extend the vessel's range. On the other hand, higher peak power can be achieved in a parallel hybrid [42]. In other words, a series-parallel hybrid is the only way to fully exploit the potential of hybridisation.

2.4.1. Battery functionalities in hybrid systems

Where fuel cells can only supply energy, batteries are more flexible as they can both store and provide energy to a system. Batteries can exhibit a number of functions to support the fuel cell. It is important to understand the differences between the functionalities and the impact on the configuration: in general, some functions require higher battery capacity. A battery may have five functionalities in a hybrid configuration, according internal research at Damen Shipyards:

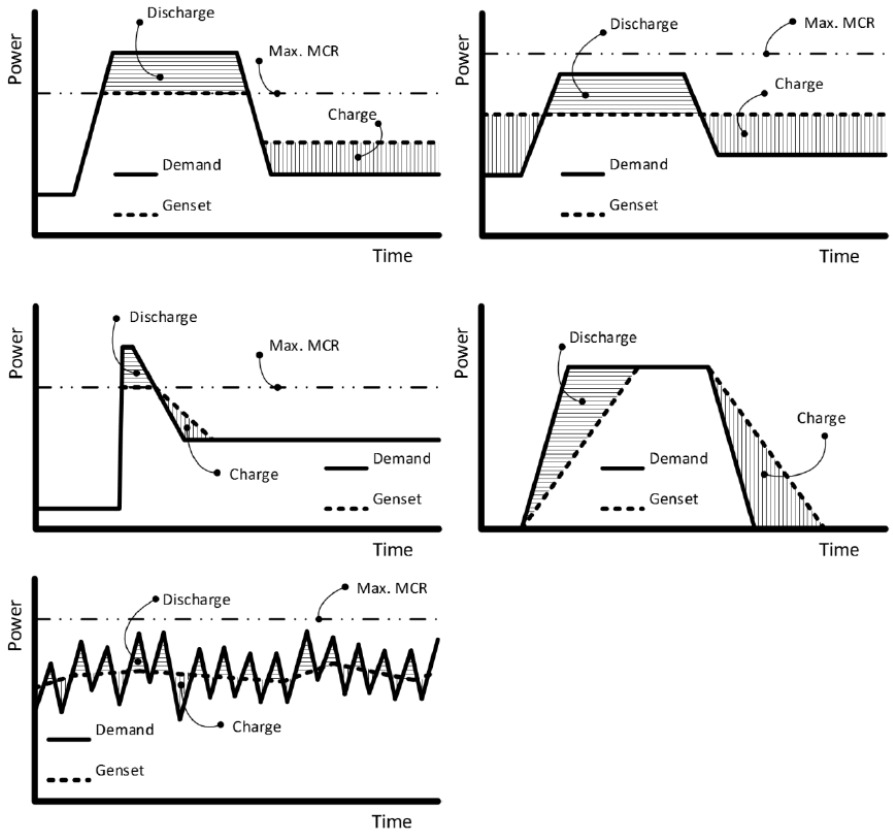

Figure 2.7: Power profiles for different battery functionalities (from left to right and top to bottom: boosting, load levelling, peak shaving, ramp support and load smoothing) [Source: Damen Shipyards Group]

1. Boosting: during boosting the load demand is higher than the maximum power from the main energy source. The battery delivers the additional energy. An example of this function is sailing at top speed. After boosting, the energy source provides more power than the required load power to recharge the battery. The endurance and maximum deliverable power is fully dependent on the size of the battery. In general, this function requires a high capacity for the desired effect.

2. Load levelling: This function aims to fix the loading point of the main energy source at the average load demand of the operational profile. If the power demand is higher than the set-point, the battery is discharged and vice-versa. In practice, it is difficult to realise this since it is impossible to predict the load profile. The battery will be either full or empty if the load demand deviates from the set-point for prolonged periods.

3. Peak shaving: load peaks above the maximum load are handled by the battery. The main difference with boosting is that these load peaks occur during very short periods. Hence, the required battery power is much lower.

4. Ramp support: this function aims to support the main energy source during large load steps. A battery has a higher responsiveness than a fuel cell [85]. This function ensures that the propulsion system is capable of following the load transients. Ramp support is a general term for both ramp-up and ramp-down support.

5. Load smoothing: batteries are better capable of handling high frequency load fluctuations than fuel cells. In this function, the main energy source, which is often the least responsive, handles the low frequency fluctuations and the battery handles the high frequency fluctuations.

The different battery functionalities of hybrid systems are visualised in figure 2.7. In reality, these functionalities are often mixed and the load distribution between battery and second energy source should be optimised in order to use all hydrogen efficiently. It is expected that desired boosting and load levelling capabilities are dominant for the sizing of the battery system.

2.5. All-electric ship propulsion

As mentioned before, electrification (and hybridisation) in marine propulsion systems is gaining popularity, due to the zero emission potential and improved overall performance for various operational conditions. The propulsion system which is studied here is classified as all-electric propulsion with hybrid (fuel cell/battery) power supply. In order to convert electrical energy in rotational motion of the propeller shaft an electric motor required.

Electric machines (motors or generators) have the main function to convert electrical energy in mechanical energy (motor) or vice versa (generator) by electromagnetism [76]. Most variable speed controlled electric motors have in common that they have a high efficiency for a wide range of loads [39]. They either run on direct current (DC) or alternating current (AC). In most electric motors the stator is on the outside and the rotor is on the inside mounted to a shaft [48].

The stator and rotor are made of highly magnetic materials. Two electromagnetic phenomena occur when conducting materials are placed in a magnetic field. First of all, voltage is created in a conductor when it is moved in a magnetic field. Secondly, a mechanical force, also known as the Lorentz force, is created when a current-carrying conductor, i.e. a rotor, is placed in this magnetic field [76]:

$$F_L = B \cdot l \cdot I \tag{2.18}$$

Where B, l and I refer to the strength of the magnetic field, length of the conductor and current, respectively. A magnetic field is created by field windings or permanent magnets, either placed in the stator or rotor. The other winding, where voltage is induced, is called the armature winding. Figure 2.8 shows a current-carrying conductor in the magnetic field of a permanent magnet stator.

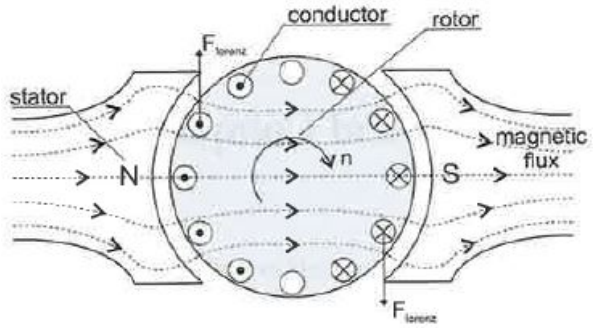

Figure 2.8: Drawing of a rotor with current-carrying conductors in a permanent magnet stator [49]

The armature windings on opposite sides of the rotor carry current in opposite direction and, consequently, all Lorentz forces contribute to a moment in the same direction. This mechanical torque (output torque) is

proportional to the magnetic flux (Φ), which is the total magnetic field that passes through an area, and the current [49]:

$$T_m = K_M \cdot \Phi \cdot I \tag{2.19}$$

Where K_M is called the motor constant. The power of the electric motor follows from the equation for the power of rotating bodies, which is the product of torque and angular mechanical velocity.

$$P_{EM} = T_m \cdot \omega_m = 2\pi \cdot T_m \cdot n_m \tag{2.20}$$

In general, electric motors can be divided in three common types [39, 48, 49, 76]:

1. DC motors: the main benefit of DC motors is the accurate control of torque. Field and armature windings are placed on the stator and rotor, respectively. The DC currents induce an alternating armature voltage, which is rectified by commutator brushes. These brushes bring maintenance issues as there is contact between the stator and rotor. Since the 1980's AC drives are more convenient for ship propulsion.

2. Induction motors: this type of motor has a relatively simple construction and is therefore widely used. The field windings are placed on the stator. The current-carrying conductors are not powered externally. In an induction motor the rotational speed of the rotor is slightly lower than the rotational speed of the electric field (the synchronous speed), hence the alternative name 'asynchronous machine'. The rotor current is generated by induction which results from the difference between the two speeds (slip).

3. Synchronous machines: the rotational speed of the rotor is synchronised with the rotational speed of the electric field, as the name says. On the stator, field windings are connected to an AC power supply. The rotor's magnetic field is either created by a DC supply or by permanent magnets. A typical characteristic of a synchronous machine is the vertical torque-speed curve: at synchronous speed the motor can deliver zero and maximum torque and everything in between.

A high efficiency, power density and reliability are important characteristics for marine applications. High powers are required for propulsion at a relatively low propeller speed. Synchronous machines meet these requirements best [17]. A permanent magnet synchronous machine (PMSM) has no rotor windings, hence there are no copper losses in the rotor. Consequently, PMSM's require less cooling and overall efficiency is improved. In addition to this, PMSM's have a wide speed range and fast torque-speed response [52]. Furthermore, PMSM's are most commonly used for marine application, according to conversations with research & development engineers at Damen. Therefore, PMSM's are considered in the sequel of this study.

3

Initial design choices for the hybrid propulsion system

Chapter 1 introduced the 'DKTI-Transport 2019' project as an inter-organisational collaboration aiming to technically and commercially validate innovative hydrogen technology applied on waterborne craft. The Damen Shipyards Groups takes part in this consortium and is responsible for the design and development of a hybrid hydrogen-electric vessel. The fast crew supplier 1204 (FCS1204) was selected for this project since it is relatively small. This means that she is a suitable vessel to bear the risks of such a project. On the other hand, the FCS1204 can still provide valuable insights in the operational aspects of hydrogen propulsion systems.

3.1. Fast crew supplier 1204

The FCS1204 is a vessel from Damen's high-speed compact class. The numbers in the name refer to a length of 12 metres and a breadth of 4 metres. The vessel is constructed from 'fibre reinforced plastic' (FRP), which reduces its weight compared to steel or aluminium. The vessel can be outfitted with various accommodation options and propulsion configurations (fixed pitch propeller, stern drive or waterjet). The product specification sheet and different configurations are included in appendix A.1. This versatility provides the ideal platform for the implementation of a fuel cell propulsion system with a minimum of design amendments [28, 98]. The main characteristics of the reference vessel are presented in table 3.1. This table includes a reference displacement, which is the displacement of the vessel (in loaded condition) where all diesel related systems and components are removed. The removal of these components reduces the weight with 2.5 t in total [98]. Other weight groups will be added if the vessel is outfitted with a FC system.

Parameter	**Unit**	**Value**
length overall	m	11.9
breadth overall	m	4.0
Depth	m	1.5
Draught	m	1.0
Max. speed	kn	26.0
Range at max. speed	nm	200
Total engine power (2x Volvo D7)	kW	390
Displacement (without diesel equipment)	t	9.0

Table 3.1: Characteristics of FCS1204

3.1.1. Power prediction

For the power prediction for a vessel it is often assumed that the ship's resistance is proportional to the square of speed [49]. The effective towing power (P_E), being the product of speed and resistance, is described by a cubic relationship with respect to speed. This is an acceptable assumption for low speeds. At high speed, however, the FCS1204 is fully planing and the assumption of a quadratic resistance curve does not hold.

$$R = c \cdot V_s^2 \tag{3.1}$$

$$P_E = R \cdot V_s = c \cdot V_s^3 \tag{3.2}$$

The research & development department of Damen has provided a power prediction for the FCS1204 for various displacements. Due to the removal of the diesel engines and all related systems, the weight might change significantly. Assuming that the weight remains unchanged with respect to the reference vessel, might result in a false impression for the required power. Furthermore, different combinations of fuel cell power and battery energy will be studied and each configuration requires more or less power with respect to the others due to variations in displacement. A displacement of 9 tonnes corresponds to the displacement without the diesel system [98].

The power speed diagram (PSD) for the FCS1204 (fig. 3.1) is based on power measurements from a slightly larger vessel with similar characteristics (FCS1605). The PSD gives the required brake power (P_b), which means that the total efficiency between the motor and propeller is taken into consideration. This includes open water efficiency, hull efficiency and gearbox efficiency among others. The diagrams provide the required powers for the semi-displacement and fully planing domain. The assumption of a cubic power curve is used for the displacement domain. This curve is fitted through the starting point of the PSD's to ensure that the power curves are continuous for the total speed domain. The power prediction is given per shaft, the total brake power can easily be found by duplicating this number (see the left and right y-axis). The data behind figure 3.1 is considered confidential information.

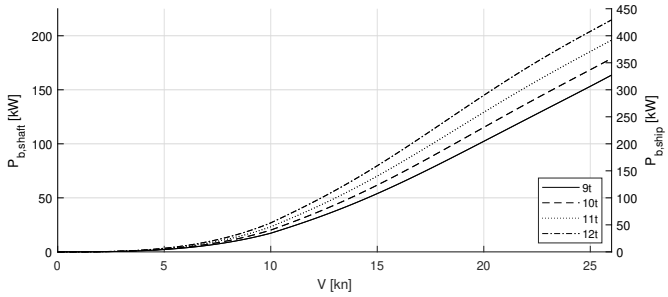

Figure 3.1: Power speed diagram for the FCS1204 for various displacements

3.1.2. Operational profiles

The FCS1204 can be used for many purposes as it is very versatile due to its modular design. For this study, two user cases are defined. These followed from the previous studies and conversations with potential users that might become involved in the 'DKTI-Transport 2019' consortium.

1. Survey vessel: the vessel sails at low speeds (7 kn) during survey operations. This is the majority of the time. For transits, however, a high speed (19 kn) is desired in order to reach the survey location in a short time. The required endurance at top speed is dependent on the distance to the survey location.

2. Harbour patrol vessel: [28] developed a detailed sailing profile for a harbour patrol vessel operating in the port of Den Helder and the Waddenzee (surrounding Texel). This profile is developed without interaction with the potential user (port authority), but it includes the major requirements for such a vessel. It sails at low speed during harbour patrol (max. 5 kn) and is capable to sail at high speed (up to 20 kn) for short periods.

The sailing profiles are shown in figures 3.2a and 3.2b. At the end of each day, the vessel must sail 50 minutes from the port entrance to the tank station (max. 5 kn) and back to the docking location.

3.2. Fuel cell/battery propulsion system

The original drive train of the FCS1204 is outfitted with two Volvo Penta D7 diesel engines, each providing 195 kW brake power. These engines drive two separate propeller shafts. A gearbox is required between the engine and propeller, since the D7 engines are four-stroke high-speed engines. Due to space restrictions, a V-drive gearbox is required.
For the hydrogen propulsion system, the diesel engine and related systems are removed from the vessel.

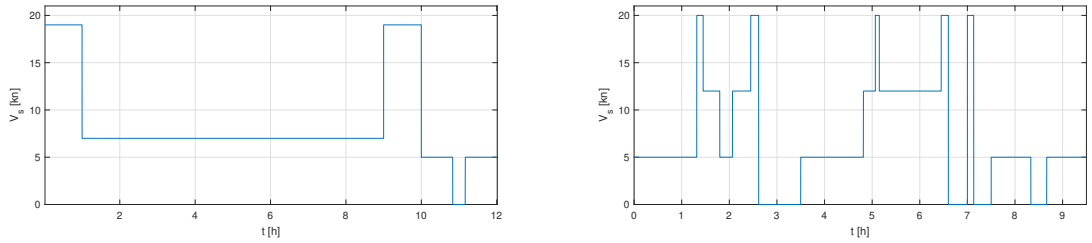

(a) Survey vessel

(b) Harbour patrol vessel

Figure 3.2: Optional operational profiles for the FCS1204H2

These are replaced by the fuel cell stack, balance of plant components, hydrogen tanks, battery, electronic components for power conversion and electric motors. PMSM's are often available with a wide range of speeds, so a gearbox is not required anymore. The propellers remain unchanged for the new propulsion system. An example of a fuel cell/battery propulsion for the FCS1204H2 is presented in figure 3.3. This example shows a propulsion system with two fuel cell stacks, where one is also optional. The diagram, as presented in figure 3.3, is based on [13] and applied to the FCS1204.

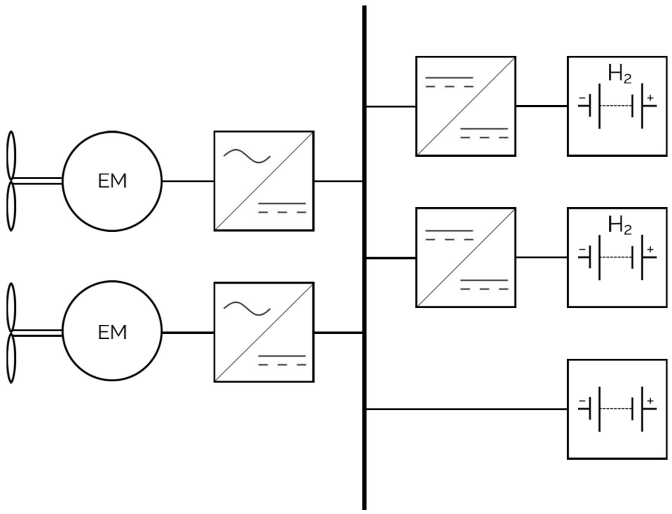

Figure 3.3: Diagram of the drive train of the FCS1204 with fuel cell/battery propulsion

3.2.1. System description

Figure 3.3 shows how the complexity has increased by implementing a fuel cell/battery propulsion system. The propulsion system under consideration can be divided in two subsystems. The hybrid power supply, where energy is generated, is presented on the right side of the DC bus. On the left side, the electric drive can be found where electrical energy is converted in forward speed. For the hydrogen propulsion system, the diesel engine is removed from the vessel. In addition, a gearbox is not required anymore as a consequence of the wide speed range of electric motors. The propellers remain unchanged for the new propulsion system.

The hybrid power supply has three components: a fuel cell module, battery and DC/DC converter. During peak power demand, both the fuel cells and battery deliver power to the electric drive. The battery functions as a power booster in this condition. The fuel cell stack is also used to deliver energy to the battery so the system is classified as a series-parallel hybrid (sec. 2.4). In this system architecture, the battery can also be used to assist during transient loading (peak shaving, ramp support and load smoothing). This chapter discusses the characteristics of these components in more detail.

'Hybrid ship propulsion' should be distinguished from 'hybrid power supply with all-electric ship propulsion'. A combustion engine (or turbine) and electric motor are coupled to one shaft for hybrid ship propulsion [18].

In the case of this study, the shaft is solely driven electrically and this is referred to as all-electric ship propulsion. Electrical energy is delivered through the DC bus and this is converter to AC power with an inverter. The rotational speed of a synchronous machine is synchronised with the frequency of the AC supply, which is a distinctive characteristic of this type of machines. Therefore, the speed of the PMSM is controlled through the electric circuit.

3.2.2. Energy versus power management

A suitable control system is a prerequisite for successful and efficient operations of hybrid fuel cell/battery systems. A basic feature is that the momentary load should be split between fuel cell stack and battery pack. On a larger timescale, the available energy should be managed properly in order to execute a mission in an energy efficient way. Energy management can be approached from different perspectives. Examples of objectives are to minimise hydrogen consumption, to sustain a battery state of charge or to maximise the fuel cell or system efficiency [13].

A control scheme of a hybrid system typically has two management levels: energy management and power management (fig. 3.4). The energy management system is at the top level to ensure that sufficient energy is provided to execute a given task. It determines the power set-points for the energy suppliers. The task may take minutes (manoeuvring) to several hours (voyages), so the timescale is generally large. For example, a given task for the battery system could be to provide boosting power for sailing at high speeds. The EMS should ensure that the battery is sufficiently charged to do so. Power, being the rate at which energy is delivered, should also be managed at a smaller timescale. The power management system (PMS) controls the current and voltage set-points to prevent that limits are exceeded.

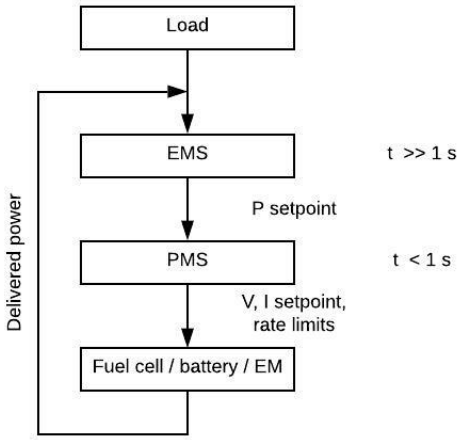

Figure 3.4: Control hierarchy for a hybrid power supply

The power converter electronics play an important role in the power management of the propulsion system. Fuel cells have relatively slow dynamics compared to batteries. A current reference ramp is often specified for fuel cells and the DC/DC converter controls the current draw to stay within the thresholds. In addition to this, the AC frequency is also controlled through the inverter.

3.3. Initial sizing

The initial sizing of the system is based on the power speed diagram (fig. 3.1) and the operational profiles from figures 3.2a and 3.2b. The survey vessel profile has a maximum speed of 19 knots. For a harbour patrol vessel it is desired that 20 knots can be reached, albeit for a maximum of 10 minutes. The top speed should be maintained much longer for the survey vessel. The influence of this difference on sizing will be discussed later in this thesis. The initial sizing is based on a top speed of 20 knots.

3.3.1. Permanent magnet synchronous machine

A sailing speed of 20 knots requires, according the PSD, a total of 296 kW for a displacement of 12 tonnes. In the PSD this was called brake power, for the electric drive this is referred to as power from the electric motor (P_{EM}). The FCS1204 has two shafts, which remains unchanged. The reference vessel has geared drive, but a power loss of 3% is associated with the gearbox, according the R&D department [98]. Besides this, electric propulsion with fuel cell stacks and batteries has the potential to be very silent. However, the gearbox creates noise so direct drive will also improve comfort onboard. Therefore, it is beneficial to select a PMSM that can accommodate direct drive. The PSD can easily be adjusted to obtain a power prediction for direct drive by compensating the original PSD for the gearbox efficiency of 97% [49]:

$$P_{EM,direct} = \eta_{GB} \cdot P_{EM,geared} \tag{3.3}$$

Damen Shipyards has selected Danfoss as supplier of electric motors for numerous projects. Due to this, a lot of information is available, such as product specification sheets and factory acceptance test reports. Danfoss has PMSM's in many sizes with a wide range of speeds. The operating envelope of a PMSM can be matched to the load by comparing power and torque with respect to rotational speed. Propeller data is also included in the power prediction from the R&D department: a propeller speed of 1200 to 1290 rpm corresponds to a ship speed of 20 knots, dependent on the displacement. The 'Danfoss EM-PMI375-T1100-1200' is considered as driving machine with a nominal speed of 1200 rpm and maximum speed of 2400 rpm.

Up to the nominal speed, PMSM's are capable of delivering the nominal continuous torque. This region is called the constant torque speed range (CTSR). Above the nominal speed, the PMSM enters the constant power speed range (CPSR) where nominal power is developed by the machine [52]. In the CPSR the maximum continuous torque decreases with speed (more on this in sec. 6.1). In other words, the torque limit decreases above the PMSM's nominal speed, but load torque keeps increasing with speed. Therefore, the load and drive torque are also compared. The propeller torque (Q) is given in the power prediction and this torque can be used to calculate the load torque as experienced by the engine. Engine speed equals propeller speed due to the removal of the gearbox. Therefore, the mechanical load torque at the engine (T_m) can be calculated by dividing propeller torque by the relative rotative efficiency (98%) and shaft efficiency (98%) [49]:

$$T_m = \frac{Q}{\eta_R \cdot \eta_S} \tag{3.4}$$

$$P_{EM} = T_m \cdot \omega_m \tag{3.5}$$

The load and drive characteristics are now presented in figure 3.5a and 3.5b. The 'EM-PMI375-T1100-1200' has a high nominal continuous torque and relatively low speed compared to other Danfoss PMSM's. This is most suitable for a for direct drive configuration, because speed is low and torque is high compared to geared drive. The selected machine has a power of 176 kW, where 144 kW is required for a displacement of 12 tonnes. This results in an engine margin of approximately 20%. The engine margin seems very high for lower displacements, but from previous studies it can be expected that the added weight of the FC system is significant. The engine margin also reduces for displacements above 12 tonnes.

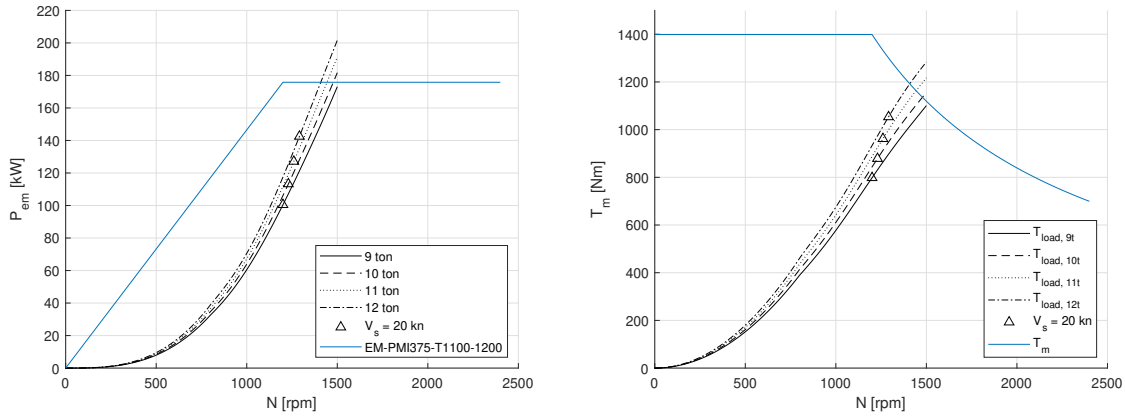

(a) Load and drive power

(b) Load and drive torque

Figure 3.5: Load and drive characteristics for various displacements and the EM-PMI375-T1100-1200

3.3.2. Fuel cell

The previous studies focused on two configurations with either one or two FC power packs with a size of 100 kW [28, 98]. The generic fuel cell model which is used in the propulsion model (ch. 4) is validated for a reference fuel cell stack with a maximum power of 120 kW and this stack is also available in the model.

The harbour patrol profile shows that the vessel sails 12 knots or less for the majority of the time with a few short periods at top speed. The PSD gives a total required power of 90 kW (sum of both shafts) for a displacement of 12 tonnes (fig. 3.1). The reference FC module has sufficient power to sail at this speed, but a power booster (battery) is required to reach top speed (20 knots). For the survey vessel, it is likely that one module, supported by a battery, will not have sufficient power to sail at a top speed of 19 knots for an extended period. This would require 270 kW according the PSD. Therefore, two configurations will be tested in this study with either one or two fuel cell stacks. The validated fuel cell model with 120 kW will be used for both configurations.

3.3.3. Hydrogen storage

The low volumetric energy density of hydrogen requires very sizeable tanks [100]. Figure 1.1 showed that it is not feasible to bunker an equivalent amount of energy carried in hydrogen compared to diesel, without losing the functionality of the vessel. It was concluded by [98] that the vessel could be outfitted with six fuel tanks at most. The hydrogen is stored in composite pressure vessels at a pressure of 350 bar. Each tank is capable of storing 8.4 kg of hydrogen, which brings the total storage capacity to 50.4 kg. These tanks are placed on the aft of the deck in open air for safety reasons [28, 98].

3.3.4. Battery

Batteries are modular, the energy can easily be increased by adding connecting multiple batteries. Toshiba Type 3-23 Li-Ion battery modules are used in this study. This battery is also considered for other electric vessels within the Damen shipyards Group. The battery module has a nominal capacity of 45 Ah. The maximum voltage is as high as 32.4 V and nominal voltage of 24.6 V. The PMSM requires a minimum DC voltage, which is dictated by the battery, of 675 V at all times. The voltage of the battery bank can be increased by adding battery modules in series. Twenty-eight battery modules are added in series to reach a voltage of approximately 690 V. The amount of battery banks that are connected in parallel will be systematically varied to analyse the most suitable degree of hybridisation. The amount of parallel banks is varied between one and five.

A concept design with a similar fuel cell/battery system is presented in figure 3.6. The figure shows how the system could be fitted in the FCS1204. This system is designed during the previous studies [28, 98]. In this render there are only five tanks visible, where six is also possible. The fuel cell stacks can be recognised by the two red boxes and the battery by the grey box underneath the superstructure. The spatial design is outside the scope of this research, but figure 3.6 is included to give an impression how the design could look like.

Figure 3.6: Concept design of a fuel cell / battery propulsion system [98]

4

Modelling of the hybrid power supply

In figure 3.3 it was seen that the hybrid power supply consists of three components: a fuel cell stack, battery and DC/DC converter. A power conversion system is required between the FC power pack and DC bus. In the following chapter, it is seen that it is likely that the fuel cell and battery will not deliver the same voltage. Therefore, at least one DC/DC converter is required to ensure that both components deliver the same voltage to the bus. Figure 3.3 shows that there is only a DC/DC converter between the fuel cell stack and DC bus. Due to this, the bus voltage is dictated by the battery and this is called a "floating" DC bus voltage. The battery voltage is relatively constant for its operational domain, compared to the fuel cell voltage, which makes it convenient that the voltage is dictated by the battery. A disadvantage of this floating voltage is that all components should be capable to deal with a varying bus voltage. Alternatively, a DC/DC converter can also be added between the battery and DC bus to obtain a constant bus voltage. This allows to use of a smaller battery bank, but it also makes system control more complex compared to a floating voltage. Therefore, the topology as shown in figure 3.3 is selected for this study.

A Simulink model for the hybrid power supply is developed. The propulsion system is modelled with Simscape Power Systems (SPS). Simscape is additional software for Simulink for multi-domain modelling, as it supports physical domains such as electrical, mechanical, thermal, fluid and hydraulic. SPS provides a library for electric power systems. In these models, the actual flow of electrons is simulated. The software enables to test the performance of a electric power systems on component-level. Therefore, it is very powerful software for the goal of this study. The fuel cell and battery model are introduced in section 4.1 and 4.2, respectively. The working principles and modelling aspects of DC/DC converters are discussed in section 4.3. The chapter is finished with the presentation of the complete model for the hybrid power supply.

4.1. Fuel cell model

In section 2.2 it was noted that fuel cell systems are most efficient in part load conditions. This is the result of fuel cell polarisation. A generic fuel cell model is developed in [71] which is available in the SPS library. It combines the thermodynamic and electrical features of fuel cells in one model. The polarisation characteristics of the fuel cell are based on the datasheet which is provided by a fuel cell manufacturer and due to this the model can be applied easily for many different fuel cell modules. This generic model is also used in this study and is introduced in this section.

4.1.1. Gibbs free energy balance

The electrochemical reaction of hydrogen in a fuel cell is reversible: the electrolysis reaction and fuel cell reaction are the opposite of each other. As molecules in a FC react, the change in chemical energy is accompanied by a release of useful energy (work). Water, at a low-energy state, can be brought back to the high-energy state through electrolysis, by adding the released energy plus extra energy to cover losses that occur during the electrochemical FC reaction.

Water is created in a LT-PEM fuel cell from oxygen and hydrogen. During the FC reaction, the total enthalpy of the constituents changes. During the formation of liquid water 285.8 kJ is released for each mole of water,

which is known as the heat of formation [14]. A part of this energy is lost to the environment as heat at temperature (T). Now, the Gibbs free energy is introduced as the maximum amount of work obtainable from a reversible reaction [56, 91]. It is the total change in enthalpy minus the transmission of energy to the environment (eq. 4.1) [79]. The reversible heat effect ($T \cdot \Delta S$) represents the heat exchange with the environment under reversible conditions. It is defined as the product of the change in entropy and temperature. The entropy of all reactants is now used to construct the energy balance of the fuel cell reaction at normal conditions (298 K and 1 bar) as presented in table 4.1.

	H_2	0.5 O_2	H_2O	Change
H [kJ]	0	0	-285.8	-285.8
S [J/K]	-130.7	-102.6	69.9	-163.4

Table 4.1: Enthalpy and entropy of fuel cell reactants [14]

$$\Delta G = \Delta H - T \cdot \Delta S \tag{4.1}$$

$$\Delta G = -285.8 - 298 \cdot (-163.4) = -237.1 \text{ [kJ/mol]}$$

A negative sign indicates that energy is released rather than consumed. It can be noted that the total change in enthalpy equals the higher heating value of hydrogen. The released energy from the reaction can be expressed per mass unit of hydrogen that is consumed, where the molar mass of hydrogen equals 2.01588 g/mol.

$$\Delta H = \frac{-285.8}{2.01588} = -141.8 \text{ [kJ/g]}, \qquad \Delta G = \frac{-237.1}{2.01588} = -117.6 \text{ [kJ/g]}$$

The latter shows that 24kJ/g of hydrogen is lost to the environment as heat. This corresponds to the heat loss of 48kJ per mole of water that was found in the Gibbs free energy balance.

Open circuit voltage

The theoretical open circuit voltage (V_0) can be derived from the Gibbs free energy as shown in equation 4.2 [56, 91]. In the FC reaction, two moles of electrons are required for the production of one mole of water ($H_2 \longrightarrow 2H^+ + 2e^-$ and $0.5O_2 + 2e^- + 2H^+ \longrightarrow H_2O$), hence n equals 2. The Faraday constant gives the electric charge of one mole of electrons (96,485 coul/mole).

$$V_0 = -\frac{\Delta G}{n \cdot F} \tag{4.2}$$

$$V_0 = -\frac{-237.1 \cdot 10^3}{2 \cdot 96,485} = 1.23 \text{ [J/coul]} = 1.23 \text{ [V]}$$

This open circuit voltage is the theoretical maximum fuel cell voltage (V_{FC}). Equation 4.1 shows how the Gibbs free energy decreases with temperature, but both enthalpy and entropy are temperature-dependent. At operating conditions of a LT-PEM fuel cell, where temperature is around 80°C, theoretical open circuit voltage stays approximately 1.23 V [50]. When components draw current from the fuel cell, the actual voltage drops. This is known as polarisation [91].

4.1.2. Fuel cell polarisation and power characteristics

When a fuel cell is put to work, the fuel cell voltage will drop below the theoretical maximum, due to irreversible losses. The following voltage behaviour is observed over a range of currents [50]: a deviation between actual no-load voltage and theoretical open circuit voltage (fuel crossover), a fast drop at low current (activation losses), a linear decrease at intermediate currents (ohmic losses) and a fast drop at high current (mass transport losses). Figure 4.1 shows the characteristics of the polarisation curve. The irreversible losses are dedicated to the following phenomena [50, 56]:

1. Fuel crossover: the deviation between no-load voltage and theoretical open circuit voltage is caused by fuel crossover. The electrolyte should only transport hydrogen ions, but it can not be avoided that some fuel is transported across the electrolyte. This causes an energy and voltage loss.

2. Activation losses: The reactions on the surface of the electrodes occur with a certain slowness. Some voltage is used to drive (or activate) these reactions. Hence, the useful voltage decreases rapidly at low current density.

3. Ohmic losses: as current increases, so does the resistance related to the flow of electrons through the electrodes. The same principle holds for the flow of ions through the electrolyte. This voltage loss is proportional to the current density, i.e. linear.

4. Mass transport or concentration losses: as current increases, reactants are consumed at a higher rate. The high current causes a reduction of partial pressures of the reactant supply systems and reactant concentration in the cell, resulting in a fast drop in voltage (and power). This loss is also known as Nernstian loss, since the Nernst equation refers concentration to voltage.

The produced power of a fuel cell is the product of current and voltage [92]. The polarisation curve relates current and voltage for the cell's complete operational domain. Hence, the power curve (or power density) can completely be derived from the polarisation curve (fig 4.1). In practice, the current is limited to avoid mass transport losses and the FC power would drop rapidly at higher currents [71]. So, maximum power occurs at maximum current. Figure 4.1 shows the polarisation curve for a reference fuel cell stack from the generic model, which is validated in [71]. This module delivers a maximum power of 120 kW. The previous studies focused on two configurations with either one or two stacks with similar size (100 kW) [28, 98]. Therefore, the validated reference stack is used for the FC model. The input data for the model can be found in table 4.2.

$$P = I \cdot V \tag{4.3}$$

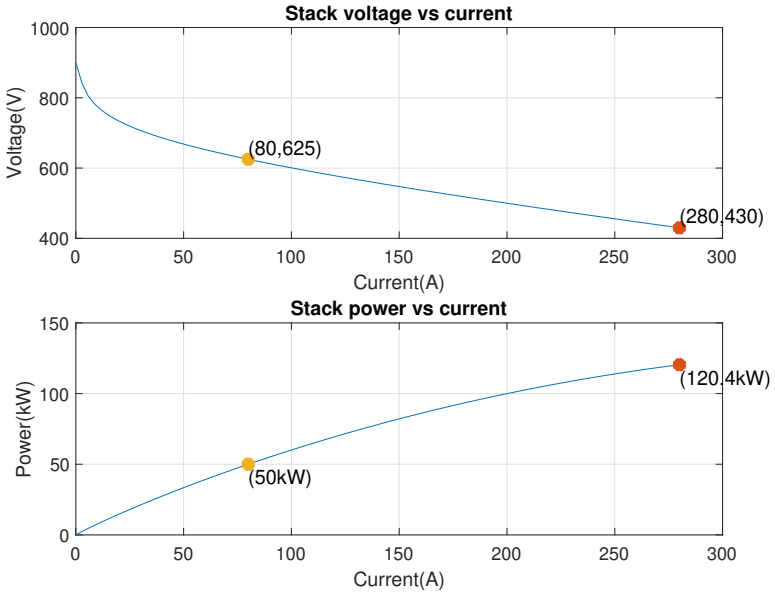

Figure 4.1: Polarisation curve of a reference LT-PEMFC from the generic Simscape^{TM} fuel cell model

For fuel cell vehicles it is most convenient to control the current output of the fuel cell [12, 13, 37, 53, 85]. Fuel cell voltage and power follow from the current draw. The fuel cell voltage at any operating condition can be modelled with the summation of Nernstian, activation and ohmic losses [51]. Crossover losses are neglected in the generic fuel cell model:

$$V_{FC} = V_{Nernst} + V_{act} + V_{ohm} \tag{4.4}$$

Nernst voltage

The shape of the polarisation curve is affected by some operational parameters, like gas concentration, pressure and temperature. The relationship between voltage and these parameters is defined by the Nernst equation (eq. 4.5) [8, 50]. The Nernst voltage is also known as the theoretical maximum (reversible) voltage for closed circuit conditions [77]:

$$V_{Nernst} = V_0 + \frac{\Delta S}{2 \cdot F} \cdot (T - 298) + \frac{R \cdot T}{2 \cdot F} \cdot \ln\left(p_{H_2} \cdot p_{O_2}^{1/2}\right) \tag{4.5}$$

The partial pressures (p_i) are dependent on the supply pressure of fuel and air, the reactant composition (y_i) and rate of conversion in the fuel cell ($\mu_{f,i}$) [60]:

$$\begin{cases} p_{H_2} = (1-\mu_{f,H_2}) \cdot y_{H_2} \cdot P_{fuel} \\ p_{O_2} = (1-\mu_{f,O_2}) \cdot y_{O_2} \cdot P_{air} \end{cases} \tag{4.6}$$

$$\mu_{f,H_2} = \frac{60,000 \cdot R \cdot T \cdot N_c}{2 \cdot F \cdot P_{fuel} \cdot \dot{V}_{fuel} \cdot y_{H_2}} \cdot I_{FC} \tag{4.7}$$

$$\mu_{f,O_2} = \frac{60,000 \cdot R \cdot T \cdot N_c}{4 \cdot F \cdot P_{air} \cdot \dot{V}_{air} \cdot y_{O_2}} \cdot I_{FC} \tag{4.8}$$

Where N_c represents the amount of cells in the fuel cell stack, $\dot{V}$ refers to the flow rate in l/min of the reactant and pressures should be provided in Pascal. This demonstrates how the Nernst voltage decreases when current increases.

Activation voltage
The activation of the cell is driven by an overpotential at the surface of the electrodes. For the activation of the cell more energy is required than thermodynamically expected [50]. The overpotential depends on the kinetics of the reaction: a slow reaction has a much higher overpotential. If overpotential is plotted againts the logarithmic function of current, a constant curve is found. This curve is known as the Tafel curve with slope A:

$$A = \frac{R \cdot T}{2 \cdot \alpha \cdot F} \tag{4.9}$$

Where α is called the charge transfer coefficient that depends on the materials of the electrodes. The activation losses are then dependent on the Tafel slope and the exchange current density (i_0):

$$V_{act} = -A \cdot \ln\left(\frac{i_{FC}}{i_0}\right) \tag{4.10}$$

The fuel cell and electrolysis reaction occur continuously in the cell, even if the current draw density (in A/cm^2) is zero. At zero current density, these reactions across the electrolyte occur at the same rate and they are in perfect equilibrium. These reactions occur at the exchange current density. If the current density is increased above the exchange current density, the reactions are "pushed" in one direction and the cell is activated [50].

Ohmic voltage
The ohmic voltage decreases due to resistance of the electrodes and electrolyte [71]. The internal resistance of the cell results in a linear voltage drop, or resistive loss, as current increases:

$$V_{ohm} = -R_{ohm} \cdot I_{FC} \tag{4.11}$$

4.1.3. Efficiency

The relationship between Gibbs free energy, enthalpy and heat loss is also related to the (theoretical) maximum efficiency of a fuel cell stack. The maximum efficiency is a relationship between the Gibbs free energy and total change of enthalpy (HHV) and can be considered as ideal efficiency of this conversion [49, 56]:

$$\eta_{max} = \frac{\Delta G}{\Delta H} = 1 - \frac{T \cdot \Delta S}{\Delta H} \tag{4.12}$$

$$\eta_{max} = \frac{-237.1}{-285.8} = 83.0\%$$

The maximum efficiency corresponds to the no-load condition and the stack efficiency decreases as the stack is loaded. The stack efficiency is now defined as the cell voltage with respect to the cell's open circuit voltage (eq. 4.13). The term μ_f appears in this expression as the fuel utilisation rate. Some excess fuel is injected to ensure that the cell is fed with fuel over its complete length. The efficiency should be corrected for the fuel utilisation [50]. The open circuit voltage was defined in equation 4.2 and is the theoretical maximum voltage [91].

$$\eta_{stack} = \mu_{f,H_2} \cdot \frac{V_{FC}}{V_0} \tag{4.13}$$

The polarisation curve shows that voltage decreases as current draw increases. Consequently, the ideal stack efficiency of 83% decreases rapidly due to activation losses, ohmic losses and mass concentration losses.

Fuel cell system efficiency
A fuel cell system requires additional components in order to generate electricity. These auxiliary components are referred to as 'balance of plant' (BoP) components, which include pumps, blowers, compressors, water management systems and system controls [95]. BoP components use parasitic power and reduce the overall efficiency of the fuel cell system. A maximum system efficiency between 50% and 60% can be expected if this taken into account [9, 37, 100]. Fuel cell systems are most efficient in part load conditions (fig. 4.2. However, as maximum power occurs at high current, there is a trade-off between high efficiency and high power.

The system efficiency is not taken into consideration in the fuel cell model, but it is important to consider during low-power operation of the fuel cell stack. The operational profiles that are presented in figure 3.2a and 3.2b show that the vessel sails a significant amount of time at low speed (5 or 7 knots). The PSD gives a total power consumption of 6.7 kW and 18.4 kW for speeds of 5 and 7 knots, respectively, and a displacement of 12 tonnes. Hence, the load factor is rather low, especially if two stacks are installed.

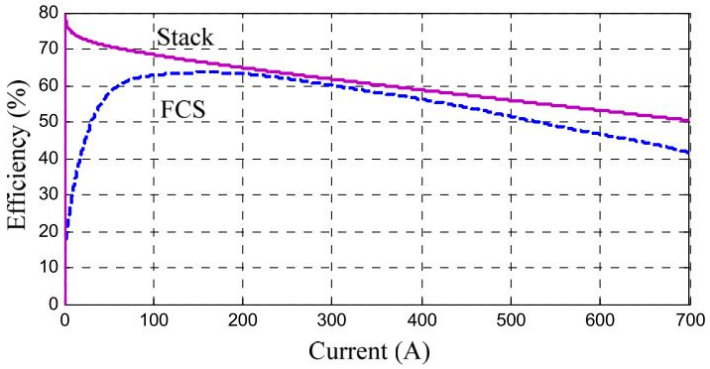

Figure 4.2: stack efficiency versus fuel cell system efficiency [37]

4.1.4. Fuel and air consumption

Two fuel cell models are available in Simscape, a simplified and detailed model. The simplified model simulates the stack at nominal operating conditions, where the detailed model allows variations of pressure, temperature and flow rates of fuel and air [71]. The detailed model is selected, because this allows the author to control the fuel flow to the stack. Supply pressure and stack temperature are assumed to be constant: both the supply system and internal temperature effects are outside the scope of this study. Hydrogen consumption, on the other hand, is an important indicator for the feasibility of fuel cell propulsion since there is a physical constraint on hydrogen storage. Therefore, the supply of fuel and air is modelled in the Simulink model. A saturation block is used to prevent that the flow of fuel becomes negative. Equations 4.7 and 4.8 can be rewritten to regulate the flow:

$$\dot{V}_{fuel} = \frac{60{,}000 \cdot R \cdot T \cdot N_c}{2 \cdot F \cdot P_{fuel} \cdot \mu_{f,H_2} \cdot y_{H_2}} \cdot I_{FC} \tag{4.14}$$

$$\dot{V}_{air} = \frac{60{,}000 \cdot R \cdot T \cdot N_c}{4 \cdot F \cdot P_{air} \cdot \mu_{f,O_2} \cdot y_{O_2}} \cdot I_{FC} \tag{4.15}$$

The FC model requires a flow rate in l/min. The term 60,000 would disappear from this equation if the flow rate is calculated in SI-units (m^3/s). The volume flow rate can then be converted to a mass flow rate:

$$\dot{m}_{H_2} = \dot{V}_{fuel} \cdot \rho_{H_2} \tag{4.16}$$

$$\dot{m}_{O_2} = \dot{V}_{air} \cdot \rho_{air} \cdot x_{O_2} \tag{4.17}$$

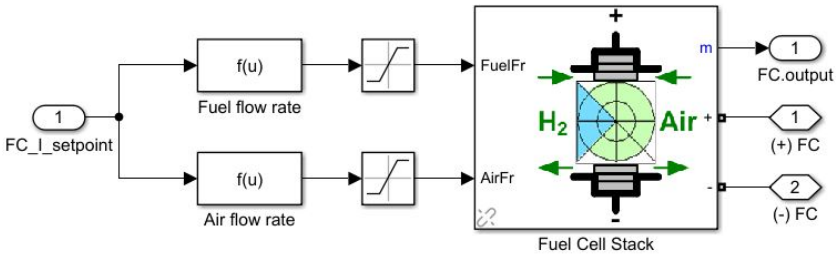

Figure 4.3: Simulink model of fuel flow regulation

The mass fraction of oxygen in air, which is 23.2%, is represented by x_{O_2} [81]. The mass flow rate is then integrated to obtain the total consumption:

$$m_{H_2} = \int_0^t \dot{m}_{H_2} \cdot dt \tag{4.18}$$

$$m_{O_2} = \int_0^t \dot{m}_{O_2} \cdot dt \tag{4.19}$$

The fuel cell model assumes that gases are ideal, which is not the case for hydrogen. The stack consumption at operational conditions (elevated temperature and pressure) is therefore expressed as stack consumption in 'standard litre per minute' (sl/min). The density of hydrogen at standard conditions (0.09 kg/m^3) is used to estimate the total consumption. Due to this, it can be assumed that gases are ideal without compromising the accuracy of the consumption calculation. Other model assumptions are that the stack is equipped with a cooling and water management system, that there are no variations across the length of a cell and that the internal resistance is constant for all operating conditions [71]. These assumptions have some implications for the performance. The cell's potential can be lost due to local flooding or drying inside the cell, even with proper water management [10]. In addition, phenomena such as pressure drops or temperature changes across the cell may increase the parasitic power consumption required for pumps or coolers.

Parameter	Unit	Value
Nominal power	kW	50.0
Nominal voltage	V	625
Nominal current	A	80
Nominal efficiency	%	55
Maximum power	kW	120.4
Voltage at maximum power	V	430
Maximum current	A	280
No-load voltage	V	900
Current reference ramp	A s^{-1}	25
Operating temperature	°C	65
Fuel supply pressure	atm	1.5
Air supply pressure	atm	1.0
Fuel utilisation rate	%	99.25
Air utilisation rate	%	70.4

Table 4.2: Input data for fuel cell model [60]

4.2. Battery model

Batteries operate electrochemically quite similar to fuel cells. Fuel cells, however, are solely energy converters, where all reactants in batteries are stored internally. Batteries have the important function to support fuel cells. This can be done in different ways, for example by delivering extra power above the fuel cell's maximum or supporting the low responsiveness of fuel cells. A similar SPS model is developed for batteries in [87]. This generic model can accurately reproduce the charge and discharge characteristics of all battery types discussed in section 2.3. A battery can be modelled fairly simple by an ideal voltage source in series with

a resistance [87]. The presented model, however, is non-linear as it also takes battery state-of-charge into consideration.

4.2.1. Battery polarisation

The polarisation of a battery is similar to fuel cell polarisation. The Gibbs free energy balance determines the open cell voltage. The open cell voltage is very dependent on battery chemistry and follows from the datasheet from the manufacturer. The battery polarisation curve relates voltage to charge level (rather than current strength as seen for fuel cells). At the beginning of the discharge cycle (the exponential zone) additional energy is required which causes an overpotential [15]. In the nominal operational zone, ohmic losses occur. Finally, a rapid voltage drop is seen if the battery is discharged beyond the nominal zone (deep discharge). At a certain voltage the battery is considered to be fully discharged and this is referred to as the end-of-discharge or cut-off voltage ($V_{B,cut}$). Figure 4.4 shows an approximation of the polarisation curve of a Toshiba Type 3-23 Li-Ion battery module. The product sheets of this battery are considered confidential information.

Up to this point, the polarisation curve of a battery seems very similar to the FC's curve. However, the state of charge plays an important role here too. The voltage of a battery diminishes as the depth of discharge increases at a fixed current [57, 74]. Also, if the battery is studied at a given SOC, then it is also observed that voltage decreases with increasing current [15]. These discharge characteristics are visualised in the figure 4.4. The current draw is related here to the battery's capacity: the rated capacity (in Ah) gives the current that a battery can deliver for one hour [87]. If current is higher than this nominal current, the battery will be discharged in less than one hour and vice versa. The ratio between the nominal current and discharge current is called the C-rate.

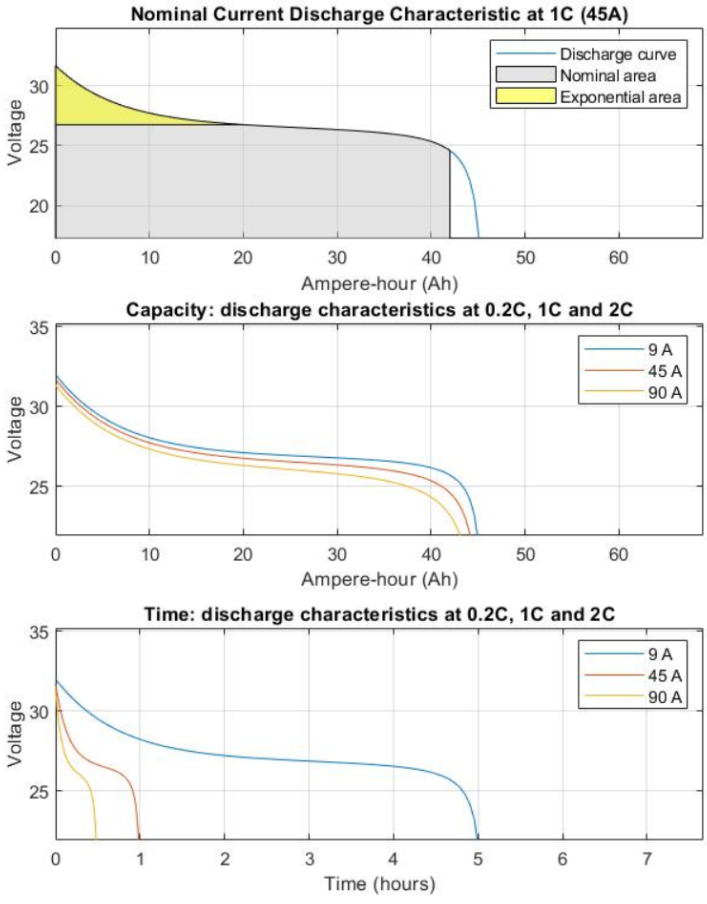

Figure 4.4: Discharge characteristics of Toshiba Type 3-23 Li-Ion battery module

The battery voltage in the presented model follows from the current draw and the actual battery charge. Similar to fuel cells, the voltage has a couple of components. For Li-Ion batteries these are discussed below.

$$V_B = V_{pol} + V_{exp} + V_{ohm} \tag{4.20}$$

Polarisation voltage
The polarisation voltage can be best compared with the Nernst voltage: it is the theoretical maximum cell voltage for closed circuit conditions. The polarisation voltage is presented by [87]:

$$V_{pol} = V_{0,nom} - K \cdot \frac{Q_B}{Q_B - \int_0^t i \cdot dt} \tag{4.21}$$

where $V_{0,nom}$, K and Q_B represent the battery voltage constant, polarisation voltage constant and the battery's capacity, respectively [87]. The battery constant voltage and polarisation voltage constant will be discussed below. The integral of time gives the actual battery charge in Ampere-hour.

Exponential voltage
The exponential voltage describes the discharge characteristic in the exponential area (fig. 4.4). It is characterised by the voltage drop in the exponential zone (A), the capacity at the end of the exponential area ($Q_{B,exp}$) and the battery charge:

$$V_{exp} = A \cdot e^{-B \cdot \int_0^t i \cdot dt}, \qquad B = \frac{3}{Q_{B,exp}} \tag{4.22}$$

Both the voltage drop and capacity at the end of the exponential area can be read from the polarisation curve of a battery. With this information it is also possible to estimate the polarisation voltage constant:

$$K = \frac{\left(V_0 + V_{nom} + A \cdot e^{-B \cdot Q_{nom}} - 1\right) \cdot \left(Q_B - Q_{B,nom}\right)}{Q_{B,nom}} \tag{4.23}$$

The parameters with index 'nom' refer to the values of these parameters at the end of the nominal area (fig. 4.4) [87].

Ohmic voltage
The ohmic losses of a battery are also caused by resistance of the electrodes and electrolyte of a battery, known as the internal resistance:

$$V_{ohm} = -R_{int} \cdot I_B \tag{4.24}$$

The battery voltage constant can be computed based on the equations presented above. $V_{0,nom}$ is defined as the no-load voltage of the battery's nominal area [87]. It is lower than the no-load voltage at the beginning of the exponential area (fig. 4.4):

$$V_{0,nom} = V_0 + K + R_{int} \cdot I - A \tag{4.25}$$

As seen in figure 4.4, different C-rates result in different polarisation curves. Each current strength results in another set of parameters (K, A, B, $V_{0,nom}$) that describe the curve. The parameters for the approximation of the nominal discharge curve of the Toshiba Type 3-23 module are presented in table 4.3.

Parameter	Unit	Value
R_{int}	mΩ	6
K	V	0.0022
A	V	5.04
B	Ah^{-1}	0.15
$V_{0,nom}$	V	27.0

Table 4.3: Battery model parameters for Toshiba Type 3-23 module

This model is a simplified version of the Shepherd model, which includes the actual current in the equation for the polarisation voltage (rather than only the integral of current that represents battery charge). This gives a non-linear polarisation voltage that causes instability in simulations [86, 87]. Therefore, actual current is

only implemented in the computation of the ohmic voltage. Besides this, variations in internal resistance and temperature effects are also not considered in the used model. Confidential product sheets show that this is not the case for a real battery. Finally, it is also assumed that the charging behaviour is the same as discharging behaviour, which means that the polarisation curves from the model are also used for the simulation of charging the battery [87].

4.2.2. Efficiency

From section 2.3 and 4.1.3 it can be expected that the efficiency of Li-Ion batteries is higher than the fuel cell's efficiency, let alone the FC system efficiency. The nominal efficiency is estimated with the following equation, which can be used to estimate the power losses in any operational condition [87]:

$$\eta = 1 - \frac{I_{nom}^2 \cdot R_{int}}{I_{nom} \cdot V_{nom}} \tag{4.26}$$

This equation gives the relationship between resistive losses and power output of the battery. The battery model does not distinguish between charge and discharge mode and uses one constant internal resistance, which is a limitation of the model. The nominal efficiency is estimated at 99% with equation 4.26. The battery efficiency is higher than values that are found in literature, which is 95% to 98% according [43]. This is a consequence of the assumption that internal resistance is constant. Therefore, the power losses are somewhat underestimated in the model. Confidential product sheets show that the internal resistance of the Toshiba SCiB battery cell is relatively constant if the battery operates at ambient temperature (between 20% and 100% SOC). Furthermore, the difference between charge and discharge mode is small for this condition. These observations do not longer hold if the battery operates in colder environments.

Furthermore, equation 4.26 shows that the battery is most efficient for low currents, if the resistance and voltage remain equal. This should be taken into account in the energy management of the system: the fuel cell system functions most efficient in part load, but it is likely to be more efficient to use a battery at low loads. Also, at high loads it might also be more efficient to distribute the load power over battery and fuel cell module. In this way, fuel cell power can be reduced and the fuel cells operates closer to its efficient domain.

4.2.3. Design of battery bank

In the generic model, the battery is modelled as an internal resistance with a voltage source. Voltage is controlled based on current and actual SOC. The battery module that is discussed before, is not capable of delivering the high power and voltage that is required in a electric vehicle. Therefore, multiple battery modules need to be connected in series or parallel to get the desired output. The necessary equations to design a battery bank are presented here. These will be used to design a battery bank based on the required power for the FCS1204.

The Toshiba battery module is in fact also a small battery bank: it is built up by connecting different cells in series and parallel. The main advantage of a series connection is the increase in voltage. Current (or capacity in Ampere-hour) is increased if batteries are connected parallel. To increase power, being the product of current and voltage, both are important. This follows from the fundamental laws of electric systems:

$$\begin{cases} V_s = V_1 + V_2 + \cdots \\ V_p = V_1 = V_2 = \cdots \end{cases} \tag{4.27}$$

$$\begin{cases} I_s = I_1 = I_2 = \cdots \\ I_p = I_1 + I_2 + \cdots \end{cases} \tag{4.28}$$

$$\begin{cases} R_s = R_1 + R_2 + \cdots \\ R_p = \left(\frac{1}{R_1} + \frac{1}{R_2} + \cdots\right)^{-1} \end{cases} \tag{4.29}$$

For a battery bank it is convenient to use a number of identical battery modules. The characteristics of this bank are then determined based on the module characteristics and the number of battery modules in series (N_s) and parallel (N_p):

$$V_B = N_s \cdot V_m \tag{4.30}$$

$$I_B = N_p \cdot I_m \tag{4.31}$$

$$Q_B = N_p \cdot Q_m \tag{4.32}$$

$$E_B = V_{B,nom} \cdot Q_{B,nom} \tag{4.33}$$

$$R_{int} = N_s \cdot \left(N_p \cdot \frac{1}{R_{int,m}} \right)^{-1} \tag{4.34}$$

By following these equations the characteristics of an equivalent battery are determined. This equivalent battery represents all battery modules that are installed as one large battery. This method is much more convenient than the independent modelling of each module. The permanent magnet requires a minimum DC voltage of 675 V at all times. The module's voltage at the end of the nominal zone 24.6 V. This means that at least twenty-eight battery modules should be connected in series to accommodate the required bus voltage. The amount of parallel modules will be systematically varied between one and five. A battery bank with twenty-eight modules in series and two parallel (2P28S) contains a total of fifty-six modules. The characteristics of these battery banks are presented in table 4.4. Notice the difference between rated and nominal capacity, where 'nominal' refers to the capacity at the end of the nominal zone.

Parameter	**Unit**	**Module**	**1P28S**	**2P28S**	**3P28S**	**4P28S**	**5P28S**
Nominal voltage	V	24.6	689	689	689	689	689
No-load voltage	V	32.4	907	907	907	907	907
Cut-off voltage	V	18.0	504	504	504	504	504
Rated capacity	Ah	45	45	90	135	180	225
Rated current (1C)	A	45	45	90	135	180	225
Nominal capacity	Ah	42	42	84	126	168	210
Maximum current	A	160	160	320	480	640	800
Internal resistance	mΩ	6	150	75	50	37.5	30
Weight	kg	14.6	409	818	1226	1635	2044

Table 4.4: Input data for battery model for various battery designs

4.3. DC/DC converter

Both a fuel cell and battery provide direct current (DC). It is therefore convenient to use a DC bus in the vessel's electric system. From the polarisation curves it was seen that there is a large difference between minimum and maximum voltage from the fuel cells. The battery voltage is much more constant for various C-rates if it is not discharged below 20% SOC. The fuel cell stack and battery modules will not deliver the same voltage during operating conditions, so it is necessary to implement a power converter to ensure that both components deliver the same voltage to the DC bus. The battery voltage should determine the bus voltage [13]. The variation of battery voltage is much smaller for various C-rates, compared to the FC voltage at various current draws.

4.3.1. Working principle

A DC/DC converter is required between the fuel cell system and DC bus to accurately control the stack output. In the essence, the device converts an unregulated input voltage to a regulated bus voltage. It does so by respecting the power balance across the converter [30]:

$$P_{in} = P_{out} \quad \longrightarrow \quad I_{in} \cdot V_{in} = I_{out} \cdot V_{out} \tag{4.35}$$

Power converters are also used to control the output of the power supply: if the bus voltage is regulated, the bus current follows from the load power. The current from the fuel cell module, for instance, is found by measuring the current at the bus side and dividing the power by the unregulated stack voltage:

$$I_{FC} = \frac{I_{DC\ bus} \cdot V_{DC\ bus}}{V_{FC}} \tag{4.36}$$

DC/DC converters either increase or reduce the output voltage. Conventional converter types are boost converters ($V_{out} > V_{in}$ and $I_{out} < I_{in}$) or buck converters ($V_{out} < V_{in}$ and $I_{out} > I_{in}$), which are also known as step-up or step-down converters, respectively. Buck-boost converters, which can operate in both states, are

also regularly used in power systems [93]. Different converter types can be distinguished based on their electrical circuit. The power balance above suggests an ideal converter with 100% efficiency, in reality efficiencies are lower (up to 95%) due to losses in the electrical circuit [30].

Most DC power converters consist of a switch network and low-pass filter as shown in figure 4.5 [30]. The switch operates at a certain switching frequency (f_s). The switch output voltage equals the input voltage when the switch is in position 1 and equals zero when the switch is in position 2. The switch is only in position 1 during a fraction of the switching period ($T_s = 1/f_s$). This fraction is called the duty cycle (D) and varies between 0 and 1. The conversion ratio is defined as the ratio between in- and output voltage and dependent on the duty cycle and differs for various converter topologies [30]:

$$M(D) = \frac{V_{out}}{V_{in}} = \frac{I_{in}}{I_{out}} \tag{4.37}$$

is o

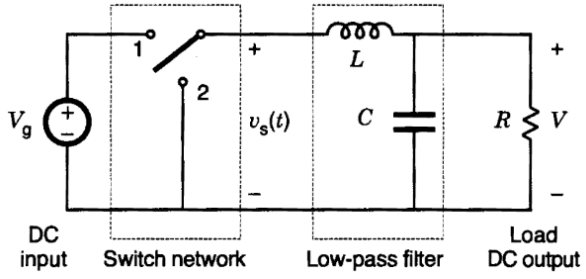

Figure 4.5: Operating principle of DC/DC buck converter [30]

Switching frequencies are often in the range of a couple of kilohertz. The system transients of interest are much slower. When this is the case, it is possible to eliminate the switching dynamics and only look at the average values. The inductor and capacitor in the circuit act as low-pass filter [30].

4.3.2. DC/DC converter model

The DC bus voltage is dictated by the motor drive. The required DC voltage is 675 V, which is within the voltage range of the batteries (tab. 4.4). The power converter should function as a buck-boost converter. However, for the applicability of this model it is important to develop a generic DC/DC converter model that can be used for boost, buck and buck-boost operation. Therefore, a bidirectional DC/DC is implemented in the model. A bidirectional converter can also be used between the battery and DC bus if more research should be conducted on alternative system topologies. The electric circuit of this converter is shown in figure 4.6. If this converter circuit is used between the FC stack and bus, a diode is needed to ensure that electrons only flow from the fuel cell system to the bus. This diode is present in the fuel cell model.

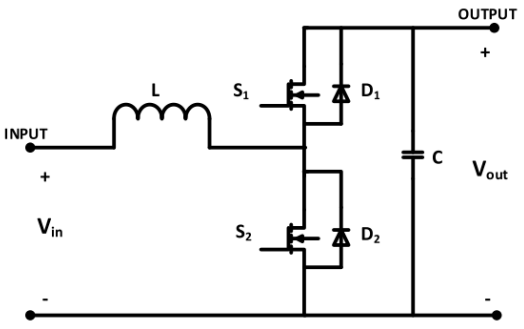

Figure 4.6: Electric circuit of a bidirectional DC/DC circuit [7]

Model complexity

In Simscape Power Systems three different model types are most commonly used: simplified, average-value and detailed models [61]. The simplified model implements the power balance from equation 4.35. The

switch network, inductor and capacitor are neglected here. These come into play in the average-value model and detailed model, where switching effects are not present in the first.

The difference between the latter can best be explained by diving into the function of the switching network. This is demonstrated for a buck converter in figures 4.7a and 4.7b for the simple circuit presented in figure 4.5. The load requires a reduction of the voltage with conversion ratio $M(D)$. If the switch is in position 1, the network is connected to the high voltage source and for position 2 this is not the case. Due to this, the voltage measured at the inductor is continuously varying between a high an low voltage. The average voltage is the required output voltage for the load and this is controlled by the duty cycle. This gives a rectangular pulsating signal with a width of $D \cdot T_s$ [30]. The variation of the voltage with respect to the average is called the 'ripple voltage'. For a properly designed converter the amplitude of the ripple is less then 1%. Ripple voltage often remains present due to the incomplete filtering of the LC network [31]. Varying current is also observed as a result of the pulsating voltage (fig 4.7b).

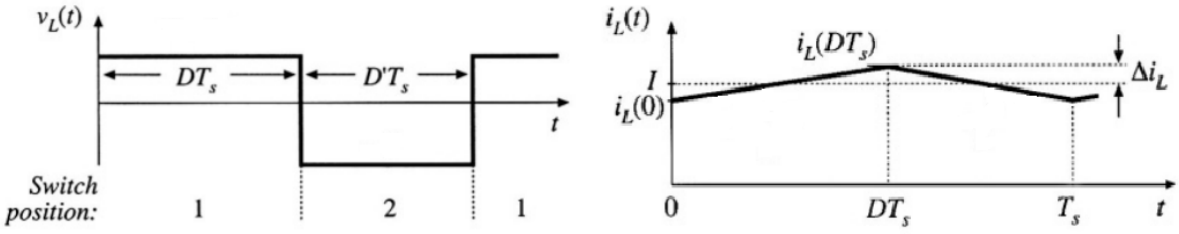

(a) Ripple voltage

(b) Ripple current

Figure 4.7: The effect of the switching network on inductor voltage and current [31]

The pulses are controlled by a so-called pulse-width modulation (PWM) generator, which is controlled by the duty cycle signal. The average-value model controls the conversion based on the duty cycle, where the detailed model implements this PWM generator. Both models significantly improve the accuracy compared to the simplified model [61]. As stated before, the system transients of interest are much slower than the time-domain of this PWM generator operates in. Therefore, an average-value model is used for this study. The Simulink model of this average-value converter is presented in figure 4.8.

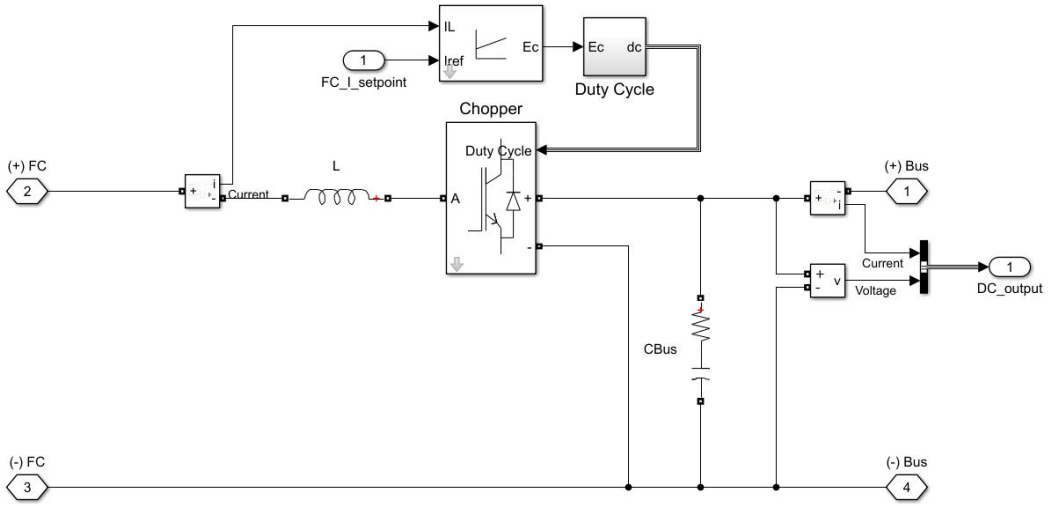

Figure 4.8: Simulink model of average-value DC/DC converter

4.3.3. Converter control

DC/DC converters have an important function in addition to the voltage conversion across the device. They also play an important role in the control of the FC output. The stack's voltage follows from its current set-point and the polarisation curve. On the other side of the converter, the bus voltage is determined by the

battery and the output current of the converter can then be determined by respecting the power balance (eq. 4.35). The current set-point of the fuel cell system is now used to determine the converter's duty cycle. This set-point is compared to the actual current and a Proportional-Integral controller maintains a stable conversion.

The average-value chopper contains a controlled current source and a controlled voltage source [61]. These sources control the stack voltage and current to the bus based on the fuel cell current, bus voltage and duty cycle. All converter types that are discussed (buck, boost and buck-boost) can be modelled with this converter model by changing the conversion ratio in the chopper. The corresponding equations for each type are given in table 4.5.

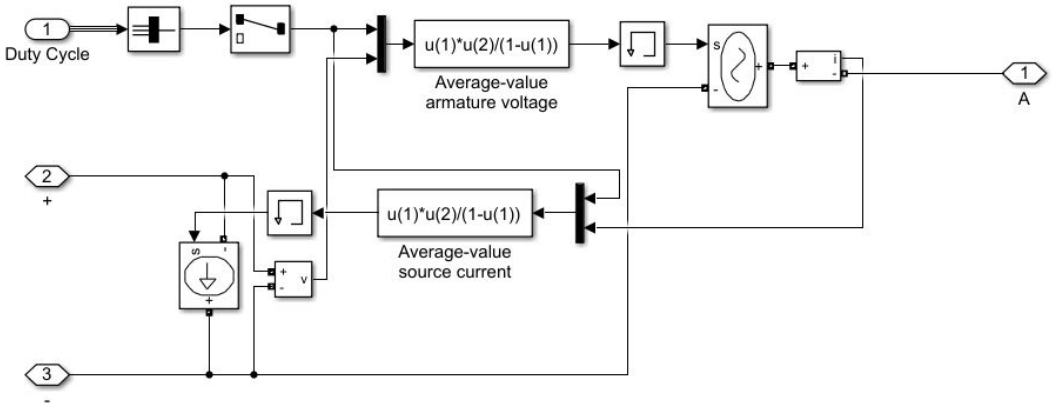

Figure 4.9: Simulink model of an average-value chopper in the DC/DC converter model

Converter type	Conversion ratio	Fuel cell voltage	DCus current
Buck	$M = D$	$V_{FC} = D \cdot V_{DC\ bus}$	$I_{DC\ bus} = D \cdot I_{FC}$
Boost	$M = 1/(1-D)$	$V_{FC} = V_{DC\ bus}/(1-D)$	$I_{DC\ bus} = I_{FC}/(1-D)$
Buck-boost	$M = D/(1-D)$	$V_{FC} = D \cdot V_{DC\ bus}/(1-D)$	$I_{DC\ bus} = D \cdot I_{FC}/(1-D)$

Table 4.5: Conversion ratio's for different converter types [30]

Discontinuous conduction mode

The conversion ratio's from table 4.5 are only valid under the assumption of 'continuous conduction mode'. Discontinuous conduction mode is explained by [31]: if the load resistance (R_0) increases, the load current will decrease consequently (if bus voltage remains constant. The magnitude of ripple currents is independent of the average current value. If the inductor current becomes too low, a point is reached where this amplitude exceeds the average value and the inductor current becomes negative. The diodes in the circuit (fig. 4.6) should prevent this, which results in three subdomains in T_s for the inductor current as illustrated in figure 4.7b (rising, falling and constant (zero) current). This behaviour is known as discontinuous conduction mode.

These switching harmonics are not present in this model due to the implementation of an average-value converter. However, inductors and capacitors are still needed to ensure stability between steady-state conditions. For example, the converter might be exposed to high-frequency variations in load and it is important that continuous conduction mode is maintained here. Therefore, the values for the inductance and capacitance are based on the critical values for continuous conduction mode. These expressions provide the minimum values for the LC values[36]:

$$L_c = \frac{1-D}{2 \cdot f_s} \cdot R_0 \tag{4.38}$$

$$C_c = \frac{1-D}{16 \cdot f_s \cdot L_c} \tag{4.39}$$

The load can be determined with Ohm's law (eq. 4.40) and equation the relationship between voltage, current and power. The nominal fuel cell load has a resistance of 9.5 Ω on the DC bus side. The duty cycle is computed

with the relationships from table 4.5. Finally, the switch frequency is 8 kHz, which is the switch frequency for the electric motor. It is assumed that the whole system would work on this frequency. This yields a critical inductance and capacitance of approximately 0.3 mH and 13 mF, respectively.

$$V = I \cdot R \tag{4.40}$$

4.4. Hybrid power supply model

The models that are discussed in this chapter are coupled according the topology from figure 3.3. Previous studies have concluded that either one or two fuel cell stacks are required. Both models are shown in figure 4.10 and 4.11. In these models, some simplifications are made, most important being the facts that 1) the balance of plant is not modelled, 2) the battery resistance is constant and 3) the DC/DC converter efficiency is neglected. The balance of plant components use parasitic power and efficiency will be further reduced, especially at low and high fuel cell power. Following the stack efficiency gives a false impression in these domains. Also, the battery efficiency is somewhat overestimated as LTO batteries have efficiencies between 95% and 98% at nominal conditions [43]. Finally, the converter is assumed to be ideal where actual efficiency is estimated at 95%. Overall, this will result in an optimistic energy consumption for the sequel of this study.

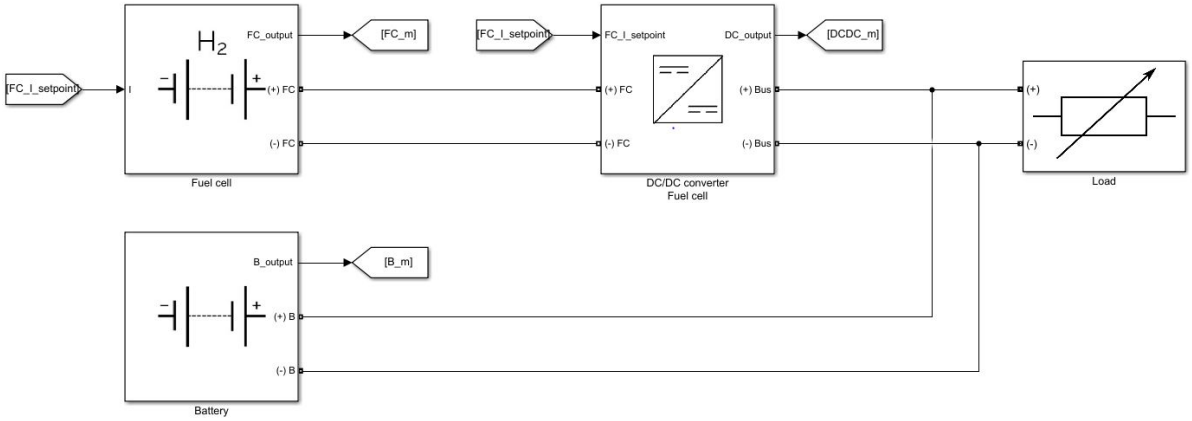

Figure 4.10: Simulink model of the hybrid power supply with one fuel cell

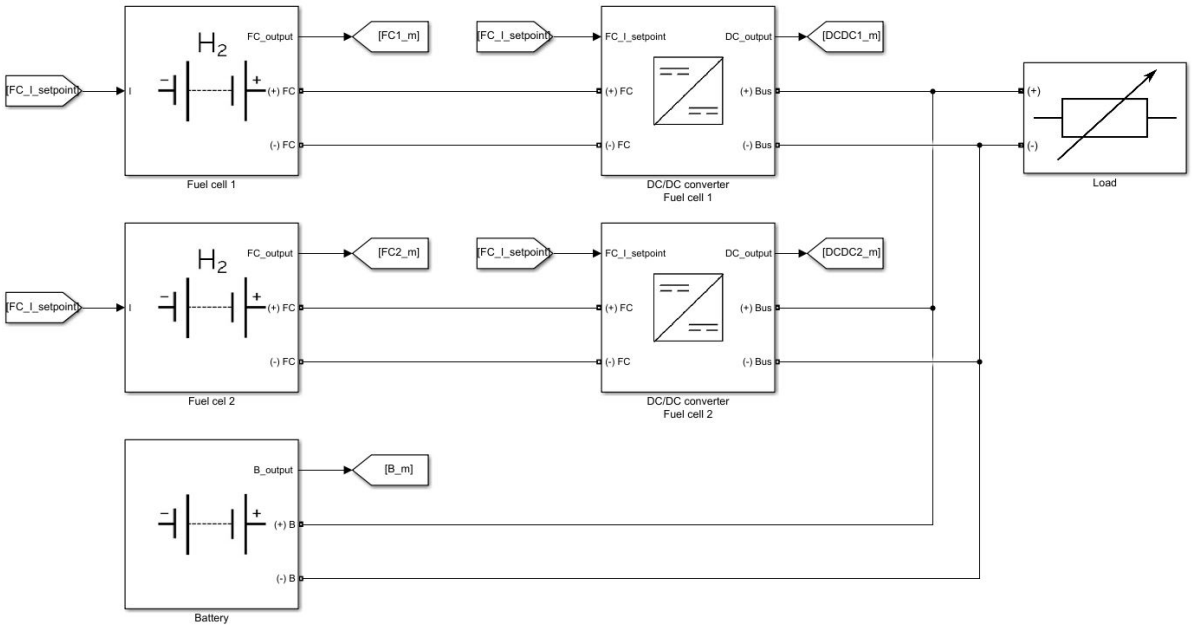

Figure 4.11: Simulink model of the hybrid power supply with two fuel cells

5

Energy analysis for operational profiles

The FCS1204 can be outfitted with different combinations of fuel cell power and battery capacity. The hybrid power supply model was introduced in chapter 4. In this model, the vessel was either equipped with one or two fuel cell stacks with a maximum power of 120 kW. A battery supports the fuel cell and delivers extra power above the stack's maximum (boosting). The configuration can be outfitted with five batteries with a capacity ranging from 45 to 225 Ampere-hour, resulting in ten configurations which are tested in this chapter in order to select the most suitable configurations for the operational profiles. The configurations are tested with the hybrid power supply model. The energy consumption is chosen as most important criterion for the selection of the configurations, but fuel consumption and stack efficiency are also discussed here.

This chapter first discusses different energy management strategies for hybrid fuel cell vehicles. State-based energy is selected as energy management strategies and the trade-offs for this decision are also discussed here. This is followed by the presentation of the settings for this management system. The operational profiles of the survey vessel and harbour patrol vessel are then simulated in the hybrid power supply model. Based on the results from these simulations, the most suitable configurations are selected.

5.1. Energy management

The energy management strategy of hybrid energy sources can have a large impact on fuel consumption, efficiency and lifetime [37]. Figure 3.4 showed the hierarchy of energy management and power management, where energy management stands at the top level. Power management is handled at a lower level and implemented in the model in the power converter. Different energy management strategies for the top level are suggested by recent studies.

5.1.1. Energy management strategies

Many different management strategies are suggested for hybrid electric vehicles by recent studies. Energy management is often approached from different perspectives. Examples of objectives are to minimise hydrogen consumption, to sustain a battery state of charge or to maximise the fuel cell or system efficiency [13]. The management strategies under consideration are suggested by [13, 37, 70] and they are briefly discussed.

Proportional-Integral control

PI controllers are relatively simple to implement. This method can be used for various objectives, such as maintaining a certain SOC. The deviation from the SOC set-point is then used by the PI controller to determine the battery power. The difference between battery power and load power is then provided by the fuel cell module. PI control can also be used to control the fuel cell power and let the battery follow the difference between reference fuel cell power and the load power. The control parameters should be tuned properly for the right balance between response time and stability.

State-based

State-based is a deterministic control strategy. It is also known as rule-based or heuristic control. Energy management is based on a set of rules which splits the power between the fuel cell system and battery. For

instance, if the load is low and SOC is very high, the rules might prescribe that the battery covers the total load. The operational states, or total set of rules, are based on the limits of the energy suppliers, state of charge and required power. This type of energy management is easy to implement and often intuitive to understand. It is fairly easy to add multiple states or other criteria. The most common objective for this type of EMS is to attain a high system efficiency of the hybrid power supply.

Equivalent fuel consumption minimisation
In ECMS energy management is a real-time optimisation strategy. The energy suppliers are given an operational range (with high efficiency). The power consumption from the battery is then expressed as equivalent hydrogen consumption. This equivalent consumption follows the idea that discharging the battery now will lead to extra fuel consumption in the future for recharging. A cost function is used to minimise the instantaneous hydrogen consumption. If the SOC is high, the "costs" for using the battery are low and vice versa. In this way, the hydrogen consumption is optimised.

Charge depleting charge sustaining
In CDCS energy management, the philosophy is to utilise all energy that is initially stored in the battery. At the beginning of the voyage the battery is fully charged. The power is first supplied by the battery until the SOC reaches its reference value (in general low). The system then switches to charge-sustaining mode where the fuel cells are used to provide the load power and maintain the SOC at the specified level. It is fairly simple to implement and has the potential to minimise the fuel consumption for the trip.

5.1.2. Selection of EMS

These energy management strategies under consideration can now be compared directly with each other. A number of criteria are formulated and based on the comparison with respect to these criteria, one EMS is selected for the FCS1204. Obvious criteria are system efficiency and fuel consumption. Simplicity and the effect on operability are added to the selection criteria.

System efficiency
The system's efficiency is expected to be largest for ECMS and state-based EMS. An efficient domain is specified for the fuel cells and battery for both management strategies. Poor efficiency regions are therefore avoided [13]. In CDCS management, the battery is prioritised. During charge depleting this results in a very high efficiency, but this is not necessarily the case during charge sustaining. In CS mode it might be more efficient to increase fuel cell power above load power and recharge the battery with the surplus, but this does not follow the CDCS philosophy. For PI strategy, the correction factor can become very large due to the integral part of the controller. This is the case when the battery is discharged below the reference SOC for a prolonged period (during power boosting for instance). If fuel cell power becomes available for recharging, this large correction factor results in maximum fuel cell power with low efficiency. An anti wind-up mechanism can improve this, however.

Fuel consumption
Obviously, ECMS is most promising when it comes to the minimisation of fuel consumption, since it is an optimisation algorithm with this purpose. The usage of the battery can be prioritised over the usage of the fuel cell stack, when the SOC is high, for the other management strategies. This would reduce the instantaneous fuel consumption. The fuel cell module is then used as range extender when the battery is discharged, either by recharging or by providing the load power.

Simplicity
Novel management systems reduce the crew's degree of control. It is important for the vessel's crew to understand the energy management philosophy in order to operate the vessel safely and with confidence. This is in line with the valid design approach of the 'KISS-principle' (keep it simple & straightforward) where unnecessary complications are avoided.

Most of the presented EMS's are fairly simple to understand. ECMS is the most complex management strategy due to the optimisation algorithm. PI control is also relatively simple, but the required anti wind-up mechanism makes it more complex compared to CDCS for instance. The concept of state-based strategy is also fairly simple, but a large set of rules could make it confusing for the vessel's crew.

Effect on operability
A lot of research has focused on the optimisation of energy management for hybrid electric vehicles for other mobility industries, such as automotive [41, 53, 70]. The main objective here is to maintain a steady SOC during operation [13, 53]. It was seen in the operational profiles for the FCS1204 that the vessel's average speed usually deviates from the top speed. For these different conditions, different SOC's might be desired.

The operational profiles that are presented in chapter 3 show that the vessel's speed varies significantly over time. One of the main functions of the battery is to provide additional boosting power when sailing at top speed, which requires a high state of charge. Both ECMS and CDCS try to maintain a steady state-of-charge which is relatively low. If the battery is fully loaded at the beginning of the trip, it can still deliver energy to sail at a high speed. However, after a number of hours of sailing, the battery charge level is maintained at a low SOC. Due to this, the vessel's operability is reduced as it can not sail at top speed at the end of the day. The profiles show that this is required for both the survey and harbour patrol vessel. The battery reference value can easily be changed during the trip for both PI control and state-based energy management.

Conclusion
A score for each criteria can now be assigned to each management strategy. The assigned scores range between 1 and 3 and the total score gives insight in which strategy seems most promising for this application. Table 5.1 shows that state-based EMS is most suitable for this study. PI control, however, can accurately control the output of components by employing a feedback loop. Therefore, PI control is used in the power management to govern the fuel cell current (and motor speed in chapter 6).

EMS	Efficiency	H_2 consumption	Simplicity	Operability	Total score
PI control	2	2	2	3	9
State-based	3	2	2	3	10
ECMS	3	3	1	1	8
CDCS	2	2	3	1	8

Table 5.1: Score table with respect to efficiency, fuel consumtpion, simplicity and operability for different energy management strategies

5.1.3. Rules for state-based EMS

It is recalled that the philosophy of hybridisation is to utilise multiple energy sources to ensure efficient operation in various conditions [74]. Many conditions can be added to the set of rules in order to realise this statement. The set of rules that is defined for this study is based on [13]. However, the battery is given higher priority compared to the original set of rules. This means that a larger fraction of the load power is assigned to the battery if the SOC is high. Also, the SOC where the FC stack takes over the load power is reduced from 50% to 15%. Due to this, only some buffer energy remains present in the battery to avoid deep discharge cycles.

A part of the CDCS philosophy is implemented by giving the battery high priority. However, a major drawback of this EMS was that the charge level remained low after charge depletion. A second mode is added to the set of rules, which is called 'charge mode'. This mode is manually activated by the vessel's crew if they anticipate that they need battery energy for boosting in the future. A time signal, which is defined by the author, is used to (de)activate battery charging. Two charge modes (M) are implemented in the model: nominal and fast charge mode. For the first mode it requires a number of hours to recharge the battery. The survey vessel has sufficient time for this. Fast charge mode could recharge the battery in one hour or less, but the charging efficiency is lower due to high current (eq. 4.26). The rules for discharge and charge mode are presented in table 5.2 and 5.3. The first number in the state number refers to the mode, where 0, 1 and 2 are used for discharge mode, charge mode and fast charge mode, respectively.

Determination of set-points
The set of rules is based on a number of set-points for the fuel cell power pack and battery. For the fuel cell system this is minimum, nominal and maximum power. The nominal and maximum power of the stack are 50 kW and 120 kW, respectively. The minimum power follows from the efficiency curve that takes parasitic losses into account. The system's efficiency is highest around the nominal power and goes towards zero at lower powers. Therefore, the minimum FC stack power is set at 10% of the nominal power, i.e. 5 kW.

SOC	State	Rule	Fuel cell power
SOC > 80%	0.1	$P_L \leq P_{FC,min}$	$P_{FC} = 0$
	0.2	$P_L \leq P_{FC,min} + P_{B,opt}$	$P_{FC} = P_{FC,min}$
	0.3	$P_L \leq P_{FC,max} + P_{B,opt}$	$P_{FC} = P_L - P_{B,opt}$
	0.4	$P_L > P_{FC,max} + P_{B,opt}$	$P_{FC} = P_{FC,max}$
15% ≤ SOC ≤ 80%	0.5	$P_L \leq P_{FC,min}$	$P_{FC} = 0$
	0.6	$P_L \leq P_{FC,min} + P_{B,opt}$	$P_{FC} = P_{FC,min}$
	0.7	$P_L \leq P_{FC,nom}$	$P_{FC} = P_L - P_{B,opt}$
	0.8	$P_L \leq P_{FC,nom} + P_{B,opt}$	$P_{FC} = P_{FC,nom}$
	0.9	$P_L \leq P_{FC,max}$	$P_{FC} = P_L - P_{B,opt}$
	0.10	$P_L > P_{FC,max}$	$P_{FC} = P_{FC,max}$
SOC < 15%	0.11	$P_L \leq P_{FC,max}$	$P_{FC} = P_L$
	0.12	$P_L > P_{FC,max}$	$P_{FC} = P_{FC,max}$

Table 5.2: Set of rules for state-based EMS in discharge mode (M = 0)

SOC	State	Rule	Fuel cell power
SOC < 100% & M = 1	1.1	$P_L + P_{B,opt} \leq P_{FC,min}$	$P_{FC} = P_{FC,min}$
	1.2	$P_L + P_{B,opt} \leq P_{FC,max}$	$P_{FC} = P_L + P_{B,opt}$
	1.3	$P_L + P_{B,opt} > P_{FC,max}$	$P_{FC} = P_{FC,max}$
SOC = 100% & M = 1	1.4	$P_L \leq P_{FC,max}$	$P_{FC} = P_L$
	1.5	$P_L > P_{FC,max}$	$P_{FC} = P_{FC,max}$
SOC < 100% & M = 2	2.1	$P_L + P_{B,rated} \leq P_{FC,min}$	$P_{FC} = P_{FC,min}$
	2.2	$P_L + P_{B,rated} \leq P_{FC,max}$	$P_{FC} = P_L + P_{B,rated}$
	2.3	$P_L + P_{B,rated} > P_{FC,max}$	$P_{FC} = P_{FC,max}$
SOC = 100% & M = 2	2.4	$P_L \leq P_{FC,max}$	$P_{FC} = P_L$
	2.5	$P_L > P_{FC,max}$	$P_{FC} = P_{FC,max}$

Table 5.3: Set of rules for state-based EMS in charge mode

According the product specification sheet one battery module has a rated capacity of 45 Ah and, hence, the nominal current is 45 A for a battery module (1C). The optimal battery power is lower as a result of increased efficiency at lower currents (sec. 4.2.2). [86] presents a rule of thumb for the optimal battery current, which corresponds to a C-rate of 0.2:

$$I_{B,opt} = 0.2 \cdot Q_{rated} \tag{5.1}$$

5.2. Energy consumption

There will be a large difference in weight between the smallest and largest configuration. The effect of a larger displacement on power was seen in figure 3.1 so it is expected that a small configuration has a lower energy consumption. The weight of the configuration is estimated with equation 5.2.

$$W_s = W_{lightship} + W_{FC} + W_B + W_{tanks} + W_{EM} \tag{5.2}$$

Other weight groups are not considered here, so this is a simplified estimation of the weight. It is expected that other weight such as auxiliary systems, crew and passengers are more or less the same for the configurations. The displacement without propulsion systems is 9 tonnes. A reference fuel cell stack is used in the model and there is no information available with respect to weight for this stack. The power density of a fuel cell module is estimated by [98] at 0.25 kW/kg and each hydrogen tank weighs 120 kg in total (112 kg for the tank and 8.4 kg hydrogen). One battery pack has a weight of 408.8 kg. The Danfoss machines have a weight of 295 kg:

$$W_s = 9 \cdot 10^3 + \frac{N_{FC} \cdot P_{FC} \cdot 10^{-3}}{0.25} + N_p \cdot 408.8 + 6 \cdot 120 + 2 \cdot 295$$

In other words, the displacement depends on two variables: the amount of fuel cell modules and the size of the battery. Each configuration is a unique combination of fuel cell power and battery energy. The required power for each configuration is estimated with a 2-D lookup table containing the information from the PSD (speed, displacement and power). The original PSD gives the brake power of the engine, but both the PMSM

and inverter induce a power loss between the DC bus and outgoing shaft. The power at the DC bus, rather than P_{EM}, is the actual load of the hybrid power supply. Therefore, the calculation includes a PMSM efficiency of 96% (app. D.1) and the DC/AC inverter efficiency is set at 97.5%, which is a representative value for Danfoss inverters that operate at 675 V_{DC} (app. D.2). It is recommended to start a trip with a fully charged battery and return with batteries discharged to 15% (to maintain a buffer). In this way, all available energy is used. Besides this, it is more expensive to recharge batteries with the vessel's hydrogen compared to shore charging.

The lightship without any equipment (9 tonnes) is used as a benchmark for the results of this energy analysis. This benchmark gives the minimum amount of energy required to complete an operational profile. Figure 5.1b and 5.1a presents the power and energy consumption for the both operations.

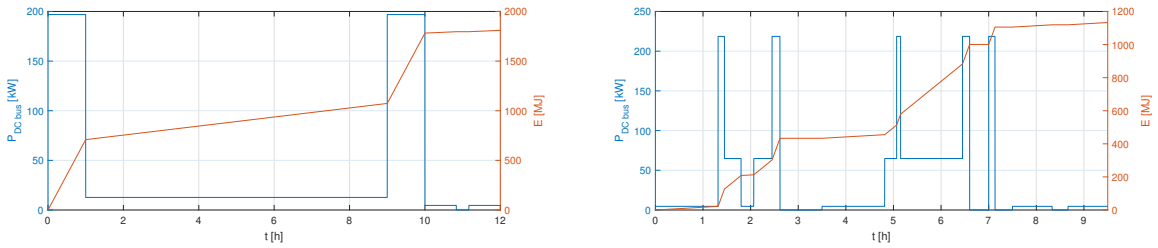

(a) Survey vessel

(b) Harbour patrol vessel

Figure 5.1: Load power and energy consumption for the benchmark case

5.2.1. Survey vessel

The survey vessel is tested first. It is recalled that the vessel sails at a low speed (7 kn) during survey operations, which takes the majority of the time. Transits between the harbour and survey location are sailed at high speed (19 kn). The required endurance at top speed is dependent on the distance to the survey location, which is 19 nm in this case. At the end of the day, the vessel has to sail from the port entrance to the tank station and back to her docking location (5 kn).

One fuel cell stack

The operational profile for a survey vessel is first tested with one fuel cell stack. The battery size is systematically varied. These results are presented in figure 5.2. It is evident that it is not feasible to execute this operation with only one stack. The batteries are discharged in such a short period, because they have to deliver a large fraction of the total required power (53% to 61%). The largest battery, with a rated capacity of 225 Ah, is discharged in 50 minutes. The batteries are not discharged below 10% to avoid deep discharge cycles and improve lifetime [15].

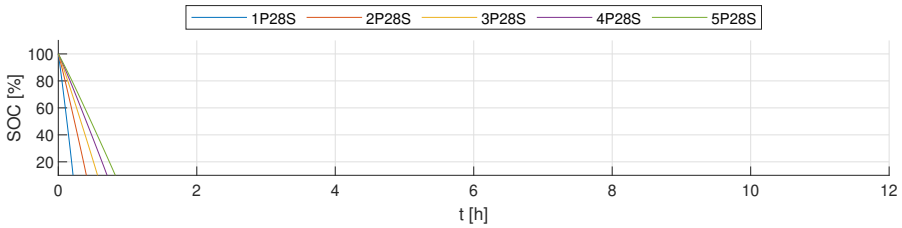

Figure 5.2: Battery state-of-charge for a survey vessel with one fuel cell stack

Two fuel cell stacks

For the second series of simulations, the number of fuel cell stacks is increased to two. Due to this, the total fuel cell power increases to 240 kW (instead of 120 kW) and during boosting, the battery power is significantly reduced. As a result of the increased fuel cell power, the operational profile of the survey vessel is feasible for all configurations. Even the smaller batteries have sufficient energy to sail at top speed for one hour according figure 5.3. The top figure shows how the battery is discharged at top speed and recharged during the survey operation. The interval that the battery is recharged is can be recognised by a rising line in the top figure. A table with all charge intervals can be found in appendix B.1.

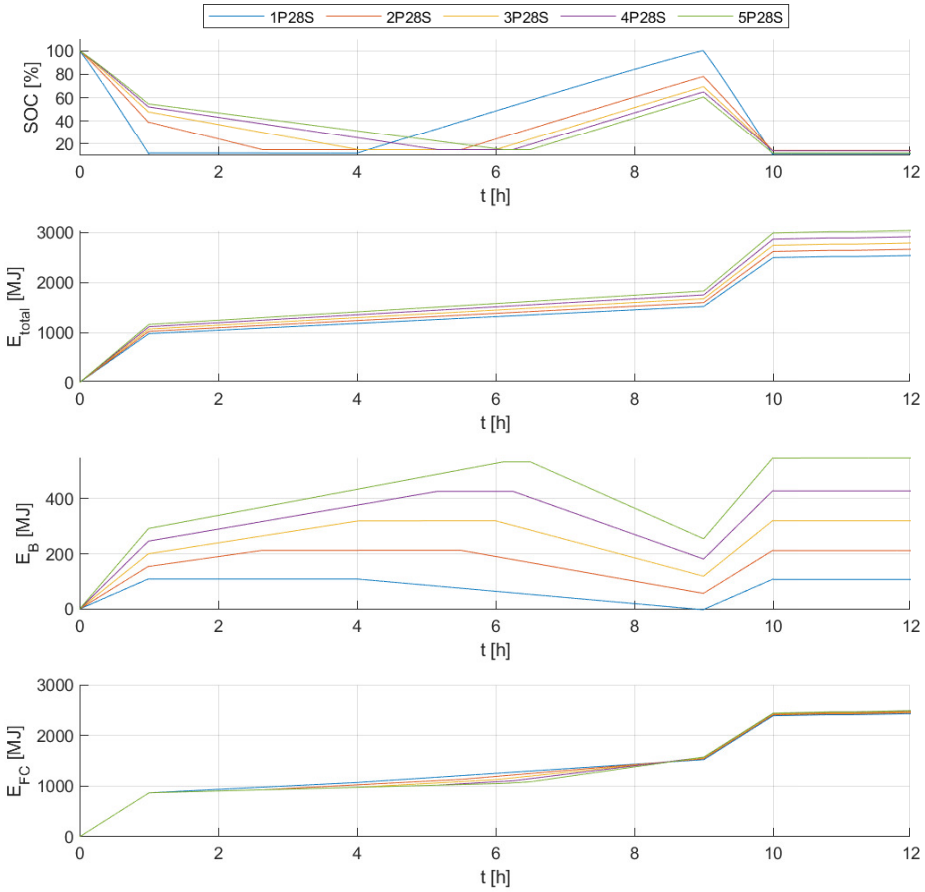

Figure 5.3: Battery state-of-charge and energy consumption for a survey vessel with two fuel cell stacks

The effect of a larger battery has a clear effect on the weight and consequently on the energy consumption (second figure). It can also be seen in the third figure that there is a significant difference between energy delivered by the various batteries. This can be expressed by the degree of hybridisation (H), which can be defined in two different ways: energy hybridisation and instantaneous power hybridisation. The first definition analyses the delivered energy over a complete profile and does also incorporate recharging. Power, being the derivative of energy, is by definition instantaneous. The power distribution during boosting (tab. 5.4) is most relevant, as top speed requirements (and endurance) dictate the sizing. Table 5.5 presents the energy hybridisation of the survey vessel. The total energy consumption is also compared to the benchmark case with a displacement of 9 tonnes (1810 MJ). This can be found under E/E_{ref}.

$$H_P = \frac{P_B}{P_B + P_{FC}}, \qquad H_E = \frac{E_B}{E_B + E_{FC}} \tag{5.3}$$

Battery	W **[t]**	P_{FC} **[kW]**	P_B **[kW]**	$P_{DC\,bus}$ **[kW]**	H_P **[%]**
1P28S	11.7	240.8	30.6	271.4	11.3
2P28S	12.1	240.8	43.4	284.2	15.3
3P28S	12.5	240.8	56.1	296.9	18.9
4P28S	12.9	240.8	68.9	309.7	22.2
5P28S	13.5	240.8	81.6	322.4	25.3

Table 5.4: Power hybridisation during boosting at 19 knots for a survey vessel with two fuel cell stacks

Battery	W [t]	E_{FC} [MJ]	E_B [MJ]	E_{total} [MJ]	E/E_{ref} [%]	H_E [%]
1P28S	11.7	2430	107	2537	140.2	4.2
2P28S	12.1	2451	212	2662	147.1	8.0
3P28S	12.5	2468	320	2788	154.0	11.5
4P28S	12.9	2485	428	2913	160.9	14.7
5P28S	13.3	2491	548	3038	167.8	18.0

Table 5.5: Energy hybridisation for a survey vessel with two fuel cell stacks (E_{ref} = 1810 MJ)

5.2.2. Harbour patrol vessel

The operational area of the harbour patrol vessel is the port of Den Helder, Wadden Sea and North Sea. It sails at low speed during harbour patrol (max. 5 kn) and is capable to sail at high speed (up to 20 kn) for short periods. The average speed outside port is 12 knots. At some instances, the vessel's speed is zero. Normally, this would not necessarily mean that power equals zero as well (bollard pull conditions for example). In this study, however, it is assumed that the power is zero.

One fuel cell stack

The harbour patrol vessel has to sail continuously at top speed for 10 minutes at most. Although top speed is 1 knot higher compared to the survey vessel, the reduced endurance has a positive effect on the set of feasible configurations. A configuration with one fuel cell module has also become feasible albeit with the four largest batteries. The smallest battery contains insufficient energy to provide the required boosting power (fig. 5.4).

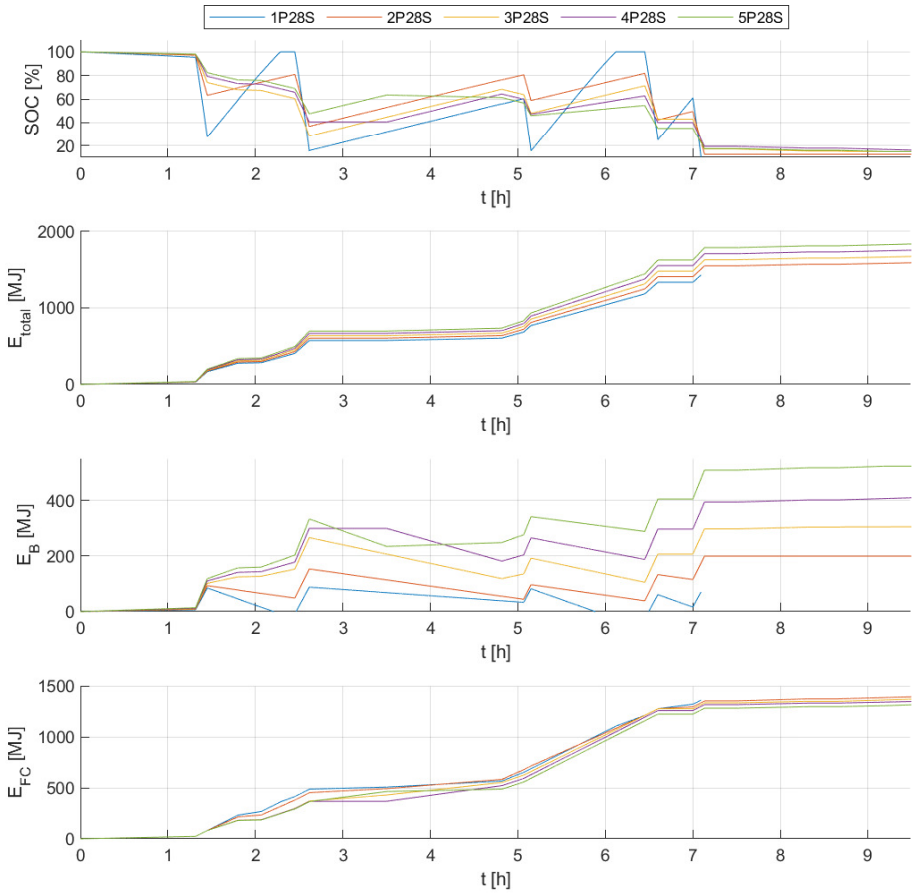

Figure 5.4: Battery state-of-charge and energy consumption for a harbour patrol vessel with one fuel cell stack

Due to the short periods of peak power requirements, the battery management should also be approached differently. For the survey vessel is was seen that there is one complete charge and discharge cycle at most. For the harbour patrol vessel with one FC module this number lies between 1 and 2, which can be derived from the third figure from the top in figure 5.4. The batteries are recharged when the load power is low between periods of sailing at top speed. For larger batteries this is required less often. The charging is modelled manually by a predefined time signal and the charge intervals are presented in appendix B.1. It works also intuitively for the crew to restore the battery charge after it has provided boosting energy.

Battery	W **[t]**	P_{FC} **[kW]**	P_B **[kW]**	$P_{DC\,bus}$ **[kW]**	H_P **[%]**
1P28S	11.2	-	-	-	-
2P28S	11.6	120.4	176.0	296.4	59.4
3P28S	12.0	120.4	189.7	310.1	61.2
4P28S	12.4	120.4	203.4	323.8	62.8
5P28S	12.8	120.4	217.1	337.5	64.3

Table 5.6: Power hybridisation during boosting at 20 knots for a harbour patrol vessel with one fuel cell stack

Battery	W **[t]**	E_{FC} **[MJ]**	E_B **[MJ]**	E_{total} **[MJ]**	E/E_{ref} **[%]**	H_E **[%]**
1P28S	11.2	-	-	-	-	-
2P28S	11.6	1392	199	1592	140.5	12.5
3P28S	12.0	1369	305	1674	147.7	18.2
4P28S	12.4	1346	409	1755	154.9	23.3
5P28S	12.8	1314	523	1837	162.1	28.5

Table 5.7: Energy hybridisation for a harbour patrol vessel with one fuel cell stack (E_{ref} = 1133 MJ)

Two fuel cell stacks

The same simulations are executed with two fuel cell stacks and the set of five batteries. The configuration with the smallest battery is now also suitable for this operational profile. The difference in top speed for the survey (19 kn) and harbour patrol vessel (20 kn) affects the power hybridisation foremost. The maximum fuel cell power remains the same for both profiles (240.8 kW). Hence, the additional energy to sail one knot faster is fully delivered by the battery. This can also be seen by comparing table 5.4 and 5.8, where power hybridisation is at least 6.6% higher for the harbour patrol vessel.

Battery	W **[t]**	P_{FC} **[kW]**	P_B **[kW]**	$P_{DC\,bus}$ **[kW]**	H_P **[%]**
1P28S	11.7	240.8	58.0	298.8	19.4
2P28S	12.1	240.8	71.7	312.5	22.9
3P28S	12.5	240.8	85.4	326.2	26.2
4P28S	12.9	240.8	99.1	339.9	29.2
5P28S	13.3	240.8	112.8	353.6	31.9

Table 5.8: Power hybridisation during boosting at 20 knots for a harbour patrol vessel with two fuel cell stacks

The harbour patrol vessel is the only vessel where it's possible to choose between one or two modules. Hence, it is also possible to compare the energy consumption directly for the two cases (tab. 5.7 and 5.9). One fuel cell stack has approximately the same weight as a battery bank, so one fuel cell stack and battery bank can be replaced for a consumption which is more or less the same. For example: one fuel cell stack with a 135 Ah battery has a similar energy consumption compared to two fuel cell stacks with a 90 Ah battery. This may have an influence on the final system sizing. From an economical point-of-view, it is likely that costs for the second configuration, with two stacks, exceed the costs for the first option due to the high costs of fuel cell stacks. This is outside the scope of this study, but it is worth mentioning.

The second fuel cell module also affects the battery management. The harbour patrol vessel sails at 5 knots in port, which results in a load power ($P_{DC\ bus}$) between 6.9 and 8.4 kW, depending on the displacement. The efficient domain of the stack starts at 5 kW. In case of two fuel cell modules, power is equally split between

Battery	W [t]	E_{FC} [MJ]	E_B [MJ]	E_{total} [MJ]	E/E_{ref} [%]	H_E [%]
1P28S	11.7	1504	102	1606	141.7	6.4
2P28S	12.1	1478	210	1688	149.0	12.4
3P28S	12.5	1446	323	1769	156.1	18.3
4P28S	12.9	1426	425	1851	163.4	23.0
5P28S	13.3	1401	532	1933	170.6	27.5

Table 5.9: Energy hybridisation for a harbour patrol vessel with two fuel cell stacks (E_{ref} = 1133 MJ)

the stacks so the fuel cells will be switched on above a load power of 10 kW. In other words, the energy is completely provided by the battery at this low speed. Table 5.2 tells that the energy is split between the fuel cells and battery for configurations with one stack, where the fuel cell will contribute 5 kW. Therefore, the batteries are discharged faster at low speed for configurations with two fuel cell stacks. On the other hand, at higher load power, the fuel cells provide a larger fraction of the consumed energy. Due to this, the battery requires less recharging in the end, which is also reflected in the number of charge and discharge cycles (fig. 5.5, app. B.1).

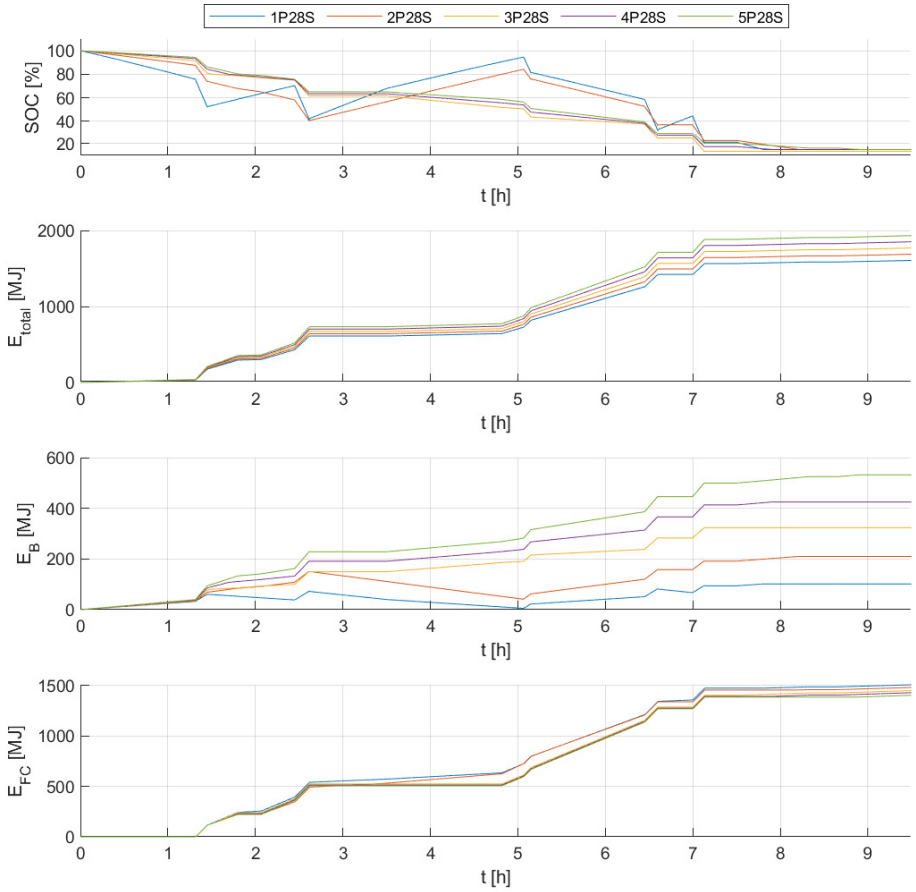

Figure 5.5: Battery state-of-charge and energy consumption for a harbour patrol vessel with two fuel cell stacks

5.3. Notes on fuel consumption and efficiency

In the introduction of this chapter it was mentioned that energy consumption is the most important criterion for the selection of the most suitable configurations. It is difficult to make a fair comparison based on fuel

consumption for hybrid vehicles with energy storage systems. To be more specific, the vessel's logistic fuel is not the only energy source since the battery is also recharged with shore energy. Therefore, the fuel consumption can only be directly compared if the net consumed energy from the battery is zero. This is the case if the vessel returns with 100% SOC, which is counter intuitive. However, fuel consumption and efficiency is important from an operator's perspective so it is worth discussing here.

5.3.1. Fuel consumption

The fuel consumption follows the same trend as the energy consumption from the fuel cells. This deviates from the total energy consumption, because the fuel cells are also used to recharge the battery. During recharging, the stack delivers more power than the instantaneous load power, so the battery becomes a power consumer in this case rather than a source. The fuel consumption plots are presented in figure 5.6a to 5.6c. The cumulative consumption of all simulations is also given in table 5.10.

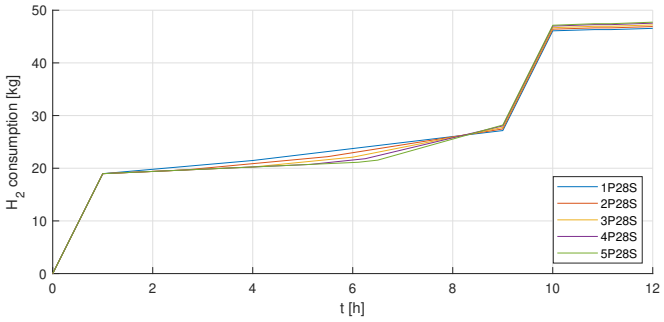

(a) Survey vessel: 2 fuel cell stacks

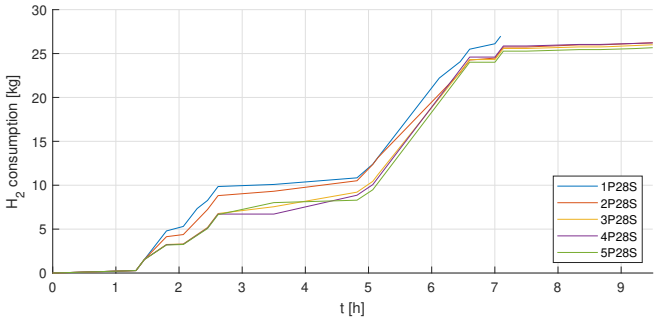

(b) Harbour patrol vessel: 1 fuel cell stack

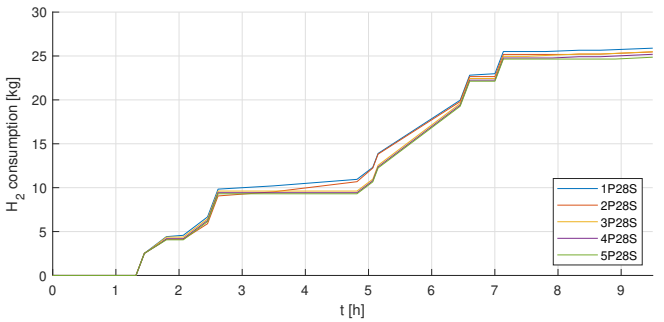

(c) Harbour patrol vessel: 2 fuel cell stacks

Figure 5.6: Hydrogen consumption consumption for the survey and harbour patrol vessel

From table 5.10 it can be seen that the cumulative hydrogen consumption for the survey vessel remains just within the limits of the hydrogen storage. There is only space for six hydrogen tanks and this gives a limit on hydrogen storage of 50.4 kg [98]. The distance to the survey location is thus limited due to the storage capacity of the vessel.

	Survey vessel		Harbour patrol vessel	
Battery	**1 FC stack**	**2 FC stacks**	**1 FC stack**	**2 FC stack**
1P28S	-	46.6 kg	-	25.9 kg
2P28S	-	46.9 kg	26.2 kg	25.5 kg
3P28S	-	47.2 kg	26.0 kg	25.5 kg
4P28S	-	47.5 kg	26.2 kg	25.2 kg
5P28S	-	47.7 kg	25.7 kg	24.9 kg

Table 5.10: Cumulative hydrogen consumption for the survey and harbour patrol vessel

The hydrogen consumption of the survey vessel shows remarkable results. Two opposite trends are observed in the relationship between battery size and hydrogen consumption. Fuel consumption increases with battery size for the survey vessel and the opposite happens for the harbour patrol vessel. It was seen that the vessel's displacement increases with battery size and so does the energy consumption. Therefore, it seems logical that hydrogen consumption does also increase as a consequence. However, a larger battery does also mean that more energy can be subtracted from the battery, which potentially reduces hydrogen consumption.

For the survey vessel it was seen that all batteries require recharging. The recharging has a large impact on the consumption as it requires much more energy to recharge a large battery. In addition to this, the power losses are also larger for a large battery as they increase with resistance and current (eq. 4.26). This can be derived from the foregoing and is emphasised by looking at the fuel consumption rate (fig. 5.7). During the survey operation (between $t = 1$ h and $t = 9$ h) three consumption rates can be seen for each line: (1) after the first period of sailing at top speed, the batteries have some residual energy and load power is split between the fuel cells and battery, (2) the fuel cells take over the total load when the battery reaches 15% SOC, and (3) if battery charging is activated, the fuel cells provide power for both sailing and recharging. Figure 5.7 is now used to subtract the consumption rate for sailing (full FC propulsion) from the total consumption rate, which results in the required consumption rate for recharging only. The integral of this rate gives the cumulative consumption for recharging. This results in values of 1.4 kg for the smallest battery and 4.1 kg for the largest battery. However, figure 5.3 showed that the smallest battery is recharged with 85% and the largest battery with only 45%. So, significantly more hydrogen is consumed for a lower charge level. For the harbour patrol vessel it is seen that the larger batteries (combined with two FC stacks) do not require recharging. So, here it seen that the increased battery size actually results in fuel savings, despite the higher displacement.

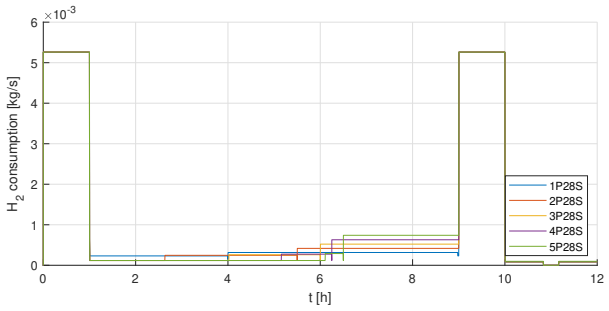

Figure 5.7: Hydrogen consumption rate for the survey vessel with two fuel cell stacks

5.3.2. Efficiency and system performance

It is relevant to check if there are no large deviations between the efficiencies for the simulations. The stack efficiency is computed by the generic model. The stack efficiency, however, gives an incomplete figure: the balance of plant efficiency, DC/DC converter losses. Also, the power losses in the battery are probably underestimated, so the actual efficiency would be lower in reality. Figure 5.8a and 5.8c show the stack efficiency and load distribution for the harbour patrol vessel with equal battery size (4P28S) and either one or two fuel cell modules. The same figures are added to appendix B.2 for all completed simulations. At some instances, where the fuel cells are switched off, the stack efficiency is equal to zero. These instances are removed from

the results and the mean efficiency is computed for the filtered data sets (tab. 5.11). The mean efficiency of the two examples, which are highlighted below, is in the same order of magnitude (57.1% vs 57.4%). However, the configuration with two fuel cell stacks consumes 1 kg less hydrogen (tab. 5.10), despite the higher displacement. This results from the fact that the fuel cells are switched off for a larger fraction of the time and the the fact that the battery does require recharging.

	Survey vessel		**Harbour patrol vessel**	
Battery	**1 FC stack**	**2 FC stacks**	**1 FC stack**	**2 FC stacks**
1P28S	-	62.2 %	-	62.8 %
2P28S	-	62.3 %	58.3 %	60.9 %
3P28S	-	62.4 %	58.0 %	58.6 %
4P28S	-	62.5 %	57.1 %	57.4 %
5P28S	-	62.7 %	59.0 %	59.0 %

Table 5.11: Mean stack efficiency for the survey and harbour patrol vessel

It should be kept in mind that the model has some simplifications. The mean stack efficiency does not give a representative figure for the total efficiency of the hybrid power supply. First of all, the battery and DC/DC converter model are simplified, resulting in a higher efficiency. The battery efficiency are expected to lie between 95% to 98% for LTO batteries at ambient temperature and the converter efficiency is also high (95%). The power loss due to BoP components is also left out of the scope. Especially at low and high FC loads these power losses can be significant, which was shown in figure 4.2. It can be expected that the mean FC system efficiency would be approximately 10% to 25% lower compared to the mean stack efficiency in table 5.11.

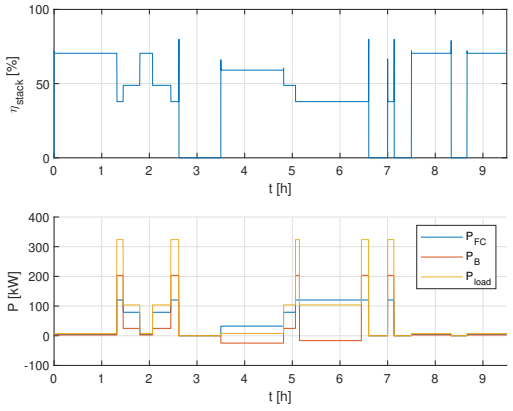

(a) 1 fuel cell stack: stack efficiency and load distribution

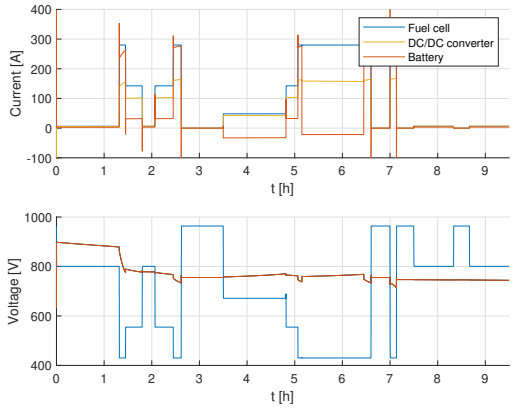

(b) 1 fuel cell stack: voltage and current

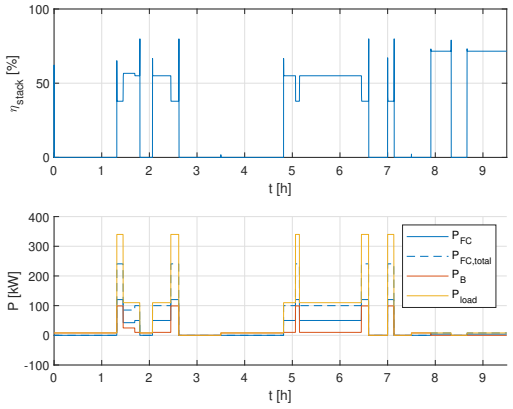

(c) 2 fuel cell stacks: stack efficiency and load distribution

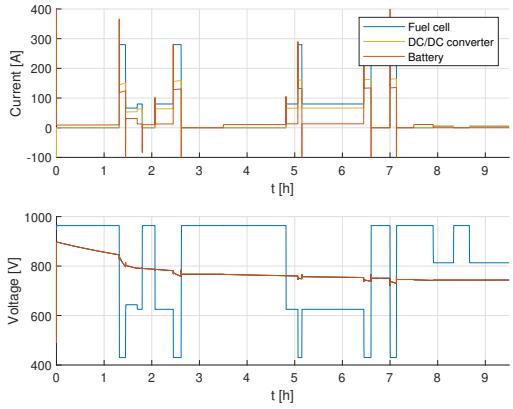

(d) 2 fuel cell stacks: voltage and current

Figure 5.8: Efficiency and system performance for a harbour patrol vessel with either one or two fuel cell stacks and a 180 Ah (4P28S) battery

In addition to this, it is also important to check if the DC system does not exceed any specified limits. The following limits are analysed for the executed simulations:

- Fuel cell current: the FC's allowable load change is approximately 10% of the maximum power per second [24], which is modelled in the power management module. This limit is explained in more detail in chapter 7. The load power, however, is modelled as a step function. Due to this, large peaks are observed in the battery current (fig. 5.8b and 5.8d). The dynamic analysis of the system will give a better insight in the actual ramp support of the battery.

- Battery current: the battery maximum battery current is dependent on battery size. The highest battery current is observed for the harbour patrol vessel with one FC module. This makes sense, because the battery power is also largest for this set. Then still, the peak current stays within the battery limits for all simulations.

- DC voltage: The AC system requires a minimum DC voltage of 675 V. For most simulations the DC voltage is sufficiently high, except for the harbour patrol vessel with one fuel cell stack and the smallest battery from the set of feasible configurations (2P28S), see appendix B.2). For this configuration, the battery's current is close to its maximum, so it is discharged at a high C-rate. In figure 4.4 it was seen that a high C-rate results in a faster voltage drop. Due to this, the voltage drops below 675 V before the battery has reached 10% SOC.

5.4. Selection of configurations

The simulated profiles give limited insights in the endurance at top speed, because only two speeds are tested (19 and 20 knots). The endurance at top speed is often an important design requirement. Therefore, a top speed-endurance diagram is developed for all speeds where the battery operates as power booster. This diagram shows the maximum endurance until the battery is fully discharged, measured in time, for various speeds and configurations. The minimum required endurance is 30 minutes, otherwise the benefit of a high top speed is very limited. These top speed diagrams are shown in figure 5.9 and help to select a battery size for the propulsion system. The maximum time at top speed drops rapidly, but the vessel can still achieve speeds in the same order of magnitude as the reference vessel with a top speed of 26 knots. However, the endurance is massively reduced. The maximum range at a speed of 26 knots is 13.5 nautical miles, where the reference vessel could sail over 200 miles. Appendix B.5 also shows the top speed-endurance diagram with respect to sailing distance. It should be noted, however, that the propulsion motors in this study are sized for a top speed of 20 kn based on the operational profiles, rather than 26 kn.

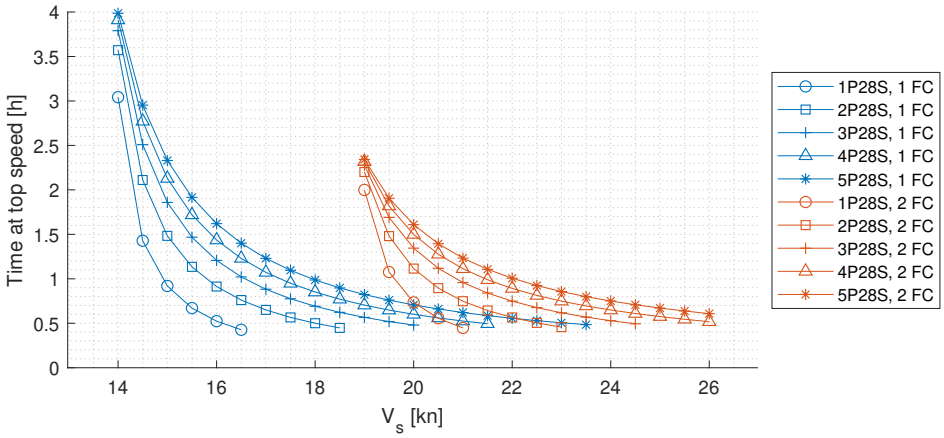

Figure 5.9: Maximum endurance during boosting at various top speeds

Two configurations are now selected as most suitable configurations for the second part of this study. In chapter 2 it was noted that batteries have a high specific power and fast response, where fuel cell systems are high specific energy sources with a slower response [57]. The endurance at top speed is higher for the survey vessel. From the PSD and energy analysis it is evident that top speed plays a major role in the energy

consumption. Hence, a high gravimetric energy density is most important for the survey vessel. The high endurance pleas for a second fuel cell (i.e. a lower degree of hybridisation). Therefore, the configuration with two fuel cell stacks and a 90Ah battery (2P28S) is selected for the survey vessel. The harbour patrol vessel has a relatively low required endurance at top speed. It can be expected that the vessel uses much energy during manoeuvring, so high specific power and fast response is important here. Therefore, the configuration with one fuel cell stack and 135 Ah battery (3P28S) is selected for this purpose. This vessel can also be used for survey purposes, but the endurance at 19 knots would then be 35 minutes at most (fig. 5.9). For both cases, the configurations with the smallest feasible battery are avoided. These batteries will result in a lighter vessel, hence less energy is required. However, these configurations have a higher risk that the voltage value of 675 V can not be maintained at high loads.

Finally, it should be noted that this energy analysis gives an optimistic impression with respect to the reality. First of all, the simplifications in the model give a higher efficiency compared to the overall system efficiency, which would be expected if the converter and balance of plant components are included in the system efficiency. The battery efficiency can also be computed more accurately by including the variation in internal resistance in the model. The power losses are expected to be underestimated in this study. This is also an argument why the smallest feasible batteries are avoided. In fact, they are selected conservatively as it is acknowledged that there would be some extra losses in reality.

In addition to this, in this energy analysis, the battery is recharged when it is at a very low SOC and the vessel returns with only 15% SOC, because it is more expensive to recharge batteries with the vessel's hydrogen compared to shore charging. It might be very well possible that a crew would be more conservative with respect to energy management. For example, it might be possible that the crew activates charge mode immediately after sailing a prolonged period at top speed. In this way, they have battery energy available at any time. As a result, the batteries may return with a higher SOC than necessary. So, in reality hydrogen consumption is probably higher due to both simplifications in the model and a potentially more conservative approach to energy management. With the harbour patrol vessel, this would not be a problem, because the vessel only uses half of the available hydrogen. The survey vessel, however, consumes over 90% of the available hydrogen, so extra hydrogen consumption can become critical.

6

Modelling of all-electric ship propulsion

The fuel cell/battery propulsion system is introduced in section 3.2. It was divided in two parts: the hybrid power supply and the electric drive. The hybrid power supply is addressed in chapter 4 and the electric drive is discussed here. In chapter 2 it was concluded that permanent magnet synchronous motors are most suitable for marine applications. This is due to their high efficiency, power density and reliability [17]. In addition to this, PMSM's have no rotor windings. Hence, there are no copper losses in the rotor and less cooling is required.

This chapter will discuss the PMSM model (sec. 6.1) and vector control shortly (6.2). The working principle of a DC/AC inverter is discussed in section 6.3 together with the inverter model. Similar to the hybrid power supply model, a set of dedicated blocks for the modelling of a PMSM is available in the SPS library. The ship and propeller models are developed in section 6.4 to work towards a complete propulsion model. This, second more-detailed, model will be used to analyse the energy flow in the system under transient conditions.

6.1. Permanent magnet synchronous motor model

The stator of a PMSM is connected to the three-phase AC supply. A rotating flux is created by a number of field windings in the stator. The rotor has the same amount of poles, created by permanent magnets. These magnets are locked onto the rotating field which is created by the stator [49]. The interaction between the current-carrying conductors of the stator and rotor magnets creates an electromagnetic torque, which is translated to a mechanical torque and rotational speed. The modelling of a PMSM requires both an electrical model for the computation of the electromagnetic torque and a mechanical model for the speed of the rotor [62].

6.1.1. Electrical model

Alternating current is, in contrast to direct current, electrical current which reverses direction and strength periodically. In a three-phase sinusoidal AC supply, each line has certain amplitude and phase difference of one third of a period with respect to the other lines:

$$\begin{cases} I_a = I \cdot \cos(\omega t) \\ I_b = I \cdot \cos(\omega t - \frac{2\pi}{3}) \\ I_c = I \cdot \cos(\omega t + \frac{2\pi}{3}) \end{cases} \tag{6.1}$$

The electrical model can be defined for three different reference frames: the 'abc' frame from the three-phase supply, frame '$\alpha\beta$' which is a four-quadrant static frame and rotating frame 'dq' [35]. The interaction between the abc and dq frames is most relevant for the model since the rotor is controlled through the dq frame (more on this in section 6.2). The transformation between these two frames is called the 'abc2dq transformation' and defined by the following relationships [63]:

$$\begin{bmatrix} V_d \\ V_q \end{bmatrix} = \frac{2}{3} \begin{bmatrix} \sin\theta_e & \sin(\theta_e - 2\pi/3) & \sin(\theta_e + 2\pi/3) \\ \cos\theta_e & \cos(\theta_e - 2\pi/3) & \cos(\theta_e + 2\pi/3) \end{bmatrix} \cdot \begin{bmatrix} V_a \\ V_b \\ V_c \end{bmatrix} \tag{6.2}$$

$$\begin{bmatrix} V_a \\ V_b \\ V_c \end{bmatrix} = \begin{bmatrix} \sin\theta_e & \cos\theta_e \\ \sin(\theta_e - 2\pi/3) & \cos(\theta_e - 2\pi/3) \\ \sin(\theta_e + 2\pi/3) & \cos(\theta_e + 2\pi/3) \end{bmatrix} \cdot \begin{bmatrix} V_d \\ V_q \end{bmatrix} \tag{6.3}$$

Where θ_e refers to the electrical angle of the motor. The electrical angle is the product of the amount of pole pairs (P) and the mechanical rotor angle (θ_m), which follows from the mechanical model. This matrix is used to express the stator (line-to-line) voltage in the rotor reference frame (dq). This results in the following relationships:

$$\begin{cases} V_{ab} = V_a - V_b \\ V_{bc} = V_b - V_c \end{cases} \tag{6.4}$$

$$\begin{cases} V_d = \frac{1}{3} \cdot \left((2V_{ab} + V_{bc}) \cdot \sin\theta_e - \sqrt{3} V_{bc} \cdot \cos\theta_e \right) \\ V_q = \frac{1}{3} \cdot \left((2V_{ab} + V_{bc}) \cdot \cos\theta_e + \sqrt{3} V_{bc} \cdot \sin\theta_e \right) \end{cases} \tag{6.5}$$

The derivation of equation 6.5 from 6.2 is presented in appendix C. The relationship between the stator voltage (expressed in the rotor reference frame), flux, motor inductance and current can then be found with the following differential equations [35, 62]:

$$\begin{cases} \frac{dI_d}{dt} = \frac{1}{L_d} \cdot \left(V_d - R \cdot I_d + L_q \cdot \omega_e \cdot I_q \right) \\ \frac{dI_q}{dt} = \frac{1}{L_q} \cdot \left(V_q - R \cdot I_q - L_d \cdot \omega_e \cdot I_d - \omega_e \cdot \Psi \right) \end{cases} \tag{6.6}$$

Similar to the electrical angle, the electrical rotational speed is the product of the mechanical rotational speed and the amount of pole pairs in the machine. The rotational speed is also computed in the mechanical model. Higher power PMSM's usually have round rotors. These have no variation in inductance for the d- and q-axis [62]. With the current, expressed in the rotor reference frame, an expression is formulated for the electromagnetic torque [35, 62]:

$$T_e = \frac{3}{2} \cdot P \cdot \left(\Psi \cdot I_q + \left(L_d - L_q \right) \cdot I_d \cdot I_q \right) = \frac{3}{2} \cdot P \cdot \Psi \cdot I_q \tag{6.7}$$

6.1.2. Mechanical model

In SPS there are three options for the input of the PMSM: mechanical torque, rotational speed or a physical shaft (which is a port that transfers the signal to the mechanical Simscape environment). The rotational speed is controlled through the AC supply. Load torque, that is computed by the propeller model, is used as input for the PMSM model. The following differential equation describes the mechanical model [54]:

$$\frac{d\omega_m}{dt} = \frac{1}{J} \cdot \left(T_e - T_m - F \cdot \omega_m \right) \tag{6.8}$$

$$\theta_m = \int_0^t \omega_m \cdot dt \tag{6.9}$$

Where J and F refer to the motor's moment of inertia and the viscous friction coefficient, respectively. The moment of inertia follows from the product specification sheet of the Danfoss motor (0.99 kgm^2). The so-called viscous damping is speed-dependent, but the damping coefficient F is assumed to be constant in the PMSM model [62]. The damping coefficient can be estimated by performing a no-load test, where the machine is running at its nominal speed without applying mechanical torque ($T_m = 0$). After starting up, the machine reaches a steady-state at its nominal speed. In this condition, the derivative of rotational speed equals zero:

$$\frac{d\omega_m}{dt} = 0 \qquad \longrightarrow \qquad T_e - T_m - F \cdot \omega_m = 0 \tag{6.10}$$

$$F = \frac{T_e}{\omega_m} \tag{6.11}$$

During the no-load test the voltage and current are measured. These give a power loss that is associated with the damping. From the electrical power loss, the electromagnetic torque in steady-state condition can be calculated:

$$P_e = T_e \cdot \omega_m \tag{6.12}$$

Equation 6.11 and 6.12 are then combined to compute the damping coefficient from the power loss. There is no factory acceptance test (FAT) report available for the selected machine. However, there is a FAT report

available for a larger machine with a similar design and losses should be the same in terms of percentage. The results of this no-load test are considered confidential. The power loss during the no-load test has a magnitude of 1.5% with respect to nominal power, which results in a damping coefficient of 0.17 Nms for the selected PMSM.

6.1.3. Drive characteristic PMSM

A distinct feature of a PMSM is that it can run at a constant speed, independent of the load. In other words, at a given speed the machine is capable of delivering a torque between zero and its maximum. This relationship between torque and speed is explained by [49]: if the machine is not loaded, the north and south pole on the stator and rotor are exactly opposite to each other. Increasing torque creates a phase lag between the magnetic fields of the stator and rotor. This is referred to as the load angle, where the rotor is lagging behind. If the load torque approaches the maximum torque, two identical poles will be opposite to each other. This torque is also called 'Pull-out torque': above this limit no torque is delivered at all, because synchronisation is lost. If the torque set-point is changed, the load angle also changes. Due to this, the machine will run out of synchronous speed for a short a short period until the new set-point is reached. The maximum torque is approximately 1.5 times as high as the continuous torque.

Up to the nominal speed, PMSM's are capable of delivering the nominal torque. This region is called the constant torque speed range (CTSR). Above the nominal speed, the PMSM enters the constant power speed range (CPSR) where nominal power is developed by the machine [52]. In the CTSR, the 'back electromagnetic force' (back EMF) is proportional to speed. At the nominal speed, the amplitude of the back EMF voltage reaches the maximum inverter output voltage (DC voltage) and the machine reaches its maximum continuous power [72]. If speed is increased further, the motor would exceed its limits and, therefore, the CPSR is normally narrow. However, if the magnetic flux is weakened above the nominal speed, the CPSR can be much wider. As a result of flux-weakening, rotational speed can be increased without increasing back EMF voltage. A wide CPSR is beneficial for electric vehicles as maximum power can be delivered for a wide speed range [52, 72]. In the PMSM model a dynamic saturation block is used that implements the torque limit from equation 6.14. Due to this, the stator current is reduced above nominal speed. The drive characteristic of the PMSM is presented in figure 6.1.

$$P_{EM} = T_m \cdot \omega_m = T_m \cdot \frac{N_{EM} \cdot 2\pi}{60} \tag{6.13}$$

$$\begin{cases} \omega_m \leq \omega_{m,nom}, & T_{m,max} = T_{m,nom} \\ \omega_m > \omega_{m,nom}, & T_{m,max} = \frac{P_{EM,nom}}{\omega_m} \end{cases} \tag{6.14}$$

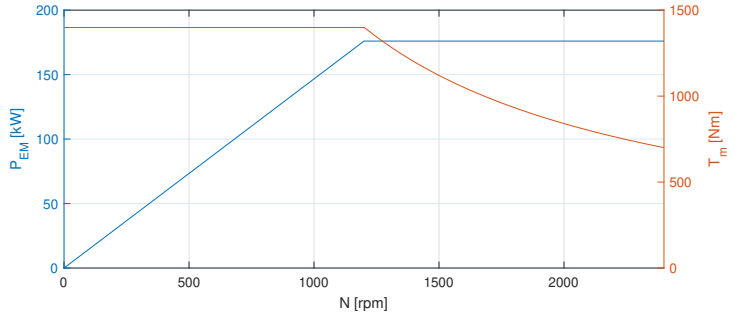

Figure 6.1: Drive characteristic Danfoss EM-PMI375-T1100-1200

The synchronous machine is controlled to maintain an optimal ratio between current and torque. This ratio is called the torque constant (K_T). It gives the ratio between electromagnetic torque and stator current I_q. The torque constant can be derived from the poduct specificication sheet, which states that peak torque (2100 Nm) is achieved with 350 A inverter (app. D.1) and this results in a torque constant of 6. Now, all parameters for the PMSM model are determined and these are presented in table 6.1.

$$K_T = \frac{T_{max}}{I} \tag{6.15}$$

Parameter	Unit	Value
Nominal power	kW	176
Nominal speed	rpm	1200
Maximum speed	rpm	2400
Nominal torque	Nm	1399
Maximum torque	Nm	2100
Nominal efficiency	%	96
Moment of inertia	kgm^2	0.99
Viscous damping coefficient	Nms	0.167
Number of pole pairs	-	6
Line-to-line voltage	V_{AC}	500
Torque constant	Nm/A	6
Weight	kg	295

Table 6.1: Input data for PMSM model

6.2. PMSM vector control

Vector control, or field oriented control, governs the current strength of the stator by controlling the magnetic field vectors (abc and dq). The stator current of a synchronous machine can be divided in two components: magnetising (I_d) and quadrature current (I_q) [102]. The quadrature current is the torque producing current, which was seen in equation 6.7. For a permanent magnet machine the direct current is controlled to be zero, as flux is provided by the magnets. The field is normally controlled with three loops: a location loop, a motor speed loop and a current loop. The first loop converts the static frame ($\alpha\beta$) to a rotating frame, but this step is not necessary in the model since only the rotating frames are considered. The PMSM control is modelled with a set of dedicated Simulink blocks for vector control.

6.2.1. Speed control

The motor's rotational speed is controlled with a PI controller. The input signal, the speed set-point, is first corrected to respect the dynamic limits of the PMSM. Due to the machine's inertia, it can not handle steps in the reference speed. A rate limiter ensures that the machine accelerates or decelerates gradually. The motor's maximum deceleration rate is 1000 rad/s^2, but the motor's inertia is smaller than the inertia of the propelling shaft. Therefore, it is expected that this limit is not exceeded if the inertia of the whole shaft is taken into consideration. The error between the reference speed and the actual speed is converted to a set-point for electromagnetic torque by the PI controller [64]. The torque set-point is the output of the speed control loop and input for the current control loop.

6.2.2. Current control

The electromagnetic torque set-point is used in the current controller to determine the value the quadrature current. This can be done by rewriting equation 6.7 to 6.16. The flux that is established by the permanent magnet is given by the PMSM model and Φ has a value of 0.67 Wb.

$$I_q = \frac{2}{3} \cdot \frac{T_e}{P \cdot \Phi} \tag{6.16}$$

The input for the magnetising current is zero, because flux was established by permanent magnets. The current set-points in the abc frame are then determined by using the 'dq2abc transformation matrix' (eq. 6.2) [65]. The voltage vectors are substituted for current vectors. The current set-points in the abc frame are then compared to the actual values and the DC/AC inverter controls the three-phase current accordingly. This gives the vector control model as presented in figure 6.2.

6.3. DC/AC inverter

The permanent magnet synchronous machine is driven by an AC power supply, while the central bus provides DC power. To go from DC to AC voltage, a device is required that is capable of producing an output voltage with both positive and negative polarity: a DC/AC inverter [31].

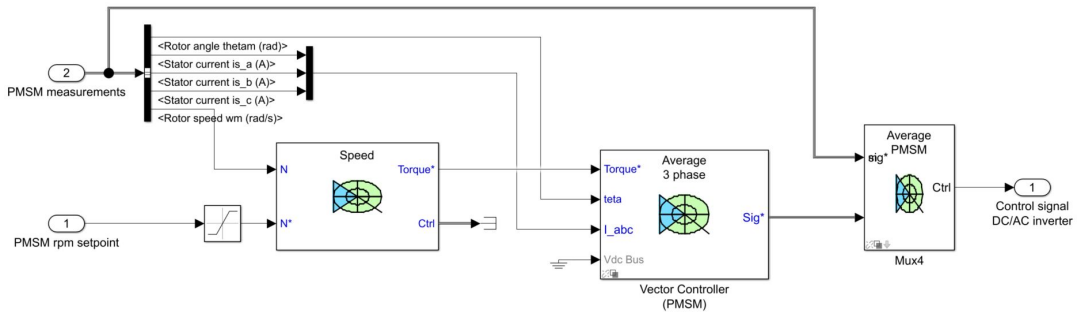

Figure 6.2: Simulink model of PMSM vector control

6.3.1. Operating principle

The three lines, described in equation 6.1, have the same amplitude with a phase difference of one third of a period. Due to this, the AC lines have their peak voltages evenly distributed over time. This gives a relatively constant power to the load [69]. From the product sheet of the Danfoss motor (app. D.1) it can be read that the motor requires a line-to-line voltage of 500 V_{AC} (V_{LL}). The line-to-line voltage is the root mean square of the sinusoidal voltages [69]. The DC voltage, however, should be capable to deliver the maximum voltage of the three phase circuit. Following equation 6.17, this results in a minimum DC voltage of 675 V. In section 4.2 it was concluded that the battery provides a voltage range between 690 V and 910 V. The relationship between phase voltage, line-to-line voltage and DC voltage is also visualised for the selected configuration in figure 6.3

$$V_{DC} = \frac{3}{\pi} \cdot \sqrt{2} \cdot V_{LL} = 1.35 \cdot V_{LL} \tag{6.17}$$

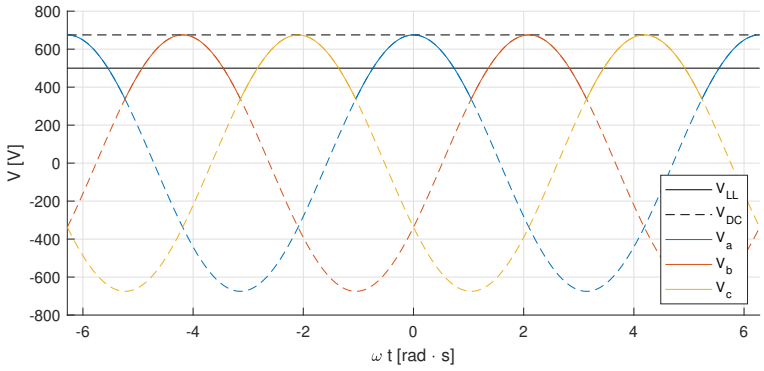

Figure 6.3: Phase voltage, line-to-line voltage and required DC voltage for a three-phase power consumer for $[-2\pi\ 2\pi]$

A sinusoidal line voltage is created by a modification to the duty cycle as introduced in section 4.3. The operating principle of an AC/DC inverter is similar to a DC/DC power converter: the conversion is regulated by switches [31]. The position of the switch, which is controlled by the duty cycle, was either open (output voltage equals zero) or closed (output voltage equals input voltage). DC/DC converters maintain the same polarity (positive) for the bus voltage. In contrast to this, the output voltage of the inverter should be positive if $D > 0.5$ and negative if $D < 0.5$, as it is sinusoidal. A duty cylce of 1 means that amplitude of the three-phase voltage equals the DC voltage. In general, this modification can be expressed as [31]:

$$V_{out} = (2D - 1) \cdot V_{in} \tag{6.18}$$

And this can be done for each line:

$$\begin{cases} V_a = (2D_a - 1) \cdot V_{DC} \\ V_b = (2D_b - 1) \cdot V_{DC} \\ V_c = (2D_c - 1) \cdot V_{DC} \end{cases} \tag{6.19}$$

6.3.2. Inverter model

Similar to the DC/DC converter model the effect of switches is not of interest in this study. The time domain of switching frequencies, which is in the order of a number of kilohertz, is much smaller than the transients of interest. Therefore, an average value model is also used for the DC/AC inverter. In this average model, the inverter has two modes. The first mode, current mode, is where the amplitude of the output voltage is smaller than the DC voltage. The model switches to 'saturated mode' if the amplitude reaches the DC voltage. The DC bus current is also controlled in the DC/AC inverter based on the power consumption of the PMSM and power losses in electric drive.

Current mode

The current set-points that follow from the PMSM vector control can directly be used if the requested AC voltage is lower than the DC voltage. The current sources in the inverter model are connected in series with the current source in the PMSM's electrical model. Two current sources that are connected in series would normally give a simulation error. However, the set-points (I^*_{abc}) from the current regulator can be controlled by adding a small resistive load. This load is rather small with a resistance of 1% of the inverter's resistance. The additional current strength to overcome this resistive load follows from Ohm's law (eq. 4.40).

$$V = I \cdot R \qquad \longrightarrow \qquad I = \frac{V}{R} \tag{4.40}$$

The voltage is computed by applying the 'dq2abc transformation' to the voltages in the 'dq' frame, which are given in the vector with measurements from the synchronous machine:

$$\begin{cases} I_a = I^*_a + \frac{V_a}{0.01 \cdot R} \\ I_b = I^*_b + \frac{V_b}{0.01 \cdot R} \\ I_c = I^*_c + \frac{V_c}{0.01 \cdot R} \end{cases} \tag{6.20}$$

Saturated mode

In saturated or voltage mode the inverter switches to a square wave output for voltage. The output voltage of the inverter is either equal to the DC voltage or zero [66]. In this mode, the voltage is controlled by a pulsating signal from the vector control. Saturated mode is activated if the amplitude of the back EMF voltage equals the DC voltage. The amplitude of the back EMF voltage is calculated with the following equation [66]:

$$V_{BEMF} = \frac{\pi}{2} \cdot \sqrt{\left(R \cdot I_d - L_q \cdot P \cdot \omega_m \cdot I_q\right)^2 + \left(R \cdot I_q + \Phi \cdot P \cdot \omega_m + L_d \cdot P \cdot I_d \cdot \omega_m\right)^2} \tag{6.21}$$

The voltage soruces are then controlled with a pulsating signal (either 1 or 0) from the vector control and the value of the DC voltage:

$$\begin{cases} V_a = Pulse\,1 \cdot V_{DC} \\ V_b = Pulse\,2 \cdot V_{DC} \\ V_c = Pulse\,3 \cdot V_{DC} \end{cases} \tag{6.22}$$

DC bus current

The DC bus current is also controlled in the inverter based on the power consumption of the PMSM. The hybrid power supply should deliver the power needed for propulsion plus the losses that are present in the electric drive. Both the PMSM and inverter are non-ideal, although they have a high efficiency. The Danfoss machine has an efficiency of 96% (app. D.1). For the inverter the efficiency is estimated at 97.5% (app. D.2). Both values are assumed to be constant as it is not feasible in the time-frame of this thesis to analyse the efficiency for different load factors. This brings the total efficiency of the AC system to 94%. The DC current follows from the power equation for electric systems and the power loss can be derived by combining Ohm's law and the power equation [66].

$$I_{DC} = \frac{P_{EM} - P_{e,loss}}{V_{DC}} \tag{6.23}$$

$$P_{e,loss} = \left(I_a^2 + I_b^2 + I_c^2\right) \cdot R \tag{6.24}$$

$$\eta_{AC} = \frac{P_{EM}}{P_{DC}} \tag{6.25}$$

The value of the resistance is determined by trying different values and check the efficiency of the AC system. A fraction of the PMSM power loss is already accounted for in the damping factor (approximately 1.5%). The electrical power loss (eq. 6.24) is thus a part of the total power loss. A value of 0.1 Ω results in an overall efficiency of 93%. This value is relatively constant for the operational domain of the PMSM. The complete inverter model is presented in figure 6.4.

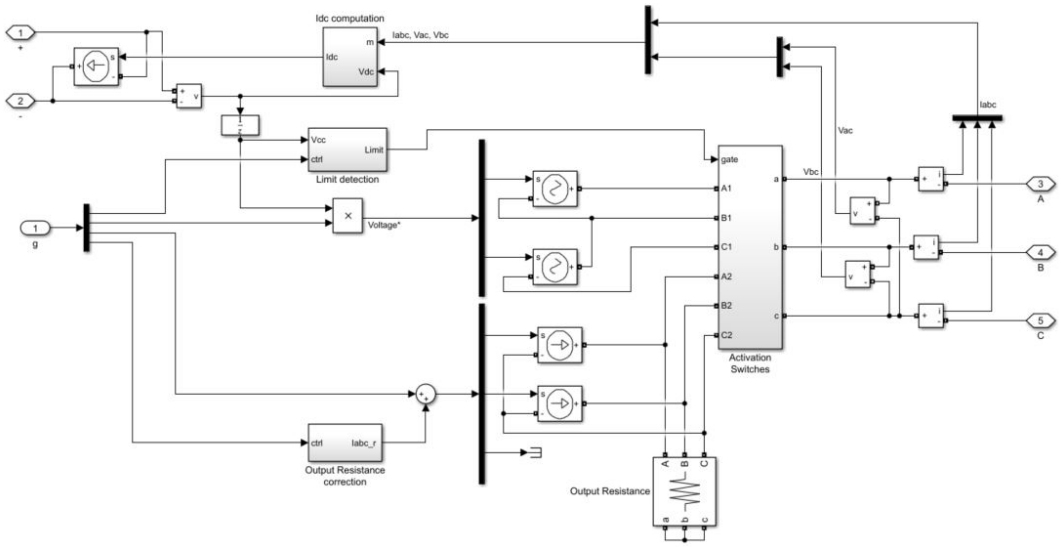

Figure 6.4: Simulink model of the DC/AC inverter

6.3.3. Start-up of the synchronous machine

During the start-up of the synchrnonous machine, the motor has no initial speed. It is not possible to start the machine with an AC supply with constant frequency [49]. In this condition the magnetic field of the rotor can not lock with the rotating field of the stator. The permanent magnets are attracted by opposite poles and rotation starts. The starting speed will be much lower than the speed of the rotating field due to inertia. Equal (repulsive) poles will pass the rotor's poles shortly after the passing of opposite poles. Due to this, positive and negative torque is developed and the average torque equals zero. The inverter controls the frequency of the AC supply, so the PMSM is started by slowly increasing the rotational speed of the stator's magnetic field from zero (eq. 6.26). Figure 6.5a and 6.5b show how the motor is brought in 10 seconds to its nominal power by linearly increasing speed and torque.

$$n_s = \frac{f}{P} \tag{6.26}$$

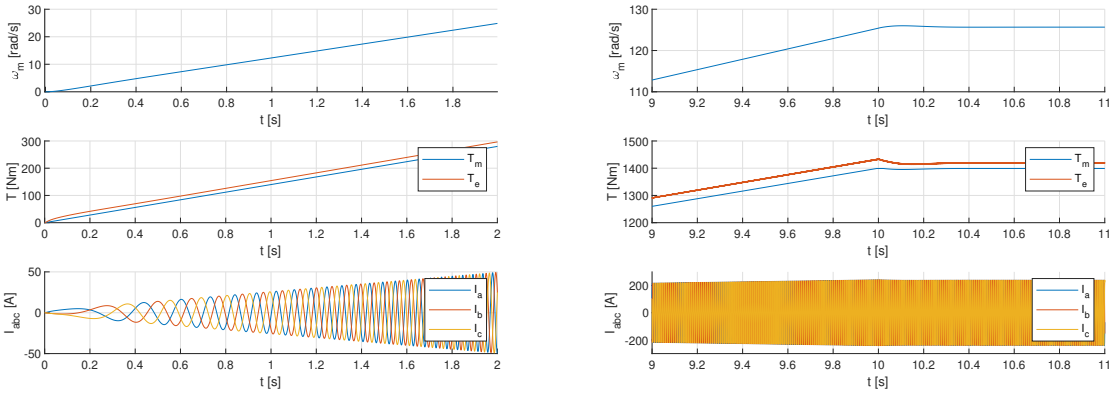

(a) Start-up from zero speed

(b) Reaching nominal speed

Figure 6.5: Speed, torque and three-phase current for the frequency controlled start-up of the PMSM

6.4. Ship and propeller model

In order to analyse the energy flow in the system under transient conditions, it is also necessary to implement the propeller and ship dynamics in the model. The ship speed and corresponding resistance dictates the required thrust from the propeller. Also, the operational condition of the propeller determines the load torque for the electric motor. The interaction between the electic drive, propeller and ship is visualised in figure 6.6. The ship model and propeller model are discussed in the following sections.

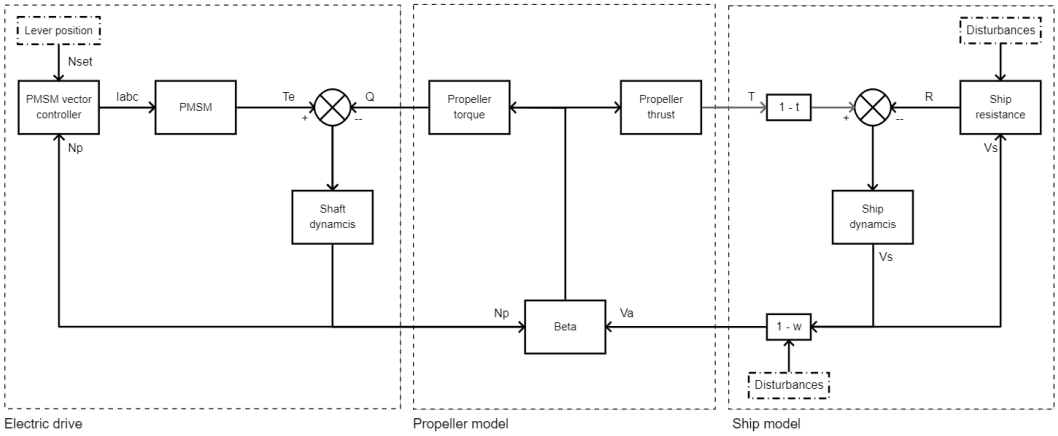

Figure 6.6: Interaction between electric drive, propeller and ship

6.4.1. Ship model

The vessel's speed is determined in the ship model. The ship speed follows from Newton's second law. In this study, only forward motion (surge) is of interest. Other ship motions are not in the scope of this study. Also, there is a lack of information with respect to hydromechanic coefficients and motion RAO's. Therefore, potential coupling between motions in various directions is also not considered here.

$$\Sigma F = m \cdot a \qquad \longrightarrow \qquad V_s = \int_0^t \frac{\Sigma F}{m} \cdot dt \tag{6.27}$$

The sum of forces consists of two components: ship resistance and thrust from the propellers. The vessel has two propellers, so the ship's resistance (fig. 6.7) should be divided by two to obtain the thrust per propeller. The thrust should be corrected for the thrust deduction, which is defined as the difference in resistance between towed condition without propeller and self propelling condition [49]:

$$T = \frac{R_s}{k_p \cdot (1-t)} \tag{6.28}$$

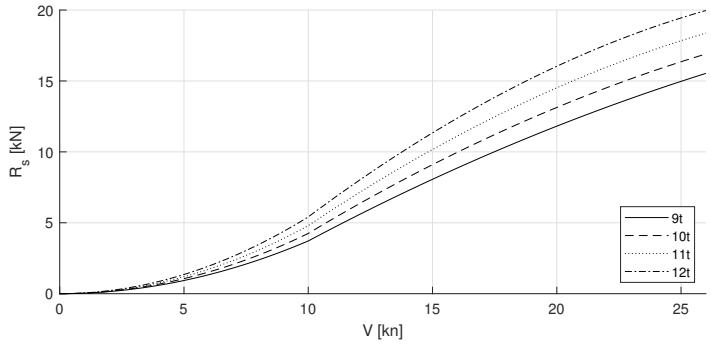

Figure 6.7: Ship resistance for various displacements

The advance speed is the input from the ship model to the propeller model. The ship speed is corrected for the vessel's wake field to obtain the water velocity through the propeller plane. According the R&D department

of the Damen Shipyards Group, the wake fraction is dependent on the ship's speed, where thrust deduction is constant (fig. 6.8). Figure 6.6 also shows two options to implement disturbances from the environment. Variations in resistance are created by wind, waves and current and variations in wake field may be the result of ship motions or (orbital) water particle motions at the location of the propeller [99].

$$V_a = (1 - w) \cdot V_s \tag{6.29}$$

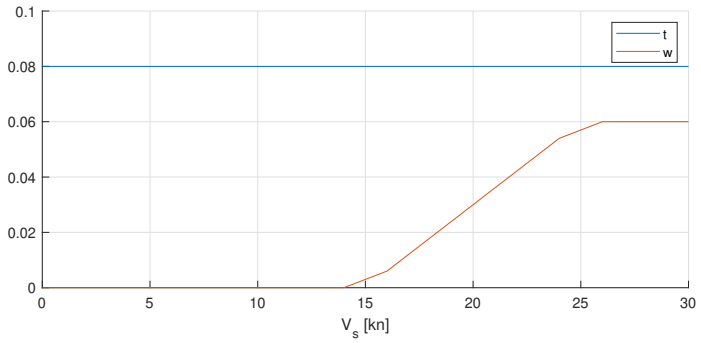

Figure 6.8: Thrust deduction factor and wake fraction for the FCS1204

6.4.2. Propeller model

The operational condition of the propeller is determined with the four-quadrant open water diagram. For stationary sailing ahead, it is also possible to use the first-quadrant open water diagram. However, this diagram does not contain sufficient information for operations like manoeuvring and sailing astern [49]. For braking, for instance, ship speed is positive where propeller speed is negative and this information is given in the third quadrant. In this research it is also the goal to study some emergency manoeuvres, so a four-quadrant diagram is required for the complete field of operation of the fixed pitch propeller.

The propeller speed (in rev/s) and advance speed are required to determine the relative water velocity (V_r) into the propeller and its angle of attack. The hydrodynamic pitch angle is defined as the angle between the advance speed and the propeller's circumferential speed, measured at the diameter where the nominal pitch angle is located (approximately 0.7 D) [33, 49]:

$$\beta = \arctan\left(\frac{V_a}{0.7 \cdot \pi \cdot n_p \cdot D}\right), \qquad V_r = \sqrt{V_a^2 + \left(0.7 \cdot \pi \cdot n_p \cdot D\right)^2} \tag{6.30}$$

If the hydrodynamic pitch angle is known, the thrust and torque coefficients follow from the propeller's geometry. This information is provided by the R&D department and presented in figure 6.9. The relationship between these coefficients, the input data and thrust or torque is now given by [33, 49]:

$$T = C_t \cdot \frac{1}{2}\rho \cdot \left(V_a^2 + \left(0.7 \cdot \pi \cdot n_p \cdot D\right)^2\right) \cdot \frac{\pi}{4} \cdot D^2 \tag{6.31}$$

$$Q = C_q \cdot \frac{1}{2}\rho \cdot \left(V_a^2 + \left(0.7 \cdot \pi \cdot n_p \cdot D\right)^2\right) \cdot \frac{\pi}{4} \cdot D^3 \tag{6.32}$$

The thrust is used for the sum of forces from equation 6.27 and the torque is used as input to the model for the electric drive. In section 3.3 we have seen the relationship between the propeller torque and the load torque as experienced by the electric motor. The motor's mechanical load torque (T_m) can be calculated by dividing propeller torque by the relative rotative efficiency and shaft efficiency [49]. Both efficiencies are constant with a value of 98%, according the R&D department. Equation 6.8 can then be rewritten to equation 6.33 to relate propeller loading to the loading of the propulsion system via the shaft dynamics (fig. 6.6).

$$T_m = \frac{Q}{\eta_R \cdot \eta_S} \tag{3.4}$$

$$\frac{d\omega_m}{dt} = \frac{1}{J} \cdot \left(T_e - \frac{Q}{\eta_R \cdot \eta_S} - F \cdot \omega_m\right) \tag{6.33}$$

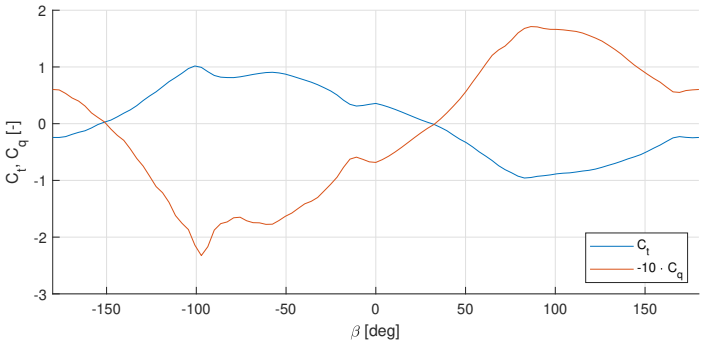

Figure 6.9: Four-quadrant open water diagram for the FCS1204 propeller

It is seen here that the propeller and ship model are closely related and therefore, they are modelled in the same subsystem in Simulink. This subsystem is presented in figure 6.10. The motion equation and the calculation of advance speed is shown on the right side. The propeller models for the two propellers and the computation of the load torque for the PMSM's is shown in the top of this diagram. Finally, the ship resistance follows from the speed loop and this completes the sum of forces together with the thrust from both propellers. Figure 6.11 shows how equation 6.30 is used as input for a look-up table to determine the propeller's operational point. The propeller's thrust and torque are then computed with equations 6.31 and 6.32.

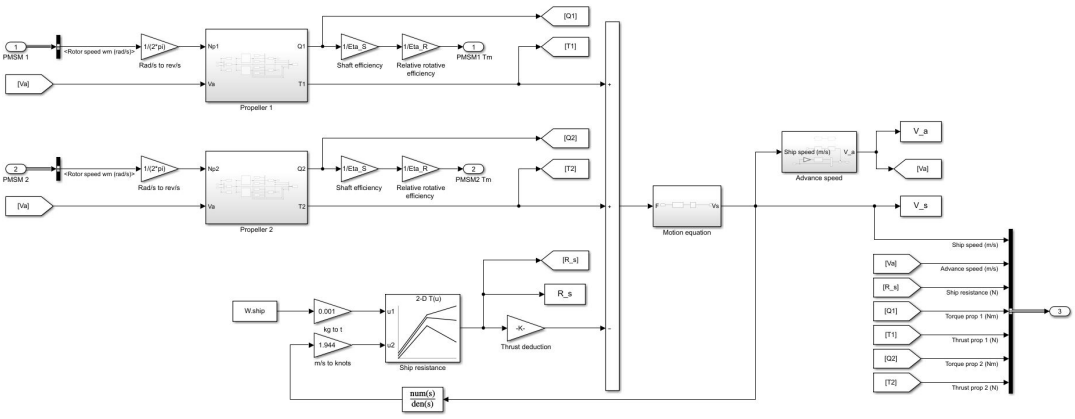

Figure 6.10: Simulink subsystem for ship and propeller model

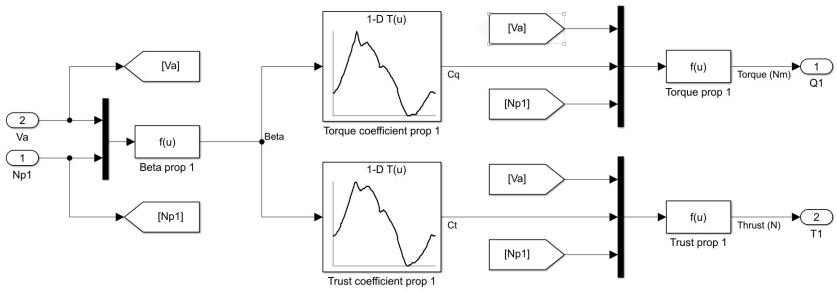

Figure 6.11: Simulink propeller model

6.5. Integrated propulsion model

The models that are developed here for the permanent magnet motor, vector control, DC/AC inverter, propellers and ship are added to the hybrid power supply models from figure 4.10 and 4.11. The ship and propeller model are both included in the separate subsystem. This results in the complete propulsion models as presented in figure 6.12 for one fuel cell stack and figure 6.13 for two fuel cell stacks.

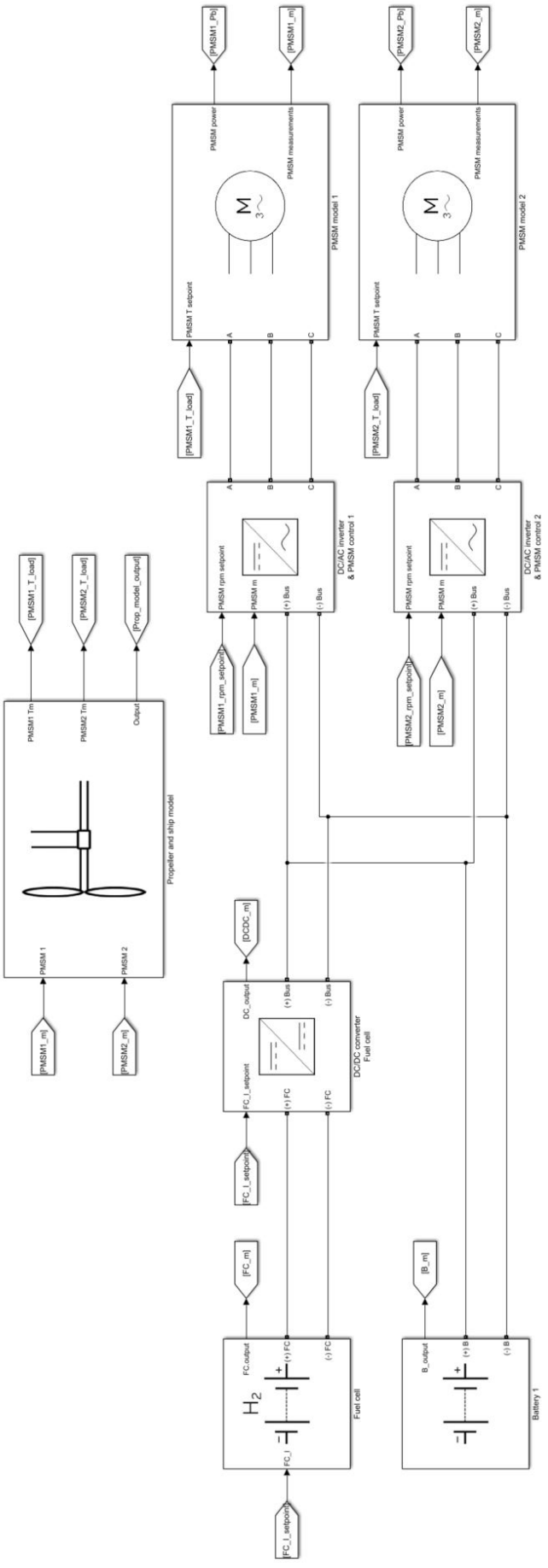

Figure 6.12: Simulink model of complete propulsion system with one fuel cell

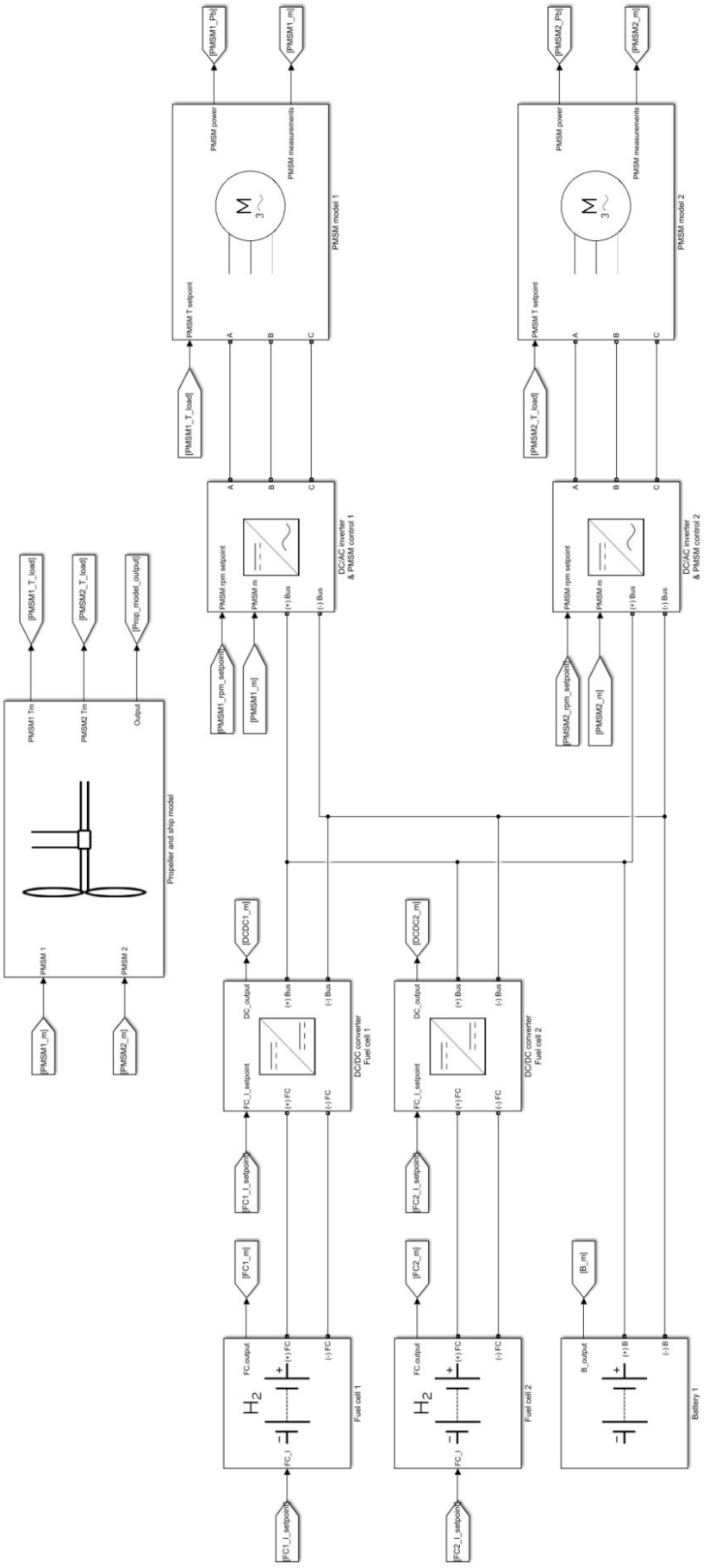

Figure 6.13: Simulink model of complete propulsion system with two fuel cells

7

Dynamic behaviour of the hybrid propulsion system

A complete propulsion model is developed in the previous chapters by coupling the 'Hybrid power supply model' from chapter 4 to the 'Electric drive model' from chapter 6. This integrated model is put to work in this chapter. Figure 3.4 showed the control hierarchy for the hybrid power supply, where energy management is at the top level. Chapter 5 covered energy management for two operational profiles. Power, being the rate at which energy is delivered, should also be managed at a smaller timescale to prevent that limits are exceeded.

In this chapter, the vessel and propeller will be exposed to a number of transient load conditions. The goal of this part of the research is to analyse how the propulsion system responds to fluctuating loads. The dynamic behaviour of a FC/battery system is a relatively unfamiliar domain for marine applications, compared to automotive applications for instance. This analysis will then be used to formulate a set of recommendations for the power management of the propulsion model, which was not modelled at a high level of detail due to a restricted time frame for this research.

Three specific cases will be studied here: sailing in waves, acceleration and deceleration. If the vessel is sailing in waves (sec. 7.2), it is continuously exposed to varying loads. For the other two scenarios, this research looks at the worst intended conditions. Therefore, two emergency manoeuvres are selected here: a slam start (sec. 7.3) and crash stop (sec.7.4. Moderate acceleration or deceleration can be managed properly if the system performs well during the worst intended conditions. However, some system limits are identified first.

7.1. Identification of system limits

The three main components of the propulsion are the battery, fuel cell stack and PMSM's. Each component is characterised by its own limits. Each limit will be discussed here.

7.1.1. Battery limits

It is recalled that it is beneficial for operational purposes to combine high specific power sources (with fast response characteristics) with high specific energy sources (slow response) [57]. In this view, fuel cells and batteries are a good combination for hybrid power supply, since batteries have a relatively high power density but low energy density (and vice versa for fuel cell systems) [42]. In other words, if there is a need for fast responsiveness, batteries are favoured over fuel cells.

However, the Toshiba Type 3-23 modules also have some limitations. Each battery bank has a maximum continuous current of 160 A and rush current of 350 A. The total allowable current strength is thus dependent on the number of battery banks that are connected in parallel. If the battery is discharged above the maximum current, this can only be maintained for a short period (known as rush current). Besides this, high discharge currents will increase the battery temperature significantly and this requires a better cooling system.

7.1.2. Fuel cell limits

For the fuel cell stack it is not possible to consult with the supplier, because a reference module is used from the SPS library. However, it is known that LT-PEM fuel cells are quite responsive compared to other types. The FC's responsiveness is determined by the rate of mobilisation of the oxidant, so it can be tweaked by changing the settings for the air blowers [24]. A higher stoichiometry inside the cell would improve the cell's response, but it sacrifices some efficiency and lifetime. For standard marine configurations it is recommended to limit the FC's rate of change to 10% of its maximum power per second (12 kW/s) [24]. In reality it is likely that current is controlled, rather than power, but no references were found for a suitable current limit (in A/s).

7.1.3. PMSM limits

The synchronous machines are very suitable as propulsion motors. According to the specification sheet (app. D.1) it is designed to produce high starting torques and it is capable of delivering full torque instantly to a non-rotating shaft. This is also reflected in some specifications: the maximum acceleration or deceleration rate is 1000 rad/s^2. The maximum acceleration/deceleration is specified for the PMSM in "unloaded" condition: the total moment of inertia of the rotating system increases due to the propeller shaft, propeller and entrained water. The moment of inertia of the propeller shaft can be estimated to be twice as high as the motor's inertia [84]. The PMSM's inertia is 0.99 kg m^2 and the inertia of the propeller, including entrained water, is 0.7 kg m^2 according to the R&D department. This results in a total shaft inertia of 3.67 kg m^2.

The specified value for the peak torque is 2100 Nm with a 350 A inverter. In section 6.1 this was defined as the torque constant. In other words, the maximum stator current (I_q) may not exceed this value of 350 A. The PMSM's maximum continuous torque is 1399 Nm and its maximum continuous power is 176 kW. The PMSM can operate for a limited time at higher loads. In an 'overtorque test' the PMSM should be able to deliver 150% of the maximum continuous torque (i.e. pull-out or peak torque) for at least 30 seconds. These dynamic limits give guidelines for the analysis of the three cases that are studied in the next sections.

7.2. Sailing in waves

When a ship sails in (irregular) waves, the waves induce added resistance and ship motions. The flow field around the propeller varies significantly in such conditions, which induces a varying propeller torque [33]. This also effects engine loading and, hence, the hybrid power supply.

7.2.1. Set-up of the experiment

The effect of continuously varying loads can be analysed by modelling disturbances in the ship model as seen before. Wind, waves and current induce variations in ship resistance and disturbances [99]. Various methods are known to estimate the order of magnitude of the wave force on a body, but there are some complications here. First of all, it is possible to estimate the first and second order wave forces by calculating the wave force on a vertical wall in the water. This can be done by integrating the wave potential derivatives (with respect to time and height) between the bottom and free surface. However, this approach would assume that all waves are reflected. The vessel under investigation has a limited depth and slender hull form, so this approach would probably lead to an overestimation of the wave force. Second of all, for other methods, such as the near- or far-field approach, there is not enough information available. It would not be feasible to dive into these methods within the time given. Therefore, added resistance due to waves is not considered.

The second type of disturbances were found in the wake field: ship motions and orbital water motions induce fluctuations in the wake field [99]. The effect of ship motions will be neglected, because this was left outside the scope of this study and, secondly, there is also a lack of information with respect to motion RAO's for the FCS1204. Therefore, it is simply not possible to include the effect of motions, such as heave, pitch and surge in this analysis, despite the fact that changes in propeller submergence due to motions will contribute to the fluctuating loads on the electric motors [84].

However, it is feasible to analyse the variations in wake field due to the orbital motions of water particles in waves. The particle velocity can be added to the forward advance speed of the vessel. This approach would give an advance speed which will fluctuate around the calm water advance speed. Wake data is often only available for calm water conditions and not known in irregular waves [84]. Therefore, it must be assumed that the vessel follows the waves and, hence, that propeller submergence remains constant with respect to

the free surface. Due to this it is also necessary to assume that the vessel sails in long regular waves. It is acknowledged that this approach will not necessarily give an representative impression of wave loads, but it will give insights in the dynamic behaviour of the propulsion system, which is the goal of this study.

7.2.2. Wake field variations in waves

The water particle velocity in forward direction can be computed from the wave potential Φ_w, which is derived in x-direction [46]. The particle velocity is computed for deep water, so the path of the particles is assumed to be circular. The expression for the particle velocity is further simplified with the dispersion relationship:

$$\Phi_w = \frac{\zeta_a \cdot g}{\omega} \cdot e^{k \cdot z} \cdot \sin(kx - \omega t) \tag{7.1}$$

$$c = \frac{\omega}{k}, \qquad k = \frac{\omega^2}{g} \tag{7.2}$$

$$u = \frac{\partial \Phi_w}{\partial x} = \zeta_a \cdot \omega \cdot e^{k \cdot z} \cdot \cos(kx - \omega t) \tag{7.3}$$

Where c, k, ζ_a and ω represent the wave speed, wave number, amplitude and frequency, respectively. It is assumed that the location of the propeller is fixed at $x = 0$. The wave frequency must now be corrected for the forward speed of the vessel. The wave frequency in the cosine is replaced by the encounter frequency between ship and wave, dependent on wave direction (μ) [46]:

$$\omega_e = k \cdot \big(c - V_s \cdot \cos(\mu)\big) = \omega - k \cdot V_s \cdot \cos(\mu) \tag{7.4}$$

Equation 7.3 shows that the particle velocity depends on the height. The propeller hub is located at 1 meter below the free surface, which can be seen in appendix A.1. This value is used as average height of the propeller. The height of the propeller can be related to the elevation of the free surface, because it was assumed that the vessel follows the wave:

$$z(t) = \zeta(t) - 1 = \zeta_a \cdot \cos(\omega_e t) - 1 \tag{7.5}$$

In the previous section it was stated that there is insufficient data available from the wake field. Therefore, the thrust deduction factor is still assumed to be constant with a value of 0.08. The wake fraction might change due to a variation in V_s. Eventually, this approach leads to the final expression for the speed at the propeller plane:

$$V_{wave} = V_a + \zeta_a \cdot \omega \cdot e^{k \cdot (\zeta_a \cdot \cos(\omega_e t) - 1)} \cdot \cos(\omega_e t) \tag{7.6}$$

The next step is to select a set of wave parameters for the simulations. This study looks at two wave directions: head waves ($\mu = \pi$) and stern waves ($\mu = 0$). The first condition is most challenging in terms of dynamic loads [33]. Stern waves are also considered, because the encounter frequency is much lower. Therefore, a fuel cell might be better capable to follow the transients in stern wave conditions. Furthermore, the vessel should be capable to operate in significant wave heights up to 1 meter, which is quite extreme for such a small vessel. Therefore, a regular wave height of 1 meter will be used here as well. Furthermore, this operation is simulated for two forward speeds (12 and 20 knots) to be able to analyse the system's behaviour at part load and during boosting. Finally, it is necessary to select a set for the wave frequencies. The vessel is operated in the Wadden Sea / North Sea area, so a JONSWAP spectrum is used for the domain of wave frequencies that are found on the North Sea. The energy spectrum of a JONSWAP spectrum lies between 0.5 and 2.5 rad/s, with the peak frequency around 0.7 rad/s. However, it is recalled that it was assumed that the vessel sails in long waves. The ratio between the wave length (λ) and wave height should not exceed 1/20 for this assumption to hold. This information is used to determine the upper limit for the wave frequency, which results in 1.7 rad/s:

$$k = \frac{2\pi}{\lambda} \qquad \longrightarrow \qquad \lambda = \frac{2\pi}{k} = \frac{2\pi \cdot g}{\omega^2} \tag{7.7}$$

	Unit	Value
Wave amplitude	m	0.5
Wave direction	°	[0 π]
Ship speed	kn	[12 20]
Wave frequency	rad/s	[0.7 1.2 1.7]

Table 7.1: Set of variables for regular waves

7.2.3. Head waves at top speed

As mentioned in the previous section, sailing in head waves is most challenging in terms of dynamic loads [33]. Peak loads follow each other quickly due to the opposite wave and ship directions, especially if the vessel sails at top speed. Figure 7.1a shows the variation in the advance speed due to the presence of waves. It can be seen that the amplitude of the variation increases with a higher wave frequency and this follows from equation 7.6. The ship speed also shows oscillations due to fluctuating thrust [68]. The amplitude, however, is much smaller than the variation in advance speed, which is a consequence of the ship's large inertia. The fact that a large mass must be accelerated or decelerated also results in a phase lag between the peaks in advance speed and ship speed.

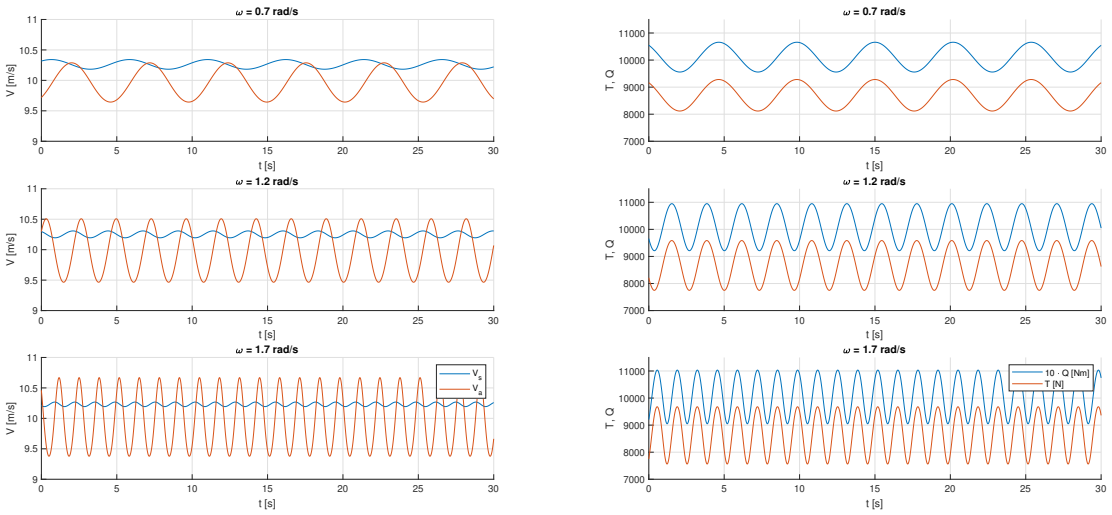

(a) Ship and advance speed

(b) Propeller torque and thrust

Figure 7.1: Speed and propeller loading in head waves with various wave frequencies at a speed of 20 knots (top: 0.7 rad/s, middle: 1.2 rad/s. bottom: 1.7 rad/s)

The oscillating advance speed causes a continuous change in the operational point of the propeller (eq. 6.30) and, hence, a continuous variation in the propeller thrust and torque is seen in figure 7.1b. These wake field variations in the propeller plane also have an effect on the shaft speed [68, 99]. This is also found in equation 6.33, where circumferential speed was defined as a function of electromagnetic torque and load torque from the propeller (fig. 7.1b). The amplitude of the shaft speed oscillation is much smaller (1% at most) compared to the variations in advance speed or propeller loading. The configurations that are selected in section 5.4 are now exposed to these waves and the behaviour of the propulsion system in discussed in the next sections. The results of all simulations are also included in appendix E.1.

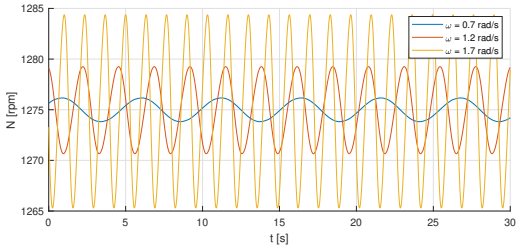

Figure 7.2: Variations in propeller speed in head waves at a speed of 20 knots

1 fuel cell stack with a 3P28S battery

The first configuration employed one fuel cell stack and a battery with three banks in parallel. This is the most suitable configuration for the harbour patrol vessel. A speed of 20 knots would require approximately a total of 290 kW in calm water conditions, according to the PSD. If this is corrected for the power losses in the

inverter (2.5%) and PMSM (4%) this would yield a power consumption of approximately 310 kW at the DC bus. This is well above the maximum power of the FC module, so it is seen that the fuel cell stack operates at maximum power. The battery provides energy for both boosting and for countering of the harmonic loads. The PMSM can follow the load accurately (fig. 7.3a) and the shaft dynamics are much faster than the ship's dynamics (fig. 7.1a) due to the lower shaft inertia [68].

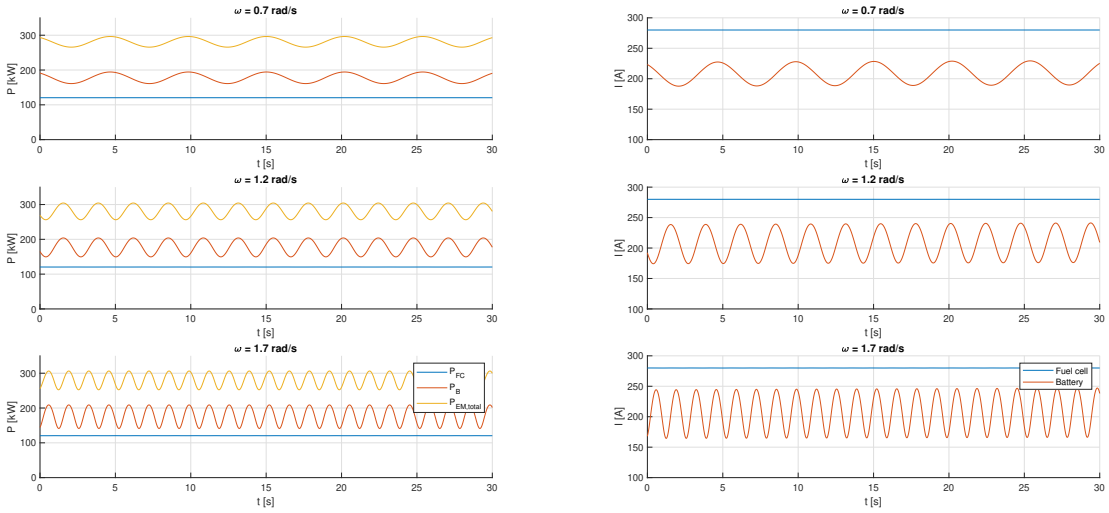

(a) Load distribution

(b) fuel cell and battery current

Figure 7.3: Loading of hybrid power supply with one fuel cell stack and a 3P28S battery, while sailing in head waves at 20 knots

2 fuel cell stacks with a 2P28S battery

Two fuel cell stacks and a battery with two banks are installed in the second configuration. The increased specific energy was favourable for operations with higher required endurance. Figure 7.3a shows large fluctuations in the propulsion power of the electric motors. By adding a FC stack, the total fuel cell power increases to 240 kW. However, it is seen that the load power does not drop below the total fuel cell power. Hence, the fuel cells operate at maximum power and the battery assists for boosting and transients.

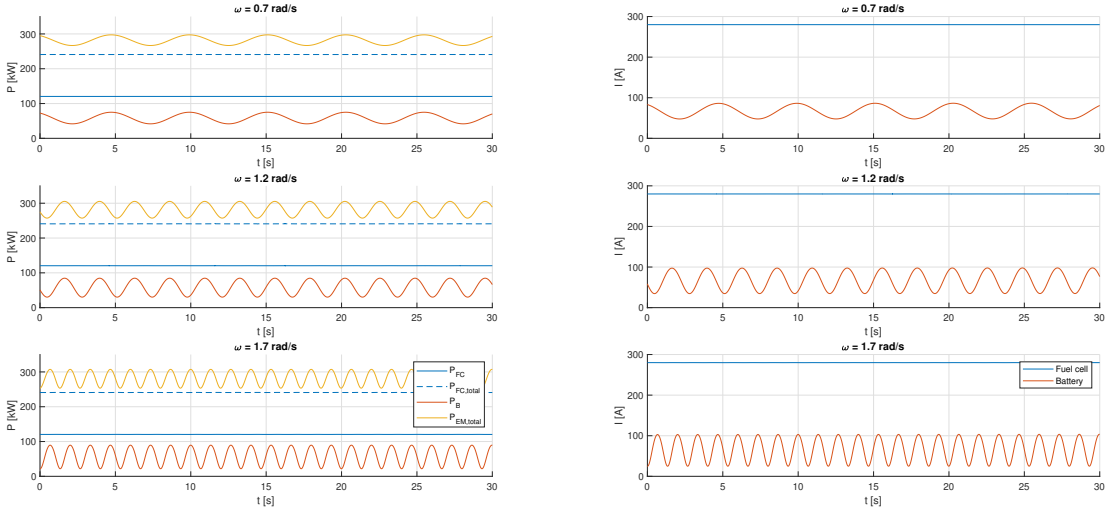

(a) Load distribution

(b) fuel cell and battery current

Figure 7.4: Loading of hybrid power supply with two fuel cell stacks and a 2P28S battery, while sailing in head waves at 20 knots

It is also seen that the total load power remains within the limits of the PMSM (176 kW for each motor). At top speed, the propeller is running at 1275 rpm and this is within the CPSR of the motor. At this speed, maximum continuous torque is 1318 Nm (fig. 6.1) and the maximum load torque, including shaft efficiency and relative rotative efficiency, is 1150 Nm. The maximum continuous torque and power are not exceeded and the motors operate within their limits.

7.2.4. Head waves at cruising speed

From the previous simulations it can be concluded that the battery accounts for most dynamic loads, because the load power exceeds the maximum fuel cell power. Reducing the load power could give valuable insights in the capabilities of the fuel cells to cope with dynamic loads. Therefore, the speed is now reduced to a moderate cruising speed of 12 knots. In this condition, the system operates at part load. Before taking a closer loop at the behaviour of the hybrid power supply, the waves are first discussed briefly. The vessel is exposed to the same incoming waves that are introduced in the previous section. This means that the amplitude of the advance speed is equal between the two cases (fig. 7.1a and 7.5a). However, the variations in propeller loading are somewhat lower due to another operational point of the propeller (as a result of lower ship and propeller speed). The amplitude of the oscillations in propeller loading is approximately 25% lower compared to the top speed case, so fluctuations are still considerable (fig. 7.5b).

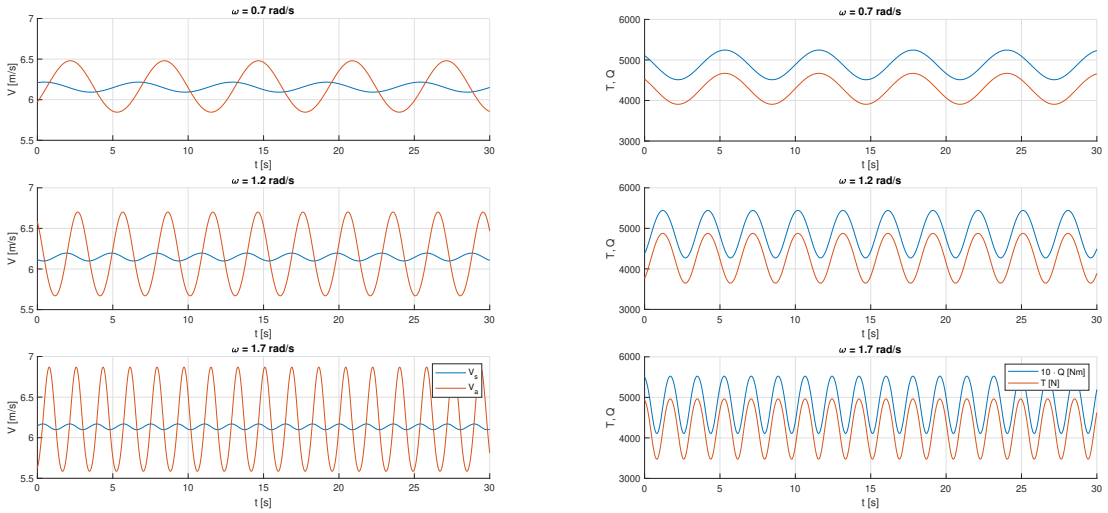

(a) Ship and advance speed

(b) Propeller torque and thrust

Figure 7.5: Speed and propeller loading in head waves with various wave frequencies at a speed of 12 knots (top: 0.7 rad/s, middle: 1.2 rad/s. bottom: 1.7 rad/s)

1 fuel cell stack with a 3P28S battery

Reducing the operational speed to 12 knots gives valuable insights in the stack's capabilities to deal with transient loads. At this speed, the system is operating at part load and the state-based EMS from section 5.1.3 provides the set-points of both components, where the battery operates at its optimal power and current and the fuel cells provide the rest of the energy. The system, however, must respect the identified limit of 10% load change per second. So the battery can also assist if the fuel cell stack can not follow the dynamic load, like it was seen in the previous section.

$$I_{B,opt} = 0.2 \cdot Q_{rated} \tag{5.1}$$

At part load, it becomes clear that the fuel cells are better capable to follow the transient loads of a low-frequency incoming wave (fig. 7.6a). If the wave frequency is increased, this figure changes significantly. As the amplitude and the frequency of the oscillations increase, the fuel cells can only follow a fraction of the dynamic load and the battery has to assist for a significant part of the load. The fuel cell stack is not capable to follow the wave form and is continuously increasing and decreasing power at a rate of 10% of maximum power per second.

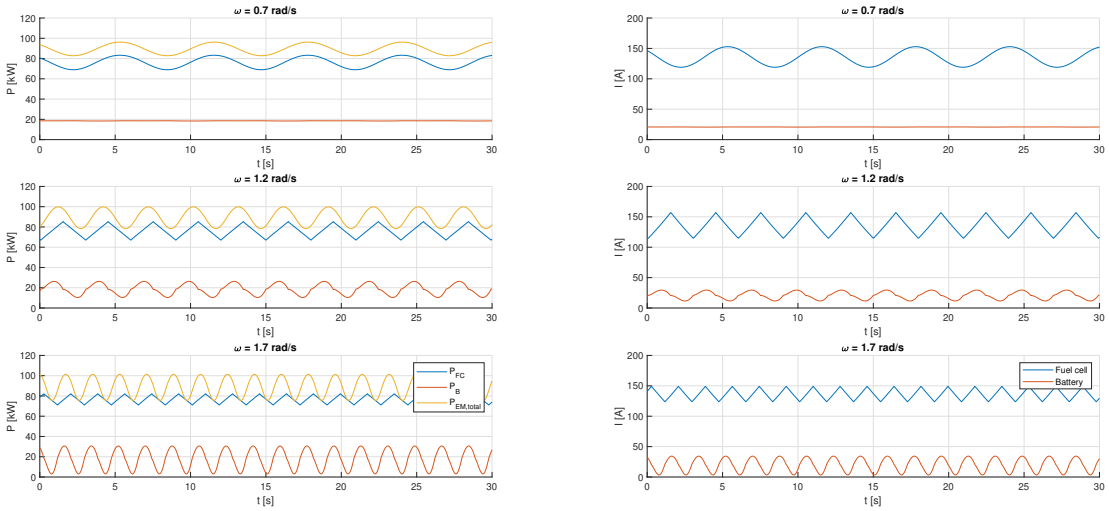

(a) Load distribution

(b) fuel cell and battery current

Figure 7.6: Loading of hybrid power supply with one fuel cell stack and a 3P28S battery, while sailing in head waves at 12 knots

2 fuel cell stacks with a 2P28S battery

A similar response can be seen if the configuration with two fuel cell stacks is tested for part load conditions. In this case, total required fuel cell power is split over two stacks and the state-based EMS still dictates that the battery should operate at its optimal power. The fuel cell power is now operating close to its nominal condition. For the two waves with low frequency (0.7 rad/s and 1.2 rad/s), a battery is not required for support.

On the other hand, support is still required for the wave with the highest frequency, because the fuel cells start lagging behind. Due to this, the battery's assist becomes more irregular (fig. 7.7a, middle figure). If the battery was only used for the transients (for example when the SOC would be below 15%), the battery would also absorb energy at some instances. This results in continuously dis- and recharging and the net effect on the charge level would be zero during the passing of one wave.

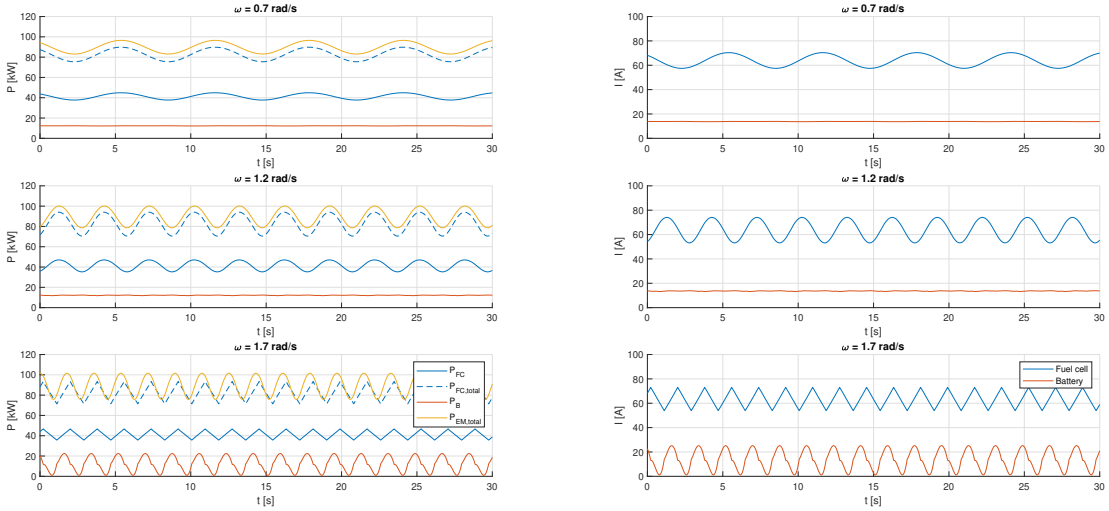

(a) Load distribution

(b) Fuel cell and battery current

Figure 7.7: Loading of hybrid power supply with two fuel cell stacks and a 2P28S battery, while sailing in head waves at 12 knots

7.2.5. Stern waves at cruising speed

In section 7.2.2 it was mentioned that stern waves are also considered. The encounter frequency is much lower here, because the wave and ship travel in the same direction. It was seen that a fuel cell module is better capable to follow low-frequency transients. In contrast to head waves, the highest encounter frequency is found for the wave with the lowest frequency. In this case, the waves travel faster than the ship. For the high-frequency wave, the ship travels slightly faster than the waves, so this results in the lowest encounter frequency. The maximum encounter frequency is 0.4 rad/s in stern waves. The minimum encounter frequency for head waves is 1 rad/s, so all waves have a lower encounter frequency if stern waves are compared to head waves. Hence, according expectations, both configurations are capable to follow the load power in stern waves when sailing at cruising speed. Stern waves at top speed are not discussed here: the fuel cells will work at maximum power anyway, since load power exceeds the maximum fuel cell power, like it was seen in section 7.2.3. All results from the simulations in stern waves are included in appendix E.1

The results that are presented in this section are generated with two models (fig. 6.12 and 6.13). These models have identical electric drives (i.e. the inverters, PMSM's and propellers), but differ on the supply side in terms of number of fuel cell stacks and battery size. Both models should give the same results with respect to ship speed, propeller speed and propeller loading. All results of these simulations are included in appendix E.1 and it can be concluded by looking at these results that both models are consistent with each other.

7.3. Slam start manoeuvre

Emergency manoeuvres induce the most stressful conditions for the driving machines and propulsion system [5]. If these emergency manoeuvres can be executed without exceeding the system limits, it can be expected that other manoeuvres can be executed without problems. The first manoeuvre is called a 'slam start' for ship acceleration.

7.3.1. Slam start procedure

A slam start is a manoeuvre where the vessel is accelerated from a low speed to full speed ahead. A slam start has to meet two criteria to distinguish it from regular ship acceleration. First of all, the bridge lever position, which controls the circumferential speed, is suddenly moved to full speed ahead [5] and, secondly, the initial speed is close to zero. The sudden change of set-points can best be modelled with a step function. The results from the slam start simulations can be compared to the sea trial report of the FCS1204 to make a comparison with the reference vessel. During sea trials, the initial ship speed was approximately 1 knot, so the same number is also selected for this study.

The characteristics of the driving machine are favourable for these type of manoeuvres. It is recalled that the PMSM can deliver full torque instantly and the PMSM can accelerate rapidly. The inertia of the ship causes a delay between the change of the set-points and the time when the reference speed is reached. It is seen that the propeller reaches its reference speed (1275 rpm) faster due to the lower combined inertia of motor, shaft, propeller and entrained water and favourable PMSM characteristics. This is shown in figure 7.8a and 7.8b.

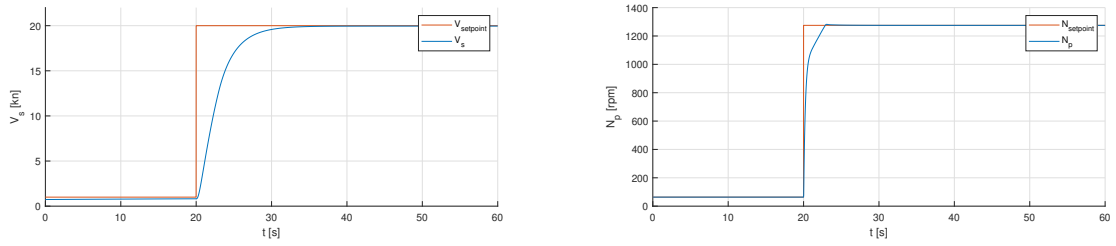

(a) Ship speed

(b) Propeller speed

Figure 7.8: Acceleration during a slam start manoeuvre

It can be seen that the vessel accelerates in 15 seconds to its requested speed. The FCS1204 with diesel engines accelerates in approximately 25 seconds, according to the sea trials report. This report is considered confidential information. It should be noted that the acceleration test during sea trials was executed to reach a speed of 26 knots, so it is estimated that the reference vessel reached 20 knots in approximately 20 seconds.

In this view, the studied propulsion system has improved the ship acceleration.

The electric motor delivers a high electromagnetic torque after the initiation of the manoeuvre. After approximately 1 second, the PMSM delivers a constant 1.8 kNm until the rpm set-point is reached, which takes 3 seconds in total. Due to this, the propeller develops a high torque and thrust (fig. 7.9a). The total thrust from two propellers is much higher than the ship's resistance and this results in the rapid acceleration. As the ship approaches the set-point of 20 knots, the peak load on the propeller diminishes and the system approaches the steady-state condition. From the bottom figure it can be noted that the thrust multiplied by 2 (for both propellers) does not equal the ship resistance at 20 knots, which is a consequence of the thrust deduction.

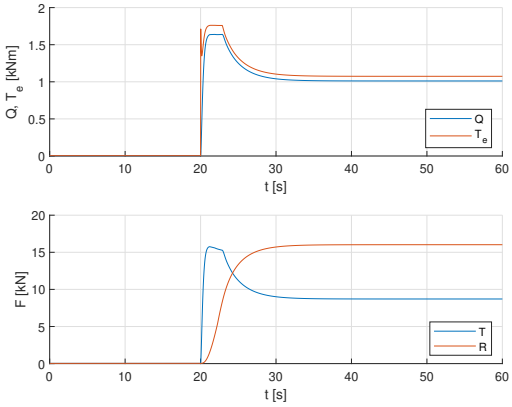

(a) Propeller loading

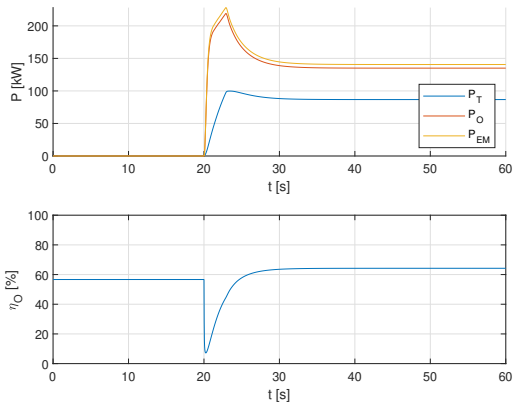

(b) Thrust power, open water power, PMSM power and open water efficiency

Figure 7.9: Propeller and engine loading during a slam start manoeuvre

The thrust power required to sail at a certain speed is provided by the electric motor at a certain rotational speed and torque [49]. It is interesting to analyse the steps between motor power and thrust power to see how the electric drive responds to this peak load. This is presented in figure 7.9b. Thrust power is computed from the advance speed and total thrust. The propeller's open water power follows from the torque from the open water diagram and its circumferential speed.

$$P_T = T \cdot V_a \tag{7.8}$$

$$P_O = 2\pi \cdot n_p \cdot Q \tag{7.9}$$

The difference in open water power and thrust power is defined by the open water efficiency and it is a measure for the conversion from rotational power to translational power. The actual delivered power is slightly lower compared to the open water condition if the propeller is attached to the hull (relative rotative efficiency) [49]. Finally, the mechanical transmission between motor and propeller also creates a small loss (shaft efficiency):

$$\eta_O = \frac{P_T}{P_O} = \frac{T \cdot V_a}{2\pi \cdot n_p \cdot Q}, \qquad P_{EM} = \frac{P_T}{\eta_O \cdot \eta_R \cdot \eta_S} \tag{7.10}$$

A peak in thrust power can be seen after approximately 3 seconds, i.e. when the propeller reaches its set-point. The open water efficiency is very low during the shaft acceleration due to a high propeller speed and low ship speed. The low efficiency explains the difference between thrust power and open water power. This peak load also diminishes after 3 seconds. During this operation the shaft accelerates at a rate of 460 rad/s^2 at most, which is lower than the motor's limit of 1000 rad/s^2. The rotational speed is increased above the nominal speed of the motor and the motor enters the continuous power speed range. In this domain, the maximum torque is lower compared to the torque limit in the continuous torque speed range (fig. 6.1). The maximum instantaneous torque is delivered during this operation, which is recognised by the flat electromagnetic torque between 1 and 3 seconds. Maximum instantaneous torque can be delivered for at least 30 seconds and here it is only required a few seconds. So, the PMSM's limits are not exceeded during the manoeuvre.

7.3.2. Response of the hybrid power supply to a slam start manoeuvre

In section 6.2 it was noted that the stator current I_q is also referred to as torque producing current. Equation 6.16 shows the direct relationship between the quadrature current and electromagnetic torque. The PMSM's are fed by the DC bus through the inverter, so a peak current is also expected at the DC bus.

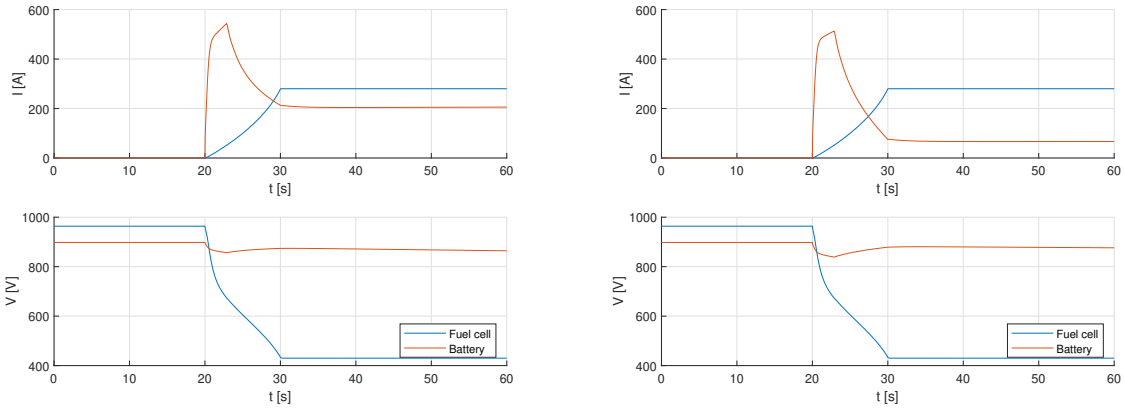

(a) 1 fuel cell stack with a 3P28S battery

(b) 2 fuel cell stacks with a 2P28S battery

Figure 7.10: Dynamic behaviour of the hybrid power supply during a slam start manoeuvre

Figure 7.10a and 7.10b show the dynamic behaviour of both selected configurations during a slam start manoeuvre. A high peak load can also be observed for the hybrid power supply. The fuel cell stack is still limited at a maximum load change, with respect to its maximum power, of 10% per second. This means that the battery provides ramp support to assist the fuel cells during this transient period. The battery peak current seems very high compared to the quadrature current, but it must be recalled that both motors are connected in parallel and, hence, the total current flow through the DC bus is twice the current that flows to each motor. Furthermore, there are no significant differences between the two configurations, although the peak current is somewhat lower for the configuration with two fuel cell stacks (510 A compared to 540 A). The fuel cell module delivers approximately 50 A after 3 seconds, but this is reduced across the DC/DC converter, which operates in boost mode when the bus voltage (i.e. battery voltage) exceeds the stack voltage. Hence, the difference between the two cases is small. When the steady-state condition is reached, the battery contributes a lower amount of the total power which corresponds to the results from the energy analysis (sec. 5.2.2).

7.3.3. Effect of speed slope limiters

High peak currents are observed for the slam start manoeuvre. A speed slope limiter for the PMSM might be an optional control strategy to reduce the magnitude of the peak load for the hybrid power supply. This control strategy is suggested by [68] for diesel engines to better match fuel flow and turbocharger speed to the operational point of the engine in transient conditions. In some way, the fuel cell power pack can also be seen as a component that supplies the "fuel" for the electric motor, albeit electrical energy. By limiting the acceleration rate, the load change of the PMSM is better matched to the capability of the fuel cells. Therefore, three settings for the speed slope limiter (Δrpm) are tested in this section: 100, 200 and 300 rpm/s. The results of these simulations are compared to the slam start manoeuvres without a speed slope limiter.

The effect of the speed slope limiter settings has a clear effect on the acceleration time (fig. 7.11a, 7.11b). The acceleration with the lowest rate results in an acceleration time of 23 seconds. The acceleration time from the sea trial report was approximately 20 seconds, so this is slower compared to the sea trials. The other cases still show improved results (15 - 18 seconds). Therefore, it should be noted that a low speed slope limiter setting reduces the performance during a slam start manoeuvre, which was also found by [5].

Figure 7.12a and 7.12b show the fuel cell and battery current for these various speed slope limiter settings. Only current is presented here, because the bus voltage is similar to the voltage curves that are presented before, but all results are included in appendix E.2. The maximum continuous and instantaneous battery current are also plotted in the figures in addition to the actual battery current during the manoeuvre. The

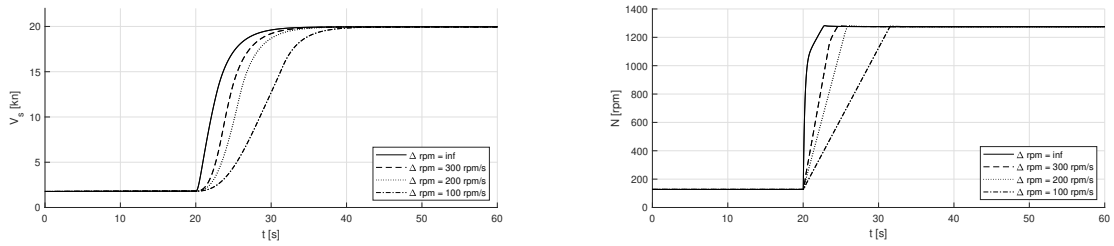

(a) Ship speed

(b) Propeller speed

Figure 7.11: Acceleration during a slam start manoeuvre with various speed slope limiter settings

maximum battery current is lower for the second configuration, because only two banks are connected parallel (tab. 4.4). The maximum continuous current is exceeded for all cases except for a slope limit of 100 rpm/s and this outcome is the same for both configurations. The rush current is 350 A per bank so this value is not exceeded for both configurations. The maximum continuous current can be exceeded for 20 seconds according to the suppliers of the battery, so the battery also remains within its limits. However, batteries heat up rapidly during rush currents, so this induces strict requirements for a cooling system. The results of this section are summarised in table 7.2.

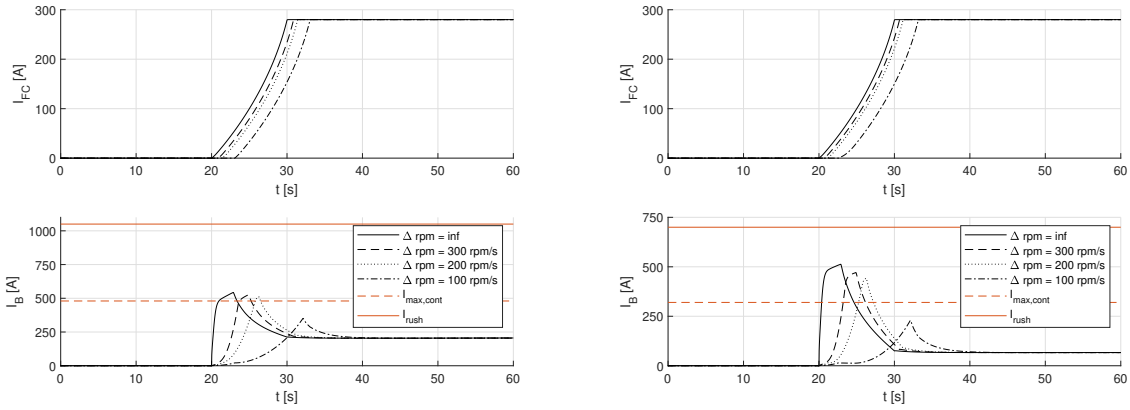

(a) 1 fuel cell stack with a 3P28S battery

(b) 2 fuel cell stacks with a 2P28S battery

Figure 7.12: Current flow of the hybrid power supply during a slam start manoeuvre with various speed slope limiter settings

			1 FC / 3P28S		2 FC / 2P28S	
Δrpm	**t [s]**	**$P_{EM,max}$ [kW]**	**$I_{B,max}$ [A]**	**dP_{FC}/dt [kW/s]**	**$I_{B,max}$ [A]**	**dP_{FC}/dt [kW/s]**
inf	15.0	228	542	12.0	512	12.0
300	16.5	228	526	12.0	471	12.0
200	18.0	227	511	12.0	441	12.0
100	23.0	190	351	12.0	230	11.5

Table 7.2: System performance during a slam start manoeuvre with various speed slope limiter settings

7.4. Crash stop manoeuvre

The second manoeuvre is called a 'crash stop' and intends to stop the ship as fast as possible. It is usually executed to avoid collisions. This condition is often most stressful for the system [5].

7.4.1. Crash stop procedure

A common way to reduce a ship's speed is to reduce propeller speed and hence reduce thrust. As a result, the vessel will start to decelerate, because the resistance exceeds the thrust. The speed drop will be large just after the change of propeller speed, but in the end the ship speed will converge slowly to the desired speed as

the magnitude of the resistance force also decreases during deceleration. However, this approach does not result in a satisfactory braking distance so the propulsion system must provide an additional braking force [101]. This is done by reversing the engine to deliver negative thrust. A crash stop manoeuvre is then defined by class societies as a manoeuvre where the bridge lever position is changed suddenly full speed ahead to full astern. There is also sea trial data available from crash stop manoeuvres, so this is also used as reference. Two control procedures can be used to stop the vessel:

- **Direct braking**: the PMSM can directly apply a braking torque to decelerate the shaft when the crash stop is initiated. The propeller reaches a negative speed rapidly and it is expected that a braking force is developed almost instantly. It is also expected that this procedure results in a short stopping distance.
- **Coasting and braking**: the second procedure is more common for vessels with internal combustion engines as driving machines. The engine's speed is reduced slowly towards a characteristic reversing speed [101]. At this speed the engine can be reversed (direct drive) or it is possible to clutch in or out (reversion via gearbox). Due to this, the ship's speed will slowly drop (i.e. coasting) and after reaching the characteristic reversing speed additional brake force is delivered. There is no such thing as a characteristic reversing speed for the PMSM, but this procedure can still be followed by going to a zero-speed condition before applying a braking force.

These procedures are further analysed in the next sections. In the foregoing section, the effect of a speed slope limiter was also looked into. This control method, however, doe not improve the stopping time for a crash stop manoeuvre. The sea trials were executed at an initial speed of 26 knots and the vessel is stopped within 11 seconds approximately. It is estimated that an initial speed of 20 knots leads to a stopping time of approximately 8 seconds. The highest speed slope limiter setting (300 rpm/s) gives a stopping time of 8.5 seconds, so the performance is even reduced for the highest slope limit. These stopping times are presented in appendix E.3.1.

7.4.2. Direct braking

The vessel has an initial speed of 20 knots at a propeller speed of 1275 rpm. After 20 seconds, the crash stop is initiated by changing the bridge lever position from 100% to -100%. The PMSM delivers a braking torque directly after the initiation of the procedure to stop the vessel. Figure 7.13a and 7.13b show the deceleration of the vessel.

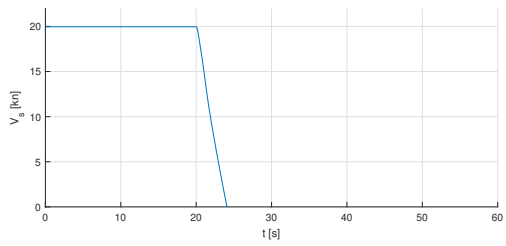

(a) Ship speed

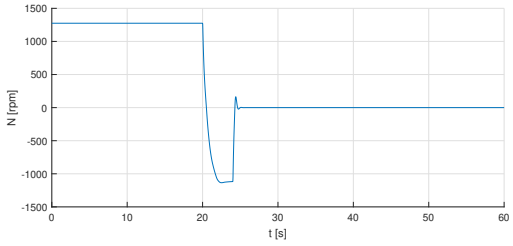

(b) Propeller speed

Figure 7.13: Deceleration during a crash stop manoeuvre with direct braking

The vessel is stopped in 4 seconds which is a significant improvement compared to the sea trial data. This stopping time gives a deceleration rate of 2.6 m/s^2, which is almost linear according to the figure 7.13a. This achieved by reversing the propeller direction. It is observed that the propeller does not reach its reversed set-point of -1275 rpm, but it is limited at -1130 rpm. This observation can be explained by looking at the propeller and engine loading (fig. 7.14a). It is seen that the engine delivers its maximum instantaneous braking torque of -1.8 kNm from 2.5 seconds onward after the initiation of the manoeuvre. Therefore, the reversed propeller speed can not be further increased.

It is also seen that each propeller delivers a thrust of approximately -13 kN, which results in a negative thrust force. The thrust power diminishes together with the ship's speed (eq. 7.8). The open water power, however, is only negative for a short moment when torque is negative and circumferential speed positive (eq. 7.9). A negative PMSM power suggests that it operates as generator so there will be an energy flow back to the DC bus [40], which should be absorbed by the battery. The PMSM power becomes positive again as soon as the

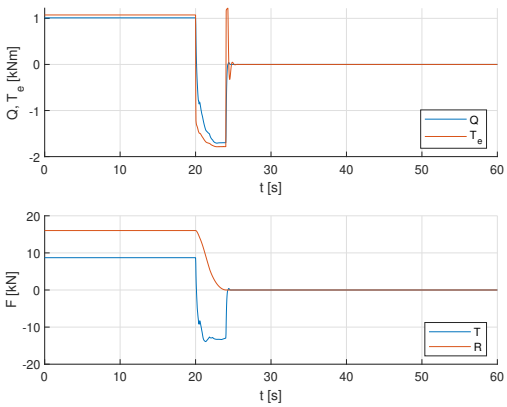

(a) Propeller loading

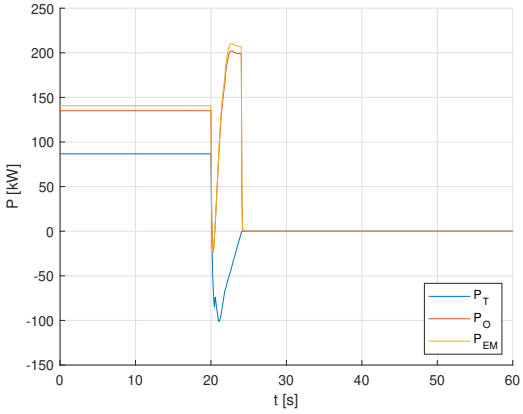

(b) Thrust power, open water power and PMSM power

Figure 7.14: Propeller and engine loading during a crash stop manoeuvre with direct braking

propeller speed and torque are both negative. Figure 7.14b shows that the negative power is followed rapidly by the positive PMSM power.

Figure 7.15a and 7.15b show the dynamic behaviour of the hybrid power supply, for both configurations, during the crash stop manoeuvre. The hybrid power supply experiences a high negative power at first. It is observed that the magnitude of the peak is much larger than the generated power from the PMSM. This is due to the fact that the stator current I_q controls the electromagnetic torque of the motor. A high current is required to generate the maximum instantaneous torque, so this induces a high load on the hybrid power supply. In addition to this, the fuel cell stack can not reduce its power instantly. Therefore, the battery also has to provide ramp-down support by absorbing the energy from the fuel cell system. This peak load is highest for the configuration with two fuel cell stacks, because the battery has to provide support for both stacks. When the vessel has come to rest, the stacks are still running at a high power, so the battery provides ramp-down support again until fuel cell power has become zero.

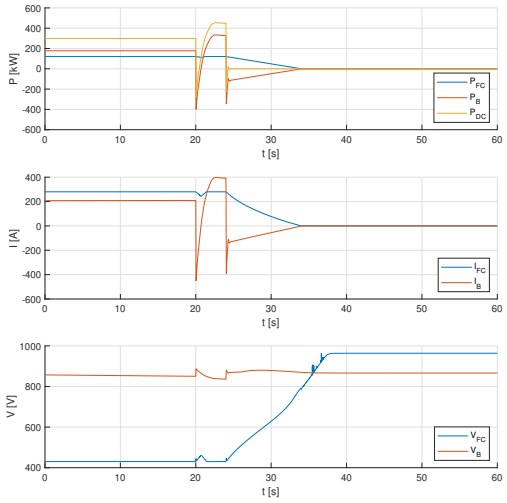

(a) 1 fuel cell and a 3P28S battery

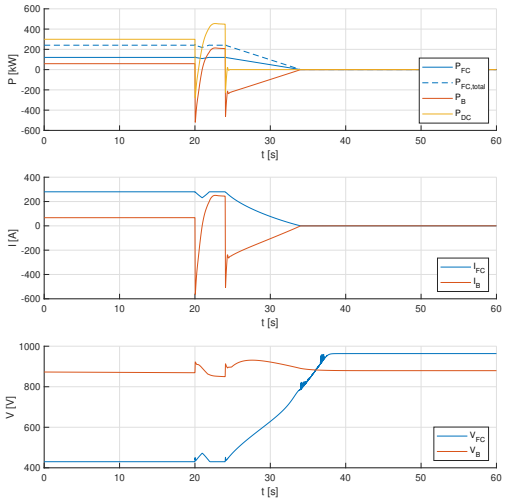

(b) 2 fuel cell stacks and a 2P28S battery

Figure 7.15: Dynamic behaviour of the hybrid power supply during a crash stop manoeuvre with direct braking (top: load distribution, middle: current, bottom: voltage)

7.4.3. Coasting and braking

When the crash stop manoeuvre is activated, the bridge lever position is changed from 100% to 0%. After 6.3 seconds, the vessel reaches a speed of 30% of the initial speed and the lever position is changed to -100% for additional braking force. The vessel comes to rest 1.7 seconds later after a total elapsed time of 8 seconds (fig. 7.16a, 7.16b). The reference vessel executes the manoeuvre in the same amount of time.

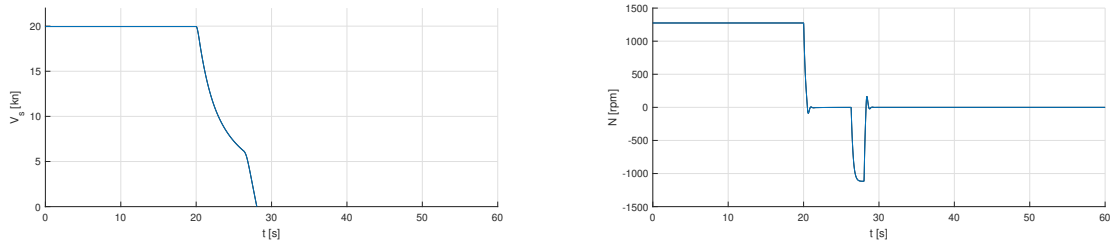

(a) Ship speed

(b) Propeller speed

Figure 7.16: Deceleration during a crash stop manoeuvre with coasting and braking

Once again it is seen that the propeller does not reach its set-point of -100%. Instead it only reaches a reversed speed 1120 rpm. In the foregoing section this was explained by looking at the propeller and motor torque. During braking, the PMSM operates at its maximum instantaneous torque, so the reversed circumferential speed can not be increased any further to its set-point.

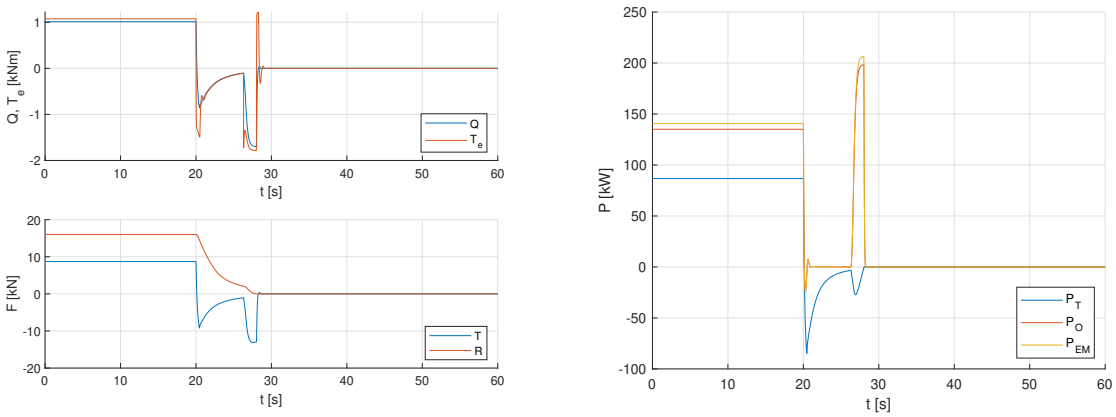

(a) Propeller loading

(b) Thrust power, open water power and PMSM power

Figure 7.17: Propeller and engine loading during a crash stop manoeuvre with coasting and braking

The propeller loading diagram (fig. 7.17a) also shows some other remarkable results. Both torque and thrust show large negative values during the coasting phase, -0.85 kNm and -9 kN respectively. During this phase circumferential speed equals zero, so at first it was expected that this would result in a condition where both torque and thrust are low. This observation can be explained by recalling the equations that are used to determine the operational point of the propeller (eq. 6.30-6.32). The hydrodynamic pitch angle equals 90° when the circumferential speed equals zero, which gives the lowest values for the torque and thrust coefficients (fig. 6.9). The advance speed is still high right after the initiation of the manoeuvre and, therefore, the torque and thrust are also high. The hydrodynamic pitch angle remains 90° during the coasting phase, but torque and thrust decrease together with the ship's deceleration. Similar to the previous case, a negative thrust power is developed and the PMSM operates as a generator for a short moment (fig. 7.17b). So, it can be concluded that a braking force is also developed during the coasting phase and this contributes to a shorter stopping time.

Finally, the dynamic behaviour of the hybrid power supply is also studied for the crash stop manoeuvre with coasting and braking. Some similarities are observed with the crash stop manoeuvre with direct braking. First of all, it is noted that the hybrid power supply has a similar response right after the initiation of the emergency stop: a large negative peak load is experienced by the system and the battery absorbs this energy.

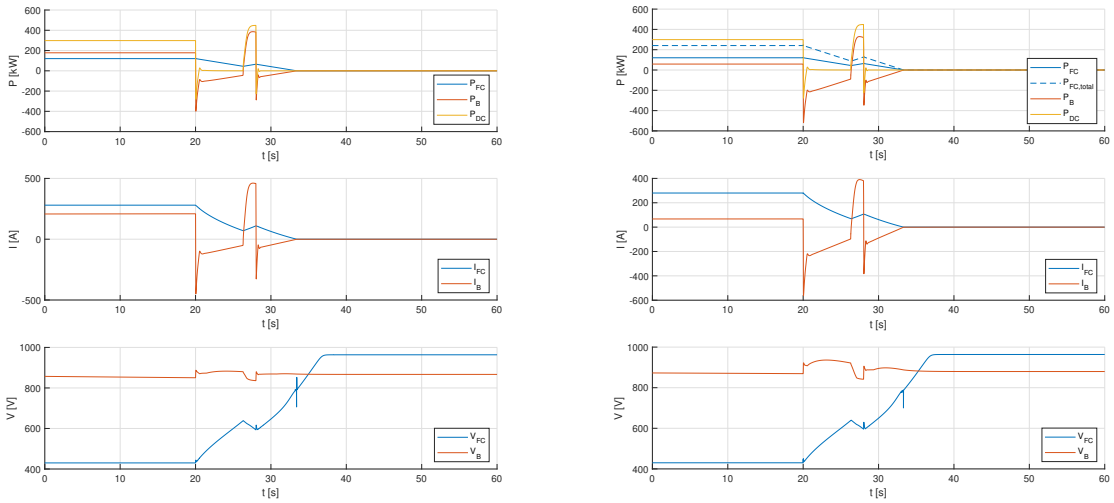

(a) 1 fuel cell stack and a 3P28S battery

(b) 2 fuel cell stacks and a 2P28S battery

Figure 7.18: Dynamic behaviour of the hybrid power supply during a crash stop manoeuvre with coasting and braking (top: load distribution, middle: current, bottom: voltage)

For the configuration with two fuel cell stacks, this peak load is highest, because the battery has to compensate for the slow transients of both fuel cell stacks. However, during the coasting phase, the load power is low and the stack's power output is slowly reduced while the battery provides ramp-down support. When the PMSM is reversed a second peak load is created and this is also handled by the battery. Finally, when the vessel has come to rest, the battery provides some final ramp-down support until the fuel cells' output equals zero and the manoeuvre is terminated.

From the crash stop simulations it is concluded that the fuel cells do not experience extreme loads by limiting its responsiveness to transient loads (10% load change per second). The PMSM and battery are exposed to these high loads. During braking, the PMSM has to deliver a maximum of 210 kW, which is above its maximum continuous power. However, the power limit is only exceeded for a number of seconds at most where maximum instantaneous power can be exceeded for at least 30 seconds. For the batteries it is important to remember that two different batteries are used in these simulations with different maximum continuous current strengths: 2P28S (320 A) and 3P28S (480 A). For the studied cases with one fuel cell stack and a 3PS28S battery, it is found that the maximum continuous current is not exceeded for any simulation. This is not the case for the configurations with two fuel cell stacks and a 2P28S battery. The maximum continuous current is especially exceeded during the large drop in current (up to -563 A) after the initiation of the crash stop. However, the maximum instantaneous current of 700 A (2P28S) is not exceeded during these manoeuvring simulations. The peak values, both positive and negative, that are found during the simulation of the crash stop manoeuvres are given in table 7.3.

			1 FC / 3P28S		2 FC / 2P28S	
Control strategy	**t [s]**	**$P_{EM,max}$ [kW]**	**$I_{B,max}$ [A]**	**dP_{FC}/dt [kW/s]**	**$I_{B,max}$ [A]**	**dP_{FC}/dt [kW/s]**
Direct braking	4.0	-24/210	-450/397	± 12.0	-563/248	± 12.0
Coasting & braking	8.0	-24/206	-450/461	± 12.0	-563/389	± 12.0

Table 7.3: System performance during a crash stop manoeuvre for direct braking and coasting & braking

7.5. Conclusion

This chapter presented the energy flow in the fuel/cell battery system under transient conditions. The results are generated with two independent models, with an identical all-electric drive. Both models are consistent with each other in terms of propeller and PMSM loading. This increases the confidence in the reliability of the presented results. Furthermore, the following conclusions can be drawn with respect to the three scenarios:

- **Sailing in waves**: first of all, it can be concluded that the system loading remains within the system's limits. In section 3.3 it was noted that the selected PMSM results in an engine margin of 20% for a displacement of 12 tonnes. Both selected configurations have a displacement of approximately the same number. The maximum continuous power is not exceeded due to this engine margin. Furthermore, as an effect of the stack's dynamic limit (10% load change per second), the fuel cells can only follow the low-frequency waves. For high-frequency transients, a battery is required. However, from a power management point-of-view it is not preferred that both the fuel cells and battery respond to the fluctuating loads as seen for head waves at cruising speed.

- **Slam start**: the PMSM's characteristics are very favourable for a slam start manoeuvre and due to this it is possible to reduce the total acceleration time compared to conventional diesel propulsion. However, rapid shaft acceleration induces a high peak in propeller loading (both torque and thrust) and, hence, the hybrid power supply experiences a high peak load as well. The PMSM and battery are capable to handle these peak loads, but only for a limited amount of time. Alternatively, the application of a speed slope limiter is a feasible method to reduce the peak current, but this increases total acceleration time during a slam start manoeuvre. Still, the moderate slope limiter settings (300 or 200 rpm/s) show improvements compared to the reference vessel.

- **Crash stop**: two approaches are suggested here for the crash stop manoeuvres: 'direct braking' and 'coasting and braking'. Both methods effectively stop the vessel within the same amount of time or faster compared to the sea trial data of the FCS1204. The application of speed slope limiters results in reduced performance compared to the reference vessel. Furthermore, both methods result in high peak loads in the hybrid power supply, which is similar to the slam start manoeuvre. The peak loads for the propulsion system are in the same order of magnitude for both methods, where is was expected that 'coasting and braking' results in lower loads. Therefore, 'direct braking' might be preferred for an actual crash stop manoeuvre, because the stopping time is shorter (4 seconds compared to 8 seconds). Furthermore, negative (generator) power is developed during braking when the PMSM applies a braking torque and the propeller is still running in forward direction. In this case, energy flows back to the DC bus which is absorbed by the battery.

8

Conclusion and recommendations

This study is finalised in this chapter. It presents the conclusions that are drawn from the research. In addition, some points of discussion are brought forward and finally recommendations are presented for future research.

8.1. Conclusion

In chapter 1 three knowledge gaps were identified, being: (1) the application of hydrogen propulsion for high-speed craft (operability), (2) the combination of fuel cells and batteries for marine vehicles (hybridisation) and (3) the capability of a fuel cell/battery propulsion system to follow dynamic loads and system control (energy and power management). These knowledge gaps have lead to the formulation of the following main research question:

What is the impact of implementing a hydrogen fuel cell-battery propulsion system on the operability of high-speed craft, based on time-domain simulations of various operational conditions?

It is recalled that 'operability' is defined as the ability to keep the vessel in a reliable functioning condition, according predefined operational requirements. The main question is answered at the end of this section after addressing the sub-questions. These questions were formulated to look at the different aspects of the problem separately.

First sub-question
To what extent is the operability reduced by respecting physical system constraints?

Two physical constraints were identified in this study: ship weight and volume of the fuel storage system. The total weight of the reference vessel was 11.5 tonnes in loaded condition, of which 2.5 tonnes is used for the diesel engine and auxiliary system. The implementation of the fuel cell/battery system results in a total weight of approximately 12 tonnes. The added weight does have consequences for the installed power, but the selected electric motors are capable to deliver the demanded power with an engine margin of 20% (fig. 3.5a). However, if it turned out that a large battery would have been required, the total weight could increase up to 13.3 tonnes (2 fuel cell stacks with a 5P28S battery). The power consumption at a speed of 20 knots would still fall within the drive characteristic, but the engine margin becomes small as a result of this added weight (6%). Alternatively, the total weight can be reduced by limiting the available weight for deck load or passengers, but this would reduce the operability with respect to the reference vessel. In this sense, it is beneficial to select a configuration with a lower weight.

The second constraint is the available volume for fuel storage. The hydrogen is stored at 350 bar in composite pressure vessels. There is space for 6 tanks with a total capacity of 50.4 kg hydrogen that should be located at the aft section of the open deck (fig. 3.6). The hydrogen storage capacity poses the main limitation to the operability of the vessel. Table 5.10 showed that the system consumes 46 to 48 kg of hydrogen for the survey operation. From these results it is evident that endurance (and top speed) are limited by the hydrogen

storage constraint. The required endurance was one hour to the survey location and one hour back to port. The endurance can not be increased over one hour (at a speed of 19 knots), because hydrogen consumption will be too high. Similarly, it is also not feasible to increase the speed to 20 knots due to the increased power at a higher speed. If it is desired to increase the vessel's endurance, it is necessary to change the storage method. Liquid hydrogen or ultimately other hydrogen carriers (such as ammonia, LNG or methanol) can be considered then.

Second sub-question
What are the trade-offs in the selection of a suitable energy management strategy to balance energy demand from the fuel cell stack and battery?

An energy management strategy can serve various objectives, like minimising hydrogen consumption, sustaining a battery SOC or maximising the fuel cell or system efficiency. The control hierarchy has two levels. Energy management, being at the top level, ensures that sufficient energy is available to execute a certain mission. Power management controls the current from the fuel cell stack and battery to prevent that limits are exceeded. Four energy management strategies (EMS) are reviewed in this study: proportional-integral control (PI), state-based, equivalent fuel consumption minimisation (ECMS) and charge depleting charge sustaining (CDCS). These management strategies are judged on the attainable system efficiency, fuel consumption, simplicity and effect on operability.

Both ECMS and CDCS try to maintain a steady state-of-charge at a relatively low level. However, the vessel requires a high SOC prior to a period of sailing at top speed, because the battery supports here as power booster. Hence, the operability, i.e. the prolonged period that the vessel can sail at top speed, is too low for these strategies. Furthermore, it is assessed that the state-based EMS scores better in terms of efficiency compared to PI control. Therefore, state-based EMS scored best overall (tab. 5.1) and is selected for the energy management to provide power set-points for the fuel cell stack and battery. PI control, however, can accurately control the output of components by employing a feedback loop. Therefore, PI control is used in the power management to govern the fuel cell current and PMSM speed (commanded by the bridge lever position).

Third sub-question
What is the most suitable degree of hybridisation for fuel cell/battery vessels?

Hybridisation can be defined in two ways: energy hybridisation and power hybridisation. The first definition analyses the delivered energy of the battery compared to total energy consumption of the vessel and does also incorporate recharging. A large battery requires less recharging and contains more energy. Therefore, it was expected that energy hybridisation increases with the capacity of the battery and this is supported by the results from chapter 5. Two operational profiles are tested in this study: a survey vessel with a high endurance at top speed (1 hour, 19 knots) and a harbour patrol vessel with a low endurance at a higher speed (10 minutes, 20 knots). It was found that a high endurance pleas for a high gravimetric energy density, because energy consumption increases rapidly at top speed. On the other hand, a lower endurance and higher speed asks for a high power density. In general, fuel cell systems score better with respect to energy density and batteries score better in terms of power density [42]. Therefore, the configuration with two fuel cell stacks and a 2P28S battery (90 Ah) was found to be most suitable for the survey vessel and this results in an energy hybridisation of 8%. The harbour patrol vessel asks for a higher power density and hybridisation. Therefore, the configuration with one fuel cell stack and a 3P28S battery (135 Ah) is selected here and this yields an energy hybridisation of 18%. The configuration which was selected for the survey vessel can also be used for the intended harbour patrol operations and gives a hybridisation of 12%. So, it can be concluded that the most suitable energy hybridisation lies between 8% and 18%.

Power, being the derivative of energy, is by definition instantaneous and the power hybridisation gives the fraction of the battery power compared to total power. Different battery functionalities require different degrees of power hybridisation. The battery peak power is highest for manoeuvring (ramp support), but the power is delivered for a very short time. Every battery can deliver a high current for a very short time (rush current). If a battery is only used in waves for the harmonic loads, it is continuously charged and discharged, because battery power oscillates around zero. Therefore, the smallest all batteries contain sufficient energy

to execute this functionality. However, the top speed and endurance at this speed dictate sizing, because the battery has to deliver a high power for a prolonged period. The difference in total fuel cell power is large for the two configurations (120 kW vs. 240 kW), so the battery has to provide much more power if only one fuel cell module is installed. This results in a power hybridisation of 61% compared to 23% for the selected configurations with one and two fuel cell stacks, respectively.

However, it should be noted that the simulations are executed with ten configurations, combining one or two fuel cell stacks and one of five different battery sizes. Therefore, the results for the hybridisation follow from a discrete problem. Therefore, it is only possible to asses which configurations result in the most suitable hybridisation, but it can not be concluded that this is the optimal hybridisation.

Fourth sub-question
What is the impact of fuel cell/battery propulsion on top speed, endurance and efficiency of high-speed craft?

First of all, the implementation of hydrogen propulsion does not necessarily affect the top speed of the FCS1204. A speed of 26 knots can only be reached with a configuration with two fuel cell stacks and a large battery (4P28S/5P28S). In theory, the vessel can sail at a speed of 26 knots for 30 to 35 minutes, which corresponds to a range of 13 to 15 nautical miles. This emphasises the largest impact of hydrogen propulsion for high-speed craft. The reference vessel can sail over 200 nm at a speed of 26 knots so the maximum range is massively reduced with 93%. Similar results followed from the previous studies at Damen, so therefore it was decided to reduce the design speed to 20 knots. However, if the vessel is equipped with the configuration with the highest specific energy, i.e. two fuel cell stacks and a 2P28S battery, the endurance is still much lower compared to the reference vessel. The FCS1204H2 can ultimately sail for 67 consecutive minutes at this speed, before the battery is completely discharged (fig. 5.9) and results in a range of 22.4 nm. The other configuration has a maximum endurance of 29 minutes and range of 9.6 nm when sailing at top speed.

The second objective in this sub-question is to analyse the efficiency of the propulsion system. However, it was not feasible to make a complete assessment with respect to efficiency within the time that is spent on this research. Balance of plant losses are not included in the fuel cell model and it is also assumed that the battery's internal resistance is constant and, therefore, the power losses in the hybrid power supply are estimated optimistically. However, it should still be noted that the mean fuel cell stack efficiency (i.e. thermodynamic efficiency) lies between 57% and 63% (tab. 5.11). A diesel engine has a nominal efficiency around 45% [81] so the thermodynamic efficiency of the energy converters is higher in the proposed system. In addition to this, from the operational profiles it is seen that high-speed craft sail at top speed for only a limited amount of time, i.e. the system operates at part load for a significant fraction of the time. The reference vessel has a direct drive diesel configuration and operates, so the mean efficiency of the diesel engine is expected to be even lower than 45%. Contrary to this, it was seen that fuel cells have excellent efficiencies in part load conditions. The philosophy of hybridisation is to utilise multiple energy sources to ensure efficient operation for both average and peak power demand [74]. The state-based EMS determines, based on load power and battery SOC, how the load is split between the fuel cell power pack and battery. In part load, this results in a power distribution where both components deliver energy at an efficient operational point (tab. 5.2, 5.3). As a consequence, the state-based EMS ensures a high system efficiency for various operational conditions and this a major benefit of the hybridisation.

Fifth sub-question
What are the characteristics of the transient response of the propulsion system to time varying loads?

Two types of varying loads are analysed in this research: continuous load changes and a change of the vessel's speed set-point. A continuous variation was tested by modelling a regular wave with a wave height of 1 meter and varying frequency, direction and ship speed. Two emergency manoeuvres, a slam start and crash stop, were simulated to analyse how the system responds to a change of set-points. If the system performs well during these emergency manoeuvres, it can be deduced that it also performs well during moderate acceleration or deceleration. For all tests, the LT-PEM fuel cells should be limited at a load change of 10% of its maximum power per second and the battery supports the fuel cell stack if it can not follow the transient loads.

The combination of frequency, direction and ship speed determines the encounter frequency of the vessel

and wave. It is found that the fuel cells can follow loads with a low encounter frequency, but it needs assistance for the high-frequency loads. The limit is found around an encounter frequency of 1 rad/s for a system with one fuel cell stack and 1.2 rad/s for a system with two fuel cell stacks. However, when the system is exposed to high-frequency loads it is observed that the fuel cells operate at their dynamic limit: the power output is continuously linearly changing at a rate of ±12 kW/s (fig. 7.6a and 7.7a), while load power has the shape of a sine wave. Especially, if the vessel is exposed to more realistic conditions, both frequency and wave height differ significantly and it is expected that the battery is continuously required to support the battery. From a power management perspective it is preferred that the fuel cells follows low-frequency loads and the battery high-frequency loads, due to the high battery responsiveness. This functionality was earlier referred to as load smoothing (fig. 2.7) and can be achieved by implementing a low-pass filter in the power management system. Furthermore, it is also concluded that the synchronous machines operate within their limits. In calm water conditions, there is an engine margin of approximately 20% and in the most extreme wave (high speed, high frequency and head waves) there is still a margin of 6% with respect to the maximum continuous power.

For the emergency manoeuvres it can be concluded that the operability is improved compared to the reference vessel with diesel propulsion. This is mainly due to the favourable characteristics of the battery and permanent magnet synchronous machines: the PMSM's are capable of delivering maximum torque instantly and they can accelerate/decelerate at a rate of 1000 rad/s^2. Due to this, it is possible to reach top speed in 15 seconds, compared to 20 seconds for the reference vessel. The total crash stop time can also be reduced with 50% from a reference time of 8 seconds. However, these simulations show that the manoeuvres induce high peak loads in the system. Both the maximum continuous power of the PMSM and maximum continuous current of the batteries are exceeded. These loads remain within the maximum instantaneous power/current. The maximum instantaneous power/current can be delivered for a limited time only, but these absolute limits are not exceeded in any simulation.

Main research question
The conclusions that are drawn from the foregoing sub-questions are now summarised for the main conclusion of this research. First and foremost, it is found that it is feasible to implement fuel cell/battery propulsion on high-speed craft, but it comes at significant costs in terms of range and top speed. First of all, hydrogen in compressed form requires a very sizeable storage system and this poses the main limitation for operability. With the available volume for fuel storage, the range at top speed is reduced up to 93%. In practice this would mean that it is possible to sail for a limited prolonged period at top speed (up to 1 hour) and refuelling is required more often (daily) compared to diesel propulsion. Second of all, boosting is one of the main functionalities of the battery system. The batteries are discharged rapidly when sailing at top speed when they deliver up to 60% of the total power. In theory, it would be possible to achieve the same top speed as the reference vessel (26 knots). However, in practice the batteries are discharged so rapidly that it is not functional to sail at such high speeds. Therefore, the intended top speed should also be reduced when implementing the proposed propulsion system. After discharging, the fuel cells take care of the recharging and therefore, the majority of the energy is delivered by the hydrogen and fuel cells (82% to 92%).

The reduced range and top speed affect the functionality of the vessel. The FCS product group is purpose-built to transport crew and supplies quickly. The hydrogen storage tanks require some deck space and, hence, the cargo capacity in terms of crew or material is also reduced. In addition to this, the vessel is not capable to operate as supply vessel for the offshore energy market, as a consequence of the low range. The sailing distance to these locations is high and the vessel can not sail a return trip with the current fuel capacity. Therefore, it is recommended to redefine the user profile of the FCS1204H2.

At top speed, the fuel cells have to operate at maximum power and this is not the most efficient domain. At part load, however, a state-based energy management system takes care of the power splitting in order that both the fuel cells and battery work at an efficient operational point. The state-based EMS is suggested here as it is easy to implement and understand. This EMS ensures a high system efficiency for various operational conditions and this is one of the major benefits of the hybrid power supply as proposed in this study.

Finally, the fuel cell/battery propulsion system has an excellent performance under transient conditions. This is mainly due to the high responsiveness of the battery and synchronous machines. LT-PEM fuel cells are

quite responsive compared to other types (SOFC's for example), but it is recommended to limit the FC's rate of change to 10% of its maximum power per second for marine configurations. Therefore, the fuel cells are only capable to follow low-frequency loads. The energy and power management system should filter these from high-frequency loads and split the power accordingly in order to respect the dynamic limit of the fuel cells. Due to this limit, the battery does also play an important role during ship acceleration and deceleration (ramp-up/ramp-down support). During emergency manoeuvres, the proposed system outperforms the original diesel configuration due to the favourable characteristics of all-electric ship propulsion. During these manoeuvres, the maximum continuous power is exceeded for both the PMSM and battery, but it remains within the maximum allowable instantaneous limits.

8.2. Discussion

The reliability of the results that are presented in the foregoing chapters of this thesis are impacted by two aspects. First of all, there are a number of model simplifications and, second of all, there is a lack of verification and validation. Therefore, there is some uncertainty in the accuracy of the results and both aspects will be discussed.

8.2.1. Model simplifications

The presented study focuses on the implementation of fuel cells in high-speed craft, rather than the internal performance of the fuel cell or battery. Therefore, it was chosen to use generic Matlab Simscape models that are readily available in the SPS library. This brings a number of simplifications and assumptions (ch. 4). For example, it is assumed that the fuel cell stack is equipped with a cooling and water management system. However, the fuel cell's potential can be lost due to local flooding or drying inside the cell and this can even occur with proper water management. So, it is assumed that a number of processes are ideal, which is obviously not the case in reality. Furthemore, there are also some simplifications inherited in the battery model. For example, it is assumed that charge and discharge characteristics are identical. The product specification sheet of the Toshiba cell shows that this is not the case, as charge voltage is in general higher. It would be possible to get rid of these simplifications by modelling the battery and fuel cells from scratch. However, then it would not have been possible to also focus on the implementation of these systems in the vessel within the time that is spent on this research.

Furthermore, it was highlighted in chapter 5 that the energy analysis presents an optimistic outlook for the energy consumption on board the FCS1204. The losses in the hybrid power supply are optimistic, because the battery efficiency is estimated optimistically and the power losses in the converter are not modelled. The battery efficiency is dependent on the internal resistance, which is assumed constant in the battery model. Therefore, it is not possible to accurately compute the battery's efficiency. The actual efficiency can be expected to lie around 95% for the converter and between 95% and 98% for the battery (under normal conditions), according to reviewed literature. These losses are acceptable, because the two configurations were selected conservatively.

In addition to this, the balance of plant components are also not modelled in the hybrid power supply. Especially at a very low fuel cell load factor, the balance of plant induces significant parasitic losses (and to a lesser extent at maximum load). If the balance of plant was included in the model, it might change the optimal power splitting at low load power. In this study, minimum fuel cell power was set at 10% of the nominal power, but maybe this number should be increased due to these parasitic losses. This potentially results in an optimal power splitting where the battery delivers all power when sailing at low speeds (5 or 7 knots in the tested profiles).

8.2.2. Validation and verification

Both the verification of the model and validation of the results is very difficult for the presented study. Similar models of hybrid propulsion systems with fuel cell stacks and batteries are found in literature but these are not publicly available. Second of all, most propulsion models, including those that are presented here, are developed for a specific research objective and these models can not be compared directly with one another. Therefore, during the development of the models, partial verification is applied where possible. In the introduction (ch. 1) it was mentioned that the propulsion model is built up iteratively with increasing scope and complexity. For the fuel cell model, for example, a reference model is used that is verified and validated by

the developer of the Simscape environment [71] and this was used as starting point. In the next step a DC/DC converter was added to the model. This converter was verified by exposing the fuel cell stack and converter to an electric load and checking the model output with manual calculations of the power balance across the converter. In this way, the whole model has been built up.

However, this approach to verification had some limitations. For example, the discharge curve of the battery model is compared to the actual discharge curve from the (confidential) product specification sheet. The discharge curve is modelled with an error less than 3% for the operational domain of the battery (i.e. avoiding deep discharge), but it is only possible to verify the discharge characteristics at normal conditions as it is assumed in the model that temperature is constant. However, it was noted that the temperature rises rapidly if the battery delivers a rush current for a period. At this moment, it can not be verified if the discharge characteristic is representative for rush currents.

Finally, the validation of the results is also not possible. Validation would have been possible if there was an identical system installed in a vessel or laboratory and if the same experiments were executed with this test set-up. However, this research project is part of a larger project at the Damen Shipyards Group, where the ultimate objective is to build and test the 'FCS1204H2'. Within this project it is not yet decided if Damen develops the complete system in-house or that it is ordered from an external supplier, while acting as a "smart customer" with this new knowledge. Anyway, the testing of the vessel will provide valuable information regarding the propulsion system's performance.

8.3. Recommendations

The first point of the discussion that is brought forward suggests that there is room for improvement in the propulsion model. It is acknowledged that the balance of plant components induce parasitic losses, but little is known about the magnitude of these losses. Therefore, it is recommended to include the balance of plant in the model for further development of the system. In addition to this, it is assumed that the stack is fed with hydrogen and air at the desired rate. The hydrogen is stored in six tanks, but it is not yet known how the supply system should be designed. For instance, it is not clear if the fuel should be supplied from a common rail system or individually from each tank. Secondly, it is also not clear how the pressure is reduced from storage pressure to inlet pressure. Therefore, it is concluded that the balance of plant and supply system should be analysed as well to gain more insights with respect to the implementation of fuel cell systems.

Second of all, it is also known that both fuel cells and batteries are negatively affected by age (or number of running hours). Fuel cell degradation results in reduced efficiency over time and, hence, a increased fuel consumption. Furthermore, the capacity of batteries decreases as the cumulative number of charge cycles increases. The reduction of performance is dependent on various parameters such as average C-rate, depth of discharge and temperature. These effects are not taken into consideration in this study, but it would be interesting to analyse the effects of fuel cell degradation and battery ageing on the system's performance. The generic battery model allows the user to simulate ageing effects: the user can define a battery age, measured in cycles, and analyse the reduction in performance due to ageing. However, more information is required about the battery to correctly simulate these effects, like capacity at the end of the battery's lifetime and cycle life at various depths of discharge. Little information is known about these parameters, so this would require closer collaboration with the battery supplier.

It was concluded that the functionality of the vessel is affected by implementation of a fuel cell/battery propulsion system. First of all, the cargo capacity in terms of crew and material is lower compared to the reference vessel. Secondly, operations with a high endurance, such as supply operations for the offshore energy market, are not feasible with the current system configuration. Therefore, it is also recommended to redefine the user profile for the FCS1204H2. The hybrid power supply model can be easily used to test a large variety of operations, such as water taxi or search and rescue operations. In addition to this, it is also recommended to revise the ship design and to optimise the design for the new user profile. For example, the hull form of the reference vessel is optimised for a top speed of 26 knots. At a speed of 26 knots, the vessel is fully planing, but it is a semi-displacement hull at a speed of 20 knots. Therefore, it can be expected that the ship hull would be revised to attain a higher efficiency at the new speed. Furthermore, the spatial design of the propulsion system should also be considered in the next steps towards realisation. The spatial design of the

reference vessel is straightforward due to the mechanical coupling of the diesel engines and propellers. The previous studies, however, have shown that the implementation of the fuel cell system brings large variety in optional spatial designs. In conclusion, it is recommended to revise the ship design based on the reduction of speed and the wide variety of potential spatial designs of the propulsion system. This is also in line with one of the main recommendations from [24], where it is advised to design the vessel around a propulsion system configuration, especially if relatively new technologies are considered.

Furthermore, it was noted that the FCS1204 is a relatively small vessel. This is a good starting point for the implementation of hydrogen propulsion, but the ultimate goal is to develop "green alternatives" for the whole high-speed craft portfolio of Damen. This portfolio can be categorised based on two characteristics: power and autonomy, where autonomy refers to the refuelling interval (fig. 8.1). A combination of LT-PEM fuel cells and hydrogen (compressed or liquid) is feasible for vessels with relatively low power and low autonomy (type 1) and this results in a relatively compact system. However, it can be expected that the low energy density of pure hydrogen becomes too much of a disadvantage for other vessel types, such as fast ferries or crew transfer vessels for the offshore wind industry (type 2) and patrol vessels (type 4). For these types it is expected that other combinations of fuel and fuel cell type result in a higher power or energy density. LNG, methanol and ammonia have considerably better energy densities and solid oxide fuel cells seem promising from a power density point of view [96]. Therefore, it is recommended to start research projects towards other configurations. The presented model can be used for these studies as well. The FCS1204 can easily be replaced by changing the PSD, resistance curve and propeller characteristics and the fuel cell model is also applicable to SOFC's.

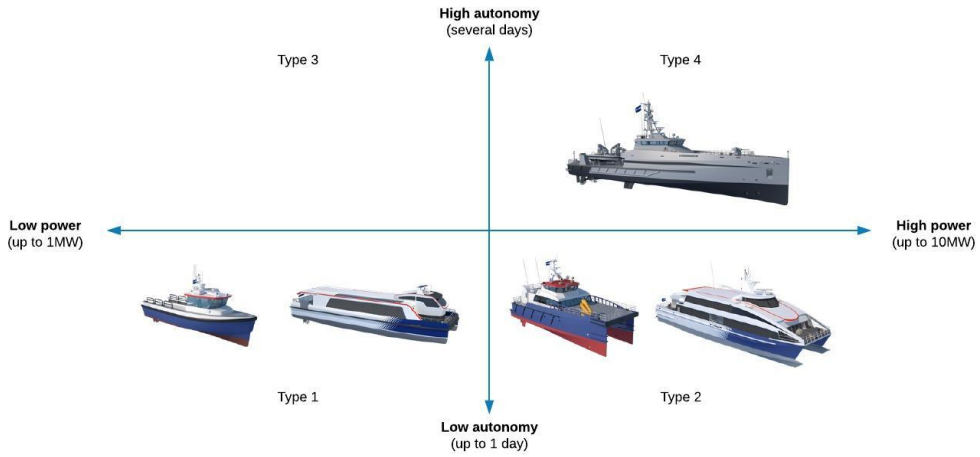

Figure 8.1: Categorisation of the portfolio of the high-speed department of the Damen shipyards group

Bibliography

[1] Aarskog, F.G., Hansen, O.R., Strømgren, T., Ulleberg, Ø. Concept risk assessment of a hydrogen driven high speed passenger ferry. *International Journal of Hydrogen Energy*, 2019. doi: https://doi-org.tudelft.idm.oclc.org/10.1016/j.ijhydene.2019.05.128. Article in press.

[2] Abbasov, F. Roadmap to decarbonising european dhipping. Technical report, European Federation for Transport and Environment, 2018.

[3] Aditya, J.P., Ferdowsi, M. Comparison of nimh and li-ion batteries in automotive applications. *Proc. IEEE Vehicle Power and Propulsion Conference*, Harbin, China, 2008. doi: https://doi-org.tudelft.idm.oclc.org/10.1109/VPPC.2008.4677500.

[4] Alaswad, A., Baroutaji, A., Achour, H., Carton, J., Makky, A.A., Olabi, A.G. Developments in fuel cell technologies in the transport sector. *International Journal of Hydrogen Energy*, 41(37):16499–16508, 2016. doi: https://doi-org.tudelft.idm.oclc.org/10.1016/j.ijhydene.2016.03.164.

[5] Altosole, M., Martelli, M. Propulsion control strategies for ship emergency manoeuvres. *Ocean Engineering*, 137:99–109, 2017. doi: https://doi-org.tudelft.idm.oclc.org/10.1016/j.oceaneng.2017.03.053.

[6] Ammar, N.R., Alshammari, N.F.S.H. Overview of the green hydrogen applications in marine power plants onboard ships. *International Journal of Multidisciplinary and Current Research*, 6:84–89, 2018. doi: 10.14741/ijmcr.v6i01.10912.

[7] Arabul, K.A., Senol, I., Arabul, A.Y., Boynuegri, A.R. Providing energy management of a fuel cell-battery hybrid electric vehicle. *International Journal of Electrical, Computer, Energetic, Electronic and Communication Engineering*, 9(8):935–939, 2015.

[8] Aravind, P.V. *Fuel cell systems*. Delft University of Technology, Delft, the Netherlands, 2019. Lecture slides.

[9] Barbir, F. *PEM Fuel Cell - Theory and Practice*. Academic Press, Cambridge, United States, second edition, 2013. ISBN 978-0-12-387710-9. doi: https://doi-org.tudelft.idm.oclc.org/10.1016/C2011-0-06706-6.

[10] Barbir, F., Gorgun, H., Wang, X. Relationship between pressure drop and cell resistance as a diagnostic tool for pem fuel cells. *Journal of Power Sources*, 141(1):96–101, 2005. doi: https://doi-org.tudelft.idm.oclc.org/10.1016/j.jpowsour.2004.08.055.

[11] Barthelemy, H., Weber, M., Barbier, F. Hydrogen storage: Recent improvements and industrial perspectives. *International Journal of Hydrogen Energy*, 42(11):7254–7262, 2017. doi: https://doi-org.tudelft.idm.oclc.org/10.1016/j.ijhydene.2016.03.178.

[12] Bassam, A.M., Phillips, A.B., Turnock, S.R., Wilson, P.A. Design, modelling and simulation of a hybrid fuel cell propulsion system for a domestic ferry. *Proc. 13th International Symposium on Practical Design of Ships and Other Floating Structures*, Copenhagen, Denmark, 2016.

[13] Bassam, A.M., Phillips, A.B., Turnock, S.R., Wilson, P.A. Development of a multi-scheme energy management strategy for a hybrid fuel cell driven passenger ship. *International Journal of Hydrogen Energy*, 42(1):623–635, 2017. doi: https://doi-org.tudelft.idm.oclc.org/10.1016/j.ijhydene.2016.08.209.

[14] Basu, P. Gasification theory and modeling of gasifiers. In Basu, P, editor, *Biomass Gasification and Pyrolysis, Practical Design*, chapter 5, pages 117–165. Academic Press, Cambridge, United States, 2010. ISBN 978-0-12-374988-8. doi: https://doi-org.tudelft.idm.oclc.org/10.1016/C2009-0-20099-7.

[15] Berndt, D. Electrochemical energy storage. In Kiehne, H.A, editor, *Battery Technology Handbook*, chapter 1, pages 25–124. Expert Verlag, Renningen-Malsheim, Germany, second edition, 2003. ISBN 0-8247-4249-4.

[16] Bloomberg. ørsted bets hydrogen is key to climate change, December 6, 2019. URL `https://gcaptain.com/orsted-bets-hydrogen-is-key-to-climate-goals/`. Accessed December, 2019.

[17] Bolvashenkov, I., Kammermann, J., Herzog, H.G. Methodology for selecting electric traction motors and its application to vehicle propulsion systems. *Proc. 2016 International Symposium on Power Electronics, Electrical Drives*, Anacapri, Italy, 2016. doi: https://doi-org.tudelft.idm.oclc.org/10.1109/SPEEDAM.2016.7525853.

[18] Boonen, E.J., Sciberras, E., Xepapa, K. Holistic fucntional design and system testing: Hybrid road ferry. *Proc. 29th CIMAC Congress*, Vancouver, Canada, 2019.

[19] Cardella, U., Decker, L., Klein, H. Roadmap to economically viable hydrogen liquefaction. *International Journal of Hydrogen Energy*, 42(19):13329–13338, 2017. doi: https://doi-org.tudelft.idm.oclc.org/10.1016/j.ijhydene.2017.01.068.

[20] Cheng, K.W.E., Xue, X.D., Chan, K.H. Zero emission electric vessel development. *Proc. 6th International Conference on Power Electronics Systems and Applications*, Hong Kong, China, 2015. doi: https://doi-org.tudelft.idm.oclc.org/10.1109/PESA.2015.7398965.

[21] Choi, C.H., Yu, S., Han, I.S., Kho, B.K., Kang, D.G., Lee, H.Y., Seo, M.S., Kong, J.W., Kim, G., Ahn, J.W., Park, S.K., Jang, D.W., Lee, J.H., Kim, M. Development and demonstration of pem fuel-cell-battery hybrid system for propulsion of tourist boat. *International Journal of Hydrogen Energy*, 41(5):3591–3599, 2016. doi: https://doi-org.tudelft.idm.oclc.org/10.1016/j.ijhydene.2015.12.186.

[22] Chryssakis, C., Brinks, H.W., Brunelli, A.C., Fuglseth., T.P., Lande, M., Laugen, L., Longva, T., Raeissi, B., Tvete, H.A. Low carbon shipping towards 2050. Technical report, DNV GL, 2017.

[23] Corbo, P., Migliardini, F., Veneri, O. Dynamic behaviour of hydrogen fuel cells for automotive application. *Renewable Energy*, 34(8):1955–1961, 2009. doi: https://doi-org.tudelft.idm.oclc.org/10.1016/j.renene.2008.12.021.

[24] Cornu, R., Stroo, K., Van de Pas, R. Fuels cells: addressing the key technical challenges. Webinar, Riviera Maritime Media Ltd., 2020. URL `https://www.rivieramm.com/webinar-library/hybrid-electric-fuel-cells/fuels-cells-addressing-the-key-technical-challenges`. Accessed June, 2020.

[25] Danfoss Drives. Robust, silent and space-saving control for all drive needs in demanding applications, 2020. URL `http://files.danfoss.com/download/Drives/DKDDPB909A502_NXP_Liquid_Cooled_LR.pdf`. Accessed July, 2020.

[26] De Miguel, N., Acosta, B., Moretto, P., Cebolla, R.O. The effect of defueling rate on the temperature evolution of on-board hydrogen tanks. *International Journal of Hydrogen Energy*, 40(42):14768–14774, 2015. doi: https://doi-org.tudelft.idm.oclc.org/10.1016/j.ijhydene.2015.06.038.

[27] DNV GL - Maritime. Assessment of selected alternative fuels and technologies. Technical report, DNV GL, 2018.

[28] Eits, J.J. *A Concept Design of a Fuel Cell System Onboard of a Small high Speed Craft*. Damen Shipyards Group, Gorinchem, the Netherlands, 2019.

[29] El-Gohary, M.M., El-Sherif, H.A. Future of hydrogen as green energy in marine applications. *Proc. 9th World Renewable Energy Congress*, Florence, Italy, 2006.

[30] Erickson, R.W. Dc-dc power converters. In Webster, J.G, editor, *Wiley Encyclopedia of Electrical and Electronics Engineering*. John Wiley & Sons, West Sussex, United Kingdom, 2000. ISBN 9780471346081. doi: https://doi-org.tudelft.idm.oclc.org/10.1002/047134608X.W5808.pub2.

[31] Erickson, R.W., Maksimović, D. *Fundamentals of Power Electronics*. Kluwer Academic Publishers, Dordrecht, the Netherlands, second edition, 2004. ISBN 0-306-48048-4.

[32] European Federation for Transport and Environment. Shipping and climate change, 2020. URL `https://www.transportenvironment.org/what-we-do/shipping-and-environment/shipping-and-climate-change`. Accessed August, 2020.

[33] Foteinos, M.I., Christofilis, G.I., Kyrtatos, N.P. Response of a direct-drive large marine two-stroke engine coupled to a selective catalytic reduction exhaust aftertreatment system when operating in waves. *Joural of Engineering for the Maritime Environment*, 234(3):1–17, 2020. doi: https://doi-org.tudelft.idm.oclc.org/10.1177\%2F1475090219899543.

[34] Fuel Cells and Hydrogen 2 Joint Undertaking. *Hydrogen Roadmap Europe: a Sustainable Pathway for the European Energy Transition*. Publications Office of the European Union, Luxembourg, Luxembourg, 2019. ISBN 978-92-9246-331-1. doi: 10.2843/341510.

[35] Gao, J., Kang, J. Modelling and simulation of permanent magnet synchronous motor vector control. *Information Technology Journal*, 13(3):578–582, 2014. doi: 10.3923/itj.2014.578.582.

[36] Gupta, A.K., Kumar, D., Reddy, B.M., Samuel, P. Bbbc based optimization of pi controller parameters for buck converter. *Proc. 2017 Innovations in Power and Advanced Computing Technologies*, Vellore, India, 2017. doi: https://doi-org.tudelft.idm.oclc.org/10.1109/IPACT.2017.8244983.

[37] Han, J., Charpentier, J.F., Tang, T. An energy management system of a fuel cell/battery hybrid boat. *Energies*, 7:2799–2820, 2014. doi: 10.3390/en7052799.

[38] Hannan, M.A., Hoque, M.M., Mohamed, A., Ayob, A. Review of energy storage systems for electric vehicle applications: Issues and challenges. *Renewable and Sustainable Energy Reviews*, 69:771–789, 2017. doi: https://doi-org.tudelft.idm.oclc.org/10.1016/j.rser.2016.11.171.

[39] Hansen, J.F., Wendt, F. History and state of the art in commercial electric ship propulsion, integrated power systems, and future trends. *Proceedings of the IEEE*, 103(12):2229–2242, 2015. doi: https://doi-org.tudelft.idm.oclc.org/10.1109/JPROC.2015.2458990.

[40] Hong-Ying, R., Hui, F., Pei-Ting, S., Jun-Jie, R. Design and research of dynamic braking circuits in electric propulsion ship. *Second International Conference on Intelligent Human-Machine Systems and Cybernetics*, Nanjing, China, 2010. doi: https://doi-org.tudelft.idm.oclc.org/10.1109/IHMSC.2010.140.

[41] Hong, Z., Li, Q., Han, Y., Shang, W., Zhu, Y., Chen, W. An energy management strategy based on dynamic power factor for fuel cell/battery hybrid locomotive. *International Journal of Hydrogen Energy*, 43(6):3261–3272, 2018. doi: https://doi-org.tudelft.idm.oclc.org/10.1016/j.ijhydene.2017.12.117.

[42] Howroyd, S., Chen, R. Powerpath controller for fuel cell & battery hybridisation. *International Journal of Hydrogen Energy*, 41(7):4229–4238, 2016. doi: https://doi-org.tudelft.idm.oclc.org/10.1016/j.ijhydene.2016.01.038.

[43] IEC. Electrical energy storage. Technical report, The International Electrotechnical Commission (IEC), 2011.

[44] International Maritime Organization. Un body adopts climate change strategy for shipping, 2018. URL `http://www.imo.org/en/MediaCentre/PressBriefings/Pages/06GHGinitialstrategy.aspx`. Accessed December, 2019.

[45] International Renewable Energy Agency, European Union. *Renewable Energy Prospects for the European Union*. Publications Office of the European Union, Luxembourg, Luxembourg, 2018. ISBN 978-92-9260-007-5.

[46] Journee, J.M.J., Massie, W.W., Huijsmans, R.H.M. *Offshore Hydromechanics*. Delft Univeristy of Technology, Delft, the Netherlands, third edition, 2015.

[47] Karden, E., Ploumen, S., Fricke, B., Miller, T., Snyder, K. Energy storage devices for future hybrid electric vehicles. *Journal of Power Sources*, 168(1):2–11, 2007. doi: https://doi-org.tudelft.idm.oclc.org/10.1016/j.jpowsour.2006.10.090.

[48] Kirtley, J.L., Banerjee, A., Englebretson, S. Motors for ship propulsion. *Proceedings of the IEEE*, 103(12): 2320–2332, 2015. doi: https://doi-org.tudelft.idm.oclc.org/10.1109/JPROC.2015.2487044.

[49] Klein Woud, H., Stapersma, D. *Design of Propulsion and Electric Power Generation Systems*. Institute of Marine Engineering, Science & Technology, London, United Kingdom, 2008. ISBN 1-902536-47-9.

[50] Larminie, J., Dicks, A. *Fuel Cell Systems Explained*. John Wiley & Sons, West Sussex, United Kingdom, second edition, 2003. ISBN 0-470-84857-X. doi: https://doi-org.tudelft.idm.oclc.org/10.1016/B978-0-12-374259-9.X5001-0.

[51] Leo, T.J., Durango, J.A., Navarro, E. Exergy analysis of pem fuel cells for marine applications. *Energy*, 35 (2):1164–1171, 2009. doi: https://doi-org.tudelft.idm.oclc.org/10.1016/j.energy.2009.06.010.

[52] Li, M., He, J., Demerdash, N.A.O. A flux-weakening control approach for interior permanent magnet synchronous motors based on z-source inverters. *Proc. 2014 IEEE Transportation Electrification Conference and Expo (ITEC)*, Dearborn, United States, 2014. doi: https://doi-org.tudelft.idm.oclc.org/10.1109/ITEC.2014.6861776.

[53] Li, X., Xu, L., Hua, J., Lin, J., Li, J. Ouyang, M. Power management strategy for vehicular-applied hybrid fuel cell/battery power system. *Journal of Power Sources*, 191(1):542–549, 2009. doi: https://doi-org.tudelft.idm.oclc.org/10.1016/j.jpowsour.2009.01.092.

[54] Lian, C., Xiao, F., Gao, S., Liu, J. Load torque and moment of inertia identification for permanent magnet synchronous motor drives based on sliding mode observer. *IEEE Transactions on Power Electronics*, 34 (6):5675–5683, 2019. doi: https://doi-org.tudelft.idm.oclc.org/10.1109/TPEL.2018.2870078.

[55] Lloyd's Register Group Limited. Hydrogen - safety considerations and future regulations, 2016. URL `https://www.fch.europa.eu/sites/default/files/3.%20Joseph%20Morelos%20-%20H2Safety.pdf`. Accessed December, 2019.

[56] Lucia, U. Overview on fuel cells. *Renewable and Sustainable Energy Reviews*, 30:164–169, 2014. doi: https://doi-org.tudelft.idm.oclc.org/10.1016/j.rser.2013.09.025.

[57] Lukic, S.M., Cao, J., Bansal, R.C., Rodriguez, F., Emadi, A. Energy storage systems for automotive applications. *IEEE Transactions on Industrial Electronics*, 55(6):2258–2267, 2008. doi: https://doi-org.tudelft.idm.oclc.org/10.1109/TIE.2008.918390.

[58] Makridis, S.S. Hydrogen storage and compression, 2017. URL `https://arxiv.org/ftp/arxiv/papers/1702/1702.06015.pdf`. Accessed December, 2019.

[59] Markowski, J., Pielecha, I. The potential of fuel cells as a drive source of maritime transport. *Proc. 2nd International Conference on the Sustainable Energy and Environmental Development*, Beijing, China, 2019. doi: 10.1088/1755-1315/214/1/012019.

[60] Mathworks. Fuel cell stack, 2020. URL `https://www.mathworks.com/help/physmod/sps/powersys/ref/fuelcellstack.html`. Accessed April, 2020.

[61] Mathworks. Multilevel modeling for rapid prototyping, 2020. URL `https://ww2.mathworks.cn/help/physmod/sps/powersys/ug/multi-level-modeling-for-rapid-prototyping.html`. Accessed May, 2020.

[62] Mathworks. Permanent magnet synchronous machine, 2020. URL `https://www.mathworks.com/help/physmod/sps/powersys/ref/permanentmagnetsynchronousmachine.html`. Accessed May, 2020.

[63] Mathworks. abc to dq0, dq0 to abc, 2020. URL `https://www.mathworks.com/help/physmod/sps/powersys/ref/abctodq0dq0toabc.html`. Accessed May, 2020.

[64] Mathworks. Speed controller (ac), 2020. URL `https://www.mathworks.com/help/physmod/sps/powersys/ref/speedcontrollerac.html`. Accessed May, 2020.

[65] Mathworks. Vector controller (pmsm), 2020. URL `https://www.mathworks.com/help/physmod/sps/powersys/ref/vectorcontrollerpmsm.html`. Accessed May, 2020.

[66] Mathworks. Inverter (three-phase), 2020. URL `https://www.mathworks.com/help/physmod/sps/powersys/ref/inverterthreephase.html`. Accessed May, 2020.

[67] McKinlay, C.J., Turnock, S.R., Hudson, D.A. A comparison of hydrogen and ammonia for future long distance shipping fuels. *Proc. LNG/LPG and Alternative Fuels Ships, Royal Institute of Naval Architects*, London, United Kingdom, 2020.

[68] Mizythras, P., Boulougouris, E., Theotokatos, G. Numerical study of propulsion system performance during ship acceleration. *Ocean Engineering*, 149:383–396, 2018. doi: https://doi-org.tudelft.idm.oclc.org/10.1016/j.oceaneng.2017.12.010.

[69] Mohan, N., Undeland, T.M., Robbins, W.P. *Power Electronics: Converters, Applications and Design*. John Wiley & Sons, West Sussex, United Kingdom, second edition, 1995. ISBN 0-471-58408-8.

[70] Motapon, S.N., Dessaint, L.A., Al-Haddad, K. A comparative study of energy management schemes for a fuel-cell hybrid emergency power system of more-electric aircraft. *IEEE Transactions on Industrial Electronics*, 61(3):1320–1334, 2014. doi: https://doi-org.tudelft.idm.oclc.org/10.1109/TIE.2013.2257152.

[71] Motapon, S.N., Tremblay, O., Dessaint, L.A. A generic fuel cell model for the simulation of fuel cell vehicles. *Proc. IEEE Vehicle Power and Propulsion Conference*, Dearborn, United States, 2009. doi: https://doi-org.tudelft.idm.oclc.org/10.1109/VPPC.2009.5289692.

[72] Pinto, J.O.P., Lawler, J.S., Filho, N.P. Extended constant power speed range of the permanent magnet synchronous machine driven by dual mode inverter control. *Proc. 2005 IEEE 36th Power Electronics Specialists Conference*, Recife, Brazil, 2005. doi: https://doi-org.tudelft.idm.oclc.org/10.1109/PESC.2005.1581789.

[73] Ren, X., Lu, Q., Liu, L., Liu, B., Wang, Y., Liu, A., Wu, G. Current progress of pt and pt-based electrocatalysts used for fuel cells. *Journal of Sustainable Energy & Fuels*, 2019. doi: https://doi-org.tudelft.idm.oclc.org/10.1039/C9SE00460B.

[74] Schofield, N., Yap, H.T., Bingham, C.M. Hybrid energy sources for electric and fuel cell vehicle propulsion. *Proc. IEEE Vehicle Power and Propulsion Conference*, Chicago, United States, 2005. doi: https://doi-org.tudelft.idm.oclc.org/10.1109/VPPC.2005.1554530.

[75] Sciberras, E.A., Norman, R.A. Multi-objective design of a hybrid propulsion system for marine vessels. *IET Electrical Systems in Transportation*, 2(3):148–157, 2012. doi: https://doi-org.tudelft.idm.oclc.org/10.1049/iet-est.2011.0011.

[76] Sen, P.C. *Principles of Electric Machines and Power Electronics*. John Wiley & Sons, West Sussex, United Kingdom, third edition, 2012. ISBN 978-1-118-07887-7.

[77] Sharma, A.K., Ahmed, K., Birgersson, E. Nernst voltage losses in planar fuel cells caused by changes in chemical composition: effects of operating parameters. *International Journal of Ionics*, 24(7):2047–2054, 2018. doi: https://doi.org/10.1007/s11581-018-2454-1.

[78] Song, M., Pei, P., Zha, H., Xu, H. Water management of proton exchange membrane fuel cell based on control of hydrogen pressure drop. *Journal of Power Sources*, 267:655–663, 2014. doi: https://doi-org.tudelft.idm.oclc.org/10.1016/j.jpowsour.2014.05.094.

[79] Spiegel, C. *PEM Fuel Cell Modeling and Simulation Using Matlab*. Academic Press, Cambridge, United States, 2008. ISBN 978-0-12-374259-9. doi: https://doi-org.tudelft.idm.oclc.org/10.1016/B978-0-12-374259-9.X5001-0.

[80] Stambouli, A.B., Traversa, E. Fuel cells, an alternative to standard sources of energy. *Renewable and Sustainable Energy Reviews*, 6(3):295–304, 2002. doi: https://doi-org.tudelft.idm.oclc.org/10.1016/S1364-0321(01)00015-6.

[81] Stapersma, D. *Diesel engines: A fundamental approach to performance analysis, turbocharging, combustion, emissions and heat transfer*. Delft Univeristy of Technology, Delft, the Netherlands, 2010.

[82] Takaoka, Y., Kegaya, H., Saeed, A., Nishimura, M. Introduction to a liquefied hydrogen carrier for a pilot hydrogen energy supply chain (hesc) project in japan. *Proc. Gastech 2017*, Tokyo, Japan, 2017.

[83] Taner, T. Alternative energy of the future: A technical note of pem fuel cell water management. *Fundamentals of Renewable Energy and Applications*, 5(3), 2015.

[84] Taskar, B., Yum, K.K., Steen, S., Pedersen, E. The effect of waves on engine-propeller dynamics and propulsion performance of ships. *Ocean Engineering*, 122:262–277, 2016. doi: https://doi-org.tudelft.idm.oclc.org/10.1016/j.oceaneng.2016.06.034.

[85] Thounthong, P., Rael, S., Davat, B. Energy management of fuel cell/battery/supercapacitor hybrid power source for vehicle applications. *Journal of Power Sources*, 193(1):376–385, 2009. doi: https://doi-org.tudelft.idm.oclc.org/10.1016/j.jpowsour.2008.12.120.

[86] Tremblay, O., Dessaint, L.A. Experimental validation of a battery dynamic model for ev applications. *World Electric Vehicle Journal*, 3(2):289–298, 2009. doi: https://doi.org/10.3390/wevj3020289.

[87] Tremblay, O., Dessaint, L.A., Dekkiche, A.I. A generic battery model for the dynamic simulation of hybrid electric vehicles. *Proc. IEEE Vehicle Power and Propulsion Conference*, Arlington, United States, 2007. doi: https://doi-org.tudelft.idm.oclc.org/10.1109/VPPC.2007.4544139.

[88] Tronstad, T., Astrand, H.H., Haugom, G.P., Langfeldt, L. Study on the use of fuel cells in shipping. Technical report, DNV GL, 2017.

[89] Tzimas, E., Filiou, C, Peteves, S.D., Veyret, J.B. *Hydrogen storage: state-of-the-art and future perspective*. Office for Official Publications of the European Communities, Luxembourg, Luxembourg, 2003. ISBN 92-894-6950-1.

[90] United Nations. Paris agreement, 2015. URL `https://unfccc.int/sites/default/files/english_paris_agreement.pdf`. Accessed December, 2019.

[91] U.S. Department of Energy, Office of Energy Efficiency & Renewable Energy. Hydrogen fuel cell engines and related technologies course manual, 2001. URL `https://www.energy.gov/eere/fuelcells/downloads/hydrogen-fuel-cell-engines-and-related-technologies-course-manual`. Accessed December, 2019.

[92] U.S. Department of Energy, Office of Energy Efficiency & Renewable Energy. Hydrogen production: Electrolysis, n.d. URL `https://www.energy.gov/eere/fuelcells/hydrogen-production-electrolysis`. Accessed December, 2019.

[93] Uysal, Z., Karaarslan, A. Comparison of one cycle and pi control method using buck-boost converter. *Proc. 13th International Conference on Technical and Physical Problems of Electrical Engineering*, Van, Turkey, 2017.

[94] Valenti, G. Hydrogen liquefaction and liquid hydrogen storage. In Subramani, V., Basile, A., Veziroğlu, T.N, editor, *Compendium of Hydrogen Energy: Hydrogen Production and Purification*, chapter 2, pages 27–51. Woodhead Publishing, Cambridge, United Kingdom, 2004. ISBN 978-1-78242-362-1. doi: https://doi-org.tudelft.idm.oclc.org/10.1016/B978-1-78242-362-1.00002-X.

[95] van Biert, L. *Solid Oxide Fuel Cells for Ships: System Integration Concepts with Reforming and Thermal Cycles*. PhD thesis, Delft University of Technology, Delft, the Netherlands, 2020.

[96] van Biert, L., Godjevac, M., Visser, K., Aravind, P.V. A review of fuel cell systems for maritime applications. *Journal of Power Sources*, 327:345–364, 2016. doi: https://doi-org.tudelft.idm.oclc.org/10.1016/j.jpowsour.2016.07.007.

[97] Van Nguyen, T., Knobbe, M.W. A liquid water management strategy for pem fuel cell stacks. *Journal of Power Sources*, 114(1):70–79, 2003. doi: https://doi-org.tudelft.idm.oclc.org/10.1016/S0378-7753(02)00591-8.

[98] Vos, B. *Hydrogen High Speed Craft, Afstudeerscriptie Maritieme Techniek*. Damen Shipyards Group, Gorinchem, the Netherlands, 2019.

[99] Vrijdag, A., Stapersma, D. Extension and application of a linearised ship propulsion system model. *Ocean Engineering*, 143:50–65, 2017. doi: https://doi-org.tudelft.idm.oclc.org/10.1016/j.oceaneng.2017.07.023.

[100] Welaya, Y.M.A., El-Gohary, M.M., Ammar, N.R. A comparison between fuel cells and other alternatives for marine electric power generation. *International Journal of Naval Architecture and Ocean Engineering*, 3(2):141–149, 2011. doi: https://doi-org.tudelft.idm.oclc.org/10.2478/IJNAOE-2013-0057.

[101] Wirz, F. Optimisation of the crash-stop manoeuvre of vessels employing slow-speed two-stroke engines and fixed pitch propellers. *Journal of Marine Engineering and Technology*, 11(1):35–43, 2012.

[102] Xu, K., Chen, W., Xu, Y., Gao, M., He, Z. Vector control for pmsm. *Sensors & Transducers*, 170(5):227–233, 2014.

A

Fast crew supplier 1204

A.1. Product sheet and design configurations

FAST CREW SUPPLIER 1204 FRP-propeller

STANDARD

GENERAL

Hull materials	FRP
Superstructure material	FRP
Basic functions	Crew and workboat duties

DIMENSIONS

Length overall	11.9 m
Beam overall	4.0 m
Depth at sides	1.5 m
Draught	1.0 m
Max deadweight	Up to 3.5 t
Max. deck load	1.5 t
Crew	Up to 2 persons
(Industrial) personnel	Up to 20 persons

TANK CAPACITIES

Fuel oil	1,500 ltr
Fresh water	60 or 130 ltr
Sewage	130 ltr

PERFORMANCES

Speed	Up to 26.0 kn
Range at max. speed	Up to 200 nm

PROPULSION SYSTEM

Main engines	2x Volvo D7
Total Power	390 bkW
Gearboxes	2x Twin Disc MG-5061 RV
Propulsion	2x fixed pitch propellers

ELECTRICAL QUIPMENT

Network	24V DC

DECK LAY-OUT

Fendering	110 mm x 110 mm D-shaped rubber fender
Anchor equipment	1x 14.4 kg Fortress FX 55 with chain and line

SHIP SYSTEMS

Fire extinguishing	Fixed Fi-Fi system in engine room (Aerosol) Hand operated fire extinguishers

NAUTICAL AND COMMUNICATION EQUIPMENT

VHF	1x
Compass	1x Magnetic

OPTIONAL

Classification	I ✠ Hull • MACH Crew Boat Sea Area 2
External communication	GMDSS A1
Fendering	160 mm x 160 mm D-shaped rubber fender 200 mm x 100 mm Foam filled fender
Sun awning	Length up to 6 m
Sanitary space	
Air-conditioning	
Generator	9.5 ekW
Network	220v 50Hz / 115V 60 Hz
Shore connection	32A
MOB platform	Electrically operated
Searchlights	2
Radars	
Navtex	
AIS transmitter	

ACCOMODATION VARIANTS

0 accommodation modules: 4 (Industrial) personnel
1 accommodation modules 12 (Industrial) personnel
2 accommodation modules 20 (Industrial) personnel

PROPULSION VARIANTS

Stern Drive version
Waterjet version

FAST CREW SUPPLIER 1204 FRP-propeller

STANDARD

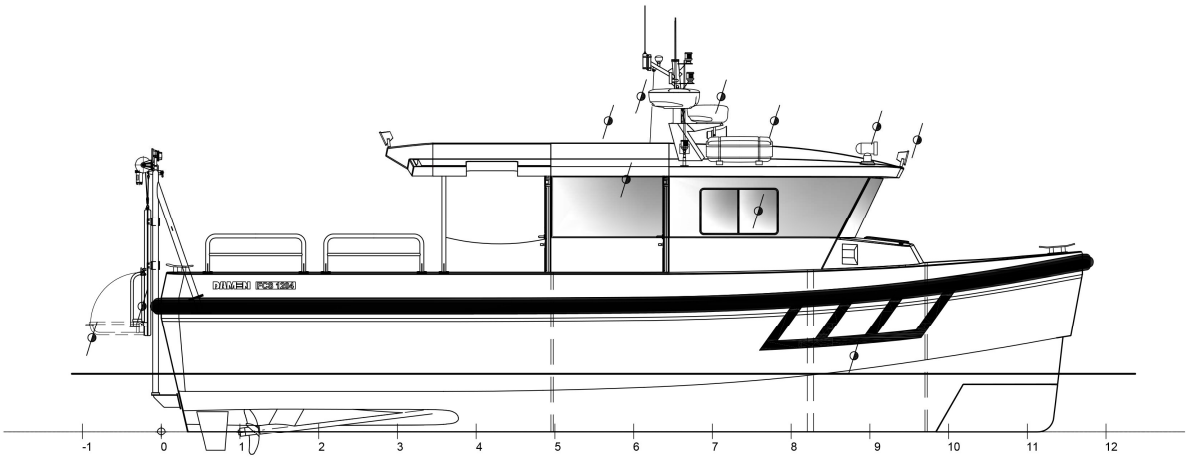

Profile

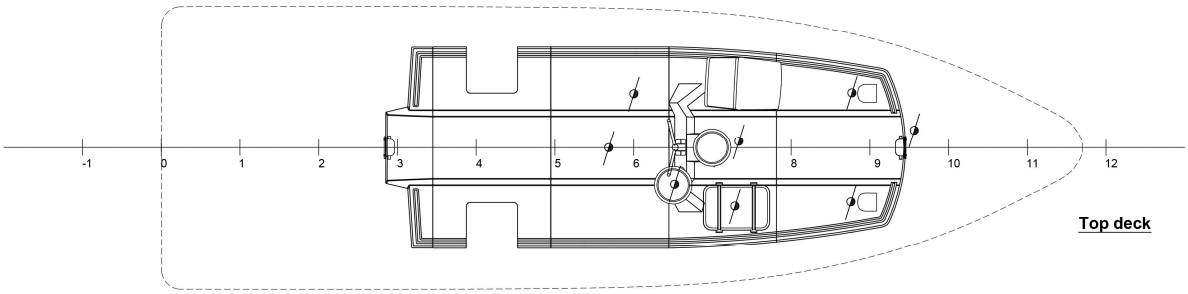

Top deck

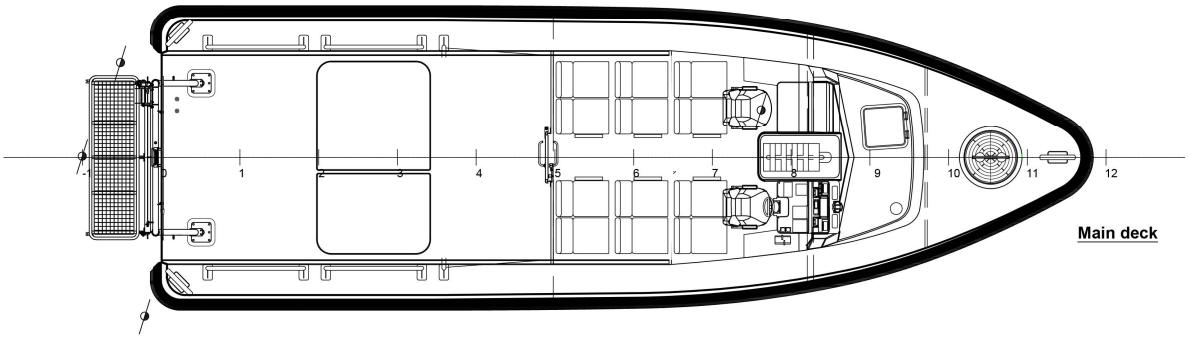

Main deck

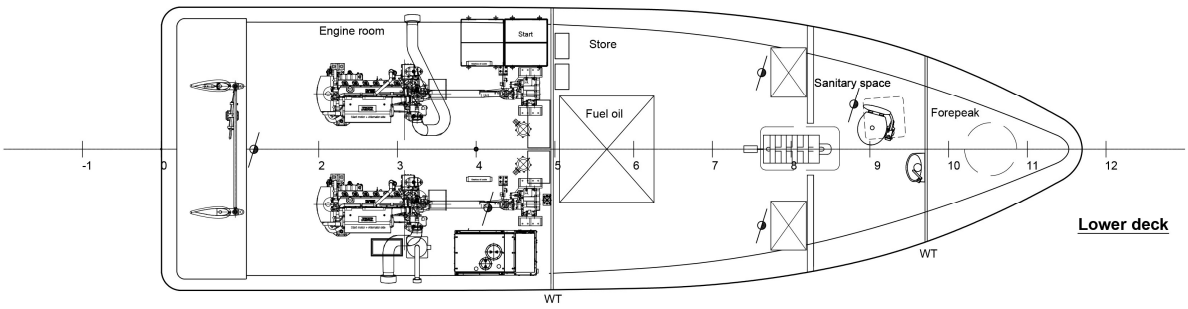

Lower deck

Items marked with ϕ are optional equipment

DAMEN SHIPYARDS GROUP

Avelingen-West 20
4202 MS Gorinchem
The Netherlands

P.O. Box 1
4200 AA Gorinchem
The Netherlands

phone +31 (0)183 63 99 22
fax +31 (0)183 63 21 89

info@damen.com
www.damen.com

September, 2019

FCS 1204 FRP

PROPULSION

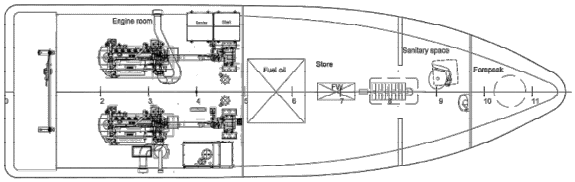

FIXED PITCH PROPULSION

Length o.a.	11.89 m
Draft max.	0.98 m
Speed	up to 25 kn
Range	200 Nm
Engine	2x Volvo D7 (390 kW)
Propulsion	2x Fixed Pith Propellers
Max modules	2 modules (20 Indus.Pers.)

DAMEN

FCS 1204 FRP

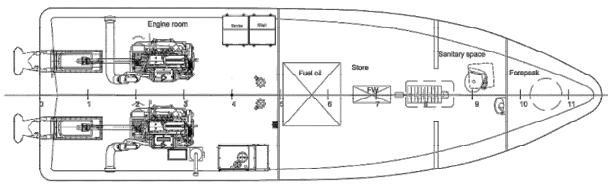

WATERJET PROPULSION

Length o.a.	12.62 m
Draft max.	0.73 m
Speed	up to 27.5 kn
Range	200 Nm
Engine	2x Cummins QSB6.7 (448 kW)
Propulsion	2x Waterjet Hamilton 274
Max modules.	2 modules (20 Indus.Pers.)

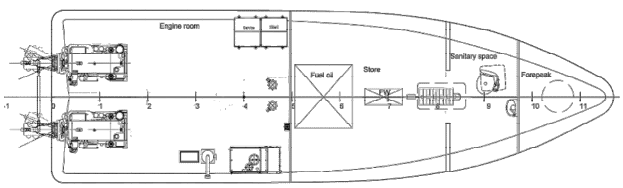

STERNDRIVE

Length o.a.	12.62 m
Draft max.	0.80 m
Speed	up to 30 kn
Range	230 Nm
Engine	2x Volvo D6-300 (442 kW)
Propulsion	2x Volvo DPH
Max modules	3 modules (28 Indus.Pers.)

Note: Non Classed

DAMEN

FCS 1204 FRP

ACCOMMODATION

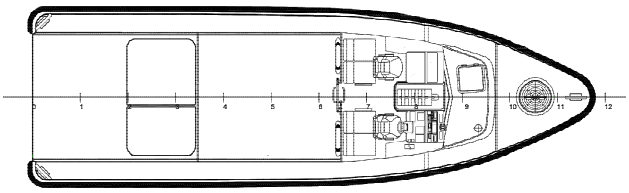

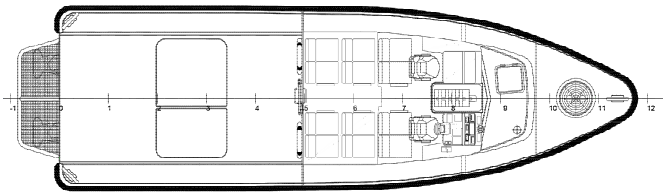

Basic superstructure

Max. Industrial personnel	4
Deck area	16.7 m²
Sun awning length	up to 6 m

Basic superstructure + 1 module

Max. Industrial personnel	12
Deck area	12.8 m²
Sun awning length	up to 4.5 m

DAMEN

FCS 1204 FRP

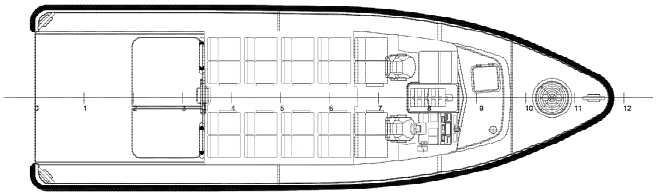

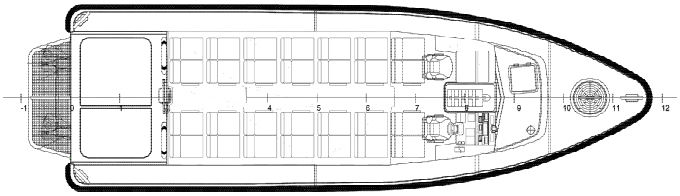

Basic superstructure + 2 modules

Max. Industrial personnel	20
Deck area	8.9 m²
Sun awning length	up to 3 m

Basic superstructure + 3 modules

Max. Industrial personnel	28
Deck area	5.0 m²
Sun awning length	up to 1.5 m

Note: only possible with sterndrive propulsion

DAMEN

B

Energy analysis

B.1. Battery charge intervals

Battery	Charge interval [hh:mm]
1P28S	04:00 – 09:00
2P28S	05:30 – 09:00
3P28S	06:00 – 09:00
4P28S	06:15 – 09:00
5P28S	06:30 – 09:00

Table B.1: Charge intervals for a survey vessel with two fuel cells

Battery	Charge interval [hh:mm]
1P28S	-
2P28S	01:27 – 02:27, 02:37 – 05:04, 05:09 – 06:27, 06:36 – 07:00
3P28S	02:37 – 04:49, 05:09 – 06:27
4P28S	03:30 – 04:49, 05:09 – 06:27
5P28S	02:37 – 03:30, 05:09 – 06:27

Table B.2: Charge intervals for a harbour patrol vessel with one fuel cell

Battery	Charge interval [hh:mm]
1P28S	01:27 – 02:27, 02:37 – 05:04, 06:36 – 07:00
2P28S	02:37 – 05:04
3P28S	-
4P28S	-
5P28S	-

Table B.3: Charge intervals for a harbour patrol vessel with two fuel cells

B.2. Survey vessel with two fuel cells

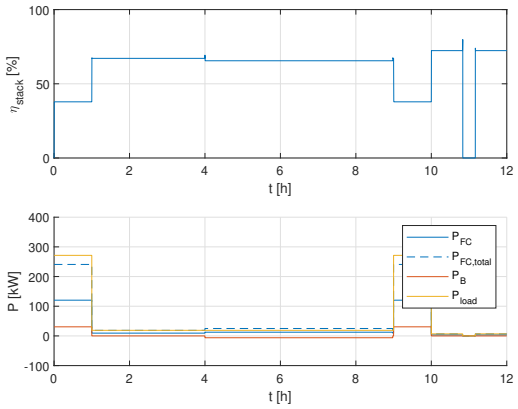

(a) 1P28S (45 Ah): stack efficiency and load distribution

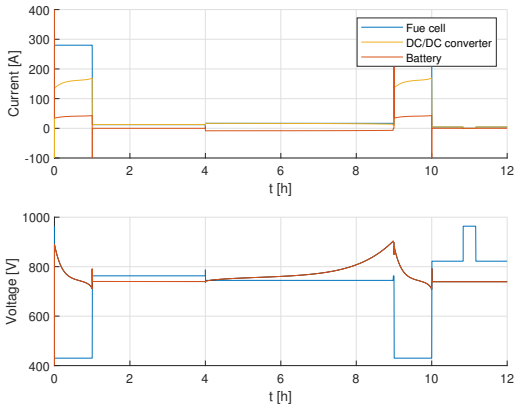

(b) 1P28S (45 Ah): voltage and current

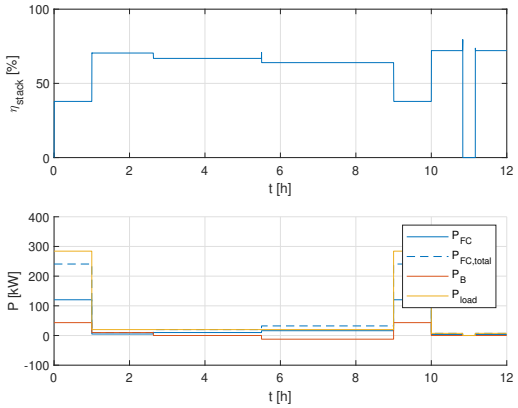

(c) 2P28S (90 Ah): stack efficiency and load distribution

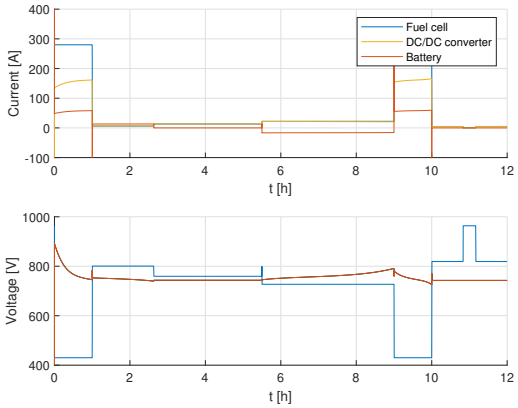

(d) 2P28S (90 Ah): voltage and current

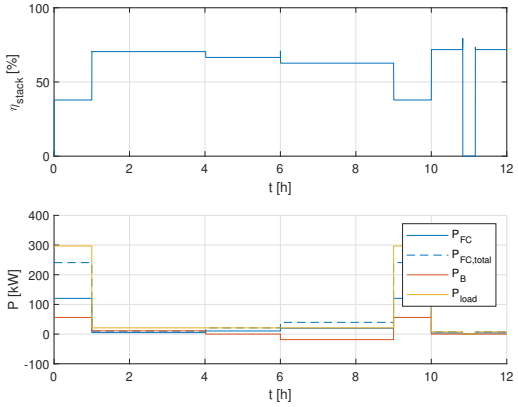

(e) 3P28S (134 Ah): stack efficiency and load distribution

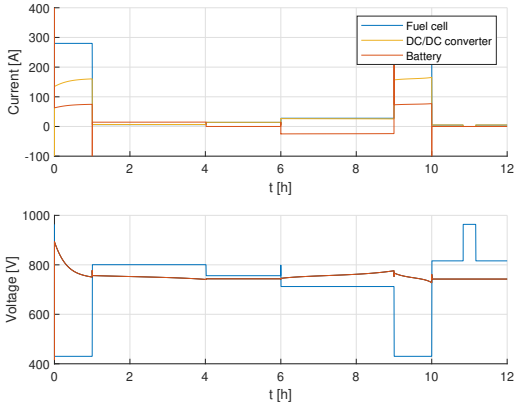

(f) 3P28S (135 Ah): voltage and current

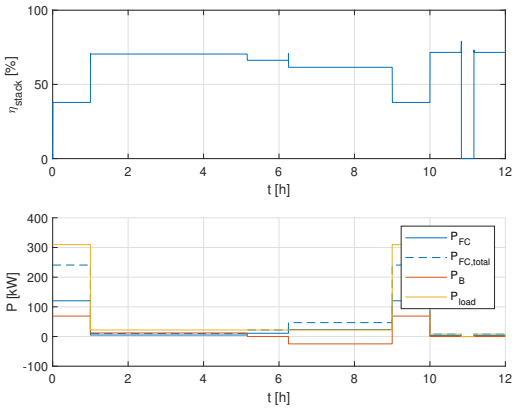

(g) 4P28S (180 Ah): stack efficiency and load distribution

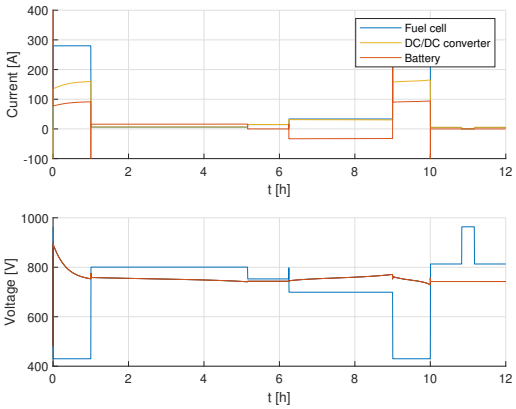

(h) 4P28S (180 Ah): voltage and current

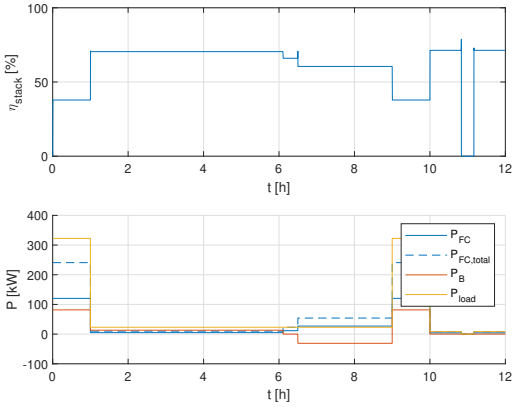

(i) 5P28S (225 Ah): stack efficiency and load distribution

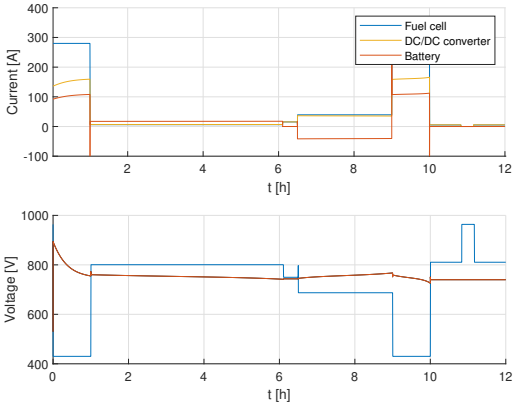

(j) 5P28S (225 Ah): voltage and current

Figure B.1: Efficiency and system performance for a survey vessel with two fuel cells and various battery sizes

B.3. Harbour patrol vessel with one fuel cell

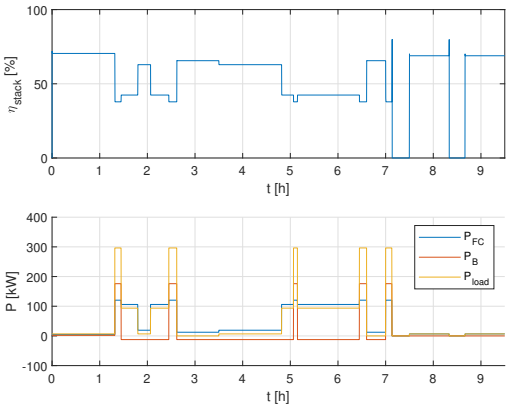

(a) 2P28S (90 Ah): stack efficiency and load distribution

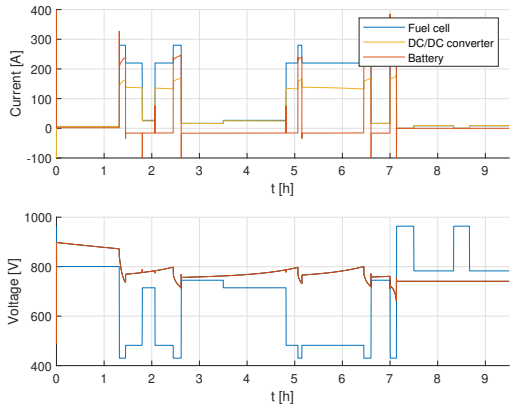

(b) 2P28S (90 Ah): voltage and current

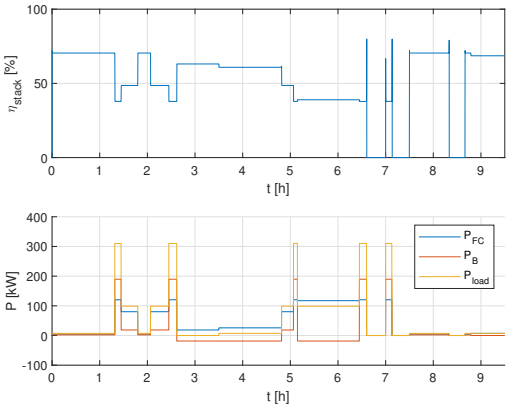

(c) 3P28S (135 Ah): stack efficiency and load distribution

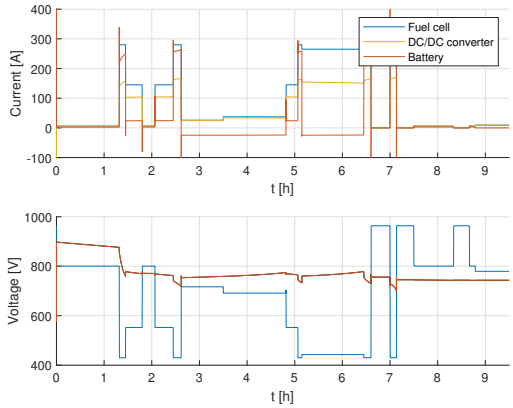

(d) 3P28S (135 Ah): voltage and current

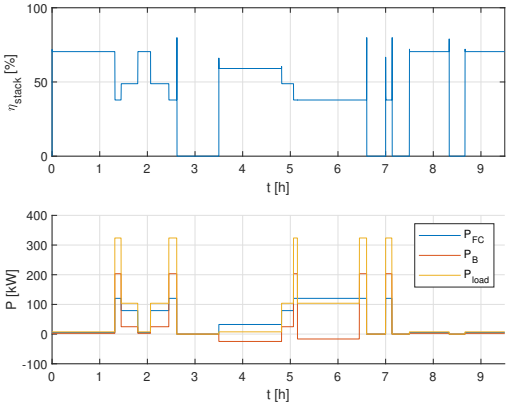

(e) 4P28S (180 Ah): stack efficiency and load distribution

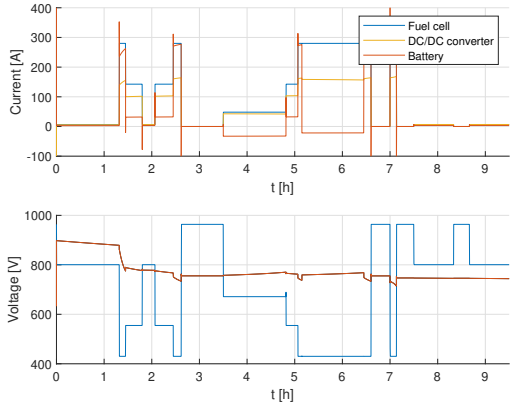

(f) 4P28S (180 Ah): voltage and current

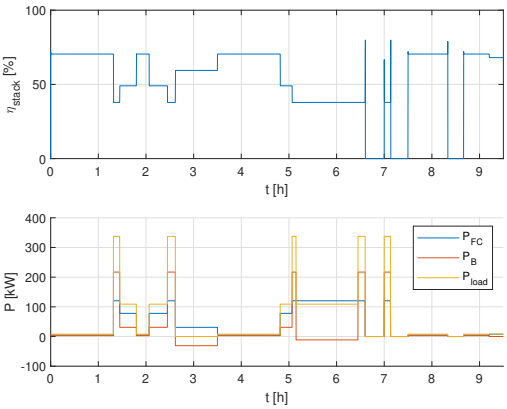

(g) 5P28S (225 Ah): stack efficiency and load distribution

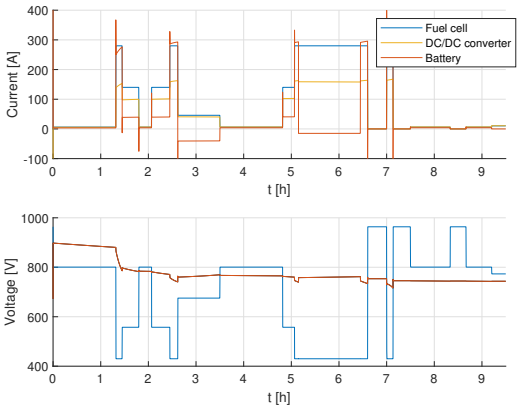

(h) 5P28S (225 Ah): voltage and current

Figure B.2: Efficiency and system performance for a harbour patrol vessel with one fuel cell and various battery sizes

B.4. Harbour patrol vessel with two fuel cells

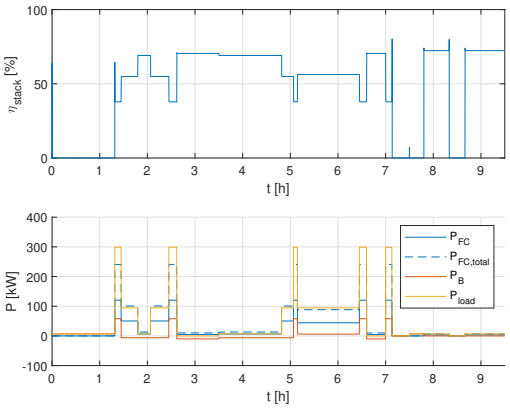

(a) 1P28S (45 Ah): stack efficiency and load distribution

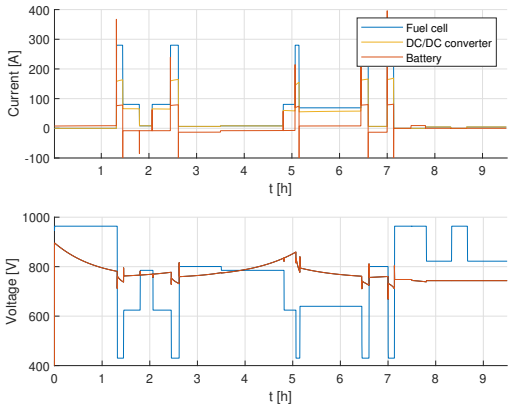

(b) 1P28S (45 Ah): voltage and current

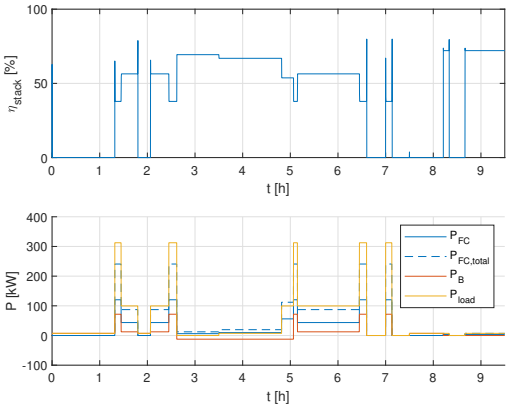

(c) 2P28S (90 Ah): stack efficiency and load distribution

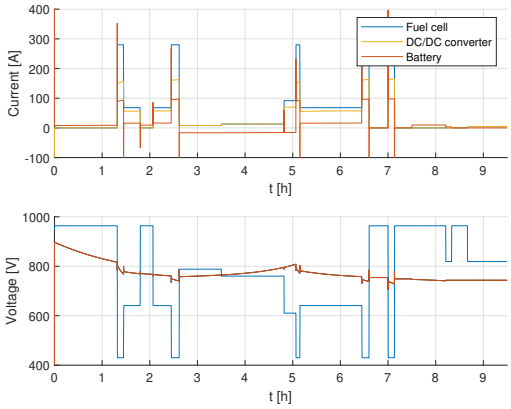

(d) 2P28S (90 Ah): voltage and current

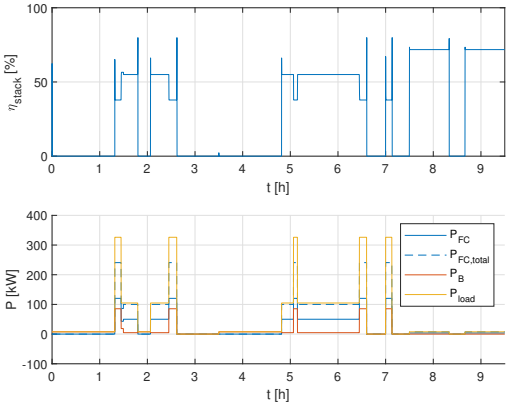

(e) 3P28S (135 Ah): stack efficiency and load distribution

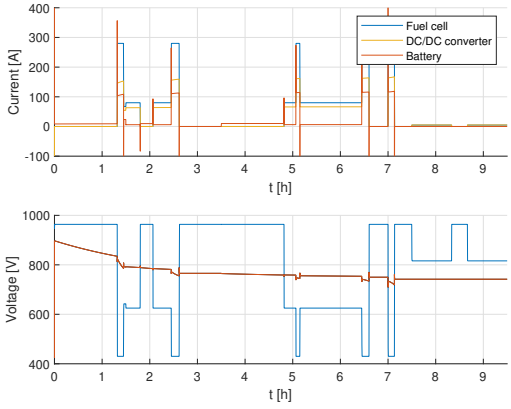

(f) 3P28S (135 Ah): voltage and current

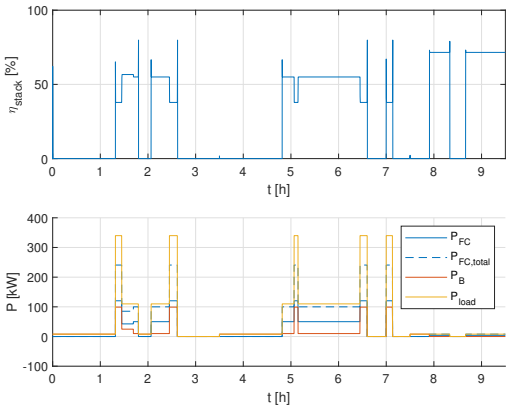

(g) 4P28S (180 Ah): stack efficiency and load distribution

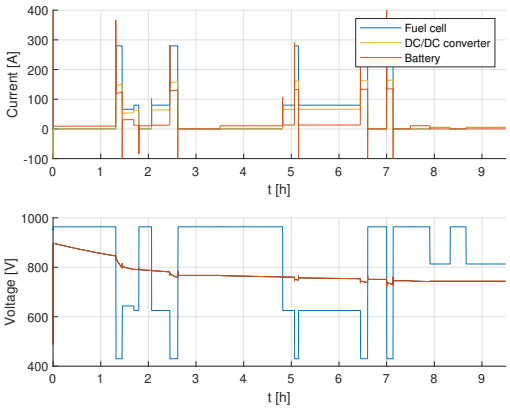

(h) 4P28S (180 Ah): voltage and current

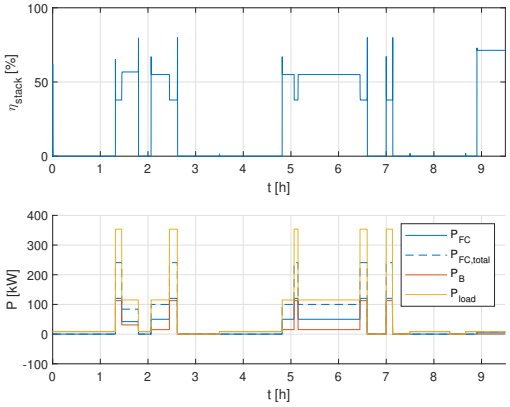

(i) 5P28S (225 Ah): stack efficiency and load distribution

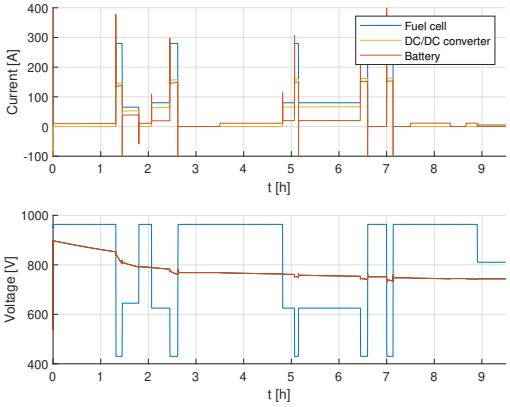

(j) 5P28S (225 Ah): voltage and current

Figure B.3: Efficiency and system performance for a harbour patrol vessel with two fuel cells and various battery sizes

B.5. Top speed-endurance diagrams

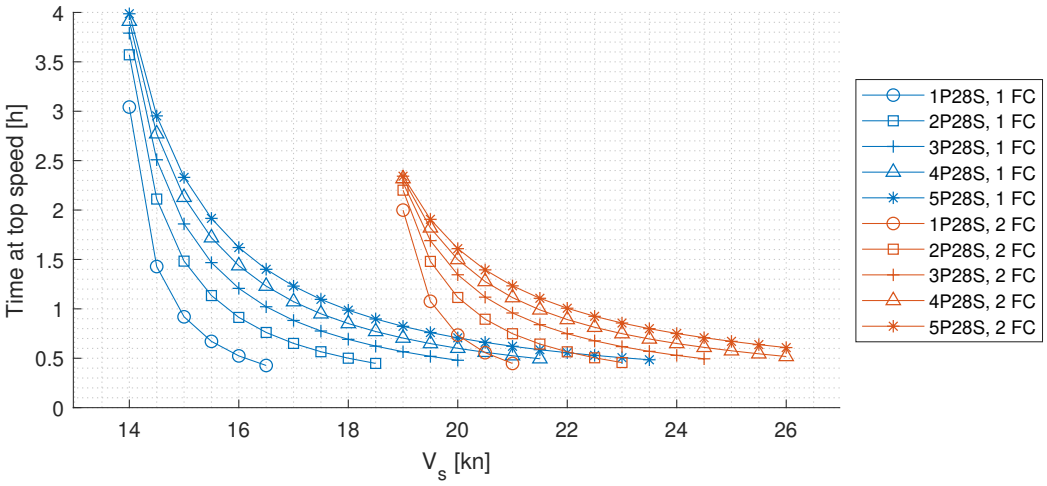

Figure B.4: Maximum endurance (time) during boosting at various top speeds

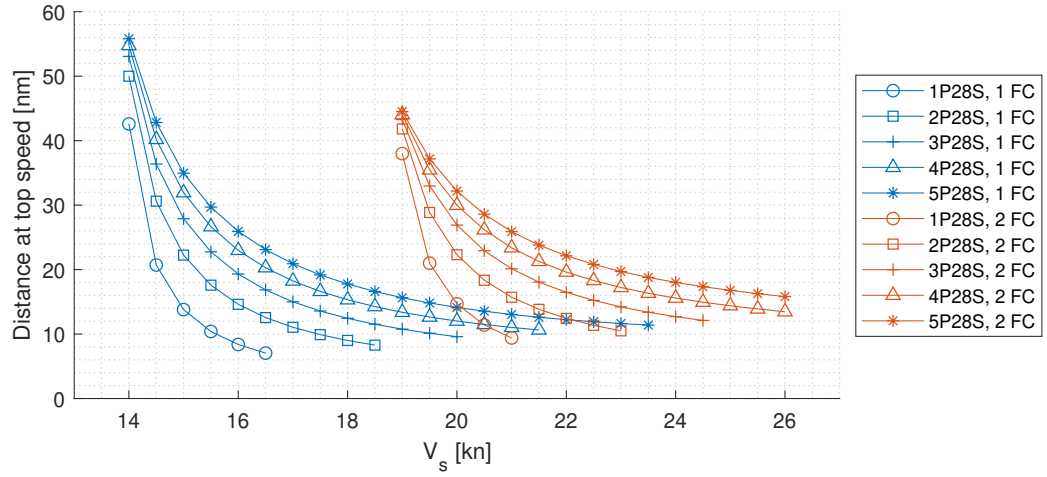

Figure B.5: Maximum endurance (distance) during boosting at various top speeds

C

ABC2dq transformation

The transformation from the ABC frame to the dq frame is defined by the following relations:

$$\begin{bmatrix} V_d \\ V_q \end{bmatrix} = \frac{2}{3} \begin{bmatrix} \sin\theta_e & \sin(\theta_e - 2\pi/3) & \sin(\theta_e + 2\pi/3) \\ \cos\theta_e & \cos(\theta_e - 2\pi/3) & \cos(\theta_e + 2\pi/3) \end{bmatrix} \cdot \begin{bmatrix} V_a \\ V_b \\ V_c \end{bmatrix}$$

$$\begin{cases} V_{ab} = V_a - V_b \\ V_{ac} = V_a - V_c \\ V_{bc} = V_b - V_c \end{cases}$$

$$\begin{cases} \sin(\alpha + \beta) = \sin\alpha\cos\beta + \cos\alpha\sin\beta \\ \cos(\alpha + \beta) = \cos\alpha\cos\beta - \sin\alpha\sin\beta \end{cases}$$

$$\begin{aligned}
V_d &= \frac{2}{3} \cdot \left(V_a \cdot \sin\theta_e + V_b \cdot \sin\left(\theta_e - \frac{2\pi}{3}\right) + V_c \cdot \sin\left(\theta_e + \frac{2\pi}{3}\right) \right) \\
&= \frac{2}{3} \cdot \left(V_a \cdot \sin\theta_e + V_b \cdot \left(\sin\theta_e \cos\frac{2\pi}{3} - \cos\theta_e \sin\frac{2\pi}{3} \right) + V_c \cdot \left(\sin\theta_e \cos\frac{2\pi}{3} + \cos\theta_e \sin\frac{2\pi}{3} \right) \right) \\
&= \frac{2}{3} \cdot \left(\left(V_a - \frac{1}{2} V_b - \frac{1}{2} V_c \right) \cdot \sin\theta_e + \frac{\sqrt{3}}{2} \left(V_c - V_b \right) \cdot \cos\theta_e \right) \\
&= \frac{1}{3} \cdot \left(\left(2V_a - V_b - V_c \right) \cdot \sin\theta_e + \sqrt{3} \left(V_c - V_b \right) \cdot \cos\theta_e \right) \\
&= \frac{1}{3} \cdot \left(\left(2V_a - 2V_b + V_b - V_c \right) \cdot \sin\theta_e + \sqrt{3} \left(V_c - V_b \right) \cdot \cos\theta_e \right) \\
&= \frac{1}{3} \cdot \left(\left(2V_{ab} + V_{bc} \right) \cdot \sin\theta_e - \sqrt{3} V_{bc} \cdot \cos\theta_e \right)
\end{aligned}$$

$$\begin{aligned}
V_q &= \frac{2}{3} \cdot \left(V_a \cdot \cos\theta_e + V_b \cdot \cos\left(\theta_e - \frac{2\pi}{3}\right) + V_c \cdot \cos\left(\theta_e + \frac{2\pi}{3}\right) \right) \\
&= \frac{2}{3} \cdot \left(V_a \cdot \cos\theta_e + V_b \cdot \left(\cos\theta_e \cos\frac{2\pi}{3} + \sin\theta_e \sin\frac{2\pi}{3} \right) + V_c \cdot \left(\cos\theta_e \cos\frac{2\pi}{3} - \sin\theta_e \sin\frac{2\pi}{3} \right) \right) \\
&= \frac{2}{3} \cdot \left(\left(V_a - \frac{1}{2} V_b - \frac{1}{2} V_c \right) \cdot \cos\theta_e + \frac{\sqrt{3}}{2} \left(V_b - V_c \right) \cdot \sin\theta_e \right) \\
&= \frac{1}{3} \cdot \left(\left(2V_a - V_b - V_c \right) \cdot \cos\theta_e + \sqrt{3} \left(V_b - V_c \right) \cdot \sin\theta_e \right) \\
&= \frac{1}{3} \cdot \left(\left(2V_a - 2V_b + V_b - V_c \right) \cdot \cos\theta_e + \sqrt{3} \left(V_b - V_c \right) \cdot \sin\theta_e \right) \\
&= \frac{1}{3} \cdot \left(\left(2V_{ab} + V_{bc} \right) \cdot \cos\theta_e + \sqrt{3} V_{bc} \cdot \sin\theta_e \right)
\end{aligned}$$

D

Danfoss product specification sheets

D.1. Danfoss EM-PMI375-T1100

ENGINEERING TOMORROW

Data Sheet

EM-PMI375-T1100

Electric machine, permanent magnet internal

FEATURES

- Synchronous Reluctance assisted Permanent Magnet (SRPM) technology
- Extremely compact and robust structure
- Highest efficiency throughout the operation range on the market (~96 %)
- Liquid cooled with plain water or water/glycol mixture
- Low coolant flow required
- Allowed coolant temperature up to +65°C
- IP65 enclosure class to maximize reliability, IP67 available as option
- Multiple mounting possibilities

GENERATOR SPECIFIC FEATURES

- Standard SAE flange mounting to match the diesel engine connection
- Wide selection of speed ratings allowing the generator to be selected to customer specific applications with various voltage requirements
- Can be also used as starter motor for the ICE

MOTOR SPECIFIC FEATURES

- Extended speed and torque capabilities compared to standard PM motors from Danfoss reluctance assisted permanent magnet motor technology
- Motor structure is designed to be able to produce high starting torques: EM-PMI motor can produce instantly full torque to a non-moving axle
- Optimized speed range to meet the most common gear ratios used in heavy mobile machinery

GENERAL

The machine is developed especially for demanding applications. It is smaller, lighter and more efficient than conventional products on the market.

TYPICAL APPLICATIONS

- Generator for diesel-electric/ serial hybrid applications
- Traction/propulsion motor
- Generator/Motor for parallel hybrid applications

SPECIFICATIONS

General electrical properties

Nominal voltage (line to line)	500 V_{AC}
Voltage stress	IEC 60034-25, Curve A: Without filters for motors up to 500 V_{AC}
Nominal efficiency	96 %
Pole pair number	6
Power supply	Inverter fed.
Nominal inverter switching frequency	8 kHz

Basic information

Machine type	Synchronous reluctance assisted permanent magnet
Mounting (IEC 60034-7)	IM 3001 (Flange)
Standard Flange D-end (SAE J617)	SAE 3, transmission housing
Standard bearings	SKF 6214 C3
Standard axle spline D-end	DIN5480 W55x2x30x26x8a
Standard Flange N-end (SAE J617)	SAE 4, flywheel housing
Standard rotation direction	Clockwise (both directions possible)
Protection class	IP65 IP67 available as option +IP67 Tests: 0.3 bar under pressure held for 120 seconds. Pressure not allowed to drop under 0.1 bar (IP65) Pressure not allowed to drop under 0.25 bar (IP67)
Duty type (IEC 60034-1)	S9
Standard color	Dark grey RAL7024 powder coating

Mechanical

Total weight	295 kg (no options)
Moment of inertia	0.99 kgm^2
Rotating mass	111 kg
Maximum static torque on the shaft	6800 Nm
Maximum dynamic torque on the shaft	4000 Nm
Maximum deceleration (shaft braking)	1000 rad/s^2

Dimensions

Length (frame)	548 mm
Diameter (frame)	450 mm

Cooling

Cooling liquid	Plain water with appropriate corrosive inhibitor (max. 50 % corrosive inhibitor)
Cooling liquid corrosive inhibitor type	Ethylene glycol Glysantin G48 recommended
Cooling method (IEC 60034-6)	IC 9S7Y7 (Liquid cooled, external heat exchanger)
Minimum cooling liquid flow	20 l/min
Coolant circuit capacity	2.8 l
Maximum operating pressure	2 bar
Pressure loss	0.4 bar with 20l/min (+25°C coolant)
Cooling liquid temperature max	+65°C (Derating required if exceeded)

Temperature rating

Insulation class (IEC 60034-1)	H (180°C)
Temperature rise (IEC 60034-1)	85°C (F) / 110°C (H)
Maximum winding temperature	175°C
Nominal ambient temperature	65°C
Min. ambient temperature	-40°C
Nominal altitude (IEC 60034-1)	1000 m

Vibration & Shock tolerance

Mechanical vibration	5.9 G_{RMS} ISO 16750-3 Test VII – Commercial vehicle, sprung masses – Table 12 Notes: test duration 8h axis (two axes tested; radial and axial) total spectral acceleration 5,91 grms Test done with EM-PMI375-T800
Mechanical shock	50 G

	ISO 16750-3 4.2.2 Test for devices on rigid points on the body and on the frame Notes: –acceleration: 500 m/s^2; –duration: 6 ms; –number of shocks: 10 per test direction. Test done with EM-PMI375-T800

Connections

Coolant connection	2 x G3/4 bore
HV cables	3 x 70 mm^2 max. (SINGLE winding model) 2 x 3 x 70 mm^2 max. (DUAL winding model)
HV cable glands	Pflitsch blueglobe TRI bg 225ms tri
HV cable	Recommended H+S Radox screened cable
HV cable lug size	35-8, 50-8, 70-8
HV connection boxes	1 x 3 phase box (SINGLE winding model) 2 x 3 phase box (DUAL winding model)
LV connector	47 pin DEUTSCH HD34-24-47PE for resolver and temperature measurement.
LV connecter type	DEUTSCH HD34-24-47PE
LV connector pin type	Gold plated
LV mating connector type	DEUTSCH HD36-24-47SE or DEUTSCH HD36-24-47SE-059
LV mating connector pin type	DEUTSCH 0462-201-1631 DEUTSCH 0462-005-2031 Plug: DEUTSCH 0413-204-2005 (size 20) Plug: DEUTSCH 0413-003-1605 (size 16)
LV connector pin configuration	See Table below.
Anticondensing heater (optional)	50W 230VAC single phase heater resistor
Heater connector (optional)	Hummel art. no. 7651 0 51 01 D
Heater mating connector	Hummel art. no. 7550 6 51 02 D
Heater connector pin type	Hummel 7010 9 42 01 1
Heater connector pin configuration	See Table below
Bearing temp. measurement connector type	4-pin M12 A coded male
Bearing temp. measurement mating type	4-pin M12 A coded female
Bearing temp. measurement connector pin configuration	See Table below

Table 1 Pin configuration of LV-connector

PIN	Description
47	Temperature 1, PT100 (P), windings
46	Temperature 1, PT100 (N), windings
33	Temperature 2, PT100 (P), windings
32	Temperature 2, PT100 (N), windings
45	Temperature 3, PT100 (P), windings
31	Temperature 3, PT100 (N), windings
30	Temperature 4, PT100 (P), windings option TEMP4
29	Temperature 4, PT100 (N), windings option TEMP4
44	Temperature 5, PT100 (P), windings option TEMP4
43	Temperature 5, PT100 (N), windings option TEMP4
28	Temperature 6, PT100 (P), windings option TEMP4
16	Temperature 6, PT100 (N), windings option TEMP4
35	Resolver, RES_COS_N, in-built non-contacting
20	Resolver, RES_COS_P, in-built non-contacting
36	Resolver, RES_SIN_N, in-built non-contacting
21	Resolver, RES_SIN_P, in-built non-contacting
22	Resolver, EXCN, in-built non-contacting
10	Resolver, EXCP, in-built non-contacting
34	Resolver, SHIELD/GROUND, in-built non-contacting

Table 2 Pin configuration of heater

PIN	Description
1	Phase, 230VAC
2	Neutral
3	Reserve
4	Reserve
5	Reserve

Table 3 Pin configuration of bearing temperature sensor connector

PIN	Description
1	PT-100
2	PT-100
3	PT-100_GND
4	PT-100_GND

PRESSURE LOSS VS COOLANT FLOW

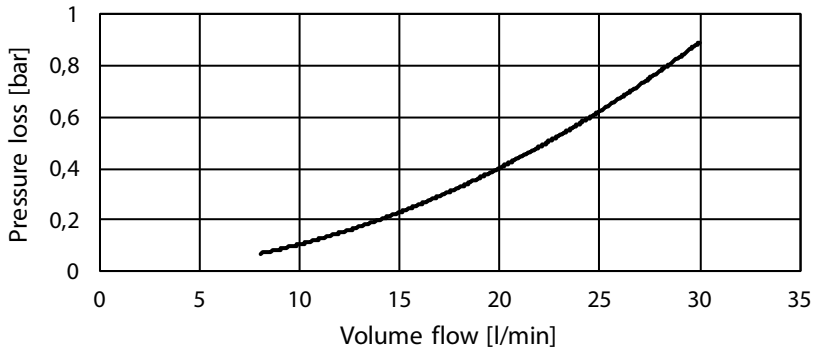

Picture 1 Pressure loss vs coolant flow

MOTORS (temperature class F, maximum winding temperature 150˚C)

Type	Coolant temperature +65°C			Coolant temperature +40°C			Coolant temperature +40 / +65°C			
	Cont. Torque [Nm]	Cont. Power [kW]	Nom. Current [A]	Cont. Torque [Nm]	Cont. Power [kW]	Nom. Current [A]	Nom. speed [rpm]	Max. speed [rpm]	Peak torque Single (*	Peak torque DUAL (**
EM-PMI375-T1100-1200	1306	164	207	1399	176	221	1200	2400	2100	3270
EM-PMI375-T1100-1500	1175	185	261	1310	206	292	1500	3000	1550	2500
EM-PMI375-T1100-1800	1077	203	271	1225	231	310	1800	3600	1380	2500
EM-PMI375-T1100-2100	995	219	288	1178	259	343	2100	4000	1100	2170
EM-PMI375-T1100-2400	952	239	323	1060	266	358	2400	4000	1040	2000
EM-PMI375-T1100-2900	896	272	367	998	303	409	2900	4000	800	1500

(Peak torque achieved with a 350A inverter*
*(** Peak torque achieved with two 350A inverters*

GENERATORS (temperature class F, maximum winding temperature 150˚C)

Type	Coolant temperature +65°C				Coolant temperature +40°C				Coolant temperature +40 / +65°C		
	Apparent power [kVA]	Cont. power [kW]	Nom. Current [A]	Power factor	Apparent power [kVA]	Cont. Power [kW]	Nom. Current [A]	Power factor	Nom. speed [rpm]	Nom. Freq. [Hz]	Volt/ speed ratio [V/rpm] (***
EM-PMI375-T1100-1200	179	175	205	0.98	193	188	219	0.97	1300	130	0.41
EM-PMI375-T1100-1500	222	205	257	0.92	251	229	288	0.92	1700	170	0.33
EM-PMI375-T1100-1800	232	214	267	0.92	266	243	305	0.92	1900	190	0.278
EM-PMI375-T1100-2100	245	230	283	0.94	293	271	338	0.93	2200	220	0.238
EM-PMI375-T1100-2400	270	248	314	0.92	302	277	351	0.92	2500	250	0.208
EM-PMI375-T1100-2900	308	281	358	0.91	344	312	401	0.91	3000	300	0.172

*(*** Back EMF for cold (20°C) generator*

MOTORS (temperature class H, maximum winding temperature 175˚C)

Type	Coolant temperature +65°C			Coolant temperature +40°C			Coolant temperature +40 / +65°C			
	Cont. Torque [Nm]	Cont. Power [kW]	Nom. Current [A]	Cont. Torque [Nm]	Cont. Power [kW]	Nom. Current [A]	Nom. speed [rpm]	Max. speed [rpm]	Peak torque Single (*	Peak torque DUAL (**
EM-PMI375-T1100-1200	1410	177	242	1515	190	263	1200	2400	2100	3270
EM-PMI375-T1100-1500	1310	206	292	1455	228	294	1500	3000	1550	2500
EM-PMI375-T1100-1800	1187	224	298	1338	252	338	1800	3600	1380	2500
EM-PMI375-T1100-2100	1070	235	310	1300	286	380	2100	4000	1100	2170
EM-PMI375-T1100-2400	1036	260	350	1155	290	386	2400	4000	1040	2000
EM-PMI375-T1100-2900	976	296	398	1098	333	456	2900	4000	800	1500

(Peak torque achieved with a 350A inverter*
*(** Peak torque achieved with two 350A inverters*

GENERATORS (temperature class H, maximum winding temperature 175˚C)

Type	Coolant temperature +65°C				Coolant temperature +40°C				Coolant temperature +40 / +65°C		
	Apparent power [kVA]	Cont. power [kW]	Nom. Current [A]	Power factor	Apparent power [kVA]	Cont. Power [kW]	Nom. Current [A]	Power factor	Nom. speed [rpm]	Nom. Freq. [Hz]	Volt/ speed ratio [V/rpm] (***
EM-PMI375-T1100-1200	211	199	239	0.94	229	213	260	0.93	1400	140	0.41
EM-PMI375-T1100-1500	251	230	288	0.92	279	253	288	0.91	1700	170	0.33
EM-PMI375-T1100-1800	252	239	292	0.95	287	269	332	0.94	2000	200	0.278
EM-PMI375-T1100-2100	264	246	305	0.93	325	306	373	0.94	2200	220	0.238
EM-PMI375-T1100-2400	293	269	343	0.92	328	300	379	0.92	2500	250	0.208
EM-PMI375-T1100-2900	332	307	385	0.93	384	349	443	0.91	3100	310	0.172

*(*** Back EMF for cold (20°C) generator*

PRODUCT CODE AND OPTIONS

Use product code including all needed options for ordering. Standard options are not given with the code as they are selected by default if a non-standard option is not selected.

Product code examples

Product code	Description
EM-PMI375-T1100-1800	Standard 1800 rpm unit with standard options
EM-PMI375-T1100-1800+BIN+RES1	Standard unit with insulated bearing in N-end and resolver

Table 3 Product code examples

		s = standard o = option		
Variant	**code**	**Description**	**Standard**	
High voltage connections	*	One 3 phase system	s	One connection box containing one 3 phase system with one M25 cable gland per phase
	-DUAL	Two galvanically isolated 3 phase systems	o	2 connection boxes each containing one 3 phase system with one M25 cable gland per phase
N-end attachement	+NE1	Flange	s	SAE 4 FH
	+NE2	Male shaft + Flange	o	DIN5480 W55x2x30x26x8a + SAE 4 FH
Bearing insulation	*	Non-insulated bearings	s	Bearing types according to BHS
	+BIN	Insulated bearing in N-end	o	SKF 6214 insulated bearing in N-end
	+BIA	Insulated bearing in both ends	o	SKF 6214 insulated bearing in both ends
Shaft grounding	*	None	s	
	+SG1	D-end shaft grounding	o	In-built grounding ring
Protection class	*	Standard protection class	s	IP65 protection class
	+IP67	IP67 protection class	o	IP67 protection class
Cable direction	*	Cable direction fixed	s	Cable direction towards D-end
	+CNE	Cable direction towards N-end	o	
Rotation sensor	*	None	s	No resolver
	+RES1	Resolver	o	In-built non contacting resolver, 6-pole pair
Winding temperature sensors	*	Temperature surveillance	s	3 x PT100 (two wire) in windings
	+TEMP4	Redundant temperature surveillance	o	6 x PT100 (two wire) in windings
Bearing temperature sensors	*	None	s	
	+BTMP1	PT100 in bearings	o	plug in connector
	+BTMP2	Double PT100 in bearings	-	
Anticondensation heaters	*	None	s	
	+HEAT1	One anticondensation heater	o	230VAC/50W,DUAL option not possible

Table 4 Option list

D.2. Danfoss DC/AC invertres

VACON® NXP Liquid Cooled inverter units, DC bus voltage 465-800 VDC

AC drive type	Drive output current			Motor shaft power		Power loss c/a/T*) [kW]	Chassis
	Thermal I_{th} [A]	Rated cont. I_L [A]	Rated cont. I_H [A]	Optimum motor at I_{th} (540 VDC) [kW]	Optimum motor at I_{th} (675 VDC) [kW]		
NXP00165A0T1IWS	16	15	11	7.5	11	0.4/0.2/0.6	CH3
NXP00225A0T1IWS	22	20	15	11	15	0.5/0.2/0.7	CH3
NXP00315A0T1IWS	31	28	21	15	18.5	0.7/0.2/0.9	CH3
NXP00385A0T1IWS	38	35	25	18.5	22	0.8/0.2/1.0	CH3
NXP00455A0T1IWS	45	41	30	22	30	1.0/0.3/1.3	CH3
NXP00615A0T1IWS	61	55	41	30	37	1.3/0.3/1.5	CH3
NXP00725A0T0IWS	72	65	48	37	45	1.2/0.3/1.5	CH4
NXP00875A0T0IWS	87	79	58	45	55	1.5/0.3/1.8	CH4
NXP01055A0T0IWS	105	95	70	55	75	1.8/0.3/2.1	CH4
NXP01405A0T0IWS	140	127	93	75	90	2.3/0.3/2.6	CH4
NXP01685A0T0IWS	168	153	112	90	110	2.5/0.3/2.8	CH5
NXP02055A0T0IWS	205	186	137	110	132	3.0/0.4/3.4	CH5
NXP02615A0T0IWS	261	237	174	132	160	4.0/0.4/4.4	CH5
NXP03005A0T0IWF	300	273	200	160	200	4.5/0.4/4.9	CH61
NXP03855A0T0IWF	385	350	257	200	250	5.5/0.5/6.0	CH61
NXP04605A0T0IWF	460	418	307	250	315	5.5/0.5/6.0	CH62
NXP05205A0T0IWF	520	473	347	250	355	6.5/0.5/7.0	CH62
NXP05905A0T0IWF	590	536	393	315	400	7.5/0.6/8.1	CH62
NXP06505A0T0IWF	650	591	433	355	450	8.5/0.6/9.1	CH62
NXP07305A0T0IWF	730	664	487	400	500	10.0/0.7/10.7	CH62
NXP08205A0T0IWF	820	745	547	450	560	12.5/0.8/13.3	CH63
NXP09205A0T0IWF	920	836	613	500	600	14.4/0.9/15.3	CH63
NXP10305A0T0IWF	1030	936	687	560	700	16.5/1.0/17.5	CH63
NXP11505A0T0IWF	1150	1045	766	600	750	18.4/1.1/19.5	CH63
NXP13705A0T0IWF	1370	1245	913	700	900	15.5/1.0/16.5	CH64
NXP16405A0T0IWF	1640	1491	1093	900	1100	19.5/1.2/20.7	CH64
NXP20605A0T0IWF	2060	1873	1373	1100	1400	26.5/1.5/28.0	CH64
NXP23005A0T0IWF	2300	2091	1533	1250	1500	29.6/1.7/31.3	CH64
NXP24705A0T0IWF	2470	2245	1647	1300	1600	36.0/2.0/38.0	2 x CH64
NXP29505A0T0IWF	2950	2681	1967	1550	1950	39.0/2.4/41.4	2 x CH64
NXP37105A0T0IWF	3710	3372	2473	1950	2450	48.0/2.7/50.7	2 x CH64
NXP41405A0T0IWF	4140	3763	2760	2150	2700	53.0/3.0/56.0	2 x CH64
2 x NXP24705A0T0IWF	4700	4300	3100	2450	3050	69.1/3.9/73	4 x CH64
2 x NXP29505A0T0IWF	5600	5100	3700	2900	3600	74.4/4.6/79	4 x CH64
2 x NXP37105A0T0IWF	7000	6400	4700	3600	4500	90.8/5.2/96	4 x CH64
2 x NXP41405A0T0IWF	7900	7200	5300	4100	5150	101.2/5.8/107	4 x CH64

The voltage classes for the inverter units used in the tables above have been defined as follows:

Input 540 VDC = Rectified 400 VAC supply

Input 675 VDC = Rectified 500 VAC supply

Figure D.1: Power loss for Danfoss VACON NXP Liquid Cooled inverter units [25]

E

Dynamic behaviour

E.1. Sailing in waves

E.1.1. One fuel cell with a 3P28S battery

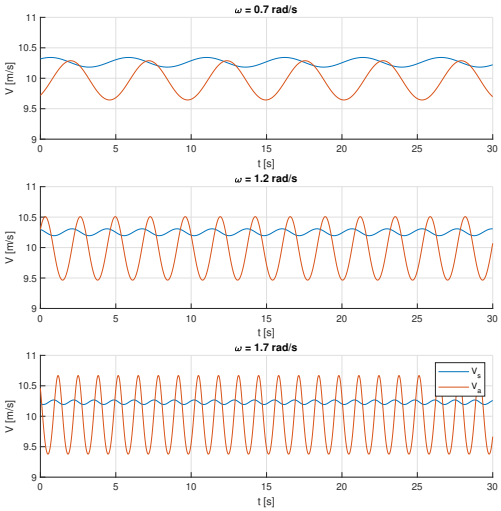

(a) Advance and ship speed

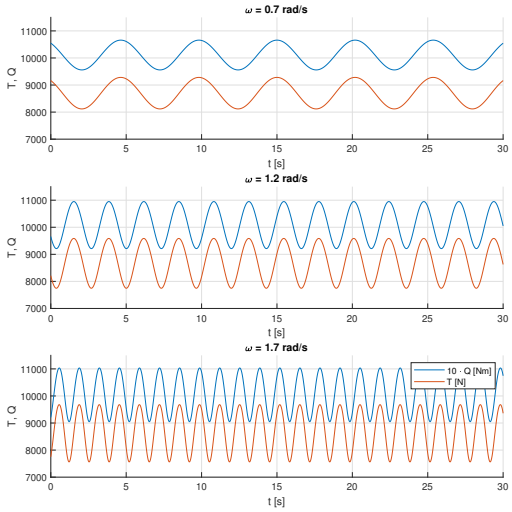

(b) Propeller loading

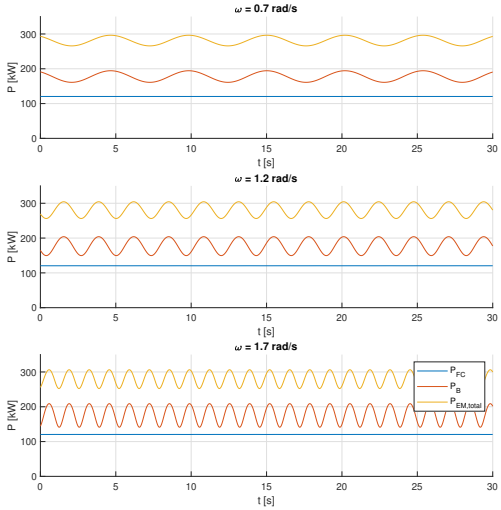

(c) Load distribution

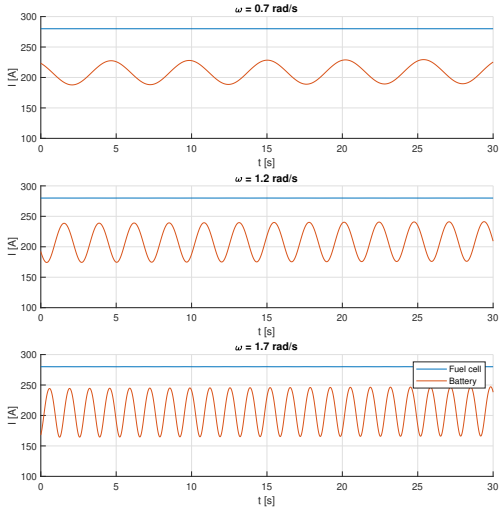

(d) Current

Figure E.1: Sailing in head waves at 20 knots (1 FC/3P28S battery)

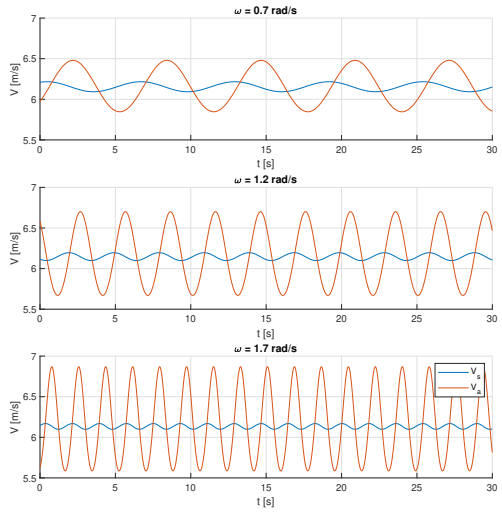

(a) Advance and ship speed

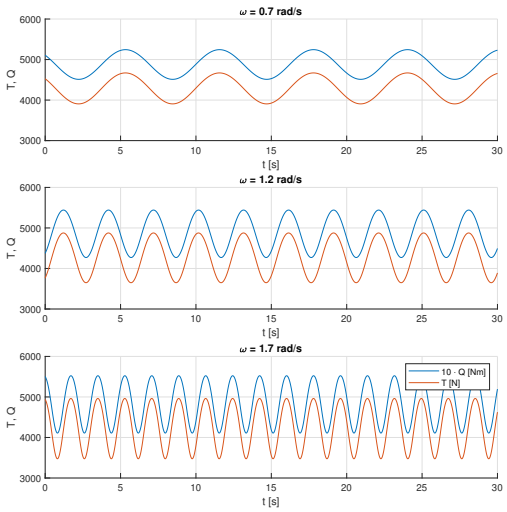

(b) Propeller loading

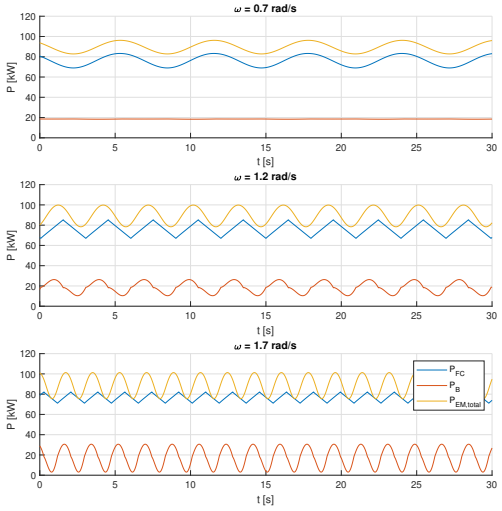

(c) Load distribution

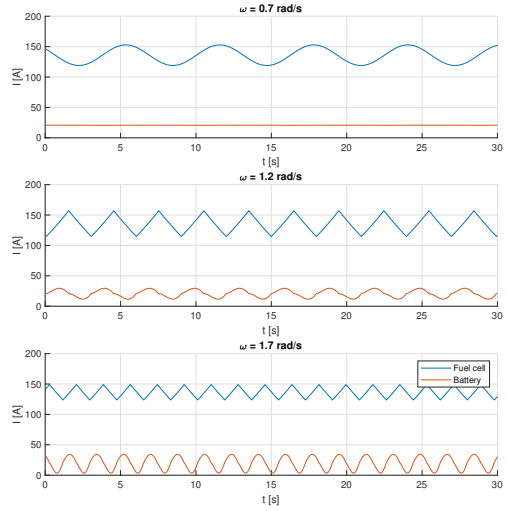

(d) Current

Figure E.2: Sailing in head waves at 12 knots (1 FC/3P28S battery)

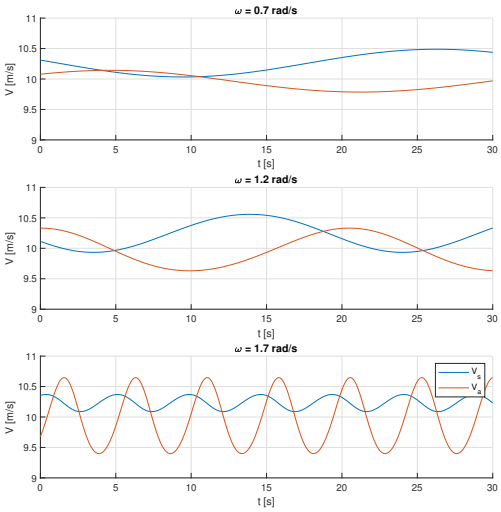

(a) Advance and ship speed

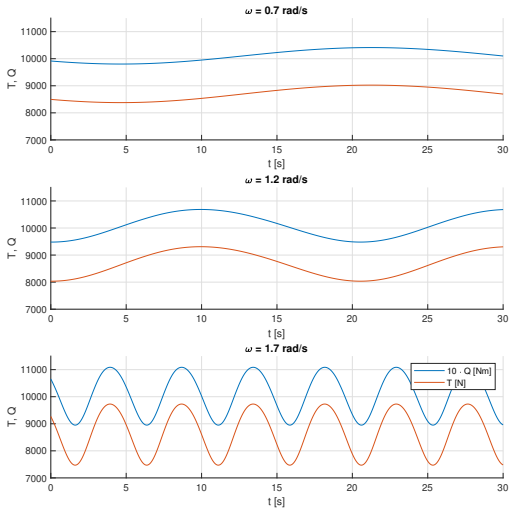

(b) Propeller loading

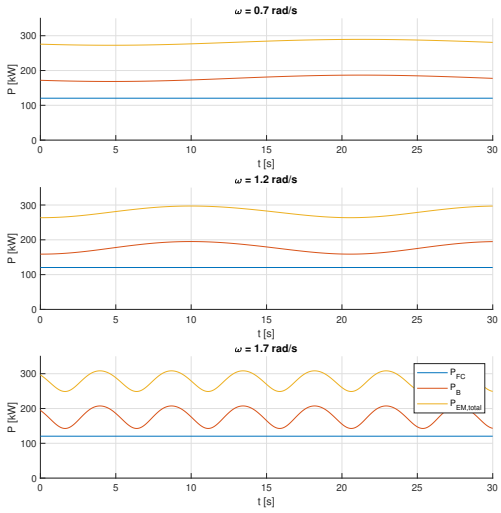

(c) Load distribution

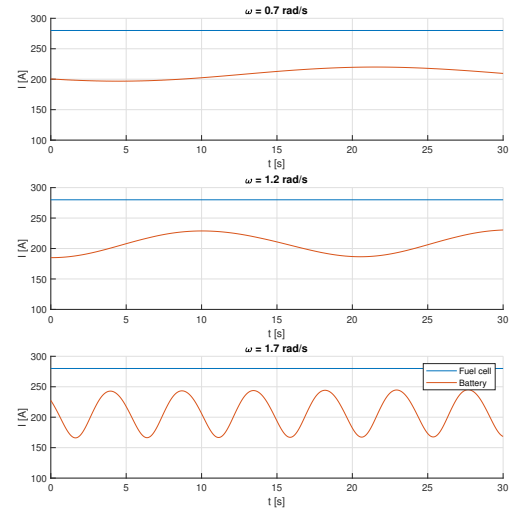

(d) Current

Figure E.3: Sailing in stern waves at 20 knots (1 FC/3P28S battery)

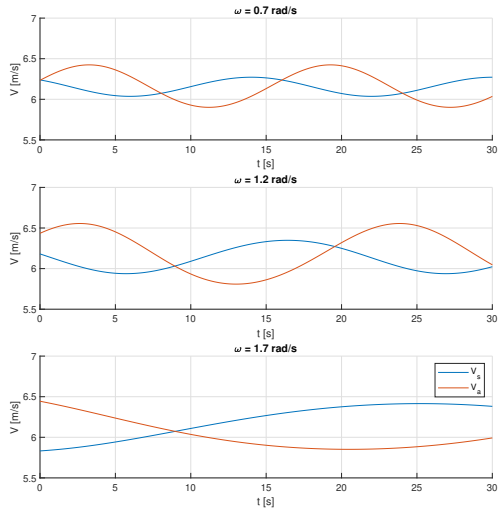

(a) Advance and ship speed

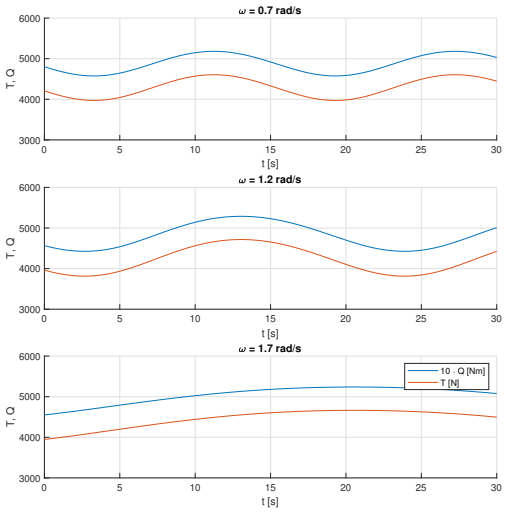

(b) Propeller loading

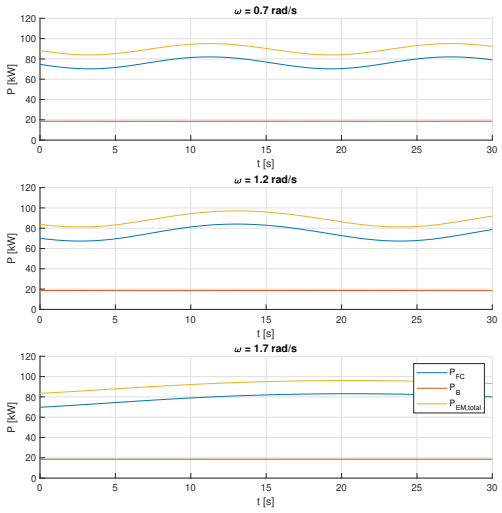

(c) Load distribution

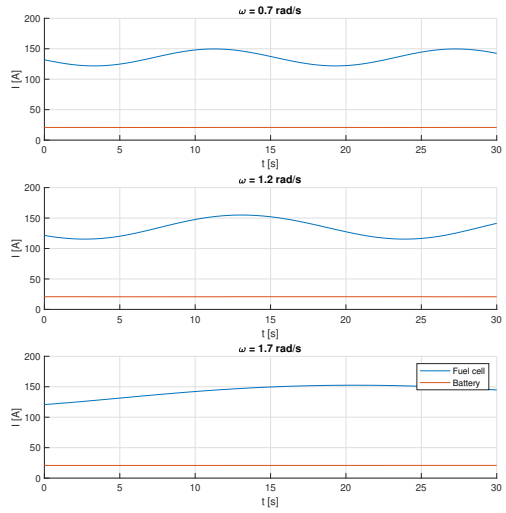

(d) Current

Figure E.4: Sailing in stern waves at 12 knots (1 FC/3P28S battery)

E.1.2. Two fuel cells with a 2P28S battery

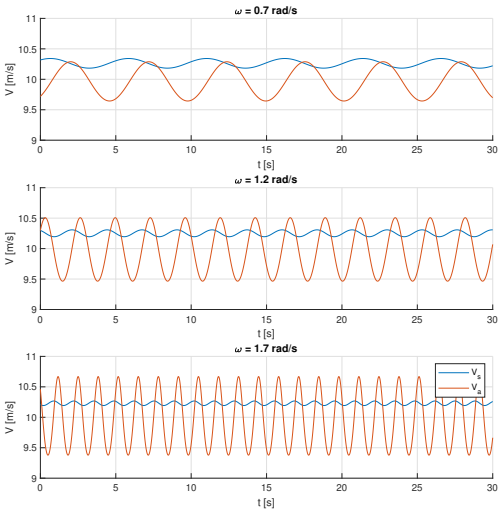

(a) Advance and ship speed

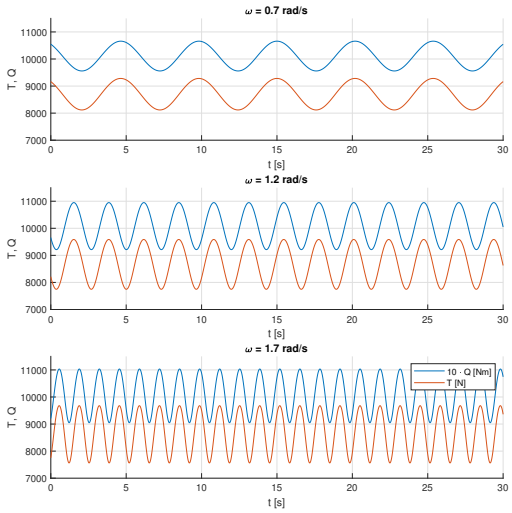

(b) Propeller loading

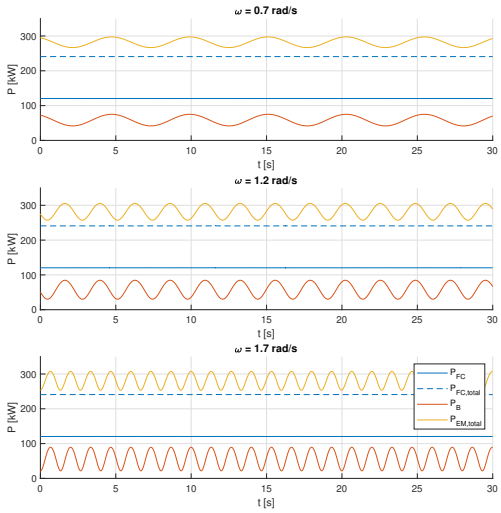

(c) Load distribution

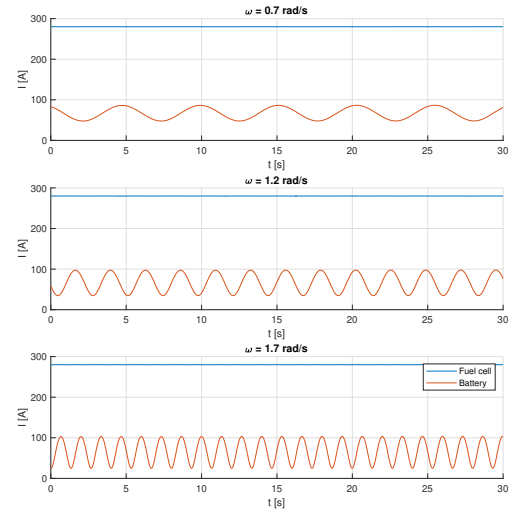

(d) Current

Figure E.5: Sailing in head waves at 20 knots (2 FC's/2P28S battery)

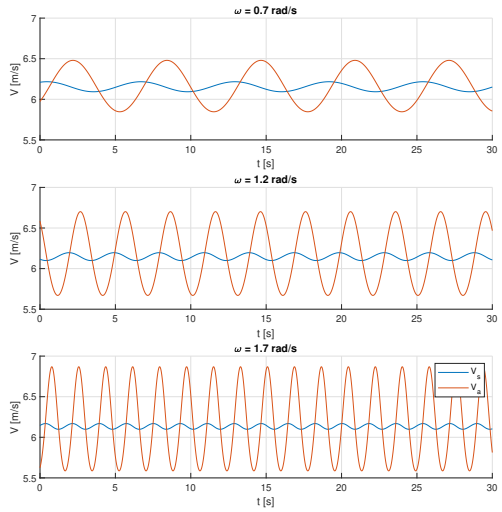

(a) Advance and ship speed

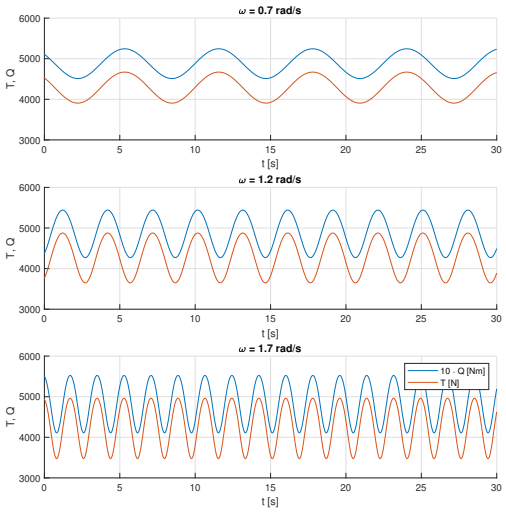

(b) Propeller loading

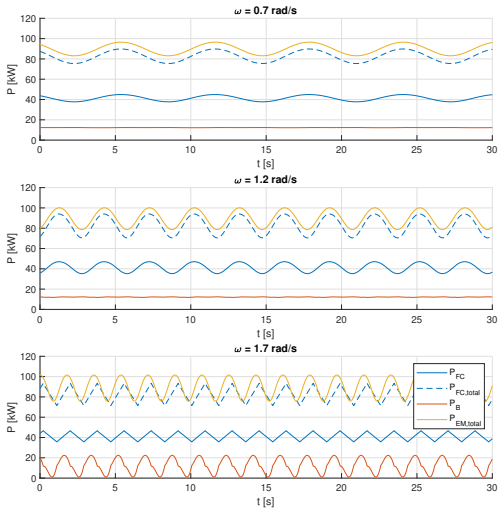

(c) Load distribution

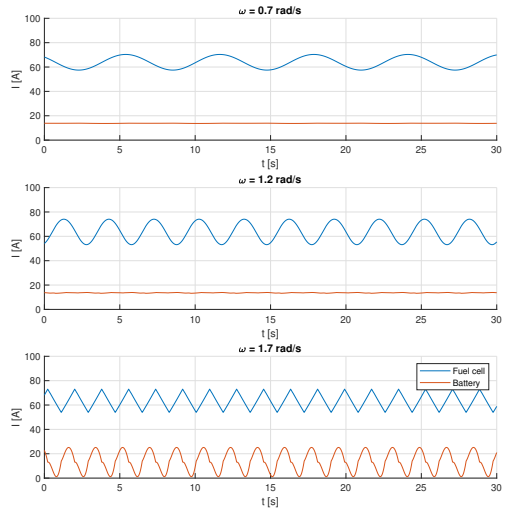

(d) Current

Figure E.6: Sailing in head waves at 12 knots (2 FC's/2P28S battery)

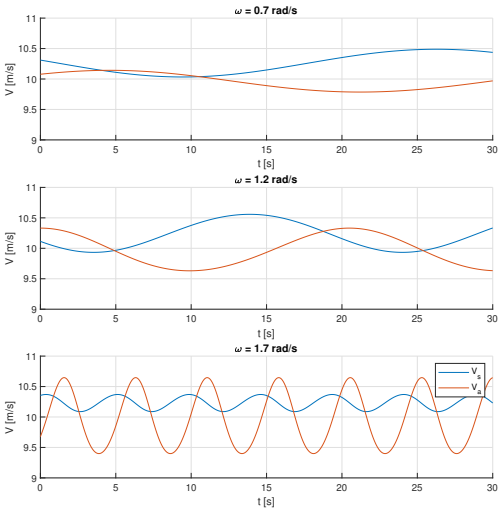

(a) Advance and ship speed

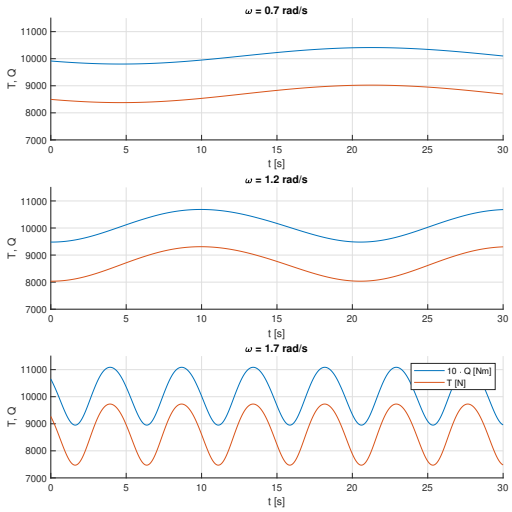

(b) Propeller loading

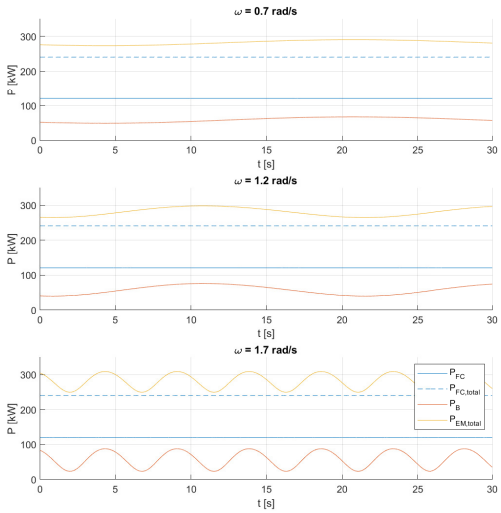

(c) Load distribution

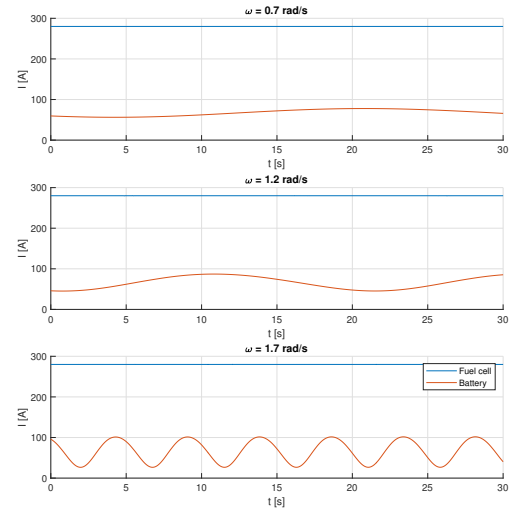

(d) Current

Figure E.7: Sailing in stern waves at 20 knots (2 FC's/2P28S battery)

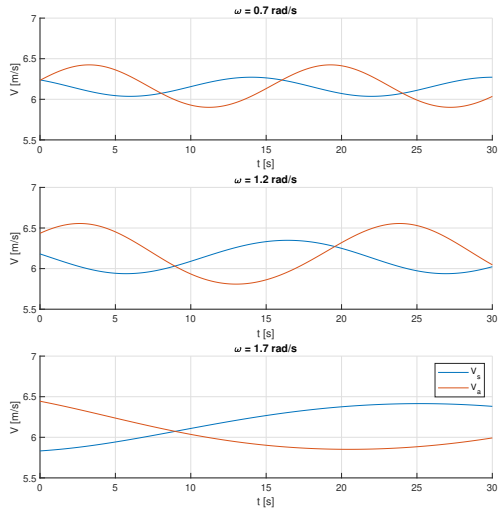

(a) Advance and ship speed

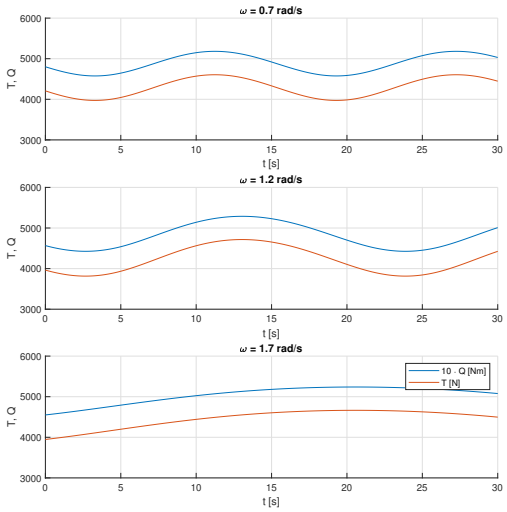

(b) Propeller loading

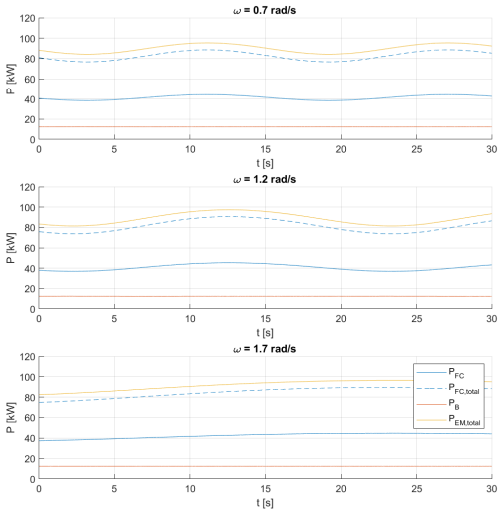

(c) Load distribution

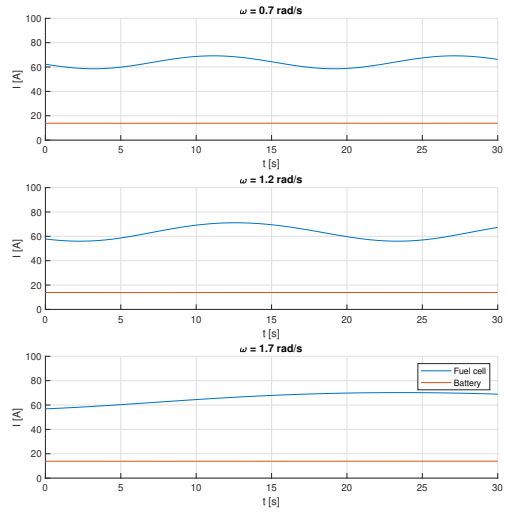

(d) Current

Figure E.8: Sailing in stern waves at 12 knots (2 FC's/2P28S battery)

E.2. Slam start

E.2.1. One fuel cell with a 3P28S battery

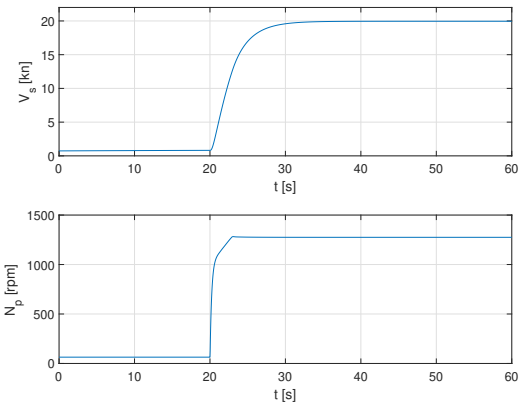

(a) Ship speed and propeller speed

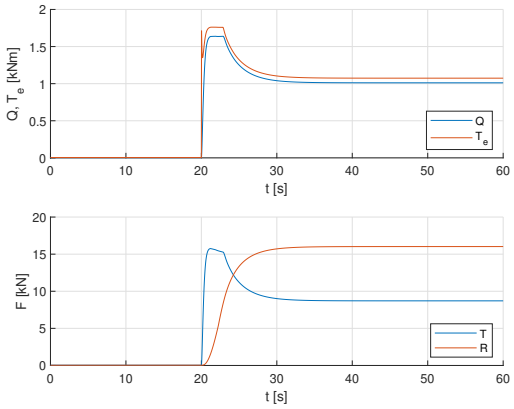

(b) Propeller loading

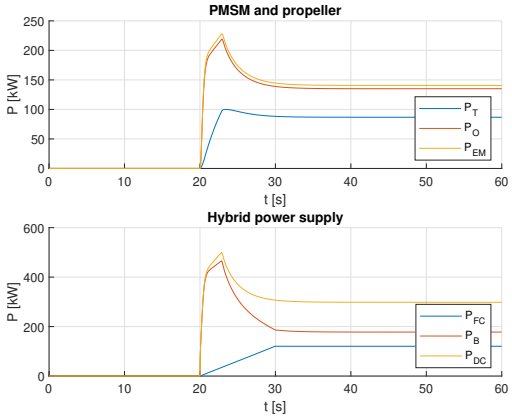

(c) Propulsive power and power distribution of the hybrid power supply

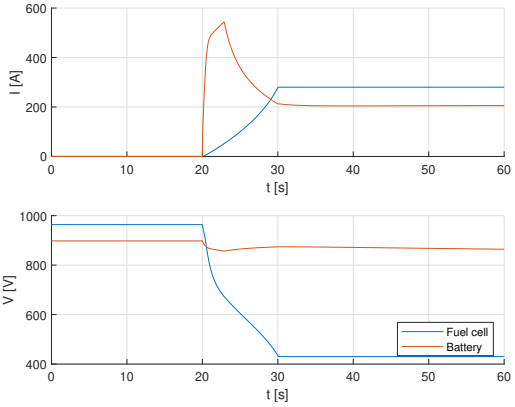

(d) Current and voltage

Figure E.9: Dynamic behaviour during a slam start manoeuvre without slope speed limitation (1 FC/3P28S battery)

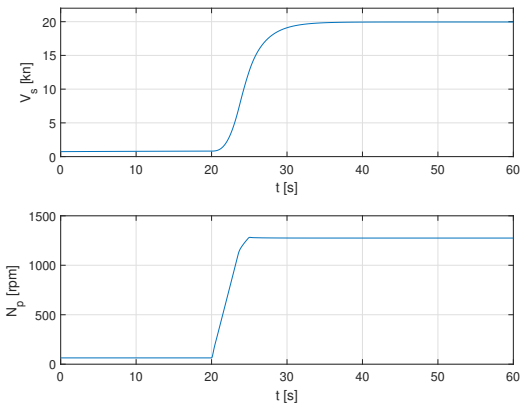

(a) Ship speed and propeller speed

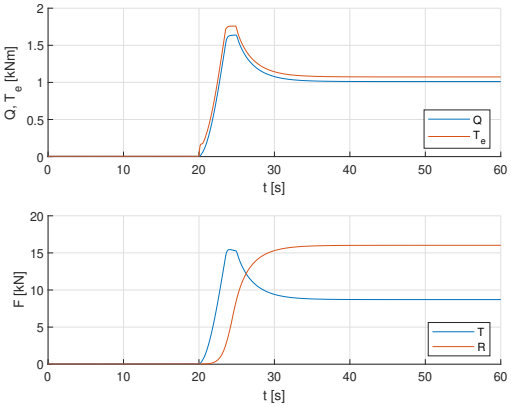

(b) Propeller loading

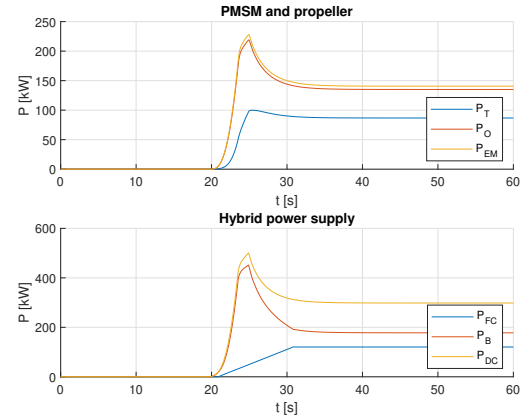

(c) Propulsive power and power distribution of the hybrid power supply

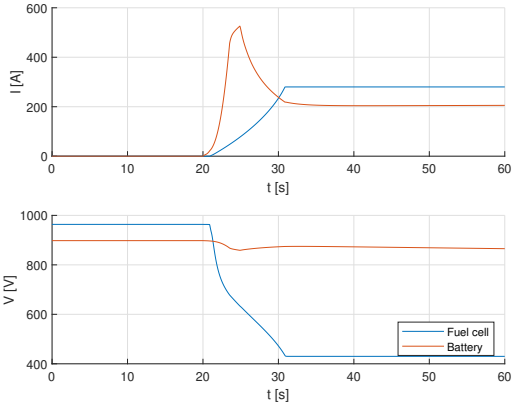

(d) Current and voltage

Figure E.10: Dynamic behaviour during a slam start manoeuvre with a slope speed limitation of 300 rpm/s (1 FC/3P28S battery)

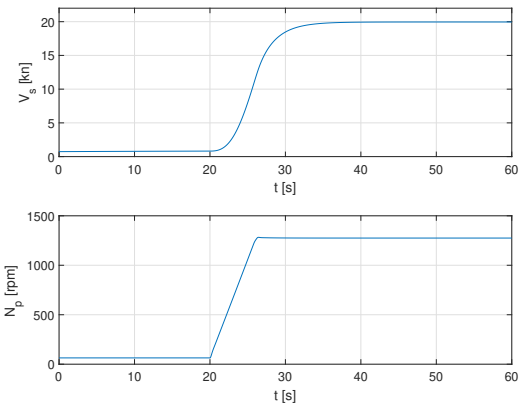

(a) Ship speed and propeller speed

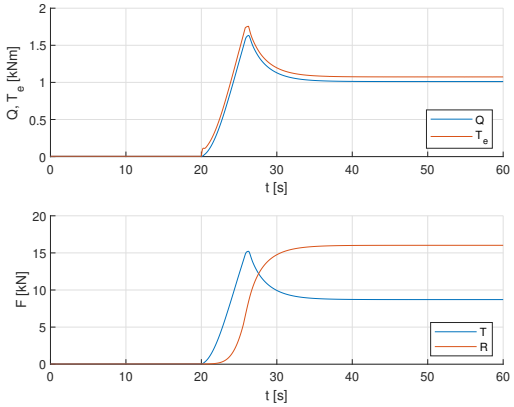

(b) Propeller loading

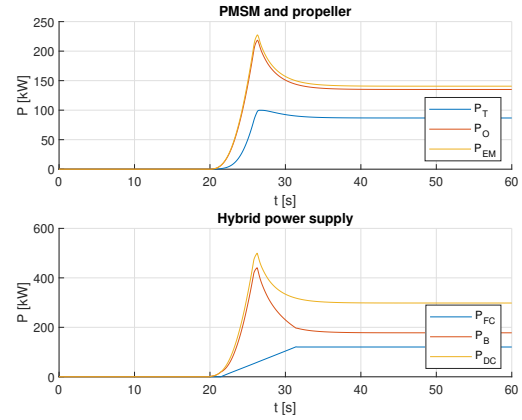

(c) Propulsive power and power distribution of the hybrid power supply

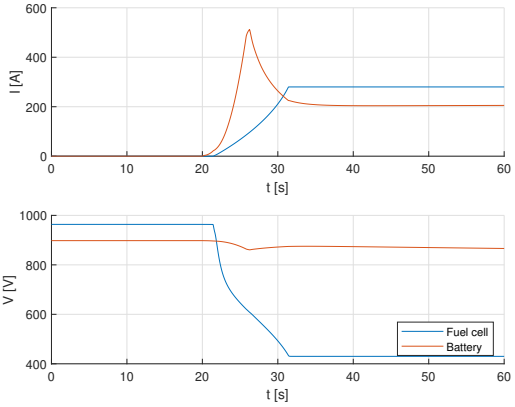

(d) Current and voltage

Figure E.11: Dynamic behaviour during a slam start manoeuvre with a slope speed limitation of 200 rpm/s (1 FC/3P28S battery)

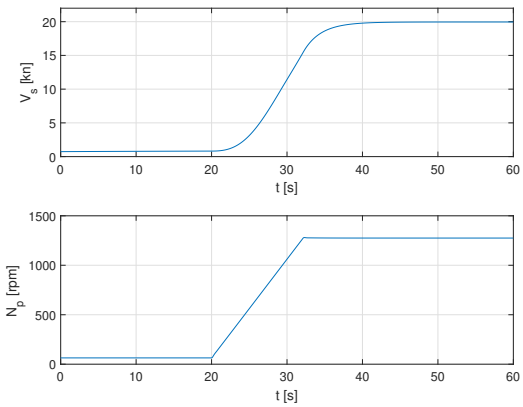

(a) Ship speed and propeller speed

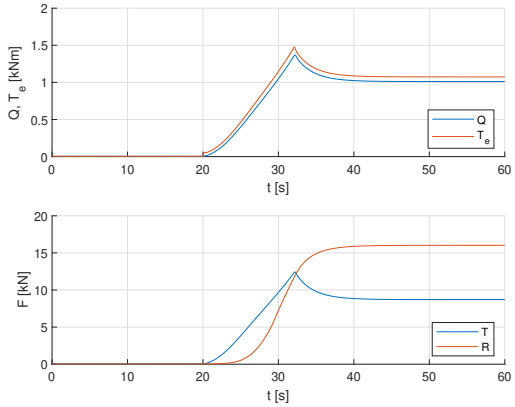

(b) Propeller loading

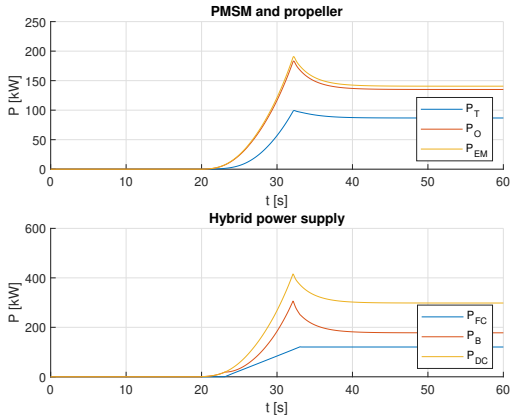

(c) Propulsive power and power distribution of the hybrid power supply

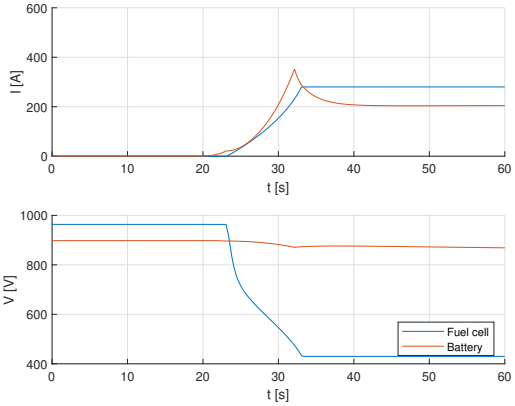

(d) Current and voltage

Figure E.12: Dynamic behaviour during a slam start manoeuvre with a slope speed limitation of 100 rpm/s (1 FC/3P28S battery)

E.2.2. Two fuel cells with a 2P28S battery

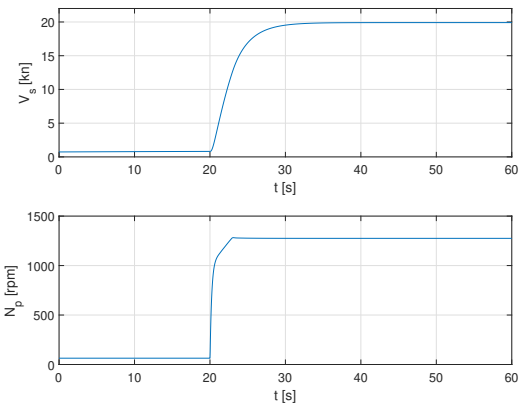

(a) Ship speed and propeller speed

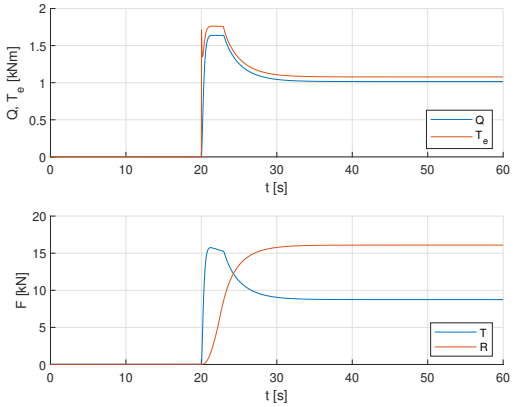

(b) Propeller loading

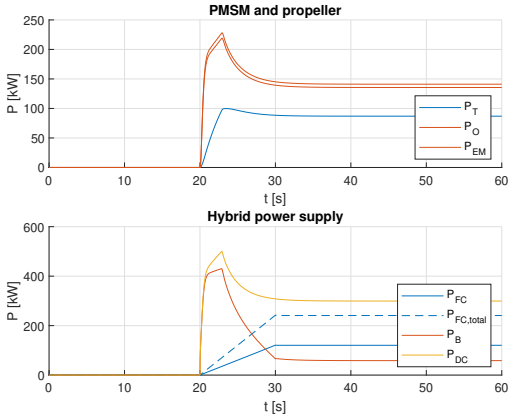

(c) Propulsive power and power distribution of the hybrid power supply

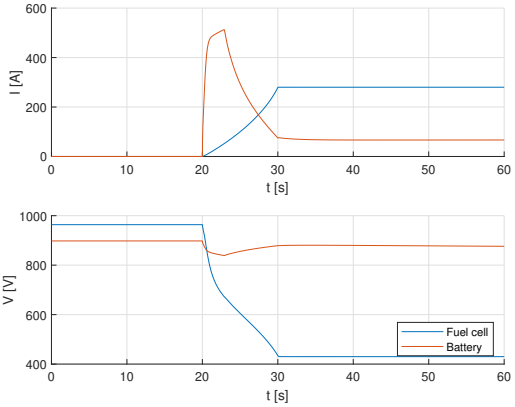

(d) Current and voltage

Figure E.13: Dynamic behaviour during a slam start manoeuvre without slope speed limitation (2 FC's/2P28S battery)

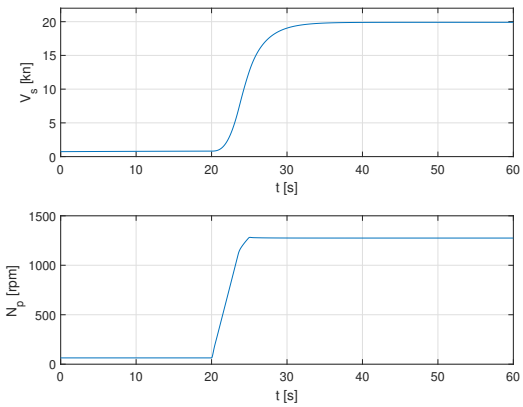

(a) Ship speed and propeller speed

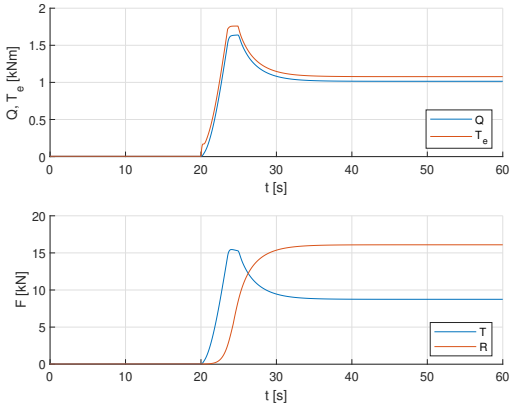

(b) Propeller loading

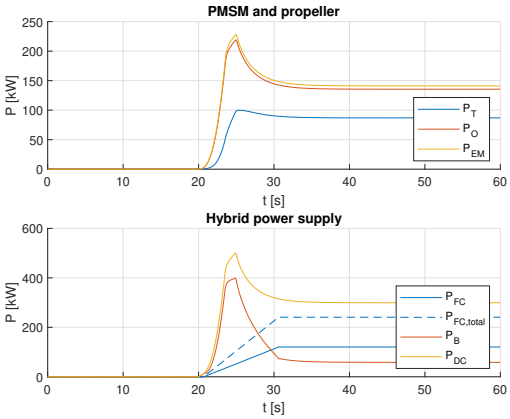

(c) Propulsive power and power distribution of the hybrid power supply

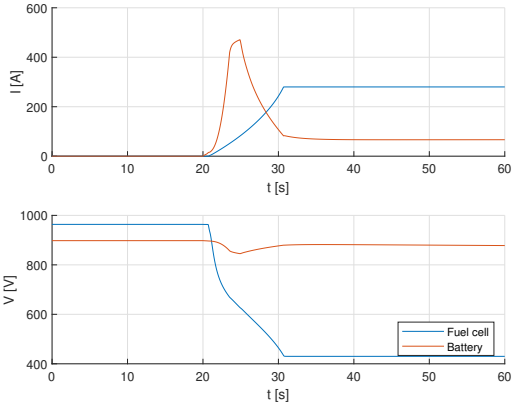

(d) Current and voltage

Figure E.14: Dynamic behaviour during a slam start manoeuvre with a slope speed limitation of 300 rpm/s (2 FC's/2P28S battery)

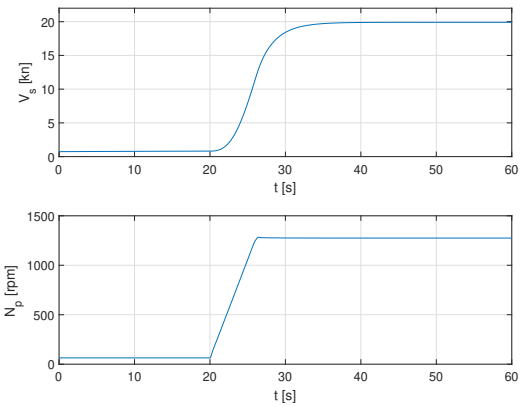

(a) Ship speed and propeller speed

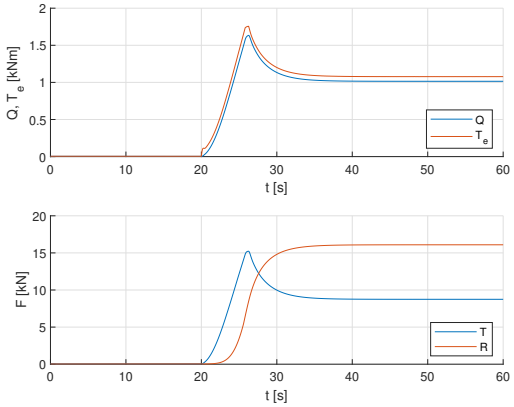

(b) Propeller loading

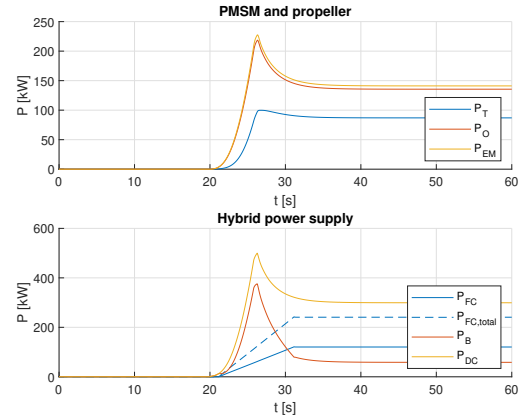

(c) Propulsive power and power distribution of the hybrid power supply

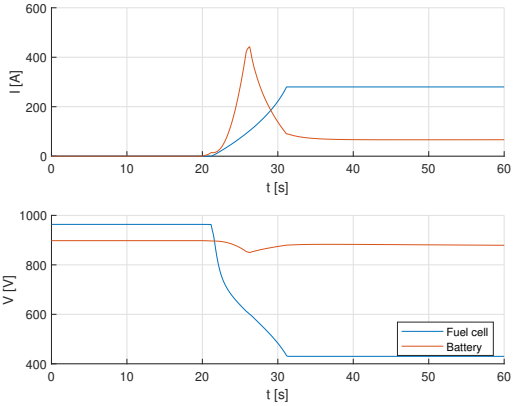

(d) Current and voltage

Figure E.15: Dynamic behaviour during a slam start manoeuvre with a slope speed limitation of 200 rpm/s (2 FC's/2P28S battery)

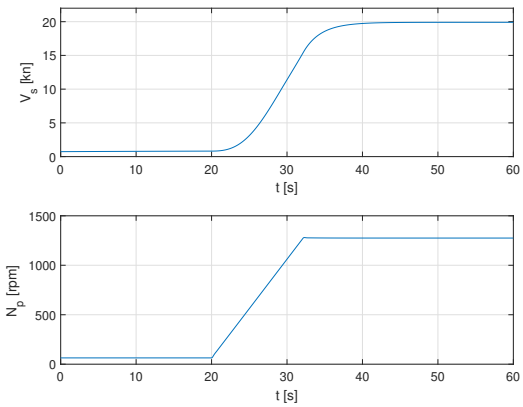

(a) Ship speed and propeller speed

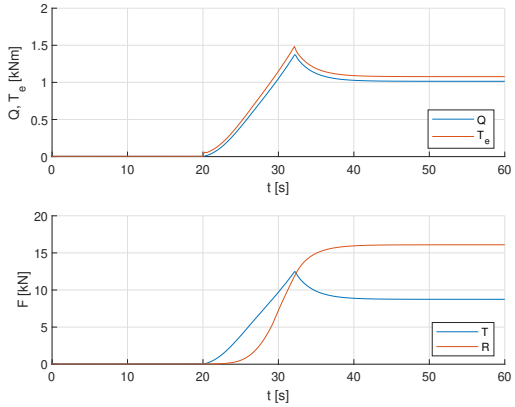

(b) Propeller loading

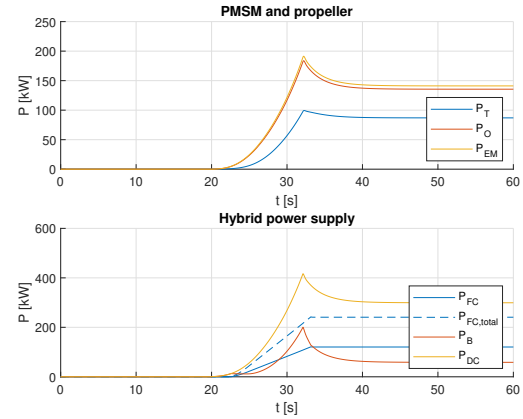

(c) Propulsive power and power distribution of the hybrid power supply

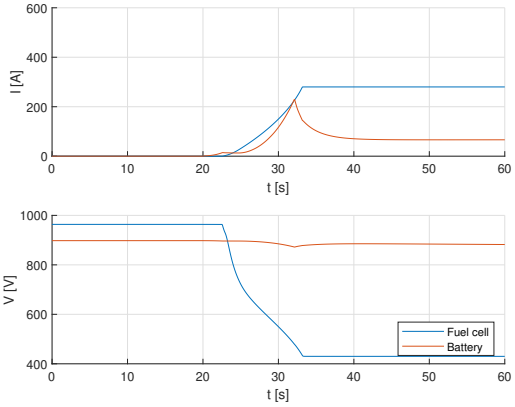

(d) Current and voltage

Figure E.16: Dynamic behaviour during a slam start manoeuvre with a slope speed limitation of 100 rpm/s (2 FC's/2P28S battery)

E.3. Crash stop

E.3.1. Effect of speed slope limiters

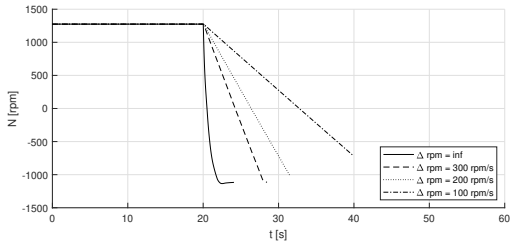

(a) Propeller speed

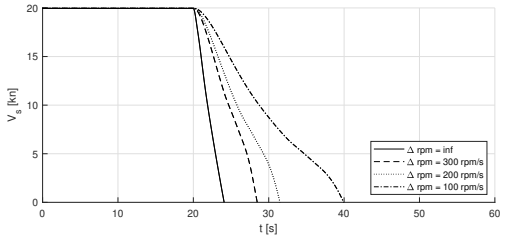

(b) Ship speed

Figure E.17: Effect of various speed slope limiter settings on stopping distance during a crash stop manoeuvre)

E.3.2. One fuel cell with a 3P28S battery

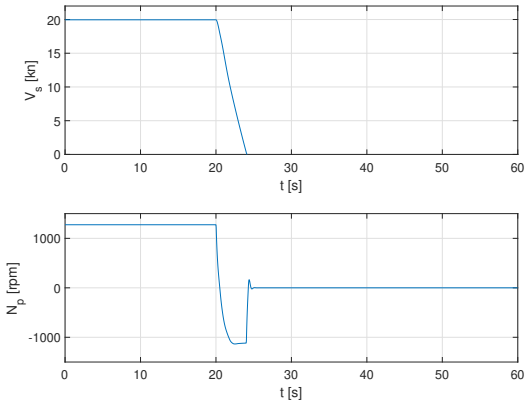

(a) Ship speed and propeller speed

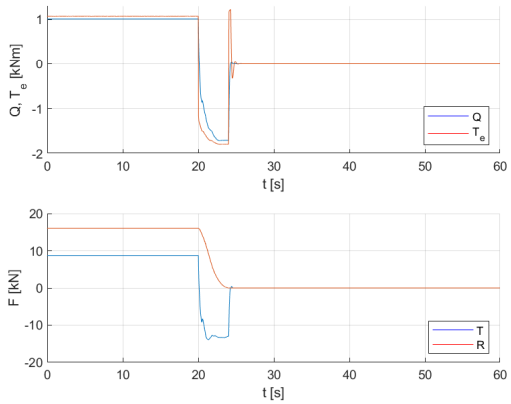

(b) Propeller loading

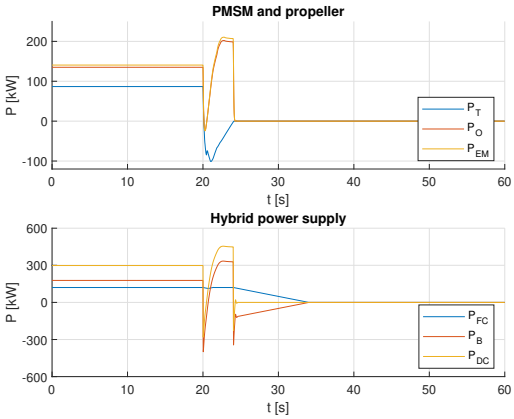

(c) Propulsive power and power distribution of the hybrid power supply

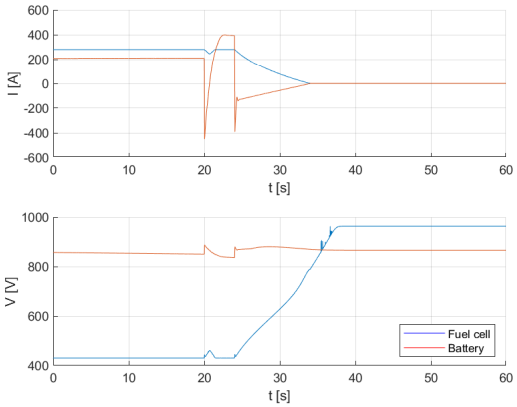

(d) Current and voltage

Figure E.18: Dynamic behaviour during a crash stop manoeuvre with direct braking (1 FC/3P28S battery)

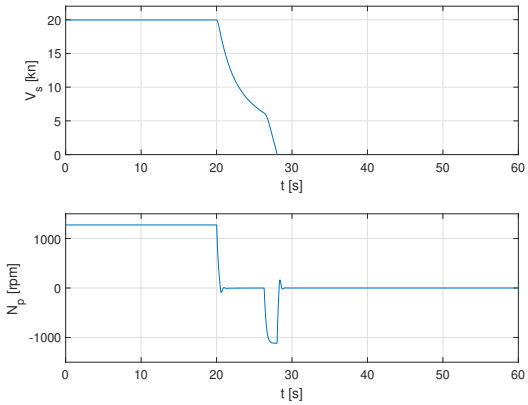

(a) Ship speed and propeller speed

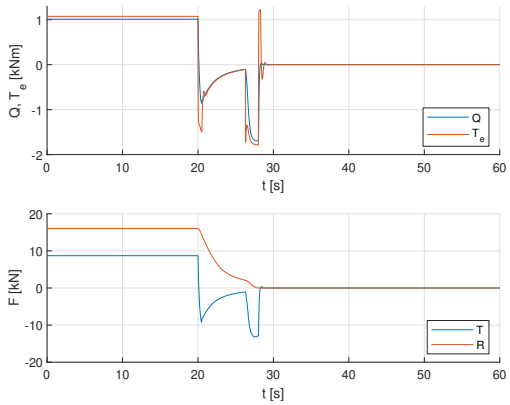

(b) Propeller loading

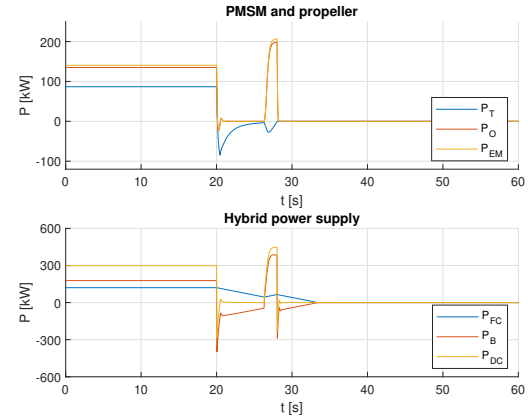

(c) Propulsive power and power distribution of the hybrid power supply

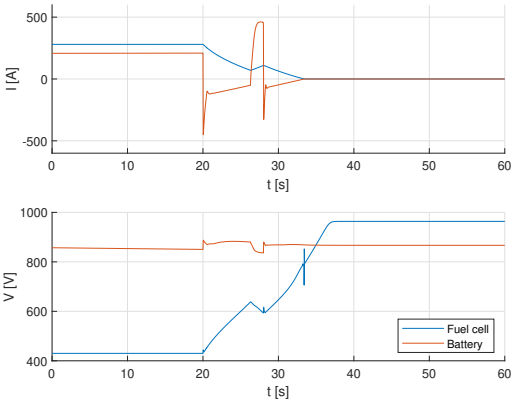

(d) Current and voltage

Figure E.19: Dynamic behaviour during a crash stop manoeuvre with coasting and braking (1 FC/3P28S battery)

E.3.3. Two fuel cells with a 2P28S battery

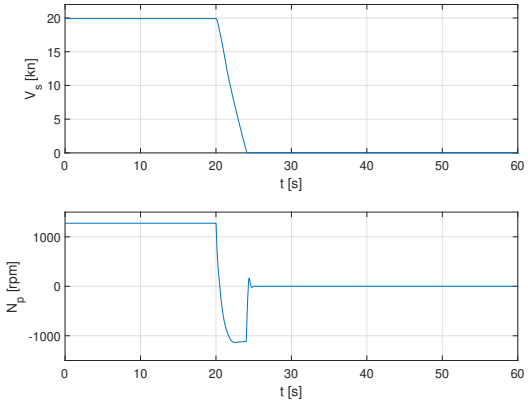

(a) Ship speed and propeller speed

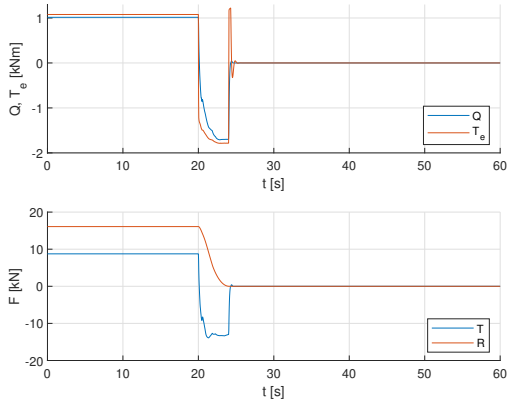

(b) Propeller loading

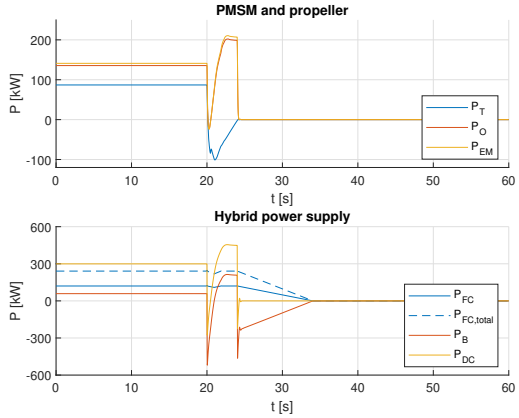

(c) Propulsive power and power distribution of the hybrid power supply

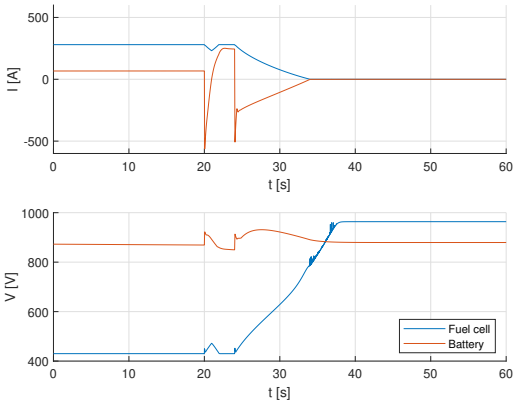

(d) Current and voltage

Figure E.20: Dynamic behaviour during a crash stop manoeuvre with direct braking (2 FC's/2P28S battery)

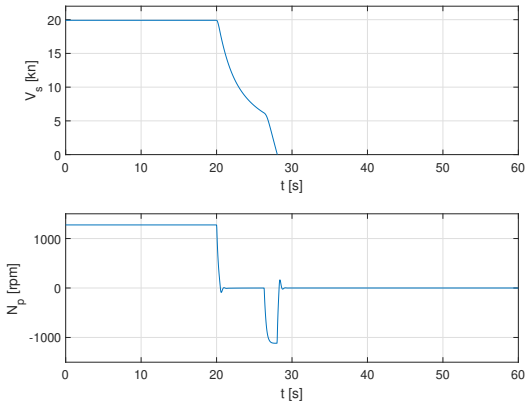

(a) Ship speed and propeller speed

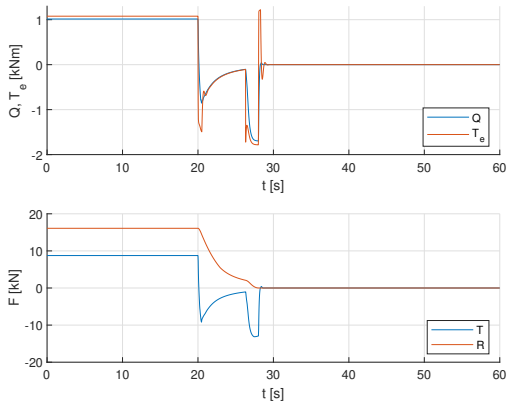

(b) Propeller loading

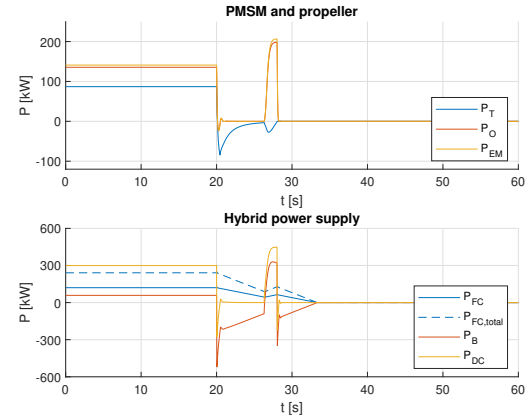

(c) Propulsive power and power distribution of the hybrid power supply

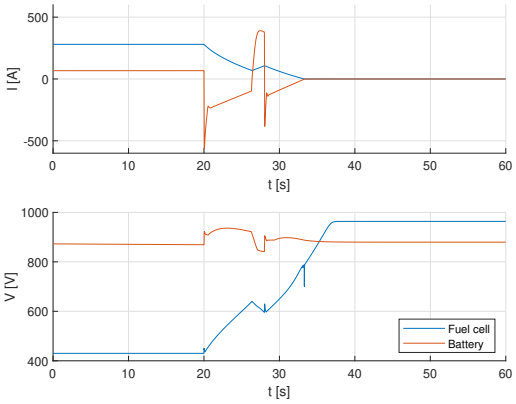

(d) Current and voltage

Figure E.21: Dynamic behaviour during a crash stop manoeuvre with coasting and braking (2 FC's/2P28S battery)